UNIVERSITY OF CALIFORNIA
SANTA CRUZ

Interplay between modes of strain release along the shallow northern Hikurangi subduction zone, New Zealand

A dissertation submitted in partial satisfaction
of the requirements for the degree of

DOCTOR OF PHILOSOPHY

in

EARTH SCIENCE

by

Erin K. Todd

March 2017

The Dissertation of Erin K. Todd is approved:

_____
Professor Susan Y. Schwartz, chair

_____
Professor Thorne Lay

_____
Professor Emily E. Brodsky

_____
Tyrus Miller
Vice Provost and Dean of Graduate Studies

Table of Contents

List of Figures

List of Tables

Abstract

Interplay between modes of strain release along the shallow northern Hikurangi subduction zone, New Zealand

Erin K. Todd

Slow slip events are well documented in global subduction zones at depths of 30-50 km. Tectonic (non-volcanic) tremor is considered to be the seismic manifestation of slow slip and is spatiotemporally correlated with slip events in most regions. Along the northern Hikurangi Margin, New Zealand, where a seamount studded igneous plateau subducts beneath the North Island, slow slip occurs shallowly at depths <15 km. Here, slow slip is associated with increases in microseismicity levels and has previously been weakly linked to tectonic tremor. Over a six-year period, the spatiotemporal progression of slow slip events along the northern Hikurangi Margin with respect to tremor, earthquake occurrence, and Coulomb failure stress changes imparted on the megathrust is analyzed. In this study, the first comprehensive tremor catalog is presented for 2010-2015. The catalog demonstrates that tremor is temporally associated with shallow slow slip events and deep tremor episodes may indicate the occurrence of previously undetected long duration slip events. A slow slip event in 2014 was recorded by the Hikurangi Ocean Bottom Investigation of Tremor and Slow Slip (HOBITSS) experiment, resulting in a detailed spatiotemporal analysis of various interplate slip processes with respect to a

local subducted seamount. Coulomb failure stress change analysis of this event suggests that seamount subduction plays a dominant role in the stress state of the shallow megathrust, and that the northern Hikurangi Margin is weakly coupled and largely releases strain through slow slip events. A detailed analysis of the Coulomb failure stress change imparted on the shallow megathrust by seven slow slip events along the northern Hikurangi Margin between 2010-2014 demonstrates that stress changes from these events influence the along strike migration of slow slip event sequences. Additionally, the stress changes dictate the spatial relationship between tectonic tremor and slow slip, with onshore tectonic tremor occurring almost wholly within regions of stress increase. Over multiple slow slip events, the shallow-most part of the plate interface experiences a net stress increase and may promote failure in future shallow earthquakes, such as tsunami earthquakes, which impact seismic hazards along the east coast of New Zealand.

Acknowledgements

The text of this dissertation includes reprints of the following previously published material. The co-authors listed in these publications directed and supervised the research which forms the basis for the dissertation.

Chapter 1: Todd, E. K., and S. Y. Schwartz (2016), Tectonic tremor along the northern Hikurangi Margin, New Zealand, between 2010 and 2015, *J. Geophys. Res. Solid Earth*, 2016JB013480, doi:10.1002/2016JB013480.

Appendix C: Todd, E. K., and T. Lay (2013), The 2011 Northern Kermadec earthquake doublet and subduction zone faulting interactions, *J. Geophys. Res. Solid Earth*, *118*(1), 249–261, doi:10.1029/2012JB009711.

I would like to acknowledge the support and assistance from numerous people and organizations, without whom this PhD dissertation would not have been the same.

First, I would like to thank Susan Schwartz for the opportunity to work on such a fantastic and interesting project. The combination of guidance and support she provided as well as the independence she afforded me allowed this project to develop organically. I would like to especially thank Susan for encouraging and allowing me to develop my professional interests such as teaching, course development, education outreach, and advising even though it meant my time was often divided between many tasks and responsibilities. I'd also like to thank my committee members Thorne Lay and Emily Brodsky for your instruction and helpfulness regarding questions or

problems I had throughout my PhD studies. Many thanks to my fellow students and postdocs in the seismology lab for all their encouragement and support over the years. Special thanks to Heather Shaddox for her help compiling the HOBITSS earthquake catalog.

A very special thank you to the E&PS department office staff, Jennifer Fish, Judy Vanleuven, Amy Kornberg, and Jenna Scarpelli, for their encouragement over the years! Thank you for your friendship, for always answering my silly questions, and all the laughs.

Another special thank you to Charles Williams for hosting me at GNS in 2014 and 2015 and for your continued support. Thanks for always having an open door, open email, and open FaceTime policy for me to ask any and all questions. Through Charles, I have been able to make many contacts and now have numerous colleagues and collaborators throughout New Zealand. I am forever grateful.

Thankfully my travel bug was not squashed during my studies and I am extremely grateful for travel support from Susan Schwartz, EAPSI (NSF), GeoPRISMS, IRIS, AGU, Yoshihiro Ito, and Kimihiro Mochizuki to attend workshops, conferences, and to have the opportunity to be a visiting researcher in New Zealand. Financial support from the EAPSI and ARCS fellowships provided me with countless opportunities that I would not have otherwise had. Additionally, I'm extremely thankful for the opportunity to be on the HOBITSS deployment and recovery cruises that allowed me to see how science is done from the ocean floor up. Thanks to the HOBITSS science party including Laura Wallace, Anne Sheehan, Kimi

Mochizuki, Stuart Henrys, Yoshi Ito, Sphar Webb, as well as the many graduate students, engineers, and crews of the R/V Tangaroa and R/V Roger Revelle.

I would not have been able to make it here without the support of my friends and family. Thanks especially to my parents, Ed & Jan Todd and Kate & Dave Seay, Betty Gustafson, Dave Santaniello, Caroline Chavez, Stephen Hernandez, Felix, and Maya for always supporting me and listening to me – even when I didn't make any sense!

Finally, I wouldn't be where I am today without the eternal love and support from Christopher Seay. Thank you for being my partner through all the crazy adventures, two cross-country moves, three years apart, through all the frustrations, successes, early mornings, late nights and everything in-between. You are my everything!

Chapter 1 - Tectonic tremor along the northern Hikurangi Margin, New Zealand between 2010 and 2015

1.1 Introduction

The detection of circum-Pacific slow slip events and associated tectonic tremor has led to numerous studies into the modes and timescales of deformation on the subduction plate boundary [e.g. *Dragert et al.*, 2001; *Kostoglodov et al.*, 2003; *Rogers and Dragert*, 2003; *Obara et al.*, 2004; *Douglas et al.*, 2005; *Wallace and Beavan*, 2006, 2010]. This discovery has shed light on a broader range of strain release processes that span from aseismic creep at plate convergence rates (cm/yr) to traditional earthquake slip rates (m/s). New Zealand has recently joined the list of regions that exhibit both slow slip [*Douglas et al.*, 2005; *Wallace and Beavan*, 2006; *Beavan et al.*, 2007; *McCaffrey*, 2008; *Wallace and Beavan*, 2010; *Wallace et al.*, 2012a; *Wallace and Eberhart-Phillips*, 2013; *Bartlow et al.*, 2014; *Wallace et al.*, 2016] and tectonic tremor [*Fry et al.*, 2011; *Kim et al.*, 2011; *Ide*, 2012; *Wech et al.*, 2012; *Chao et al.*, 2013; *Wech et al.*, 2013]. Studies indicate slow slip nucleates within the frictional stability transition between velocity-weakening (failure in earthquakes) and velocity-strengthening (stable-sliding) zones of the plate interface [e.g. *Shibazaki and Iio*, 2003; *Yoshida and Kato*, 2003; *Liu and Rice*, 2007; *Rubin*, 2008; *Segall et al.*, 2010] in locations where fluid-rich sediments may have been entrenched next to subducted features such as seamounts [*Bell et al.*, 2010; *Wang and Bilek*, 2011]. The physical, chemical, and fluid properties of the plate interface that

lead to the nucleation, propagation, and termination of slow slip are active areas of research [e.g. *Eberhart-Phillips and Reyners*, 1999; *Audet and Bürgmann*, 2014; *Bassett et al.*, 2014; *Ellis et al.*, 2015; *Montgomery-Brown and Syracuse*, 2015; *Saffer and Wallace*, 2015; *Williams and Wallace*, 2015].

Tectonic tremor collocated with or near geodetically detected slow slip provides a window into this otherwise aseismic process. Although many early tectonic tremor observations were associated with slow slip in the Nankai [*Obara*, 2002] and Cascadia [*Rogers and Dragert*, 2003] subduction zones, tremor associated with slow slip has more recently been identified in subduction zones such as Costa Rica [e.g. *Brown et al.*, 2005], Mexico [e.g. *Payero et al.*, 2008; *Brudzinski et al.*, 2010], Alaska [e.g. *Peterson and Christensen*, 2009], and New Zealand [*Kim et al.*, 2011], In addition, tremor without geodetically detectable slow slip has been observed along transform boundaries such as the San Andreas Fault near Parkfield, California [e.g. *Nadeau and Dolenc*, 2005] and the Central Alpine Fault, New Zealand [e.g. *Wech et al.*, 2012] as well as in other regions such as Central Taiwan [e.g. *Peng and Chao*, 2008], Southern Chile [*Gallego et al.*, 2013], and Sumbawa, Indonesia [*Fuchs et al.*, 2014] and is likely triggered by surface waves from teleseismic earthquakes. Tectonic tremor coincident with slow slip is nearly universally accepted to result from a multitude of low frequency earthquakes (LFE) overlapping in time such that individual body wave arrivals are rarely discernable. These events, devoid of high frequencies compared to normal earthquakes of the same magnitude, are primarily attributed to shear failure on the plate interface driven

by high pore fluid pressures [e.g. *Shelly et al.*, 2006; *Ide et al.*, 2007b; *Rubinstein et al.*, 2007; *Shelly et al.*, 2007; *Brown et al.*, 2009; *Beroza and Ide*, 2011; *Thomas et al.*, 2016].

Several plausible mechanisms for slow slip have been proposed with most sharing the notion that slow slip starts like a normal earthquake but has its slip speed arrested by some mechanism such as dilatant hardening [*Segall et al.*, 2010] or a change in frictional behavior (from velocity weakening to velocity strengthening) with increasing slip speed [*Shibazaki and Iio*, 2003; *Kaproth and Marone*, 2013]. We believe that progress in understanding slow slip can be advanced through increased observations and analysis of slow slip and tremor in many different locations and environments and the identification of those aspects that are universal and reproducible. In this study, we contribute to this effort by producing the first comprehensive tremor catalog for the northern Hikurangi Margin between 2010 and 2015 and analyzing the spatiotemporal relationships between tremor and slow slip.

1.2 Tectonic Setting

New Zealand is located on the complex boundary between the Australian and Pacific tectonic plates. Beneath the North Island the Hikurangi Plateau, a large igneous province with a crustal thickness of 35-42 km [*Reyners et al.*, 2011] overlain by a few kilometers of Mesozoic and Cenozoic sediments [*Wood and Davy*, 1994], subducts beneath the Australian Plate with convergence becoming more oblique to the south near the Chatham Rise. Moving southward, the boundary transitions into a transpressional regime and continues along the western South Island as the Alpine

Fault, a right-lateral transform fault. Further south beneath Fiordland, the Alpine fault transitions into a subduction zone with reversed polarity as the Australian Plate subducts beneath the Pacific Plate at the Puysegur Trench. The northern Hikurangi Margin, located offshore and east of the North Island (Figure 1–1), is an ideal location to investigate the various types of slip behaviors that occur along the subduction zone interface due to the shallow dip of the subducting Hikurangi Plateau beneath the Raukumara Peninsula and the resulting shallow depth to the interface (12 km near the coast) [*Eberhart-Phillips and Reyners*, 1999; *Williams et al.*, 2013]. There is also a significant along-strike change in the convergence rate which is related to a clockwise rotation of the northeastern portion of the island with faster, nearly trench-perpendicular convergence in the north and slower, oblique convergence to the south [*Wallace et al.*, 2004].

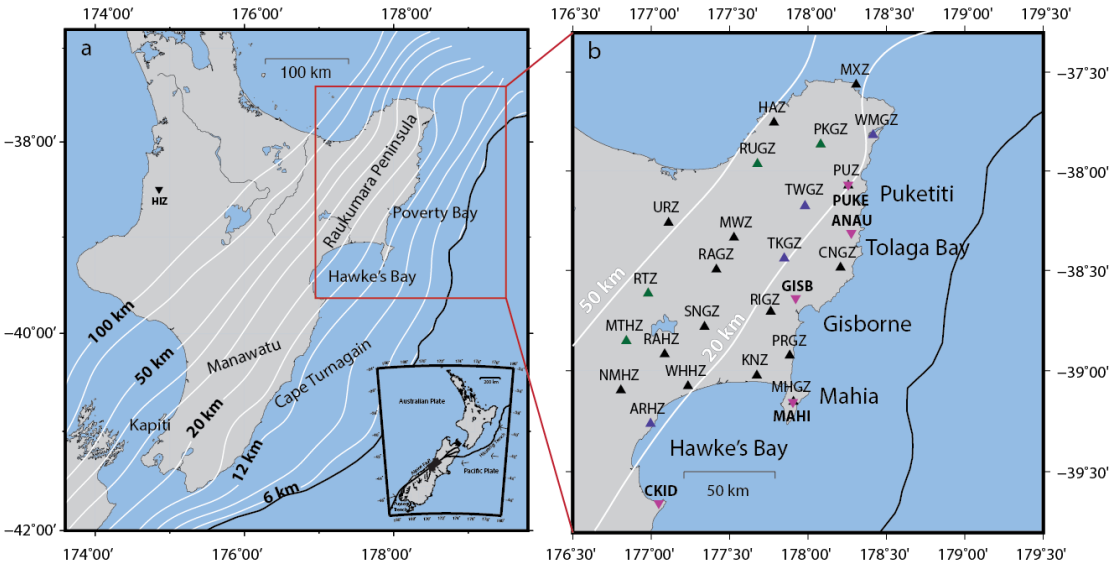

Figure 1–1. North Island tectonic setting and seismic station array.
(a) New Zealand tectonic setting with depth to plate interface (white contours) and trench location (solid black line). Megathrust depth contours are taken from *Williams et al.* [2013]. Station HIZ is a reference station used to remove false tremor detections from regional and teleseismic earthquakes. (b) Seismic stations operated by GeoNet on the Raukumara Peninsula represented by triangles color coded by when data became available (black: 2010; blue: 2011; green: 2012). Continuous GPS (cGPS) stations used in this study are shown as pink inverted triangles. The 20 km and 50 km interface depth contours are shown in white.

1.2.1 Slow slip, tremor, and the seismogenic zone along the Hikurangi Margin

The Hikurangi Margin has numerous patches with slow slip events (SSEs) exhibiting a wide range of depths, durations, recurrence intervals, and magnitudes with primarily short-duration, shallow SSEs in the north and long-duration, deep SSEs in the south. SSEs in the north primarily occur every 18-24 months at depths less than 15 km so that slip is constrained to be almost exclusively offshore. These events last for 1-3 weeks and release energy equivalent to M_w 6.3-6.8 [*Beavan et al.*, 2007; *Wallace and Beavan*, 2010]. Conversely, SSEs in the south primarily occur every 5 years at depths between 35 and 60 km and last for 12-18 months; these SSEs

release energy equivalent to ~M_w 7.0 [*Wallace et al.*, 2012a, 2014]. These larger SSEs in the south accommodate a large fraction of the plate motion and perturb the stress field to the extent that they may trigger shallow SSEs in the north [*Wallace et al.*, 2012a].

Three types of tectonic tremor are found in New Zealand: (1) triggered tremor associated with large teleseismic events in the central North Island [*Fry et al.*, 2011; *Chao et al.*, 2013], (2) sporadic (infrequent) tremor located near the hypocenters of the triggered tremor, but not associated with any geodetically detected SSEs or teleseismic events [*Ide*, 2012], and (3) tremor associated with slow slip along the Hikurangi subduction zone [*Kim et al.*, 2011; *Ide*, 2012] and the central Alpine Fault [*Wech et al.*, 2012, 2013]. Triggered tremor has been identified in the central North Island down-dip of the Manawatu slow slip patch concurrently with the passage of Rayleigh waves from the 2010 M_w 8.8 Maule earthquake and the 2011 M_w 9.0 Tohoku-Oki earthquake. *Kim et al.* [2011] presented the first evidence that tremor of any kind occurs in New Zealand. They identified tremor associated with the 16-day March/April 2010 Gisborne SSE. SSEs in New Zealand are also accompanied by an increase in seismicity [*Delahaye et al.*, 2009; *Jacobs et al.*, 2016]. The highly attenuating sediments along the northern Hikurangi Margin [*Lewis et al.*, 1998] and the lack of station density on the Raukumara Peninsula prior to 2010 likely made tremor difficult to detect in previous studies. It is likely that both tremor and an increase in seismicity accompany all SSEs in the northern Hikurangi Margin, though tremor detection is challenging.

In addition to the differences in northern and southern SSEs, inferred locking along the Hikurangi Margin also shows a significant along-strike change [e.g. *Wallace et al.*, 2004]. North of Cape Turnagain (Figure 1–1), the seismogenic zone is not well resolved and thought to be located in a narrow band offshore, up-dip of the geodetically detected SSEs. Conversely, the southern margin experiences significant locking to ~35 km depth. While no large interplate earthquakes have occurred along the southern Hikurangi Margin since 1917, in the north, two large M_w 7.2 and 7.1 tsunami earthquakes occurred in March and May of 1947 respectively [*Eiby*, 1982; *Doser and Webb*, 2003; *Bell et al.*, 2014]. Both earthquakes occurred at shallow depths <10 km beneath the continental slope offshore Gisborne and Tolaga Bay where the largest shallow SSEs occur (Figure 1–1), and have focal mechanisms consistent with locations on the subduction interface. They each produced a disproportionately large tsunami run-up for their magnitude (>10 m at some sites) along the east coast.

1.2.2 Shallow SSEs between 2010-2015

Shallow SSEs along the northern Hikurangi Margin occur predominantly offshore in 5 distinct patches: Hawke's Bay, Mahia, Gisborne, Tolaga Bay, and Puketiti (Figure 1–2). The Raukumara Peninsula has a dense (~30 km station spacing) continuous GPS (cGPS) network operated and maintained by GeoNet (www.geonet.org.nz). While there are numerous cGPS stations along the Raukumara Peninsula, slip at each of the 5 patches is most pronounced at a particular station. These cGPS stations act as characteristic stations for each distinct slow slip region

and the east-west displacement time-series for the period between 2010-2015 is summarized in Figure 1–2.

Figure 1–2. Northern Hikurangi cGPS timeseries for 2010-2016.
Location of 5 SSE patches along the northern Hikurangi Margin with the representative cGPS station for each patch. Easting component cGPS time series plotted for the study period: Puketiti (station PUKE), Tolaga Bay (station ANAU), Gisborne (station GISB), Mahia (station MAHI), and Hawke's Bay (station CKID). Transient events are highlighted in colored boxes. The two colored boxes outlined in black represent the events detailed in Figure 1–5 and are numbered according to Table 1–1. Station ANAU came online in October 2010; Tolaga Bay's first transient event is from *Wallace and Beavan,* [2010] and not shown here.

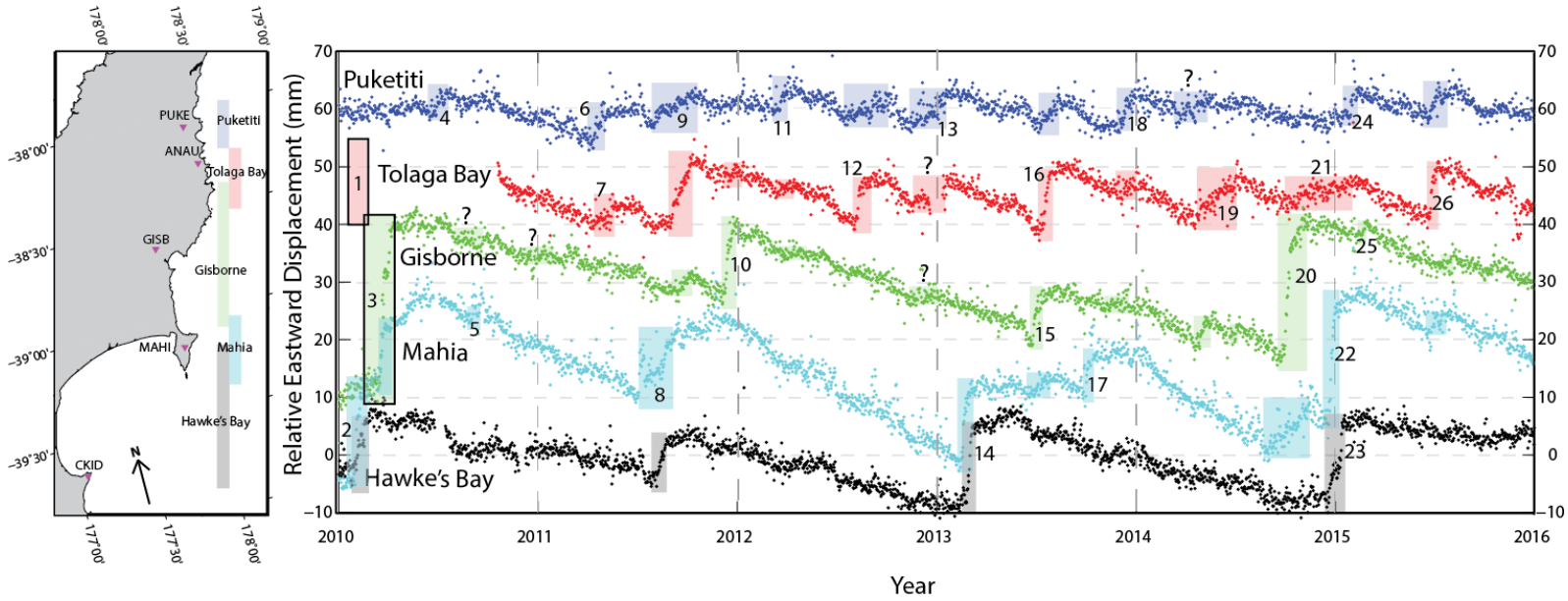
178°00'
178°30'
179°00'
-38°00'
-38°30'
-39°00'
-39°30'
177°00'
177°30'
178°00'
PUKE
ANAU
GISB
MAHI
CKID
Puketiti
Tolaga Bay
Gisborne
Mahia
Hawke's Bay
N
Relative Eastward Displacement (mm)
Puketiti
Tolaga Bay
Gisborne
Mahia
Hawke's Bay
70
60
50
40
30
20
10
0
-10
2010
2011
2012
2013
2014
2015
2016
Year

Additionally, the proximity of the network to the slip patches and shallow depth to plate interface allow for a detailed examination of these events. Displacements observed in the cGPS records that span a few days to weeks may indicate localized SSEs or SSEs that occur as part of a larger pattern along the margin (Figure 1–2). Each event listed in Table 1–1 represents displacements observed at a minimum of 3 cGPS stations along the margin; these events are identified by the characteristic station(s) for the given location.

Table 1–1. Offshore northern Hikurangi cGPS transients: 2010-2015.
Numbered transients between 2010-2015 as depicted in Figure 1–3. Location abbreviations are as follows: P- Puketiti, TB- Tolaga Bay, G- Gisborne, M- Mahia, HB- Hawke's Bay. Tremor presence is indicated as follows: Tremor is clearly spatiotemporally related to the transient (Y), tremor correlates in time with the transient, but detections are few in number and/or distant from the slip patch (?), or tremor is not detected for the transient (N).

Table 1–1. Offshore northern Hikurangi cGPS transients: 2010-2015

	Loc.	cGPS ref. station(s)	Year	Month(s)	Tremor	Reference
1	TB	--	2010	Jan-Feb	N	[*Wallace and Beavan*, 2010]
2	M	MAHI, CKID	2010	Jan-Feb	?	[*Wallace and Beavan*, 2010]
3	G	GISB, MAHI	2010	Mar-Apr	Y	[*Wallace and Beavan*, 2010]
4	P	PUKE	2010	Jun-Jul	Y	This study
5	M	MAHI	2010	Aug	N	This study
6	P	PUKE	2011	Apr-May	Y	This study
7	TB	ANAU	2011	Apr-May	N	This study
8	M	MAHI, CKID	2011	Aug-Sep	N	[*Wallace et al.*, 2012a]
9	TB	ANAU, PUKE	2011	Sep-Oct	Y	[*Wallace et al.*, 2012a]
10	G	GISB	2011	Dec	Y	[*Wallace et al.*, 2012a]
11	P	PUKE, ANAU, GISB	2012	Mar	Y	This study
12	TB	ANAU, PUKE, GISB	2012	Aug	Y	This study
13	P	PUKE, ANAU?, GISB?	2012	Dec-Jan	Y (Jan 2013)	This study
14	HB	CKID, MAHI	2013	Feb-Mar	N	[*Wallace and Eberhart-Phillips*, 2013]
15	G	GISB, MAHI	2013	Jun-Jul	Y	This study
16	TB	ANAU, PUKE	2013	Jul-Aug	Y	This study
17	M	MAHI	2013	Sep-Oct	?	This study
18	P	PUKE, ANAU	2013	Dec	Y	This study
19	TB	ANAU, GISB	2014	May-Jun	Y	This study
20	G	GISB, MAHI	2014	Sep-Oct	Y	[*Wallace et al.*, 2016]
21	TB	ANAU	2014	Sep-Jan	? (Oct & Dec)	This study
22	M	MAHI	2014	Dec-Jan	?	This study
23	HB	CKID	2014	Dec-Jan	N	This study
24	P	PUKE	2015	Jan-Feb	?	This study
25	G	GISB	2015	Feb	Y	This study
26	TB	ANAU, PUKE	2015	Jun-Jul	Y	This study

In early 2010 the Tolaga Bay and Mahia/Hawke's Bay patches experienced near simultaneous slow slip in January and February followed by a large Gisborne SSE in March and April (events 1, 2, and 3 in Table 1–1); this SSE was the largest along the margin during the study period [*Wallace and Beavan*, 2010]. In 2011 a series of shallow SSEs (events 8-10 in Table 1–1) migrated up the east coast beginning with SSEs south of Hawke's Bay in June/July. Similar to 2010, the Mahia and Tolaga Bay patches slipped first and were followed by the Gisborne patch in August, late September, and December 2011 respectively [*Wallace et al.*, 2012a]. The 2011 Gisborne SSE was a smaller magnitude event from the previous year. cGPS stations showed westward motion consistent with a locked plate interface for 2012 without any major transients. Two small magnitude events, affecting the Tolaga Bay and Puketiti patches at the northern end of the margin (events 11 and 12 in Table 1–1), occurred in March and August of that year. Activity along the northern margin began in 2013 with moderate SSEs in Hawke's Bay [*Wallace and Eberhart-Phillips*, 2013] and small slip transients in the Mahia, Gisborne, and Tolaga Bay patches (events 14-18 in Table 1–1). In 2014, a series of SSEs migrated southwestward along the margin in the opposite direction of the 2011 sequence. This series of events began in May in the Tolaga Bay patch and was followed by a large SSE in the Gisborne patch in September and October (events 19 and 20 in Table 1–1). The Mahia and Hawke's Bay patches slipped in December (events 22 and 23 in Table 1–1) and transient motions along the margin slowed down through 2015 with the exception of small Gisborne and Puketiti patch events (events 24-26 in Table 1–1). Throughout the

study period, the Puketiti patch in the north (cGPS station PUKE) experiences numerous small transients each year in what may be the frequent occurrence of very small SSEs (Figure 1–2). The observed patterns of shallow, short-duration SSEs along the northern Hikurangi margin between 2010 and 2015 suggest a complex transfer of stress along strike and likely play a pivotal role in the interplate earthquake cycle. In this study we present a catalog of tremor, associated with shallow, short duration transients, as well as deeper, long-term tremor episodes, along the Raukumara Peninsula between 2010 and 2015. For the remainder of this paper, we will refer to all displacement transients identified in Table 1–1 as SSEs. We compare the time and location of this tremor with the occurrence of both slow slip events and earthquakes.

1.3 Tremor Detection and Location

This study employs a modified version of the automated envelope cross-correlation technique [*Wech and Creager*, 2008] to search for tremor and improve tremor detection and location in New Zealand. Six years of seismic data (2010-2015) from the New Zealand National Seismic Network (operated by GeoNet; www.geonet.org.nz) are systematically analyzed to detect time windows containing coherent tremor signal across the network. We identify tremor as spatiotemporally clustered low amplitude coherent signals detected at numerous stations across the network that are deplete in high frequency energy and have durations longer than earthquakes in a similar location of a similar magnitude. An important characteristic of the tremor is that it is composed of repeating signals. We analyze the east

component of ground motion from 25 short period and broadband seismic stations in the northeastern North Island (Figure 1–1).

To define the envelopes for cross-correlation, a band-pass filter is applied in two frequency ranges: (1) 2-5 Hz to isolate tremor with energy at lower frequencies, and (2) 8-20 Hz to remove local earthquake detections that have significant energy above 8 Hz. The New Zealand National Seismic Network continued to add new stations during the study time period and these new stations are incorporated into the processing routine as data become available; the same number of stations are utilized in the cross-correlation for each calendar year of analysis, ranging from 16 stations in 2010 to 24 stations in 2015 (Figure 1–1).

After creating envelope functions, the data are low-pass filtered at 0.1 Hz and decimated to 1 Hz. Then the envelope functions are cross-correlated for all stations in 120-second time windows with a 60-second shift. Tremor is located when cross-correlation coefficients exceed 0.6 on a minimum of 7-10 station pairs. When correlations are found for a minimum of 4-5 station pairs with the 8-20 Hz band, the time window is skipped to minimize local earthquake detections. In addition to the Raukumara Peninsula stations, data from a reference station (station HIZ) located ~230 km away from the study region are filtered in the 2-5 Hz range and cross-correlated with the rest of the network. When correlations are found for a minimum of 2-3 station pairs with the reference station, the time window is skipped to minimize detections of teleseismic or regional surface waves deplete in high frequency energy in a method similar to *Kim et al.* [2011]. While these steps limit the amount of tremor

detected and located, they greatly reduce the number of false detections that survive the automated process.

To ensure the stability of the tremor detections and locations and to test the sensitivity of the input parameters, we run through the modified envelope cross-correlation process with a range of input parameters (Table A–1) based around those presented in *Kim et al.* [2011]. Tremor associated with offshore SSEs occurs in distinct spatial clusters near the coast; varying the minimum number of correlating station pairs required for tremor detection based on the number of nearby stations leads to an increase in detections for discrete tremor episodes. Only tremor detections that survive at least 50% of the iterations are kept and the remaining detections are not considered stable enough to remain in the final result. Using this method, we were able to increase the amount of tremor detected with the automated process compared to *Kim et al.* [2011] while greatly reducing the amount of false tremor detections from local, regional, and teleseismic earthquakes.

Once tremor is detected, the grid search optimization technique described in *Wech and Creager* [2008] is applied to find centroid locations that minimize S-wave travel times to correlated station pairs using a local 1-D interpretation of the New Zealand 3-D velocity model [*Reyners et al.*, 1999; *Eberhart-Phillips et al.*, 2010]. To address errors in the location process, an iterative bootstrapping process is applied that removes 10 percent of the station pair cross correlograms and searches for a location. This step is repeated 10 times, producing 10 locations for each time window of detected tremor. The final epicentral location is determined by taking the median

centroid of the 10 locations. While this process reduces the relative uncertainties in the horizontal location there are still large uncertainties on the tremor hypocentral depths. Only tremor locations with epicentral error estimates of less than 0.05-0.15° are kept before adding additional requirements to ensure the detections are indeed tectonic tremor and not correlated noise. For our study area, tremor depths are typically between 5 and 30 km and are assumed to be located on the plate interface. Tremor locations are then spatially and temporally clustered so each tremor event has a minimum of 5 additional events within 0.1 degrees and 72 hours. The clustering technique removes additional detections that likely result from correlated noise or highly attenuated local earthquakes that have lost high frequency energy and requires that the remaining detections are correlated signals that are clustered in time and in close spatial proximity, defining features of tectonic tremor [*Obara*, 2002]. Since the location method determines differential travel times using correlated waveform envelopes and not individual body wave phases, location errors are large and therefore we make no interpretations that rely on individual tremor event cluster locations that are more accurate than 10 km. Instead we interpret the spatial location of groups of tremor event clusters.

1.4 Results and Discussion

Most SSEs along the northern Hikurangi Margin are accompanied by detectable tectonic tremor (Figure 1–2) and the largest SSEs are accompanied by increases in cataloged seismicity. Detailed slip inversions have been performed for eight of the shallow SSEs (Figure 1–2) with results indicating that slow slip occurs

almost exclusively offshore. Tremor associated with shallow SSEs along the northern Hikurangi Margin is primarily concentrated onshore (Figure 1–3) and therefore at the down-dip edge of the geodetically inferred slip patches when determined. In addition to tremor that is spatiotemporally related to the shallow, offshore SSEs, tremor exists inland at greater depths. It is unclear whether this tremor is associated with previously undetected deeper slow slip events, or is regularly occurring tremor that meets the imposed time and space clustering requirements. This deeper tremor occurs in a band along strike at depths where the plate interface is between 20-50 km (Figure 1–3), at similar depths and slightly up dip of where deep slow slip events have been previously detected south of this region [*Wallace and Eberhart-Phillips*, 2013].

Figure 1–3. Tremor locations 2010-2015.
Tremor detections (circles) color coded with time of year for 2010-2015. 20 km depth contour shown with gray dashed line. Tremor episodes east of the 20 km depth contour are predominantly related to offshore SSEs with events near station PUZ related to the Puketiti patch and events between stations CNGZ and PRGZ related to the Gisborne patch. Tremor episodes are outlined with black dashed lines and numbered according to Figure 1–2 and are down dip of the offshore SSEs.

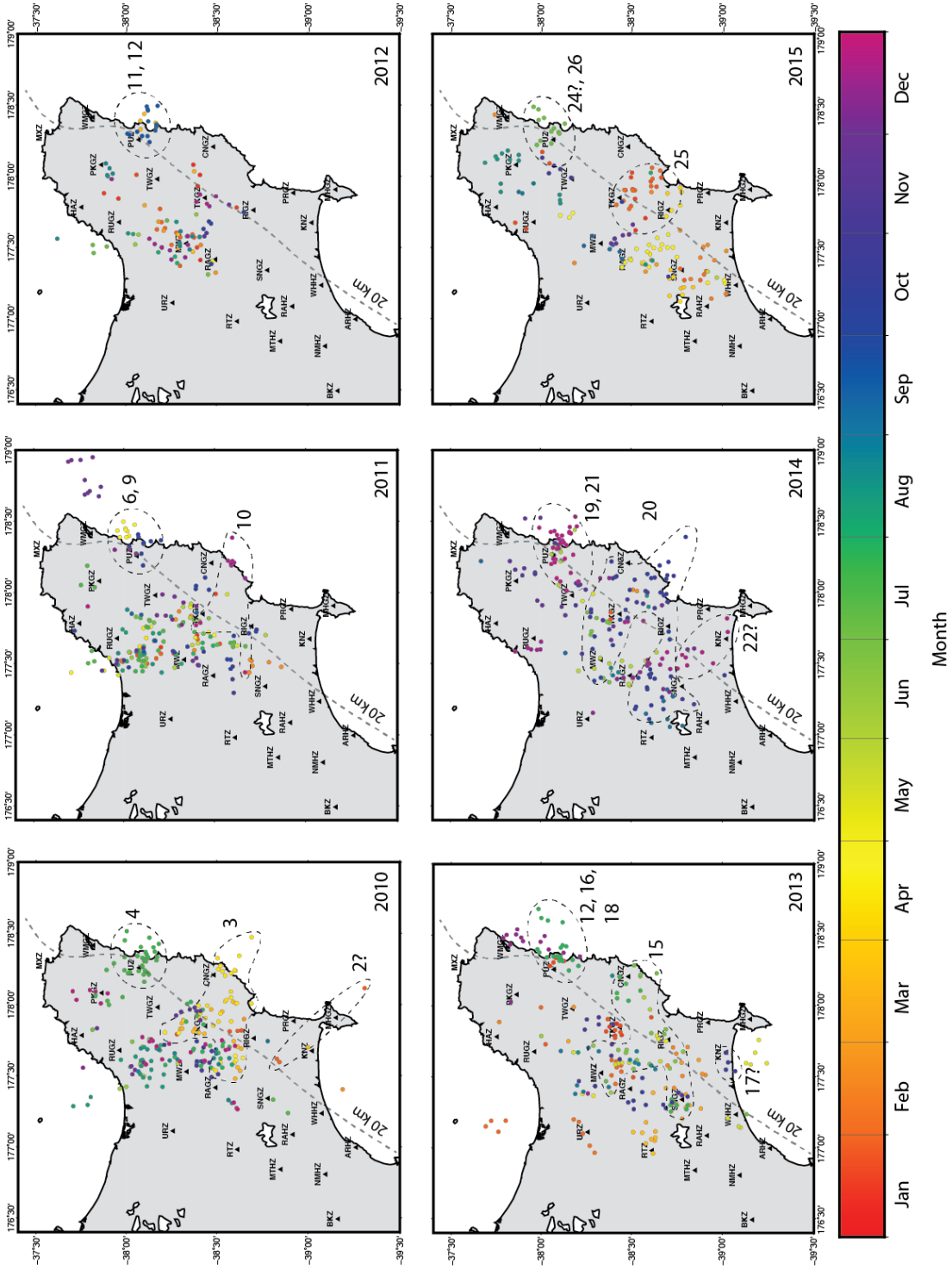
2010
2011
2012
2013
2014
2015
4
3
2?
6, 9
10
11, 12
12, 16, 18
15
17?
19, 21
20
22?
24?, 26
25
20 km
Jan
Feb
Mar
Apr
May
Jun
Jul
Aug
Sep
Oct
Nov
Dec
Month

1.4.1 Characterizing Northern Hikurangi Tremor

Tremor along the northern Hikurangi Margin consists of low amplitude coherent signals that are deplete in high frequency energy and composed of repeating events (Figure 1–4). While the highly attenuating Raukumara Peninsula provides a significant challenge to tremor detection and location, tremor along the northern Hikurangi Margin is within the range of behavior observed worldwide [e.g. *Ide*, 2012]. Tremor associated with shallow SSEs consists of numerous pulses of coherent energy across multiple stations with smaller amplitudes than local microseismicity within a time span of a few minutes (Figure 1–4). Another important identifying feature of tectonic tremor is the frequency content. Tectonic tremor along the northern Hikurangi Margin has the best signal to noise ratio between 2-5 Hz with tremor spectra falling off around 2-3 Hz and becoming indistinguishable from noise by 7-8 Hz. Conversely, the frequency content of similarly located small earthquakes remains high through 7-8 Hz and does not fall off until higher frequencies as illustrated by *Kim et al.* [2011].

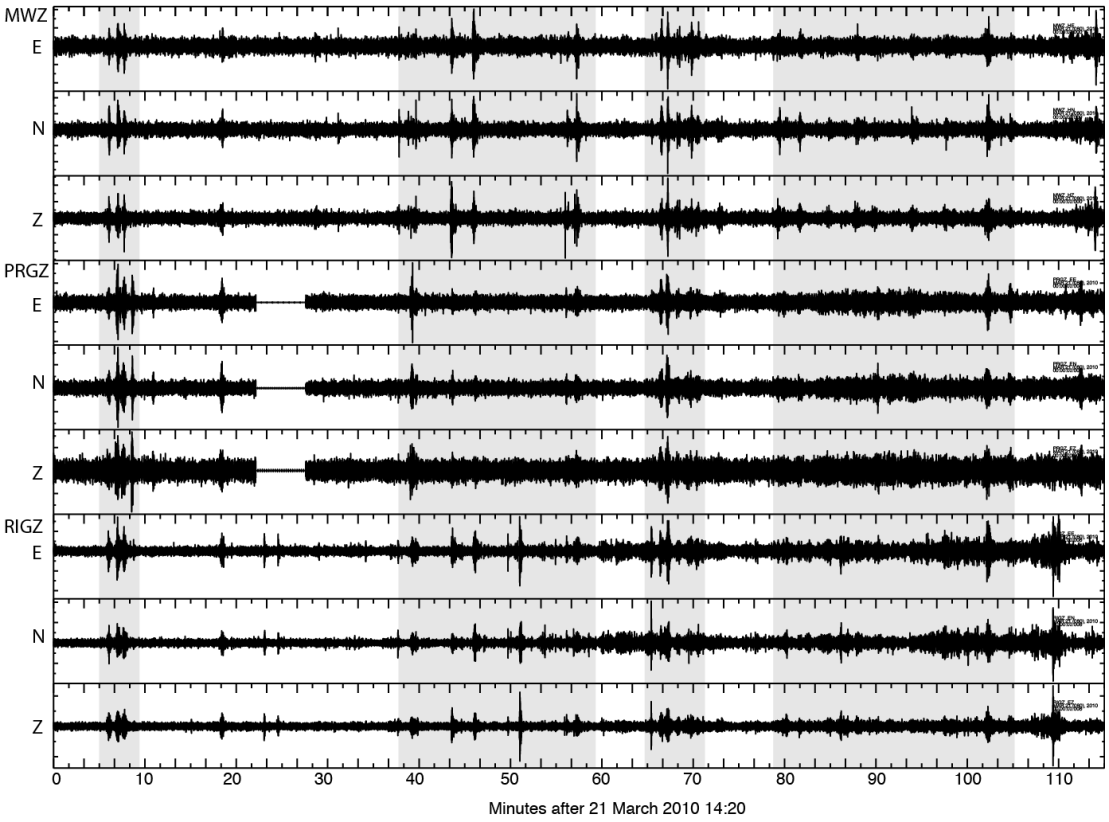

Figure 1–4. Tremor signal from March/April 2010 Gisborne SSE.
Tremor signal from 115 minutes on 21 March 2010 during peak slip of the March/April 2010 Gisborne SSE plotted on 3 components from stations MWZ, PRGZ, and RIGZ. Data are filtered between 2-5 Hz and episodes of active tremor are highlighted with gray shading.

Perhaps the most important identifying feature of tremor is that the signal is comprised of the superposition of numerous repeating low frequency earthquakes (LFEs) [*Shelly et al.*, 2006; *Ide et al.*, 2007b; *Shelly et al.*, 2007; *Brown et al.*, 2009; *Peng and Gomberg*, 2010]. Due to the low amplitude tremor signal and the high background seismicity levels in northern Hikurangi, visual identification of individual low frequency earthquakes is challenging. LFEs have been characterized as a component of tremor in a number of slow slip regions such as Shikoku [e.g. *Shelly et*

al., 2006], Cascadia [e.g. *Brown et al.*, 2009], the San Andreas Fault [e.g. *Thomas et al.*, 2009], Guerrero [e.g. *Frank et al.*, 2013], and the Alpine Fault [e.g. *Chamberlain et al.*, 2014]. Without discernable P and S waves, the emergent, low amplitude characteristics of tremor lead to challenges in accurate location. By considering that tremor is composed of repeating LFEs, location becomes more feasible.

To demonstrate that Hikurangi tremor consists of multiple repeating LFEs, LFE candidates are visually identified on at least 4 stations as impulsive arrivals within tremor episodes. A check is performed to ensure that the spectral content of the LFE differs from regular earthquakes; the identified LFEs have the best signal to noise ratio between 2-5 Hz. The best template is identified and cross-correlated with the continuous data during the largest 2010 Gisborne slow slip event following the methods of *Chamberlain et al.* [2014] to locate repeating LFEs within the tremor signal (Figure A–1). The repeating LFEs are primarily located within automatically detected tremor episodes. However, they are also found outside of automatically detected tremor and may indicate tremor close in time to earthquake signals or tremor with signal too low to be automatically detected. While it is beyond the scope of this study, a thorough matched filter analysis of tremor would likely identify additional time windows containing tremor signal that were originally skipped by the automated method. Our intent in this paper is to simply demonstrate the repeating event characteristic of the Hikurangi tremor.

Tremor detected along northern Hikurangi is shorter in duration and ‘burstier’ than tremor seen in Cascadia or Southwest Japan, but is well clustered in time around

the offshore SSEs. While the northern Hikurangi tremor is within the range of global tremor observations, the shallow depths (< 20 km) represent one end member condition. The high levels of seismicity and highly attenuating structure of the Raukumara Peninsula make automatic detection of tremor with traditional methods challenging and new methods are warranted.

1.4.2 Tremor associated with offshore slow slip events

Tremor that is spatiotemporally related to shallow SSEs is most easily detected in two regions along the margin. In the north, tremor routinely occurs in abundance along the coast near seismic station PUZ (collocated with cGPS station PUKE) during SSEs in the Puketiti/Tolaga Bay patches. This region has frequent short-duration SSEs in the cGPS record (Figure 1–2) that are highly tremorgenic (Figure 1–3); distinct tremor episodes are detected in at least 10 instances during the study period (Table 1–1). One such instance in June/July 2010 (Figure 1–5) coincides with a 5-6 mm eastward displacement at cGPS station PUKE, elevated seismicity levels, and numerous tremor detections. Although the eastward motion is relatively minor and may indicate a small local or larger offshore SSE, the amount of tremor generated is equal or greater than during much larger magnitude SSEs elsewhere along the coast.

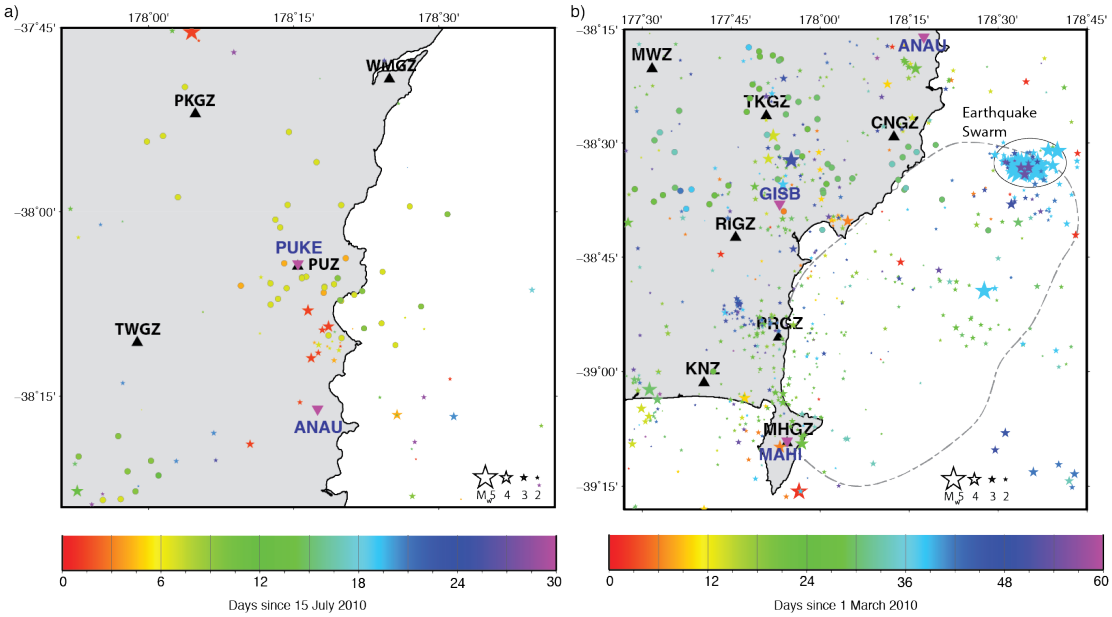

Figure 1–5. Tremor and earthquake locations for 2010 Puketiti and Gisborne SSEs. (a) Tremor (circles) and earthquakes (stars) color coded by time for the 30 days surrounding the June/July 2010 Puketiti SSE. Tremor plots in a wide area both on- and off-shore while seismicity (largest M_w 4.4) is mostly concentrated at the southern edge of the tremor at the end of the SSE. (b) Tremor (circles) and earthquakes (stars) color coded by time for the 60 days surrounding the March/April 2010 Gisborne SSE. The extent of the slow slip is outlined by the gray dashed line [*Wallace and Beavan*, 2010]. Tremor is located at the northern downdip edge of the slip patch between stations CNGZ and RIGZ and extends northwest and westward in the down dip direction. Seismicity is primarily concentrated along the shoreline to the south near the Mahia Peninsula.

Further south, tremor is routinely detected with SSEs in the Gisborne patch down dip of the northern part of the slip distribution (Figure A–2). The Gisborne region is host to the largest, and best-studied SSEs along the northern Hikurangi Margin and continues to be the target of future studies. Gisborne SSEs are specifically documented in this patch since 2002 with durations ~2 weeks, recurrence intervals of 18-24 months, and typical energy releases equivalent to M_w 6.5-6.8 [*Wallace and Beavan*, 2010]. Each substantial Gisborne SSE during the study period,

March/April 2010 (Figure 1–5), December 2011, July 2013, and September/October 2014, is correlated with productive tremor episodes between Tolaga Bay and Poverty Bay that extend in the dip direction from near the down-dip edge of the slip patch to depths around 20 km (Figure A–2). The March/April 2010 event is the largest recorded SSE in the patch with ~30 mm of eastward displacement at cGPS station GISB and is accompanied by a very productive tremor episode down dip of the northern end of the slip patch. This SSE is also accompanied by increased seismicity near the southern end of the slip patch (Figure 1–5). The December 2011 and July 2013 SSEs are smaller in magnitude, but are still accompanied by tremor in the north and earthquakes in the south of the geodetically defined slip patches. Though larger than the July 2013 SSE, the December 2011 SSE has the least productive tremor episode; there were several moderate magnitude earthquakes ($M_w > 5.0$) within the highly attenuating Raukumara Peninsula earlier in 2011. The associated aftershock sequences likely mask the tremor signal and increase the difficulty of automatic detection. In September/October 2014, another large magnitude Gisborne SSE with ~25 mm of eastward displacement at cGPS station GISB was accompanied by tremor at the north end and increased seismicity at the south end of the slip patch similar to 2010.

Tremor associated with the Mahia slow slip patch is difficult to detect in large quantities. Due to the geometry of the coastline, most of the slip is farther from land and the GeoNet seismic and cGPS stations than the northern slip patches. The coastal region extending south of Poverty Bay, along the Mahia Peninsula, and the northern

edge of Hawke's Bay is also the site of increased microseismicity observed with SSEs in the Gisborne and Mahia patches [e.g. *Delahaye et al.*, 2009; *Jacobs et al.*, 2016]. Since the methodology employed skips time windows with substantial correlations in the higher frequency band, the increased presence of microseismicity associated with SSEs adds to the existing geographic complexities with automatically detecting tremor in this region. In addition, SSEs in the Hawke's Bay patch are entirely offshore and even farther from the dense land-based seismic network, making tremor detection nearly impossible.

1.4.3 Deep inland tremor

In addition to shallow tremor (< 20 km depth) associated with offshore SSEs, tremor is detected inland where the megathrust is at 20-50 km depth (Figure 1–6). These tremor detections fulfill the same criteria as the SSE-related tremor, including spatial and temporal clustering requirements, but their origin is unclear. The inland tremor primarily occurs in 3 events throughout the study period, each lasting several months. The first tremor episode during the study period occurs predominantly north of station CNGZ in the central Raukumara Peninsula from late 2010 through 2011 for 12-14 months. While this episode does not have a clear spatiotemporal migration pattern, it extends up and down dip between 20 and 50 km depth and exists in two distinct patches. The second episode extends broadly along strike from slightly north of station CNGZ to the southern end of the Raukumara Peninsula from late 2012 through 2013 for 11-12 months. Tremor during this episode is shallower than episode 1, occurring predominantly between 20 and 35 km depth, and overlaps with a

geodetically detected deep slow slip event from 2008 near station RTZ [*Wallace and Eberhart-Phillips*, 2013]. The final tremor episode during the study period occurs south of station CNGZ between mid-late 2014 and mid 2015 for approximately 10-11 months at depths of 20-35 km, up dip of the 2006 and 2008 geodetically detected slow slip. These deep, longer duration tremor episodes occur every 1.5-2 years during the study period and have an overall southward trend along the Raukumara Peninsula.

Figure 1–6. Deep, inland tremor episodes from 2010-2015.
Inland tremor (circles) between 20 and 50 km depth color-coded by time for 2010-2015 for three distinct tremor episodes. Tremor located outside the respective tremor episodes are plotted as gray circles. 20 and 50 km depth contours plotted in black. Slip contours (in mm) of the 2006 and 2008 deep SSEs are plotted in purple [*Wallace and Eberhart-Phillips*, 2013]. Inland tremor is mostly north of station CNGZ (in red) for episode 1, in the central Raukumara Peninsula for episode 2, and south of station CNGZ for episode 3.

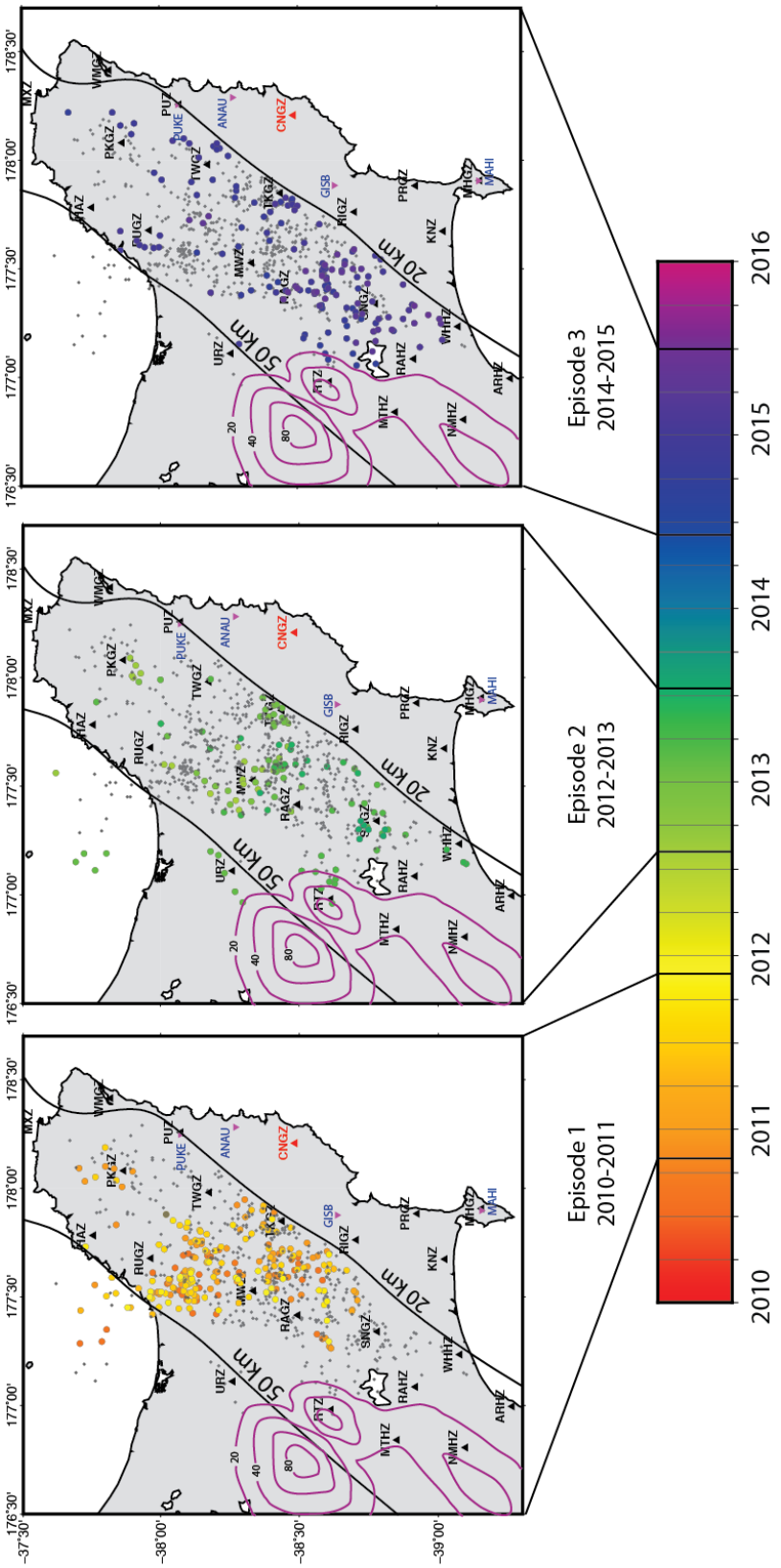
Episode 1
2010-2011
Episode 2
2012-2013
Episode 3
2014-2015
2010
2011
2012
2013
2014
2015
2016
20 km
50 km
176°30'
177°00'
177°30'
178°00'
178°30'
−37°30'
−38°00'
−38°30'
−39°00'

Wallace and Eberhart-Phillips [2013] identified the presence of deep (25-45 km), moderate duration (2-3 months) slow slip events along the central Hikurangi margin in 2006 and 2008. The slip patches of these events are inland from Hawke's Bay and extend up to the southern end of the Raukumara Peninsula. There is minimal overlap with some tremor from the longer duration episodes during this study period. It is possible that the observed long duration tremor episodes reflect undiscovered long term deep SSEs below the geodetic detection threshold adjacent to the observed shallow, short duration SSEs similar to SSEs observed near the Bungo Channel in southwest Japan [e.g. *Hirose and Obara*, 2005; *Matsuzawa et al.*, 2013].

1.4.4 Tremor and increased seismicity

SSEs along the northern Hikurangi margin are often accompanied by increases in seismicity levels above background rates [*Delahaye et al.*, 2009; *Jacobs et al.*, 2016]. These increases in seismicity often immediately follow tremor episodes associated with the shallow, offshore SSEs (Figure 1–7). For example, the March/April 2010 Gisborne SSE has a productive tremor episode that is closely followed by an offshore earthquake swarm (M_w 4.1-4.5) at the northern extent of the slip patch (Figure 1–5). *Jacobs et al.* [2016] showed that this swarm is the northern most in a series of three earthquake sequences that migrated northeast along strike from the Mahia Peninsula in 2007, 2009, and 2010. The largest earthquakes in the 2010 swarm consist of normal mechanisms and are likely intraslab events. Increased seismicity around the Mahia Peninsula at the down dip edge of the slip distribution also accompanies the first few days of this SSE, an observation associated with most

Gisborne and Mahia SSEs. Another example is the June/July 2010 Puketiti SSE, which was immediately followed by an M_w 4.4 earthquake. In this case, the earthquake and its associated aftershock sequence occurred south of the detected tremor episode at the end of the cGPS transient (Figure 1–5). Seismicity has also been shown to precede SSEs off the Raukumara Peninsula. In 2007, a Gisborne SSE began immediately after a local M_w 6.6 earthquake [*François-Holden et al.*, 2008]. Earthquakes have been shown to trigger SSEs and vice versa and while the seismicity is not always located on the megathrust, these earthquakes and SSEs are likely affecting the stress state of the surrounding area.

Figure 1–7. Weekly tremor and earthquake occurrence 2010-2015.
Histograms showing number of weekly tremor detections (top) and earthquakes (bottom) with the cumulative counts plotted in red between 2010-2015. A tremor detection is counted as an event found with the automated envelope cross correlation method that satisfies the time and spatial clustering requirements. Notable tremor and earthquake episodes are identified by region (P: Puketiti; TB: Tolaga Bay; GB: Gisborne; M: Mahia; HB: Hawke's Bay). The tremor episodes with pink identifiers are detailed in Figure 1–5 and numbers correspond with transient events in. Note that the change in slope of the cumulative earthquake plot, marked by the dashed line, and the associated decrease in over all detections is due to a change in the GeoNet catalog automatic detection procedure. This change does not affect this study, but should be noted.

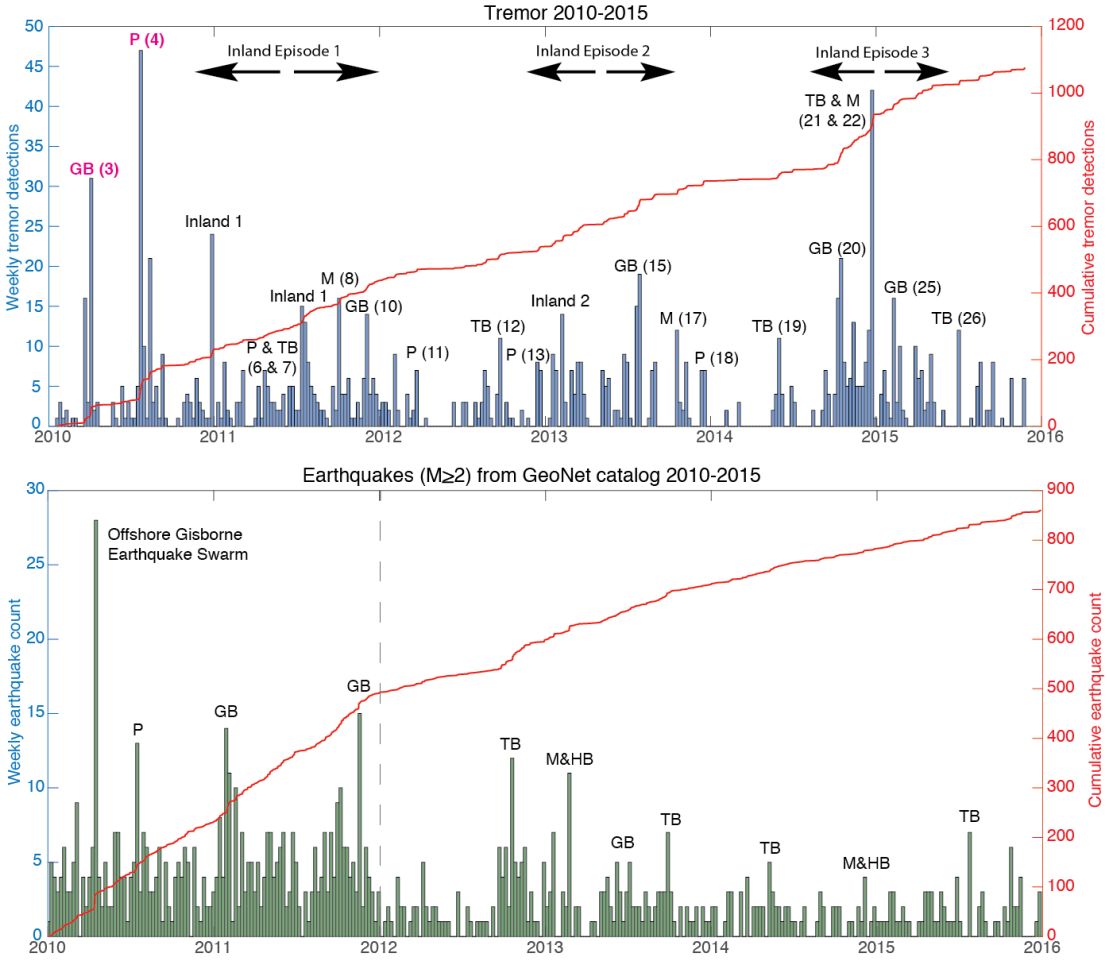
Tremor 2010-2015
Weekly tremor detections
Cumulative tremor detections
Inland Episode 1
Inland Episode 2
Inland Episode 3
P (4)
GB (3)
Inland 1
Inland 1
M (8)
GB (10)
P & TB
(6 & 7)
P (11)
TB (12)
P (13)
Inland 2
GB (15)
M (17)
P (18)
TB (19)
TB & M
(21 & 22)
GB (20)
GB (25)
TB (26)
Earthquakes (M≥2) from GeoNet catalog 2010-2015
Weekly earthquake count
Cumulative earthquake count
Offshore Gisborne
Earthquake Swarm
P
GB
GB
TB
M&HB
GB
TB
TB
M&HB
TB

After 2014, the increases in seismicity observed during or after offshore SSEs from the GeoNet catalog are greatly diminished. This is clearly evident with the September/October 2014 Gisborne SSE, which is missing the seismicity increase observed with the 2010 Gisborne SSE. Earthquakes near the Mahia Peninsula during the SSE are observed, including an M_w 4.6, but the substantial increases in seismicity observed for previous SSEs are missing in the catalog. The peak slip for this event is further offshore when compared to the 2010 Gisborne SSE, so the seismicity increases may be offshore and are therefore poorly detected and located from the land-based network. The 2014 Gisborne SSE was the target of an offshore study as part of the Hikurangi Ocean Bottom Investigation of Tremor and Slow Slip (HOBITSS) experiment and analysis of offshore seismic data is ongoing and may elucidate the missing increase in seismicity.

1.5 Conclusion

The northern Hikurangi Margin exhibits a broad range of slip processes on the plate interface and is now conclusively added to the list of subduction zones and transform boundaries that have slow slip with associated tectonic tremor. Tectonic tremor may be associated with all SSEs along the northern Hikurangi Margin, but is difficult to detect except for the largest magnitude events and in regions that are especially tremorgenic. Tremor is most abundant during large magnitude SSEs (equivalent magnitude >M_w 6.5) located in the Gisborne patch and smaller magnitude eastward transients observed in the cGPS records for the Tolaga Bay and Puketiti patches that likely represent frequent, small SSEs. Deep, inland tremor is also present

in episodes that last multiple months and may represent undiscovered long-term slow slip events occurring between 20-50 km depth. In addition to the magnitude of the SSEs, difficulties in detecting tremor stem from high base levels of seismicity, the short duration, 'bursty' nature of the signal, and the highly attenuating crust. While tremor along the northern Hikurangi Margin is primarily located down-dip of the slip patches, this may be a symptom of the location of the seismic network with respect to the SSEs. Future work with ocean datasets will likely help elucidate the up-dip extent of tremor and further characterize slip heterogeneities that exist on the subduction interface.

The broad range of tectonic tremor behavior coupled with the complex set of physical conditions present along the northern Hikurangi Margin, may expand general understanding of the range of conditions under which these phenomena occur beyond regions with more systematic relationships between slow slip and tremor like Cascadia or southwest Japan. Slow slip and tremor in these regions exhibit certain attributes that are not observed in the northern Hikurangi Margin such as regular tremor migration, rapid tremor reversals, and large infrequent SSEs that transition to smaller, more frequent SSEs with depth at the down-dip edge. The northern Hikurangi Margin may present different slow slip and tremor characteristics when compared to Cascadia and southwest Japan because of the shallow depth (<15 km) and resulting low temperatures, or the age and thickness of the incoming Pacific Plate. We may be missing some of the story in New Zealand because the slow slip is offshore, relatively far from instrumentation.

Chapter 2 - Shallow Slow Slip and Tremor Associated with Seamount Subduction Offshore Gisborne, Hikurangi Margin, New Zealand

2.1 Introduction

Slow slip events are now recognized as an important part of the spectrum of strain release processes ranging from steady aseismic plate convergence rates at a few cm/yr to traditional earthquakes with fault slip rates of a few m/s [e.g., *Schwartz and Rokosky*, 2007; *Peng and Gomberg*, 2010; *Beroza and Ide*, 2011]. Over the last decade, the list of regions with documented slow slip events has increased and diversified. Slow slip has been identified in subduction margins (Cascadia [e.g., *Dragert et al.*, 2001; *Rogers and Dragert*, 2003; *Dragert et al.*, 2004; *Szeliga et al.*, 2004; *Brudzinski and Allen*, 2007]; Japan [e.g., *Obara et al.*, 2004; *Hirose and Obara*, 2005; *Ito et al.*, 2013]; Mexico [e.g., *Kostoglodov et al.*, 2003; *Yoshioka et al.*, 2004; *Brudzinski et al.*, 2007]; Costa Rica [e.g., *Brown et al.*, 2005; *Outerbridge et al.*, 2010; *Jiang et al.*, 2012]; New Zealand [e.g., *Douglas et al.*, 2005; *McCaffrey et al.*, 2008; *Wallace and Beavan*, 2010]; Alaska [e.g., *Ohta et al.*, 2006]; Ecuador [*Vallée et al.*, 2013]; Northern Chile [*Kato and Nakagawa*, 2014]; and Italy [*Borghi et al.*, 2016]), at transform boundaries (San Andreas Fault [e.g., *Shelly*, 2009, 2010] and the Alpine Fault [*Wech et al.*, 2012; *Chamberlain et al.*, 2014]), beneath volcanic flanks (Kilauea [*Cervelli et al.*, 2002; *Brooks et al.*, 2008; *Montgomery-Brown et al.*, 2009], Mt. Etna [*Mattia et al.*, 2015], and the Lesser Antilles [*Hornbach et al.*,

2015]), and possibly in the Central Himalaya [*Mendoza et al.*, 2016]. While slow slip at most subduction margins occurs at depths of 30-50 km, slow slip along the Northern Hikurangi margin, New Zealand, the Nicoya Peninsula, Costa Rica, the Boso Peninsula, Japan and near La Plata Island, Ecuador is shallow [e.g., *Ozawa et al.*, 2003; *Protti et al.*, 2004; *Wallace and Beavan*, 2010; *Vallée et al.*, 2013], rarely occurring below 15 km, and occurs in locations where margin tectonics are dominated by the subduction of seamounts and ridges [*Mohiuddin and Ogawa*, 1998; *von Huene et al.*, 2000; *Ranero and von Huene*, 2000; *Collot et al.*, 2001; *Sage et al.*, 2006; *Tsumura et al.*, 2009; *Pedley et al.*, 2010; *Proust et al.*, 2016]. The abundant observations of slow slip have clearly indicated that it occurs under numerous depth and temperature conditions and exhibits a wide range of behaviors such as magnitude, duration, recurrence interval and tremorgenic or not.

While the exact physical mechanisms for slow slip are not well understood, it is accepted that slow slip is a manifestation of shear failure, like a normal earthquake, but with a considerably slower slip speed controlled by some other process such as dilatant hardening [*Segall et al.*, 2010], a change in frictional behavior (from velocity weakening to velocity strengthening) with increasing slip speed [*Shibazaki and Iio*, 2003; *Kaproth and Marone*, 2013], or the evolution of elastic stiffness in a localized shear fabric [*Leeman et al.*, 2015]. The mechanisms of slow slip become more difficult to constrain in regions where the subduction of topographically high features like seamounts and ridges has thoroughly fractured the upper plate [*Dominguez et al.*,

1998; *Wang and Bilek*, 2011, 2014] and plate motion can be accommodated on a network of fractures, rather than a single plane.

A large proportion of the existing slow slip observations in subduction zones come from regions where slow slip occurs at depths of 20-50 km where the slip occurs beneath land and can therefore be (relatively) easily instrumented [e.g., *Hirose et al.*, 1999; *Dragert et al.*, 2001; *Kostoglodov et al.*, 2003]. While this practice provides numerous observations and allows for the characterization of slip at these depths, behavior of the shallow, offshore portion of the subduction interface is often poorly resolved. Regions such as Costa Rica, New Zealand, Ecuador and the Boso Peninsula, Japan, where land is close to the trench and slow slip has been documented at shallow (<15 km) depths, provide a special opportunity to observe and quantify the behavior and conditions of the shallow end member of slow slip. Additionally, the presence of subducted seamounts in each of these locations provides an opportunity to address the direct role sea floor roughness has on aseismic slow slip and its associated seismic components like low frequency earthquakes, or tremor. Although the influence subducting seamounts and related high topography have on interplate behavior is controversial, most recently, subducting high relief has been more frequently associated with low seismic coupling and aseismic creep than with large megathrust earthquake failure [see *Wang and Bilek*, 2014 for a review]. Most models of megathrust locking are derived from seismic and geodetic observations made on land and suffer from the same problem of low resolution offshore as slow slip. Instrumenting the seafloor provides a high-resolution window into the range of slip

processes occurring on and near the shallow subduction interface as well as the heterogeneous conditions and deformation caused by seamount subduction. At the Nankai Trough, *Yokota et al.* [2016] provide the first evidence for the spatial coincidence of low seismic coupling, low frequency earthquakes and subducted seamounts on the shallow plate interface derived from seafloor geodetic observations. Their interpretation is that subducting seamounts generate elevated pore-fluid pressure and a complicated fracture network that results in low frequency earthquake activity and low coupling. Here we provide additional evidence from seafloor observations at the northern Hikurangi Margin that low frequency earthquakes are activated in a low-coupled region of the shallow plate interface at a subducting seamount during a large slow slip event.

2.1.1 Northern Hikurangi slow slip, tremor, and seismicity

New Zealand sits atop the complex boundary between the Australian and Pacific tectonic plates (Figure 2–1). The Hikurangi Plateau, a large igneous province with a crustal thickness of 35-42 km [*Reyners et al.*, 2011], subducts beneath the Australian Plate in northern New Zealand with near trench-perpendicular convergence of ~4.5 cm/yr [*Wallace et al.*, 2004] at the northern end of the North Island and strongly oblique convergence at the southern end of the North Island, southward to the Chatham Rise. The Hikurangi Margin can be subdivided into three segments: the northern segment, north of Hawke's Bay, the central segment from Hawke's Bay to the southern end of the North Island, and the southern segment between the southern end of the North Island and the end of subduction at the

Chatham Rise. In the northern segment, the margin is characterized by numerous seamounts on the Hikurangi Plateau and the subduction of these seamounts has played a significant role in the morphology and evolution of the frontal wedge [e.g., *Collot et al.*, 1996; *Bell et al.*, 2010; *Pedley et al.*, 2010]. There is an along strike change in the roughness of the incoming Pacific Plate with considerably fewer seamounts in the central and southern segments. The central segment is characterized by higher sedimentation rates in the Hikurangi trough, which results in a smoother incoming plate, and a wide accretionary wedge. The southern segment is dominated by highly oblique subduction [e.g., *Collot et al.*, 1996; *Pedley et al.*, 2010]. In this study, we focus on the northern Hikurangi segment.

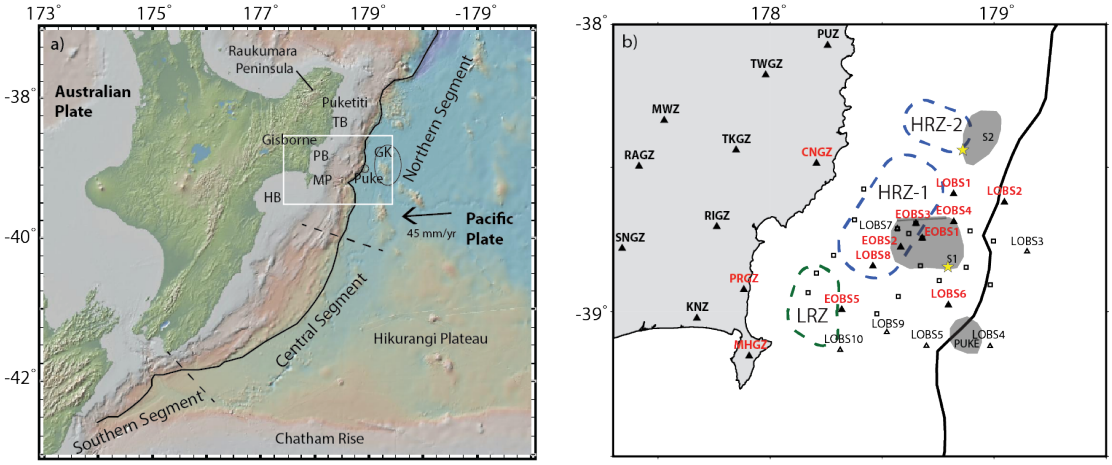

Figure 2–1. Hikurangi Margin tectonics and the HOBITSS experiment. Northern Hikurangi Margin tectonic setting. (a) Topographic/bathymetric relief of the Hikurangi Margin (trench=solid black line) showing a rough incoming Pacific Plate in the northern segment with seamounts, the sediment covered central segment, and the obliquely subducting southern segment. Place name abbreviations: HB= Hawke's Bay, MP= Mahia Peninsula, PB= Poverty Bay, TB= Tolaga Bay, GK= Gisborne Knolls. Seamounts Puke and the Gisborne Knolls are circled. The region shown in part (b) is identified by the white box. (b) Stations from the offshore Hikurangi Ocean Bottom Investigation of Tremor and Slow Slip experiment (triangles= ocean bottom seismometers; squares= absolute pressure gauges) and onshore New Zealand National Seismic Network (triangles= seismometers). Stations in red were used in the detection and location of tectonic tremor. Subducted or subducting seamounts S1, S2, and Puke are outlined in gray [*Bell et al.*, 2014]. Regions of high-amplitude interface reflectivity (HRZ) and lower amplitude reflectivity (LRZ) [*Bell et al.*, 2010] are outlined in dashed lines. Epicenters from the 1947 tsunami earthquakes are plotted as yellow stars.

The northern Hikurangi Margin (Figure 2–1) is host to a number of well-documented offshore regions that regularly experience slow slip as well as associated tectonic tremor and elevated earthquake rates [e.g., *Delahaye et al.*, 2009; *Wallace and Beavan*, 2010; *Kim et al.*, 2011; *Jacobs et al.*, 2016; *Todd and Schwartz*, 2016]. The high density of seismic and cGPS stations along the Raukumara Peninsula closest to the offshore slow slip, the shallow dip of the subducting Hikurangi Plateau, and the

resulting shallow depth to the plate interface (12 km near the coast) [*Eberhart-Phillips and Reyners*, 1999; *Williams et al.*, 2013] make the northern Hikurangi Margin an ideal location to investigate the various types of slip behaviors that occur on and near the subduction zone interface. In the northern segment of the Hikurangi Margin numerous patches experience slow slip events (SSEs) at depths shallower than 15 km that exhibit a range of durations, recurrence intervals, and magnitudes. These SSEs are primarily short in duration (< 20 days), occur at intervals < 24 months, are equivalent to M_w 6.3-6.8 [*Beavan et al.*, 2007; *Wallace and Beavan*, 2010; *Wallace et al.*, 2016] and are located almost exclusively offshore. Since 2002 when the continuous GPS (cGPS) network was installed, several SSEs in this region have been studied in detail, especially in the Gisborne patch where moderate events equivalent to M_w 6.5 occur every 18-24 months and larger events equivalent to M_w 6.8 occur every 4-6 years [*Douglas et al.*, 2005; *Beavan et al.*, 2007; *Wallace and Beavan*, 2010; *Wallace et al.*, 2012a, 2016].

Tectonic tremor accompanies many northern Hikurangi SSEs, especially those in the Gisborne and Puketiti patches, and has been predominantly located downdip of the geodetically inverted peak slip patches [*Kim et al.*, 2011; *Todd and Schwartz*, 2016] making it distinctly different from tremor in other subduction zones like Cascadia where tremor is collocated with peak slip and thought to represent the slow slip rupture front. However, tremor collocated with the offshore slow slip is difficult to detect with the land-based New Zealand National Seismic Network and may exist below current detection thresholds. Previously, seismic station density along the

Raukumara Peninsula was insufficient to detect and locate tremor associated with offshore SSEs [*Delahaye et al.*, 2009], but beginning in 2010 the seismic station separation was reduced to ~30 km over the entire peninsula and tremor could be detected and located associated with offshore SSEs [*Kim et al.*, 2011; *Todd and Schwartz*, 2016]. In addition to tectonic tremor, the largest SSEs along the northern Hikurangi Margin are also accompanied by increases in seismicity [*Delahaye et al.*, 2009; *Jacobs et al.*, 2016; *Todd and Schwartz*, 2016], especially with Gisborne and Puketiti SSEs. Although tremor detection is challenging due to highly attenuating sediments beneath the Raukumara Peninsula [*Lewis et al.*, 1998] and the lack of seismic station density prior to 2010, it is likely that both tremor and an increase in seismicity accompany most SSEs in the northern Hikurangi Margin.

The last large interplate earthquakes along the northern segment of the Hikurangi Margin were two large M_w 7.2 and 7.1 tsunami earthquakes in March and May of 1947 respectively [*Eiby*, 1982; *Doser and Webb*, 2003; *Bell et al.*, 2014]. Tsunami earthquakes are slow rupturing earthquakes at shallow depths that have anomalously high tsunami amplitude and runup for their magnitude [*Kanamori*, 1972; *Pelayo and Wiens*, 1992; *Bilek and Lay*, 2002]. These tsunami earthquakes occurred in the vicinity of the largest Gisborne SSEs at shallow depths <10 km beneath the continental slope where two seamounts have been subducted and impact the geometry of the plate interface and the upper plate (Seamounts S1 and S2; Figure 2–1). Although moderate-large interplate earthquakes along the Hikurangi margin have been rare in New Zealand's brief historic record, large upper plate and intraslab

events such as the 1855 Wairarapa, 1863 and 1931 Hawke's Bay, 2013 Cook Straight sequence, 2016 East Cape, and 2016 Kaikoura earthquakes dominate the recent seismic record and demonstrate the complex relationship between upper plate faulting and the megathrust.

The lack of large (> M_w 7.5) interplate earthquakes originating in the northern segment coupled with numerous subducting seamounts suggest that the conceptual model described in *Wang and Bilek* [2011] applies to the northern Hikurangi Margin. Subducting seamounts and the resulting complex shear network on the plate interface and in the upper plate likely dominate the subduction-related strain accumulation and release processes [see review in *Wang and Bilek*, 2014]. Additionally, subducting seamounts are thought to aid in the subduction of thick fluid-rich sediment packets that become overpressured as they are trapped downdip of the seamount [*Bell et al.*, 2010; *Bassett et al.*, 2014; *Ellis et al.*, 2015]. Working within this framework, we attempt to identify and analyze the relative contributions of the range of slip processes observed in the northern segment and their relationship to seamount subduction. While the rough Hikurangi Plateau appears to primarily be subducting aseismically in the northern segment of the margin, tectonic tremor and earthquakes accompany shallow slow slip. To elucidate the relationship between tremor, earthquakes, and shallow slow slip, and to understand their relative roles and relationship to seamount subduction in northern Hikurangi subduction, we use data from the Hikurangi Ocean Bottom Investigation of Tremor and Slow Slip (HOBITSS) experiment in concert with land-based seismic data to detect and locate

tremor and earthquakes during a moderate-large SSE offshore Gisborne in 2014. We also compute the changes in Coulomb failure stress imparted on the plate interface by the SSE to estimate the impact these SSEs have in influencing the occurrence and distribution of seismic slip processes on the megathrust. Additionally, we examine seven cGPS transients in the Puketiti patch, interpreted to be small SSEs [*Todd and Schwartz*, 2016], to analyze the spatial relationship between abundant tremor and earthquake episodes.

2.1.2 Seamount subduction

Early studies on the seamount subduction postulated that the topographic relief of the subduction interface increases interplate coupling and provides strongly locked areas that can promote failure in large-great subduction earthquakes [e.g., *Kelleher and McCann*, 1976; *Lay et al.*, 1982; *Cloos*, 1992; *Dmowska et al.*, 1996]. More recent studies of seamount subduction in regional and global contexts have found that seamounts likely break through the upper plate, creating a complex network of fractures and subduct predominantly aseismically [e.g., *Huene*, 2008; *Mochizuki et al.*, 2008; *Pedley et al.*, 2010; *Wang and Bilek*, 2011, 2014; *Bassett and Watts*, 2015; *Yokota et al.*, 2016]. Seamount subduction greatly impacts the evolution and morphology of the margin [*Lewis and Pettinga*, 1993; *Collot et al.*, 1996; *Davy and Collot*, 2000; *Lewis et al.*, 2004; *Barker et al.*, 2009; *Kukowski et al.*, 2010; *Pedley et al.*, 2010]. By trapping fluid-rich sediments at the leading front of the seamount in what has been observed on seismic reflection profiles as regions of high amplitude interface reflectivity (HRZ) [*Bell et al.*, 2010] and generating a large,

complex fracture network in the upper plate, seamount subduction influences the budget and distribution of fluids on and around the plate interface. The HRZ can become overpressurized if fluids released during dehydration and compaction are trapped at the downdip edge of the seamount [*Ellis et al.*, 2015]. This effect on overpressure is not well understood as the network of complex fractures generated by seamounts breaking through the upper plate [*Wang and Bilek*, 2014] likely create pathways for fluid migration and the level to which the HRZ can become overpressured is unconstrained. Slow slip occurs in highly overpressurized regions with low effective stress [e.g., *Kodaira et al.*, 2004; *Bell et al.*, 2010; *Kitajima and Saffer*, 2012; *Bassett et al.*, 2014] and seamounts predominantly subduct aseismically at shallow depths and may promote weak interplate coupling [e.g., *Huene*, 2008; *Mochizuki et al.*, 2008; *Wang and Bilek*, 2011, 2014] where slow slip is the dominant form of interplate slip.

2.1.2.1 Seamount subduction along the northern Hikurangi Margin

The Hikurangi Plateau is a seamount studded triangular volcanic plateau bounded by the Rapuhia Scarp and the southern Kermadec Trench in the north, and the Chatham Rise in the south that subducts westward beneath the North Island [*Wood and Davy*, 1994; *Collot et al.*, 1996; *Davy and Collot*, 2000; *Davy et al.*, 2008]. The along strike variation of roughness on the incoming Hikurangi Plateau allows the Hikurangi Margin to be subdivided into 3 zones. The northern segment, from the Rapuhia Scarp to Cape Kidnappers, is identified by a narrow, sediment starved erosive margin [e.g., *Davy and Wood*, 1994; *Wood and Davy*, 1994; *Collot et*

al., 1996] with numerous outboard seamounts and knolls (Figure 2–2). Seamount subduction in the northern segment has dictated the geomorphology of the margin as evidenced by the presence of numerous submarine landslides and presently subducting seamounts. These include the Ruatoria slide in the north that formed 2.0-0.16 Ma and is interpreted to be the result of an obliquely subducted seamount [*Collot et al.*, 2001; *Lewis et al.*, 2004; *Pedley et al.*, 2010], the currently subducting Puke seamount, the Riwha slide, and the Poverty Indent. Between the Ruatoria slide and the Povety Indent, the margin is steep (up to 10°) [*Collot et al.*, 1996; *Barker et al.*, 2009]. Further south at the transition between the northern and central segments, the Rock Garden is a region with oversteepened accretionary ridges of 10-20° atop a subducted seamount. Critical taper analyses show this area to be close to failure and suggest that a sudden change in fluid pressure, such as during strong shaking from a nearby large earthquake, could lead to voluminous mass wasting that would likely be accompanied by a destructive local tsunami [e.g., *Barnes et al.*, 2010; *Ellis et al.*, 2010; *Kukowski et al.*, 2010]. The central segment of the Hikurangi Margin (Figure 2–1), from Cape Kidnappers to Cook Strait, is characterized by a wide accretionary prism with a smoother incoming plate where seamounts on the Hikurangi Plateau are less frequent or buried by sediment [e.g., *Collot et al.*, 1996]. The southern Hikurangi Margin (Figure 2–1), between Cook Strait and the Kaikoura Peninsula, is identified by highly oblique subduction with a rapidly accreting frontal wedge and an absence of seamount subduction [e.g., *Barnes and de Lépinay*, 1997].

The presence of numerous seamounts on the shallow plate interface of the northern segment of the Hikurangi Margin (Figure 2–1) and outboard on the northern Hikurangi Plateau (Figure 2–2) coupled with the existence of shallow slow slip along the length of the segment suggest that very rough incoming plates are correlated with the occurrence of shallow episodic slow slip. The northern Hikurangi margin is established as a region of low interseismic coupling based on GPS measurements [*Wallace et al.*, 2004, 2009]. Additionally, the shallow SSEs have been shown to accommodate much of the accumulated strain on the plate interface [*Wallace and Beavan*, 2010]. Between Hawke's Bay and Tolaga Bay (Figure 2–2), the presence of subducted seamounts likely promotes interplate failure in the form of shallow slow slip and promotes the occurrence of tsunami earthquakes. The March (M_w 7.0-7.1) and May (M_w 6.9-7.1) 1947 tsunami earthquakes offshore Gisborne and Tolaga Bay at the edges of seamounts S1 and S2 [*Bell et al.*, 2014] serve as further evidence that the northern margin is weakly coupled and predominantly releases strain through slow slip and tsunami earthquakes.

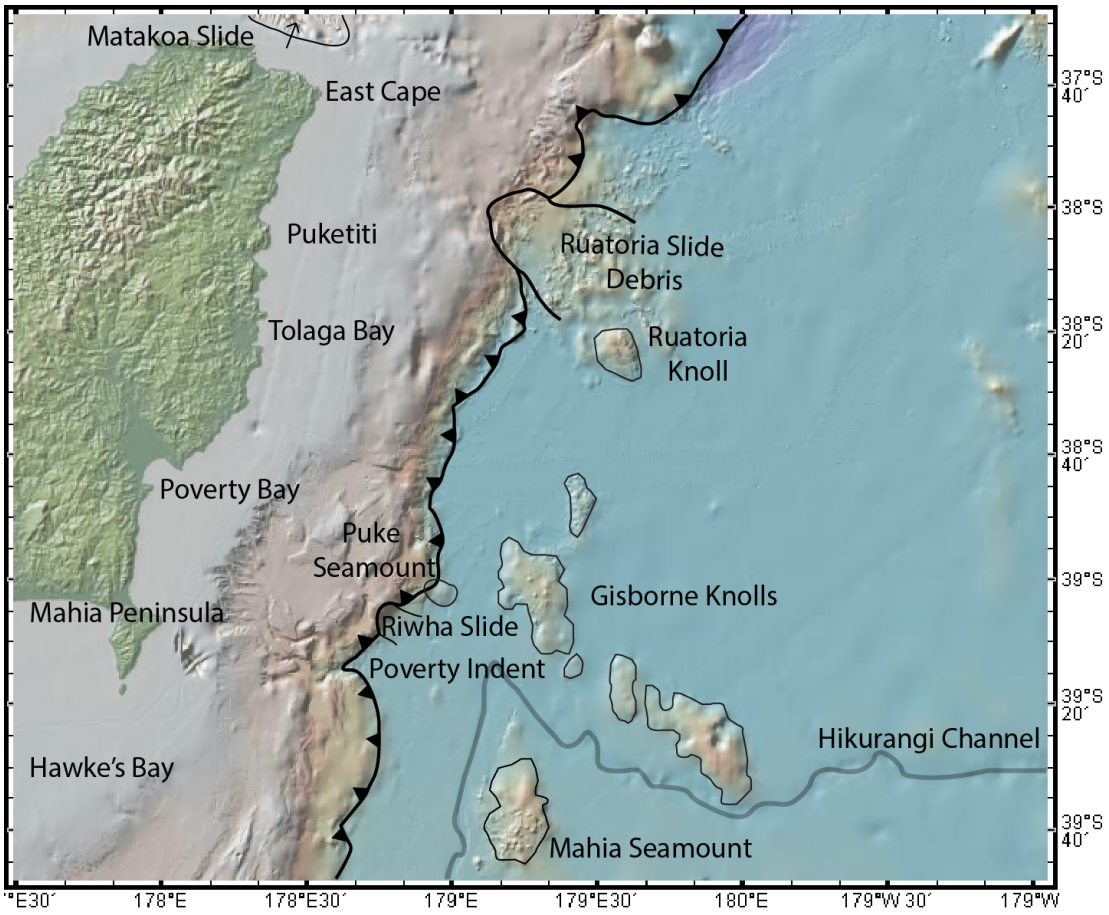

Figure 2–2. Northern Hikurangi Margin seamounts.
Detailed bathymetry for the northern Hikurangi Margin showing numerous outboard seamounts and knolls. Indentations and submarine slide debris fields are shown along the subduction trench.

2.2 The HOBITSS experiment

Since the shallow slow slip along the northern Hikurangi is entirely offshore, the best way to obtain a high-resolution slip distribution is to instrument the sea floor directly above the slip patch (Figure 2–3). In May 2014, the HOBITSS experiment deployed 24 absolute pressure gauges (APGs) in a near-source array to quantify the extent of seafloor deformation during the next large Gisborne SSE [*Wallace et al.*,

2016]. Additionally, 15 ocean bottom seismometers (OBSs) were deployed to detect and locate offshore tectonic tremor and microseismicity and improve the offshore seismic velocity structure. By combining seafloor pressure-change data with seismic data, we can elucidate the spatiotemporal relationship between slow slip, tremor, and seismicity to improve our understanding of the nature of deformation and stress transfer associated with slow slip. With a well-located offshore earthquake catalog and a well-defined slow slip patch, these data allow for a high-resolution examination of the spatial extent of seismic and aseismic slip.

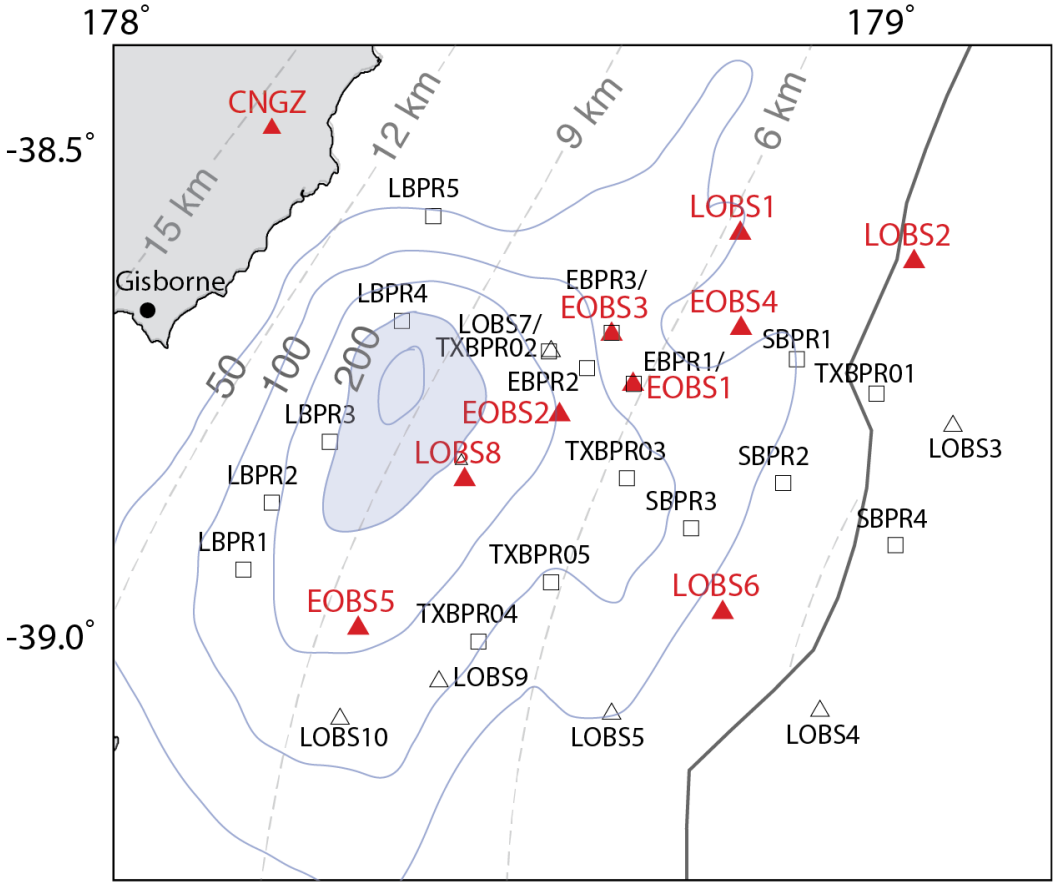

Figure 2–3. The HOBITSS experiment and the 2014 Gisborne SSE. Ocean bottom seismometers (OBS) and absolute pressure gauges (APG) from the HOBITSS experiment plotted as triangles and squares respectively. The Hikurangi trench (solid black line) and megathrust depth contours (dashed gray lines) are plotted [*Williams et al.*, 2013] with respect to slip contours (solid blue lines; displacement in mm) from the 2014 Gisborne SSE [*Wallace et al.*, 2016]. The seismic stations with good timing that were used in this study are in red.

Nine of the 15 deployed OBS stations returned data with good timing that could be used for detailed, time-sensitive analyses like tremor detection and phase picks for earthquake detection (EOBS 1–5, LOBS 1, 2, 6, and 8; Figure 2–3). Unfortunately 2 stations (LOBS 4 and 5; Figure 2–3) did not return seismic data during the slow slip event, and 4 stations (LOBS 3, 7, 9, and 10; Figure 2–3) had

moderate to severe timing errors associated with the seismic data. While the timing errors on data from LOBS 3, 7, and 9 may be corrected so these stations can contribute to future investigations, this study only employs data from the original 9 stations with adequate timing.

A large Gisborne SSE occurred in September/October 2014 directly beneath the array and a moderate SSE occurred in December 2014/January 2015 to the south of the array. Slip from the September/October Gisborne SSE covered an area of approximately 70 km by 100 km between 12 km and <2 km depth (Figure 2–3). The peak displacement (>200 mm) was located due east of Poverty Bay at around 9 km depth beneath the continental shelf [*Wallace et al.*, 2016]. This study provides a detailed analysis of the spatial and temporal relationships between slow slip, tremor, and earthquakes for the September/October 2014 Gisborne SSE with respect to subducted seamounts using seismic and cGPS data from land stations in the New Zealand National Seismic Network (operated by GeoNet; www.geonet.org.nz) in concert with data from the HOBITSS experiment.

2.3 Methods

2.3.1 Tremor detection and location

Offshore tectonic tremor is detected and located using the same modified version of the automated envelope cross-correlation and grid search methodology described in *Todd and Schwartz* [2016]. Due to increased noise on OBS stations below 3 Hz, the 2-5 Hz band-pass filter used to detect tremor with land stations from

the New Zealand National Seismic Network does not adequately isolate tremor energy from background noise or energy from local and regional earthquakes. As a result, envelopes for cross-correlation are defined by applying a band-pass filter in two frequency ranges: (1) 4–10 Hz to isolate tremor with energy at lower frequencies, and (2) 12-20 Hz to remove local earthquake detections that retain energy above 12 Hz. We analyze the east component of ground motion from 4 broadband and 5 short period ocean bottom seismometers in addition to 3 land-based coastal seismic stations to increase azimuthal coverage around the geodetically detected slow slip patch for September and October 2014 (Figure 2–3). Tremor is located when cross-correlation coefficients on a minimum of 7 station pairs exceeds 0.6. When adequate correlations are detected for at least 5 station pairs in the 12-20 Hz band, the time window is skipped to minimize local earthquake detections. Additionally, data from a reference station located outside the study region are filtered in the 4–10 Hz range and cross correlated with the ocean network and when adequate correlations are detected for at least 3 station pairs that include the reference station, the time window is skipped to minimize false detections from regional or teleseismic waves deplete in high frequency energy. Though they limit the amount of detected tremor, these steps reduce the number of false tremor detections from the automated process. Since tremor depth is poorly constrained, we assume tremor is located on the plate interface.

To ensure the tremor signal is distinct from local microearthquakes, we compare the spectral characteristics of the tremor signal to that of nearby earthquakes.

The power spectral densities for 56 10-second time windows of tremor are compared to background noise and nearby earthquakes thought to be on the plate interface at station LOBS8 (Figure 2–4). These earthquakes are distinguished from tremor because they retain high frequency energy above 10 Hz while tremor is indistinguishable from noise above 10 Hz. Additionally, background noise on OBS stations remains high until 2-3 Hz, so tremor signals are most apparent between 4-10 Hz. While the spectral character of tremor between ~3.5-10 Hz is expected, the exact cause of the rise in power below ~3.5 Hz is unclear and warrants further investigation.

Figure 2–4. Stacked power spectral densities for earthquakes, tremor and noise. Left: Stacked power spectral densities for earthquakes, tremor, and background noise at station LOBS8. Tremor signals remain above the noise above 2 Hz and fall off rapidly with a corner frequency ~7 Hz, reaching noise levels by 10 Hz. Nearby earthquakes have a higher corner frequency and retain energy above 10 Hz before dropping to noise levels ~25-30 Hz. Noise on OBS drops off between 2-3 Hz, therefore tremor signals have the highest signal to noise at 4-10 Hz. Right: 10 minutes of seismic data from station LOBS8 bandpass filtered at 4-10 Hz with short bursts of tremor (top) and a local M_w 2.2 earthquake (bottom) highlighted in gray. Abundant microseismicity and noisy OBS stations make the detection of low amplitude tremor signals difficult for extended durations.

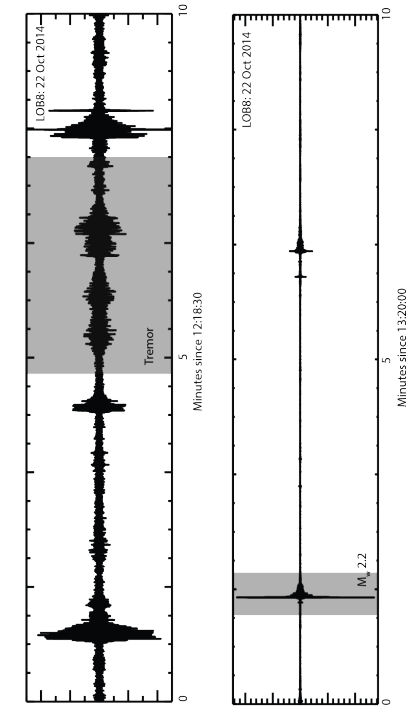
LOB8: 22 Oct 2014
Tremor
0
5
10
Minutes since 12:18:30
LOB8: 22 Oct 2014
M_L 2.2
0
5
10
Minutes since 13:20:00

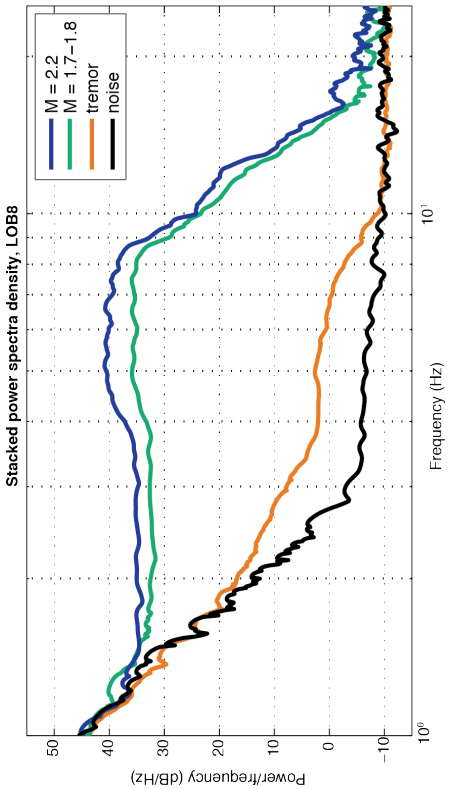
Stacked power spectra density, LOB8
M = 2.2
M = 1.7–1.8
tremor
noise
Power/frequency (dB/Hz)
50
40
30
20
10
0
−10
10^0
10^1
Frequency (Hz)

2.3.2 Detecting and locating local earthquakes

Earthquakes were manually detected for September and October 2014 by picking *P* wave arrivals at up to nine OBS stations and 16 land seismic stations for over 850 visually identified events. Using a local 1-D interpretation of the New Zealand 3-D velocity model [*Reyners et al.*, 1999; *Eberhart-Phillips et al.*, 2010], preliminary hypocenters for over 600 events were found using Antelope's *dblocsat2* algorithm that minimizes travel times over a 3-D grid search. Hypocentral locations were improved by relocating events with NonLinLoc v.6.0, a probabilistic non-linear relocation program that calculates the maximum likelihood hypocenter through a 3-D grid search [*Lomax et al.*, 2000]. Emphasis was placed on events located near the slow slip displacement shown in Figure 2–3. Initially, a local 1-D interpretation of the 3-D New Zealand velocity model [*Eberhart-Phillips et al.*, 2010] is mapped onto a specified 3-D grid and synthetic travel times are computed for stations in the catalog. Earthquake locations are determined with phase picks from the catalogs and the "Oct-Tree" search method in NonLinLoc. The oct-tree method begins with a coarse grid with spacing of 10s of km and determines the probability that the potential hypocentral location is in a particular sampled cell by multiplying the probability density function (PDF) in the center of each grid cell by the cell volume. Sampled cells with high probability are then subdivided into 8 new cells, which generates a new set of sampled cells and calculated probabilities. This procedure is repeated until either a predefined number of process nodes (7.5×10^5) is reached or the predefined smallest node size (0.25 km) is reached [*Lomax*, 2011]. Throughout the iterative

process, the solution converges rapidly and the final location is determined as the point of maximum likelihood within the final PDF solution. Errors in the original phase time picks and travel time calculations are assumed to be Gaussian and the errors in the resulting hypocentral location are dictated by the predetermined minimum node size. This method improves upon a traditional 3-D grid search that treats every potential hypocentral location equally by prioritizing the search based on the probability that the hypocenter is located within a coarser sampled cell before refining the grid and reiterating the search. The oct-tree method produces the same result as the traditional 3-D grid search, but is faster because it prioritizes sampled cells with the highest probability and therefore samples fewer cells.

2.3.3 Calculating changes in Coulomb failure stress

In order to elucidate the effects of slow slip on the stress state of the surrounding plate boundary, we employ a recently quantified geometry of the Hikurangi subduction interface [*Williams et al.*, 2013] and PyLith, a sophisticated finite-element crustal deformation modeling tool [*Aagaard et al.*, 2013, 2016], to compute stress changes on the plate interface. Initially, the slow slip distribution determined by *Wallace et al.* [2016] and produced using an elastic half-space dislocation model [e.g., *Okada*, 1985, 1992] is seamlessly transferred from the coarse grid used in the geodetic inversion to the Hikurangi megathrust geometry and placed onto the fine mesh with a bilinear interpolation. The slip distribution is then smoothed to mitigate the effects of stress singularities at the edges where there are strong gradients in the slip distribution. PyLith is then used to compute the traction changes

for each element in the fault mesh. We determine the change in coulomb failure stress by using the computed normal stresses and by mapping the computed traction changes on the direction of plate convergence [*Wallace et al.*, 2012b] for each element in the mesh to calculate the shear stresses. In this study, we used geodetic slip inversions from the 2014 Gisborne SSE [*Wallace et al.*, 2016] and compute the change in Coulomb failure stress imparted on the megathrust.

2.4 Results and Discussion

2.4.1 Tremor collocated with slow slip and subducted seamounts

Prior to the HOBITSS experiment, tremor could only be detected with seismic data from land stations after the network achieved sufficient density in 2010. For the Gisborne SSEs, these detections are predominantly located onshore in bands that extend east and northeast from the downdip edge of geodetically detected slow slip (Figure 2–5). While northern Hikurangi tremor is temporally coincident with offshore SSEs, offshore tremor spatially collocated with slow slip has not been observed. The occurrence of tremor downdip of the slow slip patch has distinguished the northern Hikurangi Margin from other tremorgenic subduction zones such as Cascadia or Nankai where tremor is identified to be collocated with the slow slip rupture front [e.g., *Ito et al.*, 2007; *Ghosh et al.*, 2009]. The slow slip with collocated tremor in these regions is located significantly deeper (30-50 km) than slow slip along the northern Hikurangi Margin (< 12 km); at this depth, the slow slip and tremor sit

directly beneath landmasses that can be well-instrumented for real-time monitoring, thus making tremor detection easier and more robust.

OBSs and APGs have previously been deployed on the ocean floor along the northern segment of the Hikurangi margin as part of small ~4 instrument campaign-style experiments for the last few years, but the station quantity and density were not sufficient to systematically observe low amplitude signals like tectonic tremor in the offshore region. In spite of the timing and data corruption issues with some of the HOBITSS OBS stations, there is sufficient coverage of the SSE slip patch to detect and locate offshore tectonic tremor (Figure 2–5).

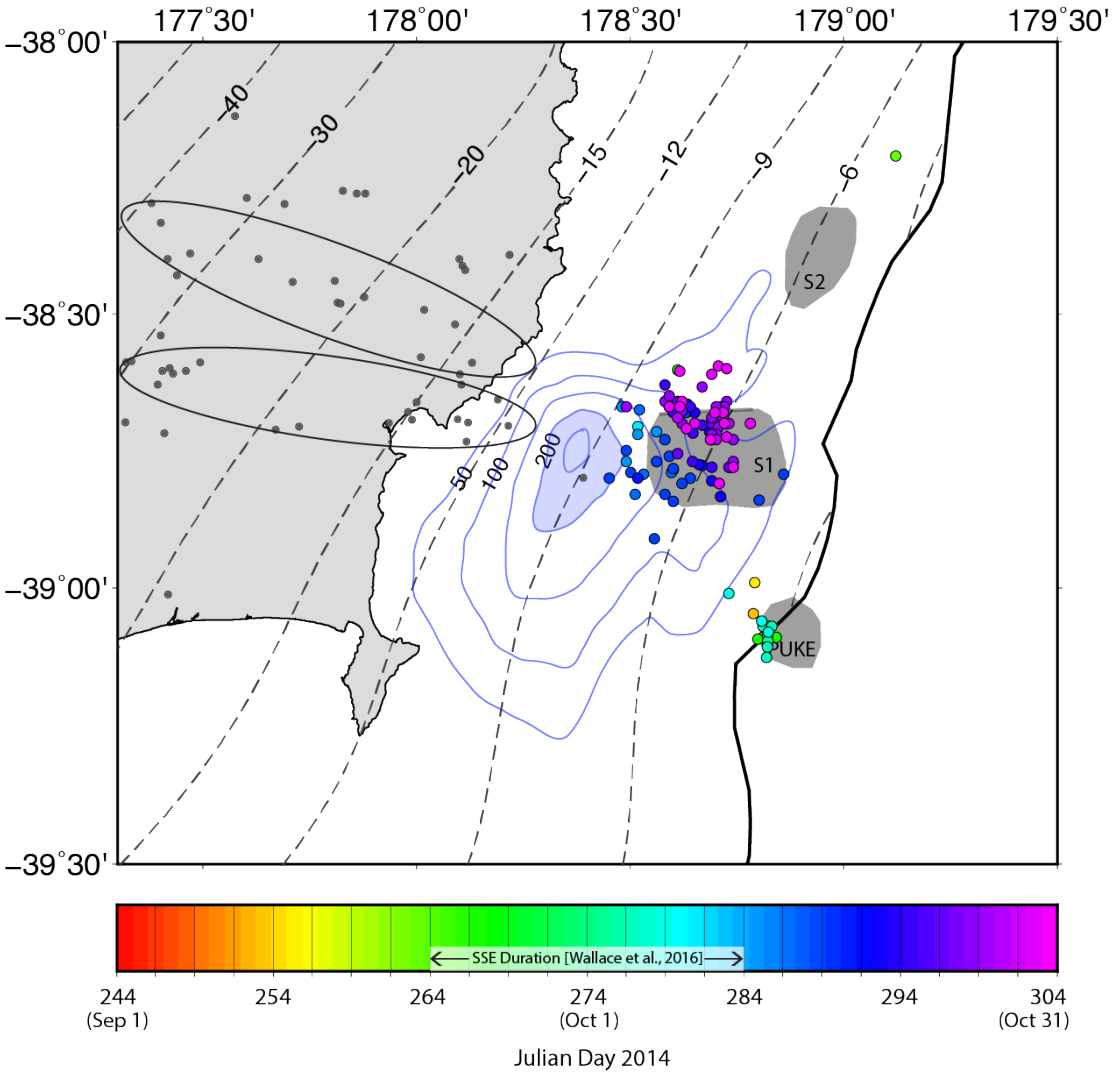

Figure 2–5. Tectonic tremor associated with the 2014 Gisborne SSE.
Offshore tremor (circles color-coded by time) is primarily located on and adjacent to subducted seamount S1, updip of the peak displacement in the slip event. Onshore tremor events located with land-based stations in the New Zealand National Seismic Network (gray circles) are located down dip of the peak slip in two bands extending in the dip direction. We assume tremor is located on the plate interface.

Offshore tremor associated with the 2014 Gisborne SSE is clustered updip of the northern end of the geodetically detected peak (200+ mm) slip [*Wallace et al.*, 2016] atop and around a large subducted seamount (seamount S1; Figure 2–5). This

cluster of events forms an offshore extension of the two lobes of previously detected tremor activity that extend onshore and downdip from the slow slip patch. Tremor has been detected in the same onshore region, downdip of the slow slip patch for every Gisborne SSE since 2010 [*Todd and Schwartz*, 2016]. Here, we present the first observation of offshore tremor that is collocated with geodetically detected slow slip along the northern Hikurangi Margin.

Wallace et al. [2016] show that APGs across the HOBITSS network experience upward movement of the ocean floor beginning on Julian days (JD) 262-265 for 2-3 weeks. This time period corresponds with a small shallow episode of tremor south of station LOBS6 near the trench where seamount Puke is currently subducting (Figure 2–5). After infrequent tremor for the first 10-15 days of slow slip, a burst of tremor activity begins between JD 275-277. Toward the end of the upward motion detected on the APG, a second, longer episode of tremor begins near station LOBS8 on JD 279 and continues across subducted seamount S1 toward station LOBS1 in a northwest trend through the end of the month (JD 304). While the observable upward motion on the APGs tapers off around JD 283-290, tremor activity continues to move northeastward across the seamount for an additional 2-3 weeks. If this episode of tremor corresponds with a slowly moving rupture front with seafloor deformation below the APG detection threshold, this tremor migration may indicate that the slow slip duration is longer than previously thought. Additionally, the delayed onset of tremor with respect to the upward motion of the seafloor may indicate a fluid-related process required for collocated tremor.

The large northeastward migrating tremor episode corresponds to a rupture velocity of ~0.7 km/day (Figure 2–5), a considerably smaller velocity than tremor migration observed in Cascadia and Nankai with velocities of 5-15 km/day [*Kao et al.*, 2006; *Obara and Sekine*, 2009; *Ide*, 2010; *McCausland et al.*, 2010]. Furthermore, the slow tremor migration velocity may be due to the shallow depth of the slip. Assuming the tremor is located on or near the plate interface, this tremor migration occurs along strike between 3-9 km depth, beneath the accretionary wedge.

The only large historical Gisborne interplate events are two tsunami earthquakes in March and May of 1947 that likely originated at the edge of subducted seamounts at depths < 10 km [*Bell et al.*, 2014] (Figure 2–1). These subducted seamounts appear as uniquely identifiable features on seismic reflection profiles and are interpreted to be zones of frictional instability that can initiate or arrest shear slip [*Mochizuki et al.*, 2008; *Bell et al.*, 2010; *Wang and Bilek*, 2014]. Immediately downdip of the subducted seamounts exist zones of high-amplitude interface reflectivity (HRZ) that are interpreted to be overpressured fluid-rich sediments trapped by the seamount [*Bell et al.*, 2010; *Bassett et al.*, 2014; *Ellis et al.*, 2015]. While the peak slip in the 2014 Gisborne SSE overlaps with the HRZ, tremor appears to predominantly exist just updip, over one of the subducted seamounts (Figure 2–5) where slow slip has a smaller amplitude and the March 1947 tsunami earthquake is thought to have originated (Seamount S1; Figure 2–1). Both identifiable bursts of offshore tremor activity occur over and adjacent to subducted seamounts Puke and S1 (Figure 2–5) suggesting that a complicated network of shear fractures surrounding the

subducted seamounts may be required for tremorgenesis in the northern segment of the Hikurangi Margin. Although seamounts are shown to primarily subduct aseismically [*Wang and Bilek*, 2014], tectonic tremor, assumed to be located on the plate interface, that is strongly spatially correlated with slow slip and seamounts may be a seismic manifestation of seamount subduction. Additionally, the complex fracture pattern generated by the "breaking through" method of seamount subduction [*Dominguez et al.*, 1998; *Wang and Bilek*, 2011, 2014] creates numerous connected fluid pathways that may promote low magnitude slow slip across the seamount.

2.4.1.1 Puketiti tremor and seismicity: evidence of a subducted seamount?

North of the Gisborne and Tolaga Bay patches, cGPS records for the Puketiti patch identify numerous transients inferred to be small SSEs [*Todd and Schwartz*, 2016]. Though the total eastward displacement experienced during each event is less than other SSEs along the northern Hikurangi Margin, Puketiti SSEs are frequently associated with prolific episodes of tectonic tremor and seismicity (Figure 2–6). Puketiti SSEs occur once or twice per year, last for 10-15 days, and experience 5-10 mm of eastward displacement at cGPS station PUKE. While there are no geodetically inverted slip distributions for Puketiti slip events, we analyze the spatial relationship between tremor and earthquakes associated with 7 events between 2010-2015 (Figure 2–6).

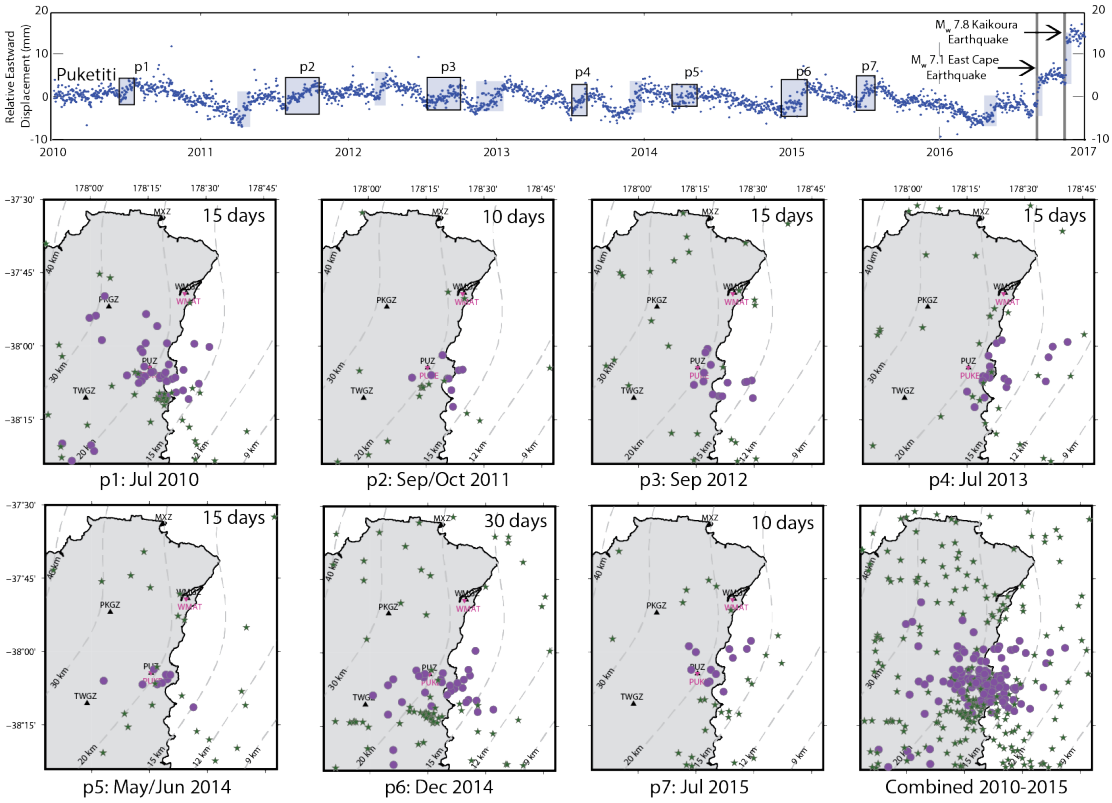

Figure 2–6. Tremor and earthquakes associated with Puketiti SSEs from 2010-2015. Top: cGPS record for station PUKE identifying numerous transients interpreted to be small SSEs (shaded boxes). Tremor and earthquakes associated with labeled events p1-p7 are plotted below. Bottom: Tectonic tremor (purple circles) and earthquakes (green stars) coincident with eastward transients from cGPS station PUKE. Seismic stations are plotted as black triangles and cGPS stations are plotted as inverted pink triangles. Tremor is clustered in a small region southwest of seismic station PUZ and earthquakes are concentrated further south along strike. The final frame plots tremor and earthquakes associated with events p1-p7.

Tectonic tremor episodes associated with Puketiti SSEs are spatially concentrated along the coast southwest of seismic station PUZ and cGPS station PUKE (Figure 2–6). Compared to tremor episodes associated with other slow slip events along the northern Hikurangi Margin [*Todd and Schwartz*, 2016], robust tremor episodes accompany each Puketiti SSE, last for 10-15 days, and predominantly originate from a single source region. Additionally, Puketiti SSEs are

associated with microseismicity sequences adjacent to the tremor episodes (Figure 2–6). We suggest that these tremor and earthquake episodes are the seismic manifestation of slow slip at the downdip edge of a subducted seamount in and adjacent to another region of overpressured fluid entrained sediments.

Earthquake sequences associated with Puketiti SSEs tend to occur immediately before or after the slow slip events. Figure 2–7 shows 30 days of the tremor and earthquake sequences associated with the most productive Puketiti event in our study period (event p6; Figure 2–6). There are two earthquake sequences in the first 15 days, with the largest earthquakes having M_w 3.3 and M_w 4.9. The initial sequence is located in the upper crust above the tremorgenic zone. This is followed by a second sequence located downdip of the tremorgenic zone. Immediately after the second sequence, starting with the M_w 4.9 earthquake, 15 days of tremor begin with eastward motion on cGPS station PUKE (Figure 2–7). The initiation of slow slip by small magnitude earthquakes indicates that the plate interface in this region is weakly coupled and predominantly slips in SSEs. The along strike change in the frequency and duration of SSEs from north to south along the margin may indicate an along strike change in interplate coupling.

Figure 2–7. December 2014 Puketiti SSE earthquake and tremor episodes.
Top: Tectonic tremor (circles) and earthquakes (stars) color coded by time for event p6 in December 2014 (Figure 2–6). Bottom: Cross-sectional view of earthquakes located inside the dashed rectangle in the top plot. The two largest earthquakes are M_w 3.3 and M_w 4.9. Tremor located in the shaded region and eastward displacement begins immediately after the M_w 4.9 earthquake.

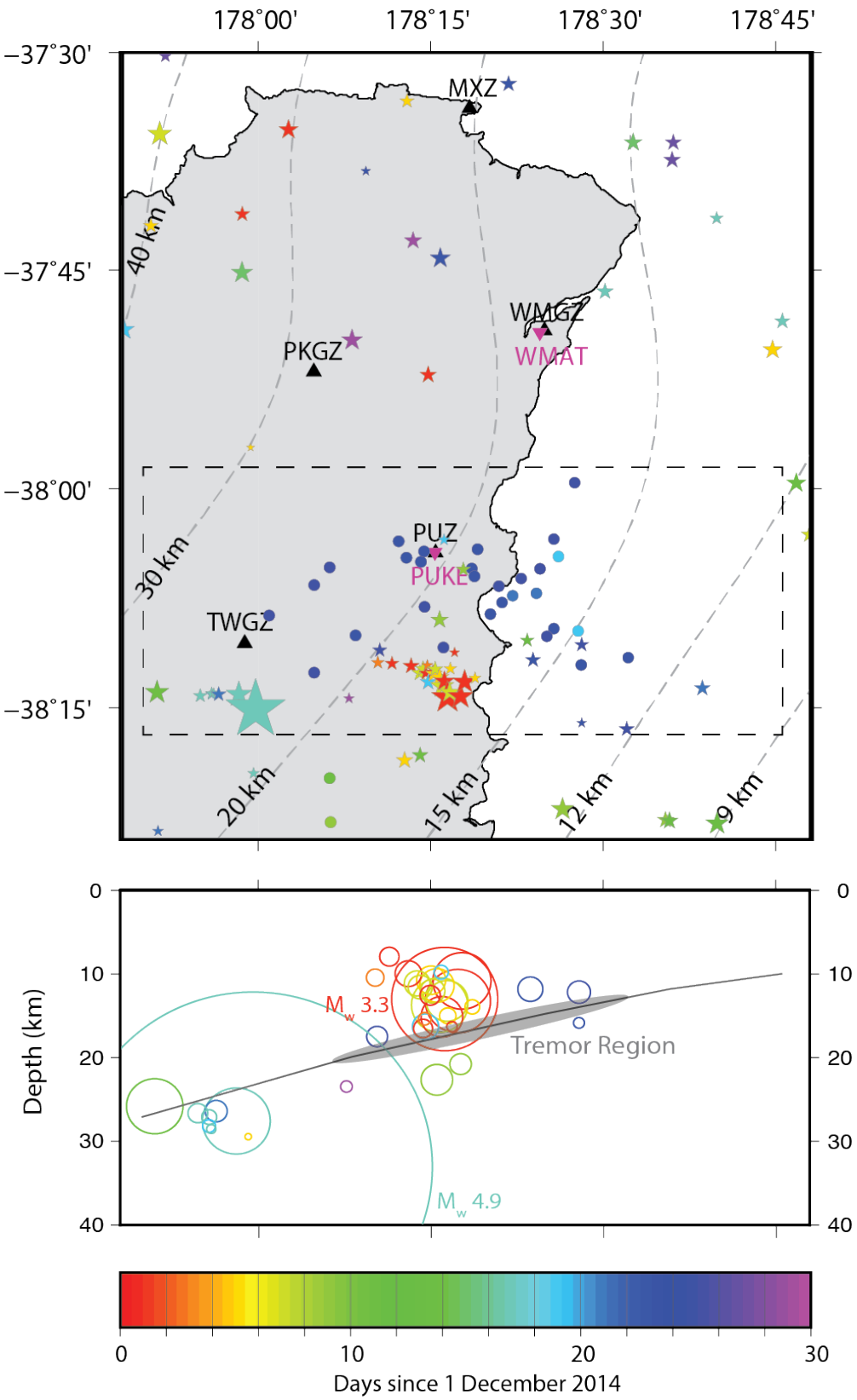
178°00'
178°15'
178°30'
178°45'
−37°30'
−37°45'
−38°00'
−38°15'
MXZ
WMGZ
WMAT
PKGZ
PUZ
PUKE
TWGZ
40 km
30 km
20 km
15 km
12 km
9 km
Depth (km)
0
10
20
30
40
M_w 3.3
M_w 4.9
Tremor Region
Days since 1 December 2014

2.4.2 Seismicity before, during, and after slow slip

SSEs along the northern Hikurangi Margin are accompanied by increases in seismicity. Clear seismicity increases do not accompany every shallow SSE, but significant increases have been identified with the largest shallow SSEs such as the 2004 and 2010 Gisborne SSEs, and the 2011 Cape Turnagain SSE [*Delahaye et al.*, 2009; *Bartlow et al.*, 2014; *Jacobs et al.*, 2016]. The 2014 Gisborne SSE has a small increase in seismicity starting at the beginning of the geodetically detected slip and continuing for several days afterward. Focusing on earthquakes located near the shoreline and offshore provides a detailed look at where earthquakes are occurring before, during and after the 2014 Gisborne SSE (Figure 2–8). Earthquakes detected before the SSE are either located onshore between Poverty Bay and the Mahia Peninsula or offshore, north of seamount S1 and downdip from seamount S2 in the region that will slip in the event between 6 and 9 km depth. Once the SSE begins, earthquakes continue at the updip edge of the slip, adjacent to seamount S1 until ~JD 279 when several earthquakes occur on the plate interface (within 5 km) in the vicinity of the peak displacement (>200 mm) from the slow slip. The presence of interplate earthquakes in the northern finger of the slip patch, prior to the geodetically determined onset of slow slip, followed by earthquakes in close proximity to the peak displacement suggests that slow slip may have initiated in the north, downdip of seamount S2 as early as JD 252 before advancing southward along strike. After the end of geodetically detected slow slip, earthquake activity in the peak slow slip patch ceases and seismicity continues around the northern and updip edge of the slow

slipping region. This extended activity includes a few events located over seamount S1 (Figure 2–8). These events are too small to determine focal mechanisms for, but are limited to be within 5 km depth of the plate interface and may be located in the fractures above the seamount. Since the slow slip is offshore, small offshore earthquake sequences may accompany all Gisborne SSEs, but are difficult to detect with the land-based seismic network.

Figure 2–8. Earthquakes associated with the September/October 2014 Gisborne SSE. Top: Earthquakes (stars, color-coded with time) before, during, and after geodetically detected slow slip with respect to subducted seamounts and slow slip displacement. Events with bold outlines are located within 5 km of the plate interface. Earthquakes are located in the region of peak slip at the start of the SSE and are concentrated on the north edge of the slip patch after the SSE. Bottom: Daily earthquake count for September and October 2014 (JD 244-304) in blue and cumulative earthquake count in red. The earthquake rate changes once the slow slip begins (~JD 264) and increases more in the final days of the SSE around JD 278.

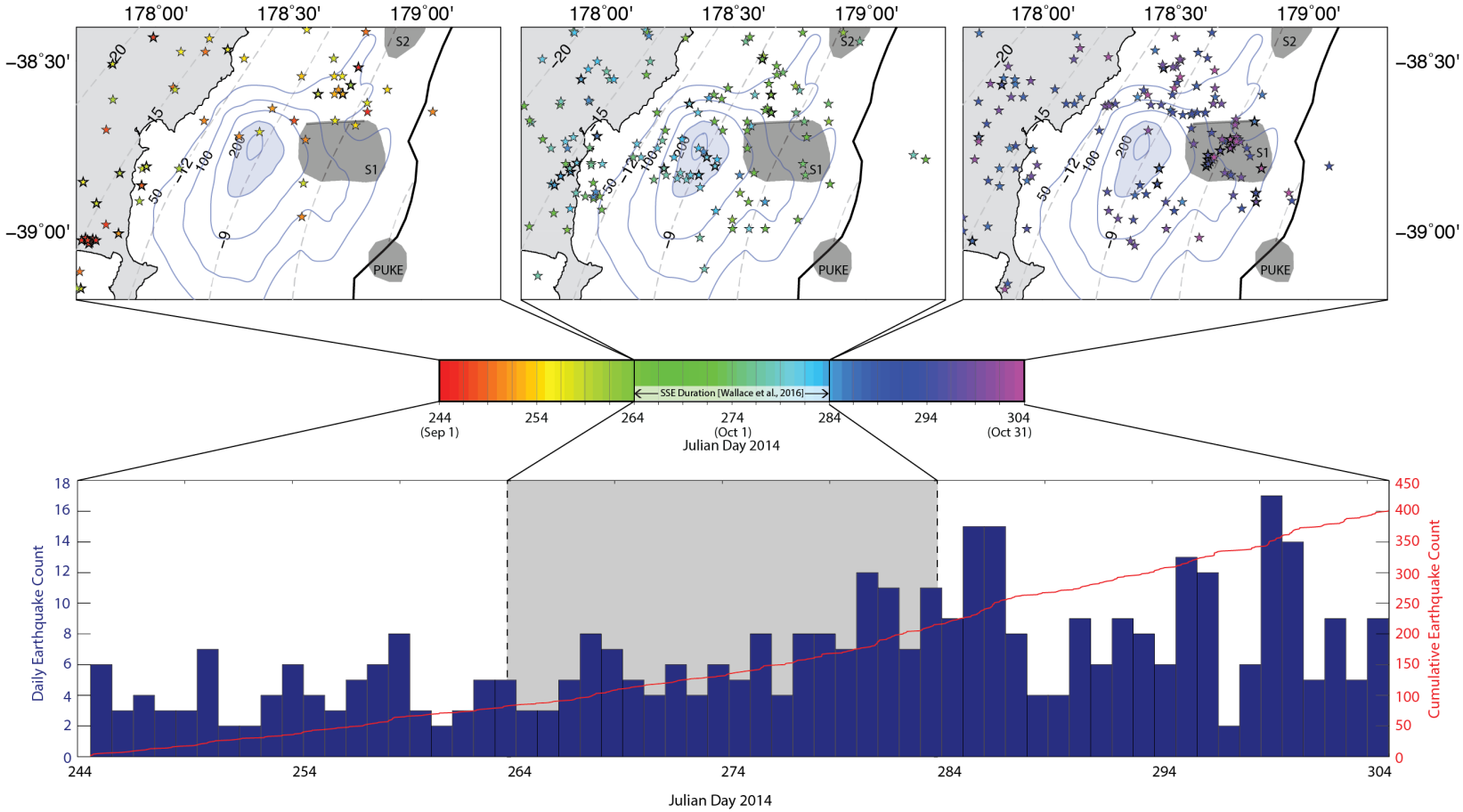
178°00'
178°30'
179°00'
−38°30'
−39°00'
S1
S2
PUKE
SSE Duration [Wallace et al., 2016]
244
(Sep 1)
254
264
274
(Oct 1)
284
294
304
(Oct 31)
Julian Day 2014
Daily Earthquake Count
Cumulative Earthquake Count

2.4.3 Change in Coulomb failure stress on megathrust from slow slip

The relationship between the distribution of aftershocks and the static increase in Coulomb failure stress (CFS) has been well established [e.g. *Stein and Lisowski*, 1983; *Stein et al.*, 1992; *Toda et al.*, 1998; *Stein*, 1999]. Additionally, earthquakes and tectonic tremor can be dynamically triggered by the passage of seismic waves from regional and teleseismic earthquakes [e.g., *Hill et al.*, 1993; *Prejean et al.*, 2004; *Peng et al.*, 2009; *Fry et al.*, 2011; *Chao et al.*, 2013]. To further investigate the relationship between slow slip, tremor, and earthquakes on or near the plate interface we compute the change in CFS on the plate interface and look at the regions of static stress increase with respect to the tremor and earthquake distribution during and after the 2014 Gisborne SSE. Results from our CFS calculations are shown in Figure 2–9 where most of the slow slip region sees a decrease of >30 kPa (Peak ~180 kPa). The only part of the slow slip patch that does not experience a stress decrease >30 kPa is where seamount S1 is located. Slip inversions with land stations and the APG data predict less displacement (<150 mm) across the seamount and this is reflected in the CFS calculations as the peak stress decrease wraps around the seamount's downdip edge. Downdip of the peak slip and seamount S1, the plate interface experiences an increase in CFS of >30 kPa with a peak of around 50 kPa. A CFS increase is also experienced updip of the southern part of the slow slip patch with an increase of >30 kPa. These values of CFS increase are similar to the increases computed for regular earthquakes similar in magnitude to the 2014 Gisborne SSE (equivalent M_w 6.7-6.8);

the 2002 M_w 6.7 Nenana Mountain earthquake, foreshock to the M_w 7.9 Denali Earthquake, had a CFS increase of 30-50 kPa [*Anderson and Ji*, 2003].

Figure 2–9. Coulomb failure stress change from the 2014 Gisborne SSE.
(a) Calculations of the Coulomb failure stress change (CFS) imparted on the megathrust by the 2014 Gisborne SSE. Regions of stress increase are shown in red and regions of stress decrease are shown in blue. (b) Earthquakes (stars, color-coded with time) located within 5 km of the plate interface (and assumed to be on the plate interface for the purposes of this discussion) are plotted with the CFS change and seamounts Puke, S1, and S2. Stress changes from the SSE do not appear to greatly impact interplate faulting. Depths of earthquakes along transect A-A' are plotted in Figure B–1.

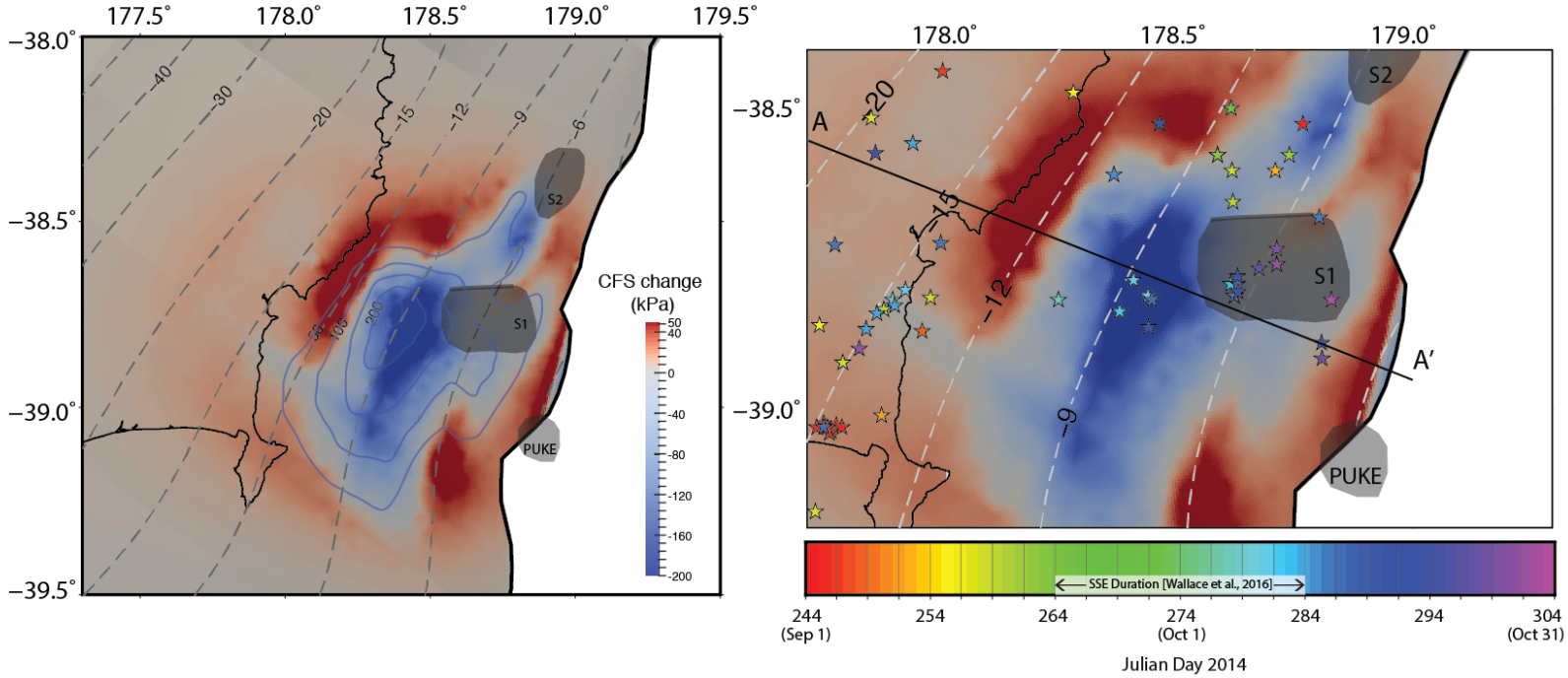
177.5°
178.0°
178.5°
179.0°
179.5°
−38.0°
−38.5°
−39.0°
−39.5°
40
30
20
15
12
9
6
S2
S1
PUKE
CFS change
(kPa)
50
40
0
-40
-80
-120
-160
-200
A
A′
SSE Duration [Wallace et al., 2016]
244
(Sep 1)
254
264
274
(Oct 1)
284
294
304
(Oct 31)
Julian Day 2014

Earthquakes within 5 km of the plate interface are plotted with the CFS change calculations in Figure 2–9 and are considered to be on the plate interface for the purposes of this study (Figure B–1). These earthquakes are clustered at the northern edge of the slow slip patch, immediately north of seamount S1. Earthquakes within the slow slip patch begin around JD 278-284 in the region that experiences the greatest displacement (>150 mm) and the greatest decrease in CFS in the final days of the geodetically detected slip event. During the same time period, earthquakes occur downdip of the slow slip patch along the coast between Poverty Bay and the Mahia Peninsula as well as along the northern coast of Hawke's Bay. Interestingly, there is no clear concentration of earthquakes on the megathrust in the regions experiencing the largest increase in CFS. Rather, many of the event locations appear to be nearly anti-correlated with the CFS increases. It is important to note that the earthquakes within 5 km of the subduction interface are a small minority of the earthquakes observed with the 2014 Gisborne SSE and most offshore earthquakes are not located on the plate interface. Therefore it is not expected that the spatial distribution of these earthquakes is correlated with the calculated CFS changes. With the majority of earthquakes occurring at the northern edge of seamount S1 inside a region of geodetically detected slow slip, it appears as though the subduction of the seamount is dominating the stress field and that SSEs in the Gisborne patch do not generate enough static stress change on the plate interface to control the distribution of interplate earthquakes.

2.4.4 Slip heterogeneity on the shallow megathrust

Seamount subduction produces a heterogeneous environment on the shallow subduction interface where each slip mode in the spectrum of fault slip occurs in close proximity, as evidenced by the Gisborne slow slip patch. Traditionally, the offshore nature of shallow slow slip makes the effects of seamount subduction on interplate slip processes elusive. Figure 2–10 illustrates the spatial heterogeneity of the various slip modes on the interface observed with the 2014 Gisborne SSE. Each unique mode of interplate slip, fast normal earthquakes, slow small earthquakes or tremor, slow large earthquakes or tsunami events, and slow slip, are largely grouped together. However, this slip mode segregation is not perfect as we observe some intermixing. For example, during the SSE, several interplate earthquakes occur inside the slow slip patch inside the HRZ zone referenced in Figure 2–1, near the peak slow slip displacement and CFS decrease. Although low magnitude slow slip is observed as shallow as 2 km depth and may extend completely to the trench through seamount S1, the geodetically inverted slip patch shows that the updip limit of slip above 150 mm arrests at the downdip edge of the seamount. Additionally, tremor and a few interplate earthquakes overlap with seamount S1 beginning in the last few days of the geodetically determined slow slip and continuing for 2-3 weeks. Further analysis of these events is warranted to determine if they are indeed on the plate interface or in the fractured upper plate above the seamount. The tsunami earthquake of March 1947 also originated at the updip edge of seamount S1 and may have ruptured across the

seamount, implying that this seamount is controlling the stress state and mechanism of interplate slip.

Our observations support a model where the diverse stress state, complex fracture system and pore fluid pressure conditions generated by seamount subduction host a wide range of transient events with varied magnitudes and slip rates in close proximity. While the majority of the shallow plate interface at the northern Hikurangi margin slips too slowly to radiate seismic energy, some small patches slip fast enough to generate tremor while larger patches are able to nucleate tsunami earthquakes.

Figure 2–10. Slip modes on the megathrust from the 2014 Gisborne SSE.
Various modes of slip on the plate interface are plotted together with the changes in CFS from the 2014 Gisborne SSE. Slow slip displacement (blue contours; displacement in mm), tectonic tremor (circles) and interplate earthquakes (stars). 1947 tsunami earthquake epicenters plotted as open black stars. Tremor is concentrated at subducted seamounts and interplate earthquakes are primarily located onshore or in the slip patch.

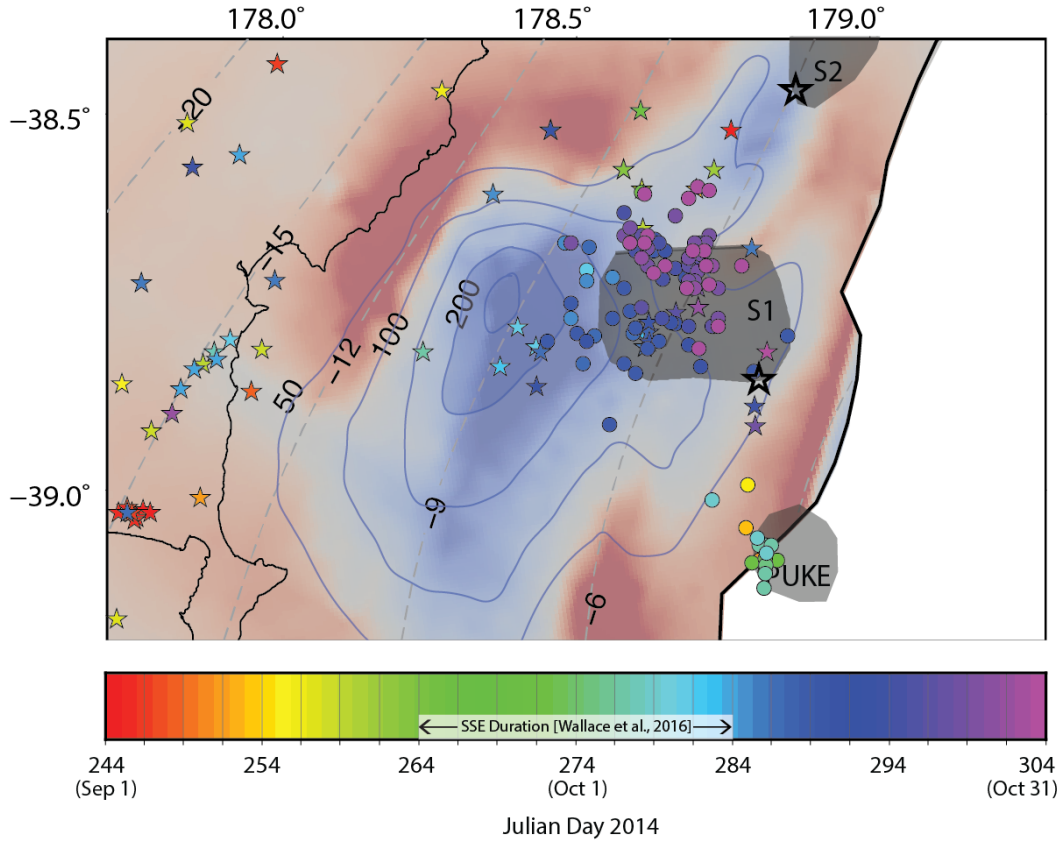
178.0°
178.5°
179.0°
−38.5°
−39.0°
S2
S1
UKE
20
15
12
9
6
200
100
50
SSE Duration [Wallace et al., 2016]
244
(Sep 1)
254
264
274
(Oct 1)
284
294
304
(Oct 31)
Julian Day 2014

2.5 Conclusions

One of the primary goals of the HOBITSS experiment was to determine if slow and fast interplate slip modes spatially overlap or are spatially segregated. The northern segment of the Hikurangi Margin experiences seamount subduction that produces a heterogeneous environment that hosts a range of inter-fingered interplate slip processes. This adds the northern Hikurangi to a short list of regions like the Nicoya Peninsula, Costa Rica, the Boso Peninsula, Japan, and near La Plata Island, Ecuador that experience shallow slow slip and seamount subduction. Due to the shallow, mostly offshore nature of these shallow SSEs, offshore seismic and geodetic experiments are needed to obtain high resolution images of the spatial extent of slow slip, tectonic tremor generation, microseismicity on the plate interface, and the spatial relationship between tremor, seismicity, and subducted seamounts. Using data from the HOBITSS experiment, it is clear that tremor is not only temporally correlated with slow slip as it occurs onshore, downdip of the slip patch, but is collocated with slow slip offshore. We detect two distinct tremor episodes that strongly overlap in space with the locations of two shallow subducted seamounts. The latter of these tremor episodes shows a slow northwest migration across seamount S1. Additionally, the Puketiti patch experiences numerous short-duration slow slip events that are accompanied by prolific bursts of tremor and earthquakes. While northern Hikurangi seamounts appear to primarily subduct aseismically, their subduction may generate elevated pore-fluid pressures and a complex, interconnected fracture network such that during shallow slow slip, tremor and microseismicity may join tsunami

earthquakes as a seismic component of subduction. CFS change calculations show stress increases similar to earthquakes of the same magnitude, but have a near anti-correlation with the location of interplate earthquakes. Most earthquakes on the megathrust occur during the geodetically detected slow slip and are in regions of stress decrease. This detailed investigation into the 2014 Gisborne SSE indicates that the megathrust may be uncoupled or loosely coupled all the way to the trench due to seamount subduction and that the seamounts themselves may experience slow slip, tremor, microseismicity, and large tsunami earthquakes, rupturing the same region in a range of slip processes.

Chapter 3 - Effects of slow slip events on the stress state of the shallow subduction interface along the northern Hikurangi Margin, New Zealand

3.1 Introduction and Motivation

Slow slip events are now well established as an important component of interplate slip processes that release strain in plate boundary environments like global subduction zones [e.g., *Dragert et al.*, 2001; *Kostoglodov et al.*, 2003; *Obara et al.*, 2004; *Brown et al.*, 2005; *Douglas et al.*, 2005; *Ohta et al.*, 2006; *Vallée et al.*, 2013; *Kato and Nakagawa*, 2014; *Borghi et al.*, 2016] transform faults [e.g., *Shelly*, 2009; *Wech et al.*, 2012], and in continental collision zones [*Mendoza et al.*, 2016], as well as beneath volcanic flanks away from plate boundaries [e.g., *Cervelli et al.*, 2002; *Hornbach et al.*, 2015; *Mattia et al.*, 2015]. It is now understood that interplate slip occurs over a wide range of temperature and pressure conditions and a spectrum of slip velocities, spanning aseismic creep at plate convergence rates (cm/yr), slow slip events (cm/day to cm/week), small slow earthquakes such as tremor, low frequency earthquakes and very low frequency earthquakes, large slow earthquakes such as tsunami earthquakes, and fast normal earthquakes (m/s) [e.g., *Ide et al.*, 2007a; *Peng and Gomberg*, 2010]. Slow slip nucleates in the transition zone between velocity weakening and velocity strengthening regions of the plate interface [e.g., *Shibazaki and Iio*, 2003; *Kaproth and Marone*, 2013; *Leeman et al.*, 2015] where slip begins as shear failure like a normal earthquake, but the slip speed is arrested due to a change in

frictional properties, dilatant hardening [e.g., *Segall et al.*, 2010], a build up of pore pressure [e.g., *Ougier-Simonin and Zhu*, 2015], or some combination thereof. In many subduction zones, this transition occurs at depths of 30-50 km, but in northern New Zealand, Costa Rica, Ecuador, and the Boso Peninsula in Japan, slow slip occurs shallowly at depths <15 km [e.g., *Ozawa et al.*, 2003; *Brown et al.*, 2005; *Wallace and Beavan*, 2010; *Vallée et al.*, 2013].

3.1.1 Slow slip along the northern Hikurangi Margin 2010-2016

New Zealand is located along the complex boundary between the Australian and Pacific Plates. The Hikurangi Plateau, an over-thickened large igneous province of Cretaceous age [*Davy and Wood*, 1994; *Strong*, 1994; *Wood and Davy*, 1994; *Mortimer and Parkinson*, 1996], subducts westward beneath the North Island with near trench-perpendicular subduction in the north and highly oblique subduction in the south near the Chatham Rise (Figure 3–1). The Australian-Pacific boundary continues along the west coast of the South Island as the Alpine Fault, a right-lateral transpressional fault, to the Puysegur Trench where the Australian Plate obliquely subducts beneath the Pacific Plate. Slow slip events (SSEs) have been observed along the entire Hikurangi Margin and along the central Alpine Fault [e.g., *Douglas et al.*, 2005; *Beavan et al.*, 2007; *Wallace et al.*, 2012a; *Wech et al.*, 2012].

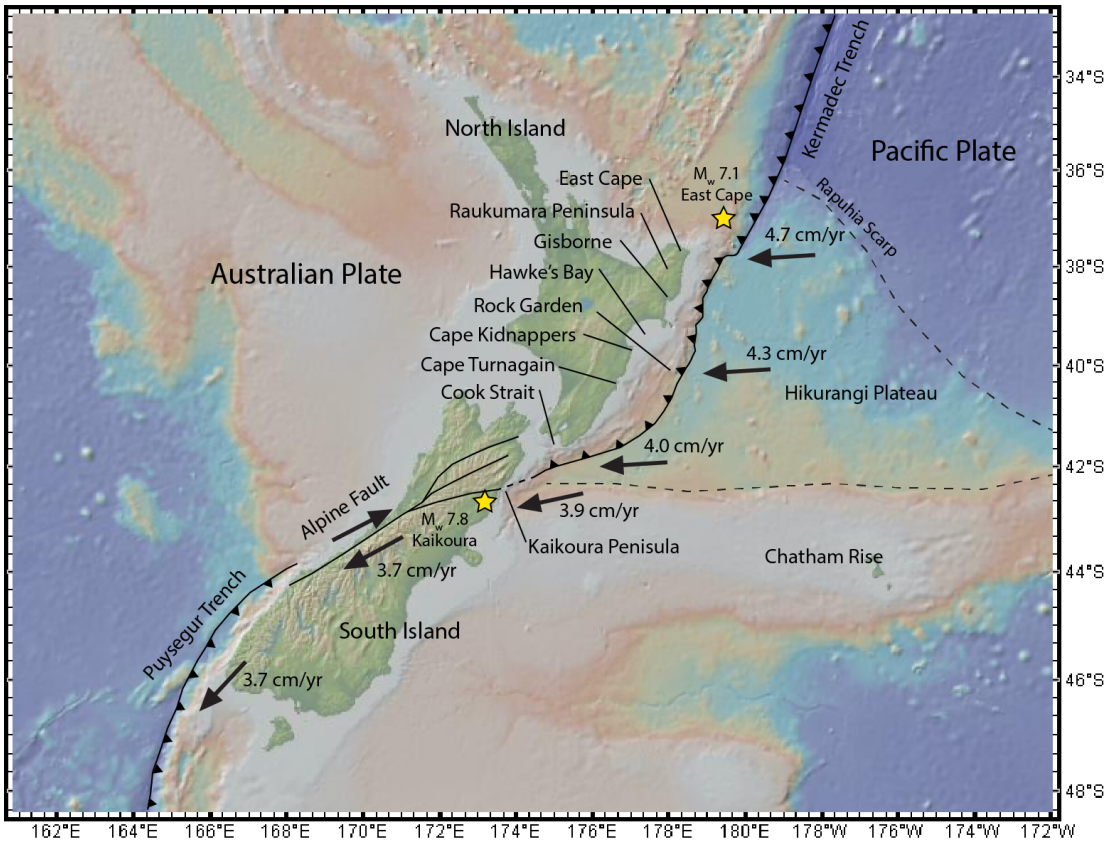

Figure 3–1. New Zealand-wide tectonic setting.
New Zealand tectonic setting showing the subduction of the seamount studded Hikurangi Plateau beneath the North Island, the transpressional Alpine Fault through the South Island, and the highly oblique Puysegur Trench with underthrusting of the Australian Plate in the south. Yellow stars represent the epicentral locations of two $M_w > 7$ earthquakes in 2016.

Geodetic observations indicate that the Hikurangi Margin experiences a sharp along-strike change in plate coupling and slow slip behavior around Cape Turnagain with off-shore shallow, weak coupling to the north and strong coupling in the south down to depths of 25-30 km [*Wallace and Beavan*, 2006; *Beavan et al.*, 2007; *Wallace and Beavan*, 2010]. Down dip of this locked zone in the south, the southern Hikurangi experiences slow slip at depths of 35-60 km with 12 to 18 month duration

every ~5 years [*Wallace and Beavan*, 2010; *Wallace et al.*, 2012a]. In contrast, the northern Hikurangi experiences slow slip at shallow depths <15 km with 1 to 3 week duration every 18-24 months. Slow slip behavior varies along strike between East Cape and Hawke's Bay with frequent, small events in the north and less frequent, larger events in the south (Figure 3–2). The largest SSEs along the northern Hikurangi occur in the Gisborne patch with moderate events (M_w ~6.5) every 18-24 months and larger events (M_w ~6.8) every ~4 years [*Wallace and Beavan*, 2010].

There is great interest in the connection between slow slip events and regular earthquakes on faults. In recent years, precursory relationships have been demonstrated around the world where SSEs have immediately preceded large earthquakes near their hypocenters [e.g., *Murakami et al.*, 2006; *Segall et al.*, 2006; *Reyners and Bannister*, 2007; *Iinuma et al.*, 2009; *Kato et al.*, 2012; *Ito et al.*, 2013; *Ruiz et al.*, 2014; *Radiguet et al.*, 2016]. Similarly, it has long been understood that aseismic slip frequently occurs within or adjacent to the mainshock rupture patch for days to years after large earthquakes [e.g., *Savage and Church*, 1975; *Marone et al.*, 1991; *Heki et al.*, 1997; *Freed*, 2005]. Thus, SSEs triggered by earthquakes may be one mechanism in a spectrum of afterslip processes. There is also documentation of slow slip events being triggered at regional or teleseismic distances [*François-Holden et al.*, 2008; *Itaba and Ando*, 2011; *Zigone et al.*, 2012]..

Figure 3–2. Northern Hikurangi cGPS timeseries: 2010-2016.
Easting component of continuous GPS (cGPS) timeseries with displacement in mm along the northern Hikurangi Margin for five patches that experience frequent slow slip for 2010-2016. Transients are located in the shaded boxes. Coulomb stress changes are calculated for labeled SSEs in the Tolaga Bay, Gisborne, Mahia, and Hawke's Bay patches. The vertical solid black lines indicate origin times for the 2016 East Cape and Kaikoura earthquakes

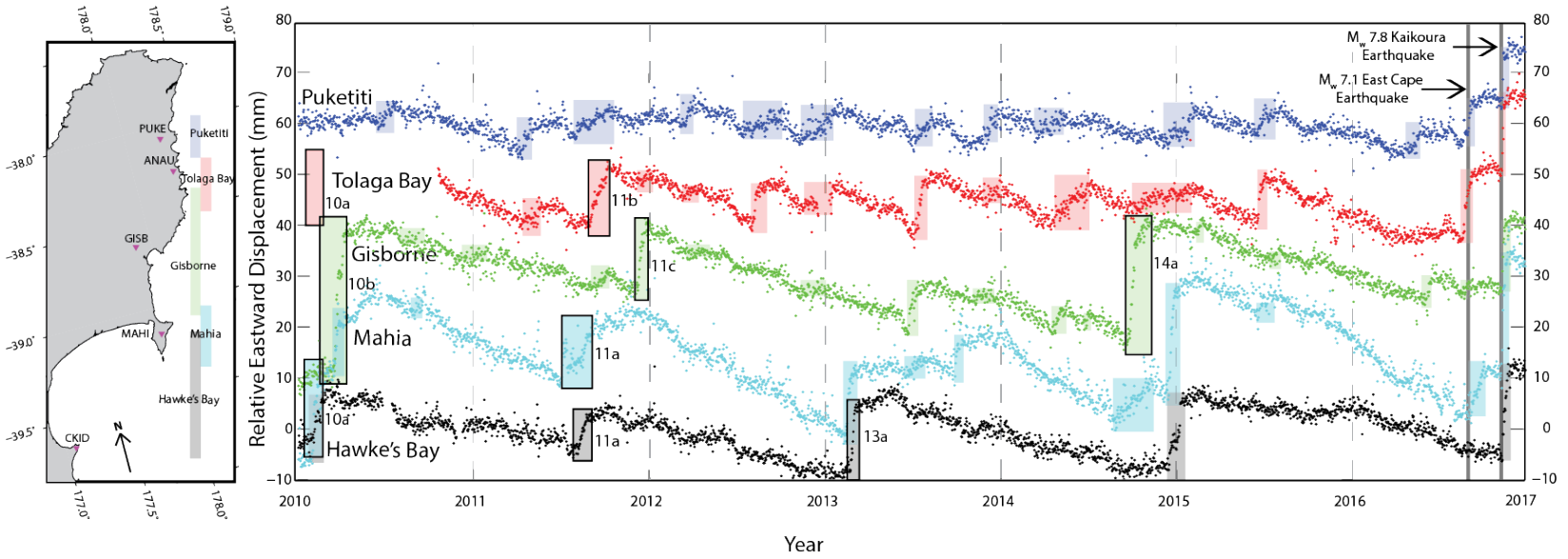
178.0°
178.5°
179.0°
PUKE
Puketiti
ANAU
Tolaga Bay
GISB
Gisborne
MAHI
Mahia
Hawke's Bay
CKID
N
-38.0°
-38.5°
-39.0°
-39.5°
177.0°
177.5°
178.0°
Relative Eastward Displacement (mm)
Year
Puketiti
Tolaga Bay
Gisborne
Mahia
Hawke's Bay
10a
10b
10a
11b
11c
11a
11a
13a
14a
M$_w$ 7.8 Kaikoura Earthquake
M$_w$ 7.1 East Cape Earthquake
2010
2011
2012
2013
2014
2015
2016
2017

Hikurangi Margin SSEs have also been shown to have relationships with moderate to large local and regional earthquakes. Recently along the Hikurangi Margin the 2016 East Cape earthquake (Figure 3–1) initiated slow slip in the Puketiti patch and may have arrested an ongoing slow slip event in the Tolaga Bay patch (Figure 3–2). A dramatic example of SSEs being dynamically triggered by a regional earthquake is for the November 2016 Kaikoura earthquake which initiated simultaneous SSEs along the entire Hikurangi Margin in regions of prior SSEs (Figure 3–2). These spatial and temporal relationships between slow slip and earthquakes demonstrate that in addition to the transfer of static stresses, dynamic stresses play a crucial role in the initiation or termination of SSEs. The earthquake-SSE interaction along the North Island supports previous findings that the northern Hikurangi Margin is weakly coupled and close to failure for slip in SSEs [e.g., *Beavan et al.*, 2007].

The plate interface and upper plate in the northern Hikurangi segment is likely composed of a network of fractures around and in the wake of numerous subducted seamounts as discussed in Chapter 2 [e.g., *Wang and Bilek*, 2014]. Seismic reflection profiles show the location of at least three prominent subducted seamounts trenchward of the North Island [*Barker et al.*, 2009; *Bell et al.*, 2010]. In a detailed analysis of these shallowly subducted seamounts (S1, S2, and S3; Figure 3–3), *Bell et al.* [2010] identify three regions of high amplitude interface reflectivity in the Hawke's Bay, Gisborne, and Tolaga Bay slow slip patches (HRZ-HB, HRZ-G, HRZ-TB; Figure 3–3) at the leading (downdip) edge of these seamounts and interpret them

to be zones of overpressured fluid-entrained sediments. Based on their analysis, it follows that HRZ regions may exist downdip of many shallowly subducted seamounts. Frequent moderate slow slip events occur within and around HRZ-HB, HRZ-G, and HRZ-TB. Additionally, tremor and earthquakes occur around these regions with tremor occurring downdip of HRZ-G and HRZ-TB [*Todd and Schwartz*, 2016], along the coast in the Puketiti patch north of HRZ-TB, and updip of HRZ-G over seamount S1 (Chapter 2), and earthquakes occurring primarily downdip of all three HRZ regions.

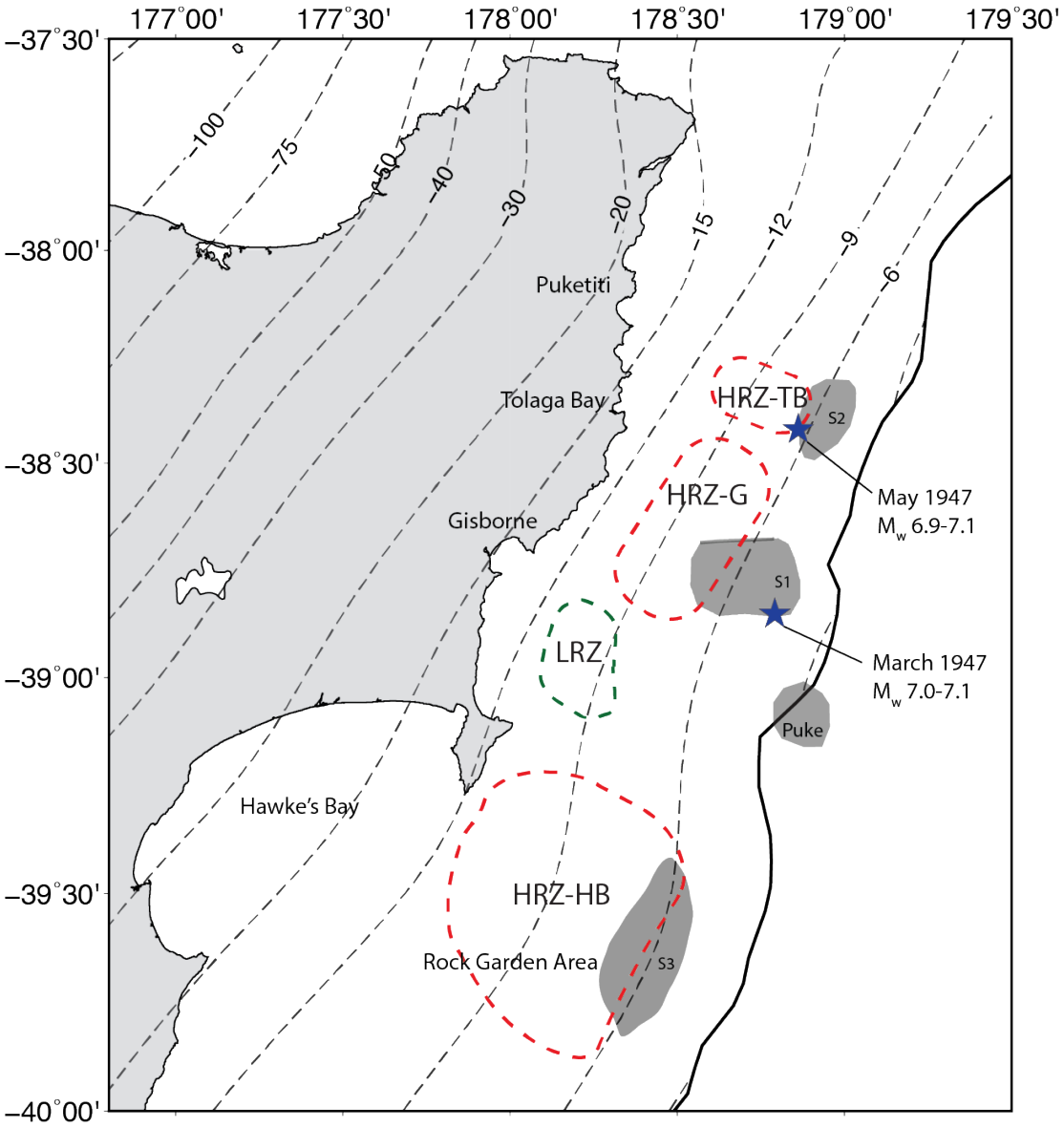

Figure 3–3. Northern Hikurangi subducted seamounts.
Subducted seamounts and associated high amplitude interface reflectivity (HRZ) and lower amplitude (LRZ) regions [*Bell et al.*, 2010] are depicted with plate interface depth contours in km [*Williams et al.*, 2013]. The epicentral locations of two tsunami earthquakes are plotted as blue stars [*Bell et al.*, 2014].

Tectonic tremor accompanies most, if not all, slow slip events along the northern Hikurangi Margin [*Kim et al.*, 2011; *Todd and Schwartz*, 2016], but is most

extensively associated with slip events in the Gisborne and Puketiti patches (Figure 3–2). Elevated seismicity levels also accompany these slow slip events with earthquakes predominately located near the edges of the geodetically detected slow slip distribution [*Delahaye et al.*, 2009; *Jacobs et al.*, 2016]. While the Gisborne patch has been the subject of numerous studies [e.g., *Wallace and Beavan*, 2010; *Wallace et al.*, 2016], the less investigated Puketiti patch experiences frequent small eastward transients interpreted to be small slow slip events (Figure 3–2). These events are frequently accompanied by prolific tremor and earthquake episodes and may indicate the presence of a yet to be directly imaged subducted seamount (Chapter 2). To elucidate the relationship between tremor, earthquakes, and shallow slow slip, as well as how the occurrence of frequent slow slip events affects the stress state of the megathrust over time, we calculate the changes in Coulomb failure stress imparted on the plate interface by seven SSEs between 2010-2014. By identifying regions of stress change over time with respect to earthquake activity, we seek to understand the role of slow slip in loading the megathrust throughout the slow slip and earthquake cycle.

3.2 Data and Methods

3.2.1 Error estimation in tremor and earthquake locations

3.2.1.1 Tremor location

Following the methods of *Todd and Schwartz* [2016] tremor presented in this study is detected using a modified version of the automated envelope cross-

correlation technique [*Wech and Creager*, 2008] with seismic data from 19-25 New Zealand National Seismic Network stations (operated and maintained by GeoNet; www.geonet.org.nz). Tremor is located through a 3-D grid search method that minimizes S wave travel times between potential source locations and correlated station pairs. Between the location process and the spatial and temporal clustering requirements, the location of groups of tremor event clusters are robust, but any interpretations that rely on spatial patterns of individual tremor event locations are not robust at length scales less than 10 km or outside of our 0.05-0.15° epicentral error estimate.

3.2.1.2 Earthquake location

Earthquakes presented in this study are from two sources, the New Zealand National Seismic Network earthquake catalog for earthquakes between 2010-2014 and manually detected earthquakes from ocean bottom stations as part of the Hikurangi Ocean Bottom Investigation of Tremor and Slow Slip (HOBBITS) experiment as summarized in Chapter 2 for September and October 2014. These earthquakes are all relocated with NonLinLoc, a probabilistic non-linear earthquake location program [*Lomax et al.*, 2000] that calculates the maximum likelihood hypocenter over a 3-D grid search.

3.2.2 Coulomb failure stress calculations

To understand the stress perturbation impact of SSEs on the subduction interface we compute the Coulomb failure stress (CFS) for seven well-characterized

SSE's between 2010 and 2014 (Table 3–1). CFS change analysis has been extensively used to interpret the locations of aftershocks in earthquake sequences [e.g., *Harris and Simpson*, 1992; *Stein et al.*, 1992; *Harris*, 1998; *Toda et al.*, 1998; *Stein*, 1999; *Toda and Stein*, 2003]. The change in CFS is defined as

$$\Delta CFS = \Delta\tau - \mu(\Delta\sigma_n - \Delta p) \quad (1)$$

where $\Delta\tau$ is the change in shear stress, $\Delta\sigma_n$ is the change in normal stress, and Δp is the change in pore fluid pressure.

Table 3–1. Slow slip events used in Coulomb failure stress change calculations

Event[1]	**Location**	**Peak CFS increase (kPa)**	**Peak CFS decrease (kPa)**	**Source of geodetic slip distribution**
10a	Tolaga Bay & Mahia	43	208	*Wallace and Beavan* [2010]
10b	Gisborne	73	293	*Wallace and Beavan* [2010]
11a	Mahia	15	44	*Wallace et al.* [2012a]
11b	Tolaga Bay	15	99	*Wallace et al.* [2012a]
11c	Gisborne	27	62	*Wallace et al.* [2012a]
13a	Hawke's Bay	84	278	*Wallace and Eberhart-Phillips [2013]*
14a	Gisborne	182	384	*Wallace et al.* [2016]

[1]Event labels correspond to Figure 3–2.

In this study, the change in CFS for slow slip events on the northern Hikurangi Margin is computed using the following procedure. Initially, slip on the

plate interface for the SSEs in Table 3–1 previously determined by inversion of horizontal and vertical cGPS displacements in a homogeneous velocity model [see *Wallace and Beavan*, 2010; *Wallace et al.*, 2012a, 2016; *Wallace and Eberhart-Phillips*, 2013 for geodetic slip inversion methodology] is placed onto a more detailed interface geometry mesh [*Williams et al.*, 2013] with a bilinear interpolation. The slip distribution is smoothed over a finite length scale (10 km) to minimize the effects of stress singularities where there are strong gradients in the slip distribution. This interpolated geodetically determined slip distribution forms the initial slip condition for each vertex on the fault.

Next, we use the initial slip conditions and prescribed material properties, an elastic half-space [e.g., *Okada*, 1985, 1992] and homogeneous velocity model, as input parameters to our finite-element model. Using PyLith [*Aagaard et al.*, 2013, 2016], a finite-element code designed for the solution of tectonic problems, we use the displacement boundary conditions to compute the traction change for each element in the fault mesh [*Aagaard et al.*, 2016]. The computed traction changes are then used to calculate the change in Coulomb failure stress. To preserve self-similarity between the input slip conditions and the PyLith-computed slip, we ensure that the detailed fault mesh used for the finite-element slip inversion contains the original rectangular course mesh used in the initial geodetic slip inversions.

Williams and Wallace [2015] demonstrate the importance and efficacy of utilizing realistic material properties such as the New Zealand wide 3-D seismic velocity model [*Eberhart-Phillips et al.*, 2010] in geodetic slip inversions and find

that for shallow offshore SSEs where cGPS observations are located away from the slip patch, homogeneous half space models may underestimate the amount of slip and therefore underpredict the size of the event. The Williams and Wallace study highlights the need for more realistic subduction interface geometries and material properties for future slow slip modeling. These methods are currently being tested as part of an ongoing study utilizing realistic material properties to produce slip inversions and compute resultant CFS changes. In this study, however, we use a homogeneous velocity structure consistent with the original slip inversions and investigate the affect of different pore pressure response modes on CFS changes [*Beeler et al.*, 2000].

For the northern Hikurangi Margin, numerous studies have investigated and quantified the subduction interface geometry [e.g., *Barker et al.*, 2009; *Williams et al.*, 2013] and spatial extent of interface properties based on seismic reflection data [e.g., *Eberhart-Phillips and Reyners*, 1999; *Reyners et al.*, 1999; *Eberhart-Phillips and Chadwick*, 2002; *Eberhart-Phillips et al.*, 2005; *Bassett et al.*, 2010; *Bell et al.*, 2010; *Eberhart-Phillips et al.*, 2010, 2013; *Bassett et al.*, 2014; *Eberhart-Phillips and Bannister*, 2015; *Ellis et al.*, 2015]. This wide body of research in concert with numerous past (and future planned) marine geophysical experiments such as the HOBITSS experiment makes the northern Hikurangi Margin an exceptional location to model shallow slow slip with variations in frictional properties. CFS calculations were conducted with the constant apparent friction and isotropic poroelastic pore pressure response models outlined in *Beeler et al.* [2000].

Using the traction changes from the finite-element model, we calculate the shear and normal stresses across the fault. Shear stresses are computed for each element by projecting the traction changes onto the plate convergence direction as determined by crustal block rotation poles in *Wallace et al.* [2012b] and normal stresses are computed for each element in the fault mesh. *Beeler et al.* [2000] stressed the importance of not exclusively using a constant apparent friction model in CFS studies because it could lead to errors in predicted stress changes. As a result, we applied each pore pressure response model identified by *Beeler et al.* [2000], the constant apparent friction model and the isotropic poroelastic model, to our CFS calculations. The constant apparent friction model assumes that pore pressure changes can be combined with friction into the apparent frictional parameter, μ', and assumes that μ' is a material constant such that the change in Coulomb stress can be represented by

$$\Delta CFS = \Delta\tau - \mu'\Delta\sigma_n \tag{2}$$

and

$$\mu' = \mu(1 - B) \tag{3}$$

where B is Skempton's coefficient. The assumption that μ' is a material constant only holds if stress-induced changes in pore fluid pressure are proportional to the change in normal stress. As a result, this model may misrepresent the relationship between fault strength and pore fluid pressure changes in earthquakes.

The isotropic poroelastic model allows the apparent friction to change with location and fault orientation such that

$$\Delta CFS = \Delta\tau - \mu(\Delta\sigma_n - B\Delta\sigma_m) \quad (4)$$

where $\Delta\sigma_m$ is the change in mean stress and is related to changes in pore pressure by $\Delta p = B\Delta\sigma_m$. In this model μ' is not a material constant and allows changes in pore pressure to be proportional to changes in mean stress across the fault surface.

Figure 3–4 shows the effects of using the constant apparent friction model compared to the isotropic poroelastic model. The difference between the constant apparent friction and isotropic poroelastic models is only 1-2%, but we present results from the isotropic poroelastic model since the apparent frictional parameter, μ', should not be treated as a material constant and should vary based on the changes in mean stress across the fault.

Figure 3–4. Coulomb failure stress change results for the 2010 Gisborne SSE. Coulomb failure stress change results exploring the effects of various pore pressure response models from *Beeler et al.* [2000] for the large 2010 Gisborne SSE (Event 10b). The first two panels represent the CFS calculation for each pore pressure response model and the last panel shows the difference between the constant apparent friction and isotropic poroelastic pore pressure response models.

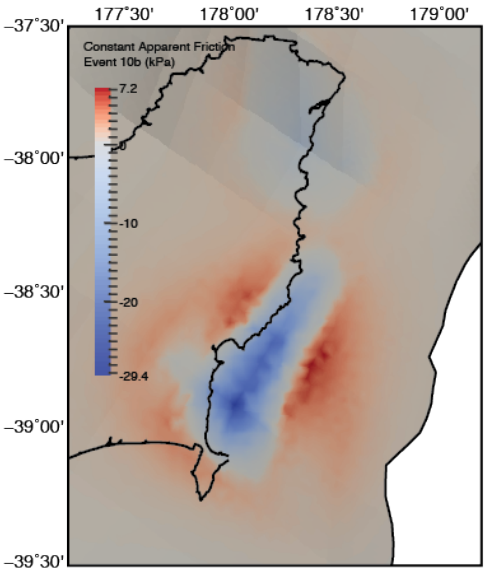

Constant Aparent Friction

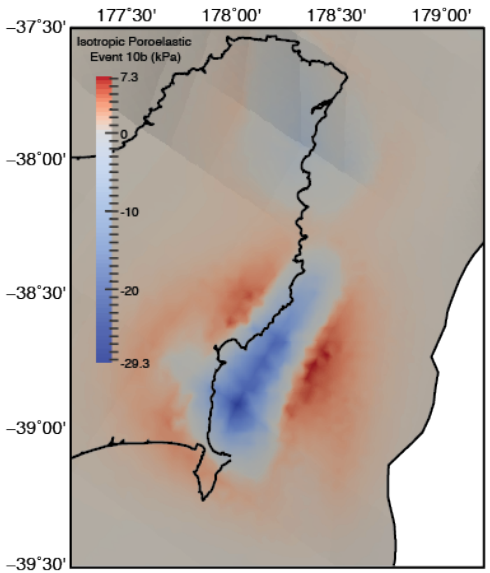

Isotropic Poroelastic

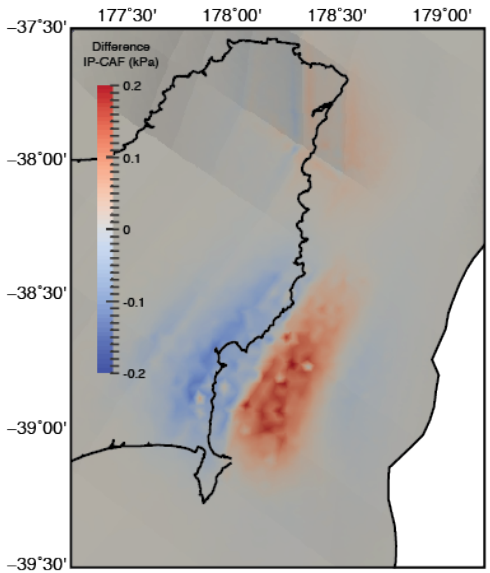

Difference (IP-CAF)

3.3 Results and Discussion

3.3.1 Coulomb failure stress from select SSEs 2010-2014

We compute the change in Coulomb failure stress associated with seven SSEs along the northern Hikurangi Margin between 2010-2014 (Figure 3–5). In 2010 and 2011, the SSEs are part of sequences that migrate along the margin, and the 2013 Mahia/Hawke's Bay SSE is part of the southern extent of shallow slow slip along the northern Hikurangi Margin. In 2014, the HOBITSS experiment was conducted to obtain near-source observations of a shallow SSE to constrain the spatial extent of slow slip and to search for offshore tremor and seismicity as summarized in Chapter 2. All CFS change results presented are based on the isotropic poroelastic pore pressure response model.

Figure 3–5. Minimum and maximum Coulomb failure stress changes imparted on plate interface from seven SSEs between 2010-2014.
SSEs correspond with labeled events in Figure 3–2. Dark red regions represent the greatest stress increase and dark blue regions represent the greatest stress decrease for each event as listed in Table 3–1. Interface depth contours (in km) [*Williams et al.*, 2013] and subducted seamounts Puke, S1, S2, and S3 are plotted for reference [*Bell et al.*, 2010].

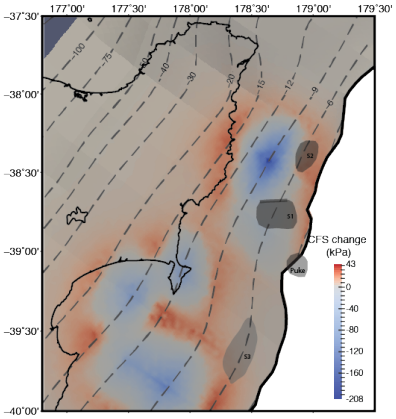

10a: Mahia & Tolaga Bay

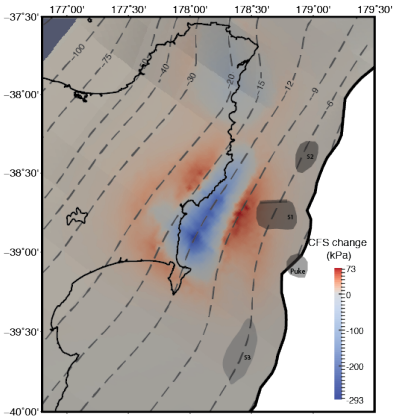

10b: Gisborne

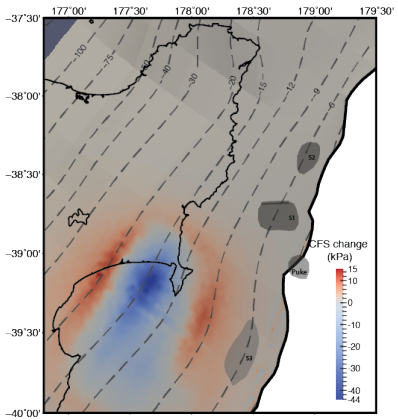

11a: Mahia & Hawke's Bay

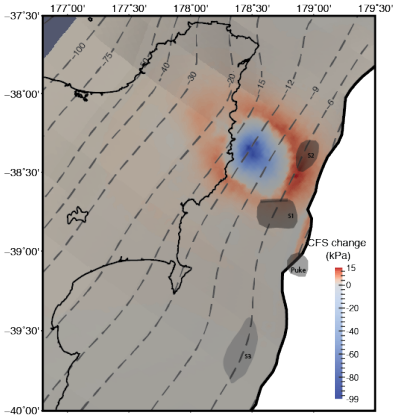

11b: Tolaga Bay

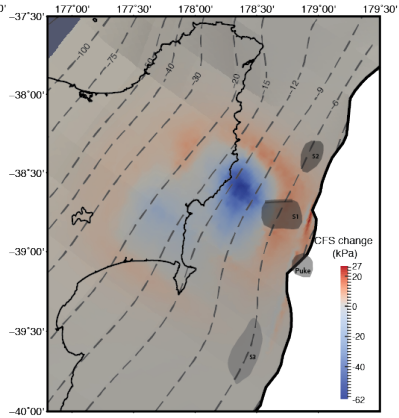

11c: Gisborne

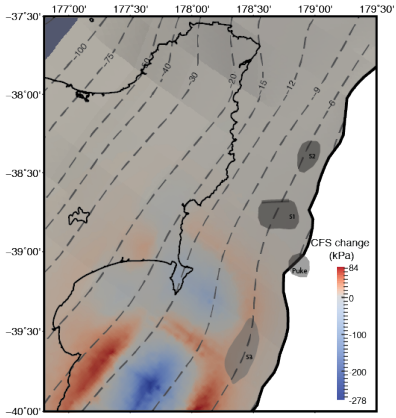

13a: Mahia & Hawke's Bay

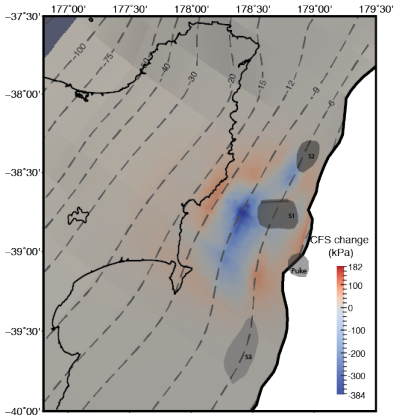

14a: Gisborne

3.3.1.1 Gisborne SSEs

The largest SSEs (equivalent M_w ~6.7-6.8) along the northern Hikurangi occur in the Gisborne patch. Figure 3–6 illustrates the slip distribution and change in CFS imparted on the megathrust by the large 2010 and 2014 Gisborne SSEs (10b and 14a from Figure 3–2). The slip distribution from the 2010 SSE is determined with land-based cGPS stations [*Wallace and Beavan*, 2010] and the distribution of the 2014 SSE is determined from land-based cGPS and ocean-bottom absolute pressure gauges from the HOBITSS experiment [*Wallace et al.*, 2016]. While this difference affects the resolution of the updip extent of the geodetically inverted slip near the trench, both the 2010 and 2014 large Gisborne SSEs rupture inside and adjacent to the HRZ-G region, downdip of seamount S1 (Figure 3–6). In addition to large SSEs every 4-5 years (Event 10a peak CFS increase 73 kPa and peak CFS decrease 293 kPa; event 14a peak CFS increase 182 kPa and peak CS decrease 384 kPa), the Gisborne patch also hosts moderate sized SSEs every 18-24 months (Event 11c peak CFS increase 27 kPa and peak CFS decrease 62 kPa; Figure 3–2). Between 2010 and 2016, the 2010 and 2014 large events are accompanied by moderate events in December 2011, July 2013, July 2016, and November 2016 in response to the M_w 7.8 Kaikoura earthquake.

Figure 3–6. Slip and CFS changes from the 2010 and 2014 large Gisborne SSEs. Slip from the 2010 (a) and 2014 (c) large Gisborne SSEs. Dark orange regions represent slip >10 cm. Positive (red) and negative (blue) Coulomb failure stress changes from the 2010 (b) and 2014 (d) Gisborne SSEs. Dark red regions represent CFS increase >50 kPa and dark blue regions represent CFS decrease >200 kPa. The 2010 event has a peak CFS increase of 43 kPa and a peak decrease of 208 kPa. The 2014 event has a peak CFS increase of 182 kPa and a peak decrease of 384 kPa (Table 3–1). The primary slip region for the 2014 event is located trenchward of the slip region for the 2010 event, though the difference may be due to the use of ocean-bottom absolute pressure gauges from the HOBITSS experiment in the slip distribution inversion, and therefore higher resolution of the updip extent of slip.

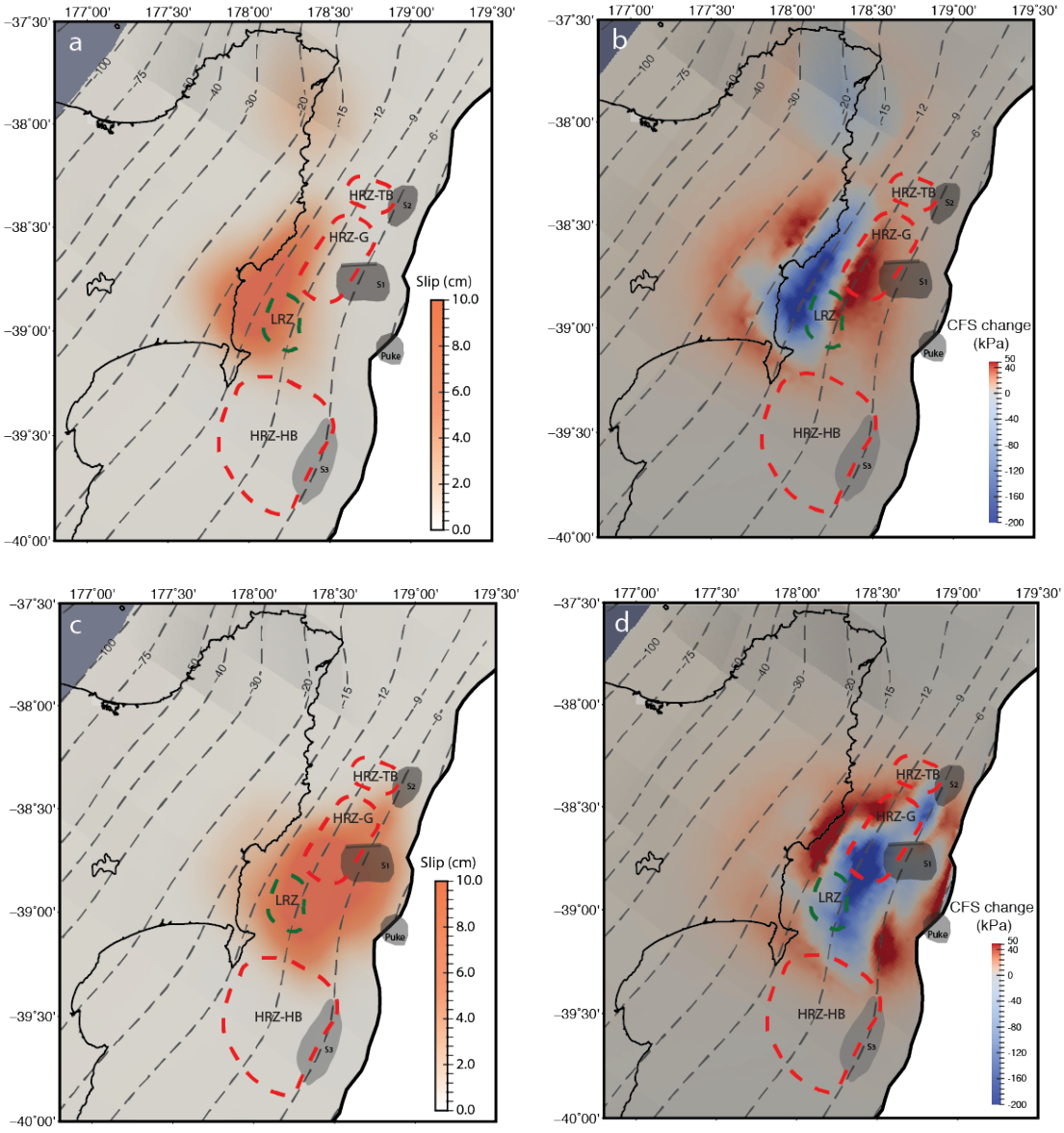
a
b
c
d
177°00'
177°30'
178°00'
178°30'
179°00'
179°30'
-37°30'
-38°00'
-38°30'
-39°00'
-39°30'
-40°00'
HRZ-TB
HRZ-G
HRZ-HB
LRZ
S1
S2
S3
Puke
Slip (cm)
10.0
8.0
6.0
4.0
2.0
0.0
CFS change
(kPa)
50
40
0
-40
-80
-120
-160
-200

Gisborne SSEs often occur immediately before or after SSEs in the neighboring Mahia and Tolaga Bay patches [*Wallace and Beavan*, 2010; *Wallace et al.*, 2012a] and are associated with tectonic tremor [*Kim et al.*, 2011; *Todd and Schwartz*, 2016] and increased seismicity levels [*Delahaye et al.*, 2009; *Jacobs et al.*, 2016]. Figure 3–7 shows the total slip for 2010 (a) and 2011 (d) from slow slip events in the Mahia, Tolaga Bay, and Gisborne patches and accompanying tremor and earthquakes. In 2010, near simultaneous SSEs in the Mahia and Tolaga Bay patches (Event 10a peak CFS increase 43 kPa and peak CFS decrease 208 kPa) preceded the largest recorded SSE in the Gisborne patch (events 10a and 10b; Figure 3–2). In 2011, a series of SSEs migrated up the east coast from Cape Turnagain to Tolaga Bay (events 11a, 11b, and 11c; Figure 3–2) suggesting that stress transfer plays an integral role in the occurrence of northern Hikurangi slow slip [*Wallace et al.*, 2012a]. First, a moderate SSE occurred in the Mahia patch in late August and was immediately followed by a SSE in the Tolaga Bay patch in early September, some 80 km away. While it is difficult to quantify the stress change between events 11a and 11b with this methodology (Figure 3–7e), the two events produced a combined CFS increase of 5-10 kPa in the Gisborne patch. Three months later, a moderate sized Gisborne SSE occurred in December. The distribution of HRZ regions and their trenchward bounding seamounts presented in *Bell et al.* [2010] overlap with the 2011 Tolaga Bay (September) and Gisborne (December) SSEs and are adjacent to the 2011 Mahia/Hawke's Bay (August) SSE (Figure 3–7). In both cases, the SSEs in the Mahia and Tolaga Bay patches loaded the Gisborne patch by 20-25 kPa in 2010 and 5-8 kPa

in 2011 and were followed by moderate-large Gisborne SSEs as shown in Figure 3–7. In 2014, this pattern occurs again with slip in the Mahia patch (August/September) preceding a large SSE in the Gisborne patch in September/October (Figure 3–8).

Tremor detections for the 2010 and 2011 SSEs (green circles; Figure 3–7a and 7d) are primary located on land, downdip of the slip patches [*Todd and Schwartz*, 2016] in regions of CFS increase. The low amplitude tremor signal and highly attenuating upper plate make offshore tremor nearly impossible to detect with a land-based seismic network. The majority of onshore tremor detected with northern Hikurangi SSEs is associated with the Gisborne and Puketiti patches and tends to repeat in the same location for each event. Figure 3–7 shows that tremor is more abundant for the large 2010 Gisborne SSE with distributed CFS increases >50 kPa and a peak CFS increase of 73 kPa when compared to the smaller 2011 Gisborne SSE with a peak CFS increase of 27 kPa. Similarly, the 2010 SSEs have more associated seismicity (black circles; Figure 3–7) than the smaller 2011 SSEs, suggesting that SSEs may require CFS increases on the order of several 10s of kPa to produce prolific onshore tremor episodes and notable increases in seismicity.

Figure 3–7. Cumulative slip and CFS changes for 2010 and 2011 SSEs.
(a) Cumulative slip for events 10a and 10b with associated tremor (green circles) and relocated earthquakes (black circles). (b) CFS changes for the 2010 Mahia and Tolaga Bay SSEs (event 10a) showing CFS increase (white number) in the Gisborne patch with the extent of slip for event 10b. (c) Cumulative CFS changes for the 2010 Mahia and Tolaga Bay SSEs and the 2010 Gisborne SSE (event 10b) with the extent of slip for event 10b. The total CFS decrease in the Gisborne patch is in white. (d) Cumulative slip for events 11a, 11b, and 11c with associated tremor (green circles) and relocated earthquakes (black circles). (e) Cumulative CFS for the 2011 Mahia (event 11a) and Tolaga Bay (event 11b) SSEs showing a minimal stress increase (white number) in the Gisborne patch with the extent of slip for event 11c. Note the different scale between the 2010 and 2011 CFS changes; the 2011 events are smaller in magnitude than the 2010 events (Table 3–1). (f) Cumulative CFS for events 11a, 11b, and 11c with the extent of slip for event 11c. The total CFS decrease in the Gisborne patch is in white. Similar to 2010, Mahia and Tolaga Bay SSEs loaded the Gisborne patch and the subsequent Gisborne SSE filled in the gap, leading to a decrease in CFS along the entire northern margin.

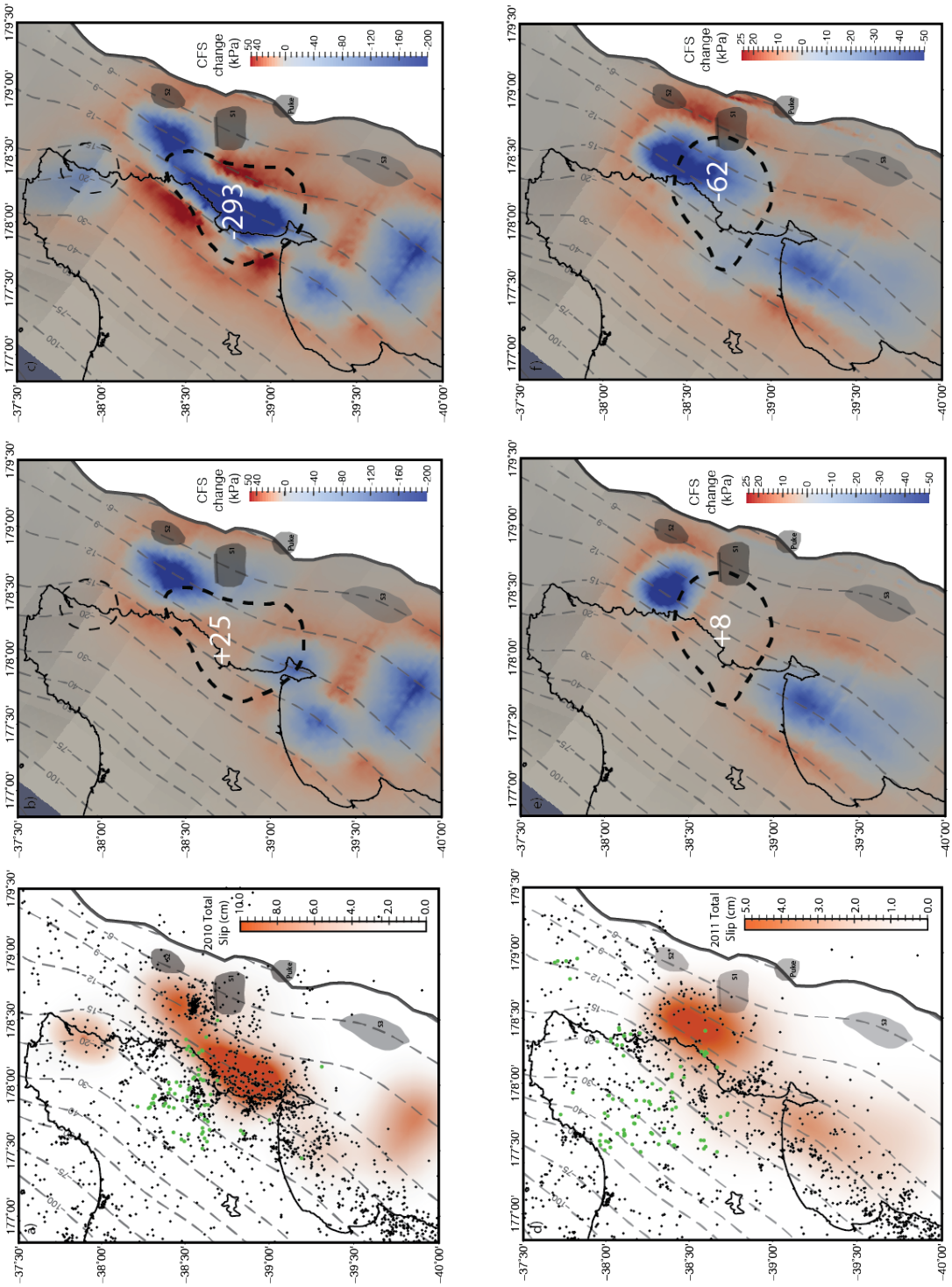
a)
2010 Total Slip (cm)
10.0
8.0
6.0
4.0
2.0
0.0
b)
CFS change (kPa)
+25
c)
CFS change (kPa)
-293
d)
2011 Total Slip (cm)
5.0
4.0
3.0
2.0
1.0
0.0
e)
CFS change (kPa)
+8
f)
CFS change (kPa)
-62
Puke
S1
S2
S3
-37°30'
-38°00'
-38°30'
-39°00'
-39°30'
-40°00'
177°00'
177°30'
178°00'
178°30'
179°00'
179°30'

Figure 3–8. Spatiotemporal evolution of slow slip along the northern Hikurangi margin 2010-2013.
Coulomb failure stress calculations for six SSEs (10a-13a; Table 3–1) with respect to the extent of slip (black dashed line) for the subsequent SSE. Color saturation is based on the smallest event (11a) to illustrate the relative magnitudes of the SSEs. Dark red regions represent CFS increase of >15 kPa and dark blue regions represent CFS decrease of <44 kPa. Events 10a-11c occur sequentially and the maximum CFS increase (kPa) within the subsequent slip patch is shown in white. Additional SSEs occurred between events 11c and 13a as well as events 13a and 14a, so peak CFS in the subsequent slip patch is not included for these events. In nearly every case, the next SSE is immediately adjacent to the previous event with minimal overlap. The Mahia and Tolaga Bay patches are an exception as they can slip simultaneously (event 10a) or in immediate succession (events 11a and 11b).

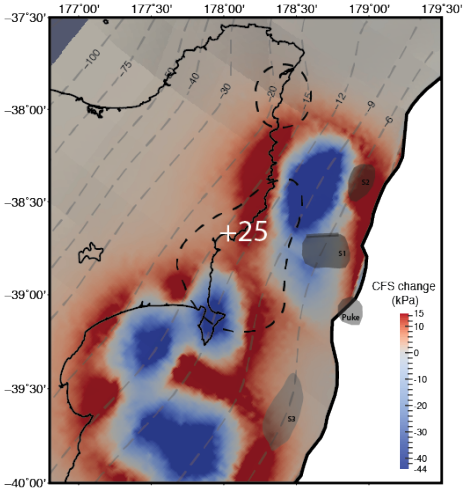

10a CFS with 10b slip outline

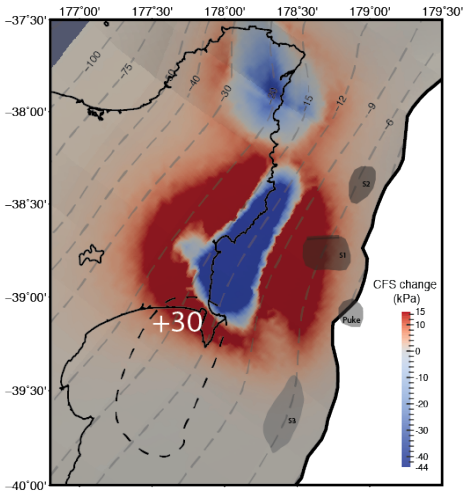

10b CFS with 11a slip outline

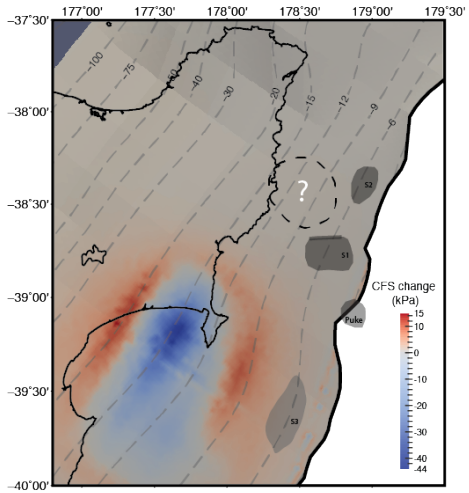

11a CFS with 11b slip outline

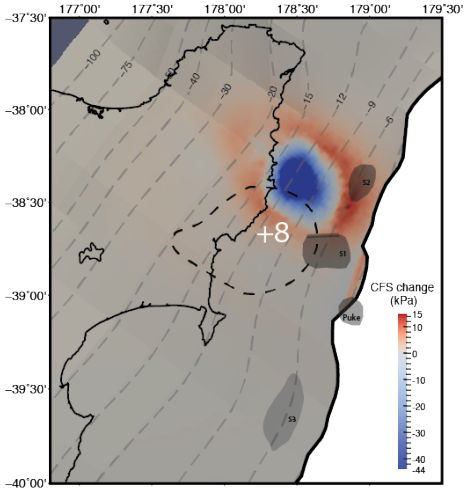

11b CFS with 11c slip outline

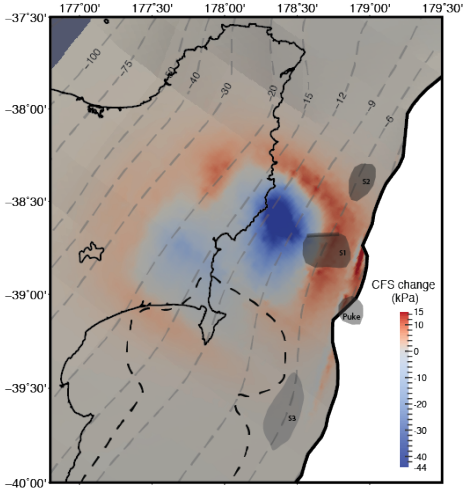

11c CFS with 13a slip outline

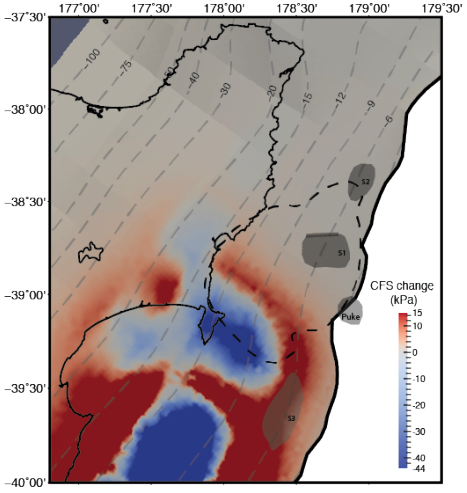

13a CFS with 14a slip outline

CFS changes have a clear impact on the spatiotemporal migration of SSEs on the northern Hikurangi Margin. Figure 3–8 illustrates the CFS for events 10a-13a (Table 3–1) with an outline of the slip extent for the subsequent event. In nearly every example, the two SSEs are immediately adjacent to each other, which suggests that CFS increases from the previous event helped to nucleate the subsequent event. For events 10a-11c, the CFS increase ranges from 8 to 25 kPa in the subsequent slip patch (Figure 3–8) indicating that a low CFS increase is required to help initiate the next SSE. Additionally, the subsequent events do not re-rupture regions of CFS decrease from the previous event. This is especially observed for events 10a-11c (Figure 3–8) that occur sequentially. Exceptions include the Mahia and Tolaga Bay patches that can have simultaneous SSEs or occur in immediate succession. While the underlying mechanism for this phenomenon is unclear, even minor changes in stress from each SSE over time appears to influence the location of the subsequent SSE.

While the large Gisborne SSEs rupture the entire Gisborne patch between the Mahia Peninsula in the south and Tolaga Bay in the north (Figure 3–6), a distance of ~80 km, the small Gisborne SSEs appear to only rupture the northern section of the patch near HRZ-G (event 11c; Figure 3–5). Assuming this is true for most moderate Gisborne SSEs, the remainder of the slip patch and the region adjacent to seamounts S1 and S2 experiences a CFS increase of over 60 kPa over time from neighboring SSEs (events 10a-13a) as illustrated in Figure 3–7 before rupturing in a large event. Over our study period, this increase in CFS is primarily accommodated by subsequent SSEs (Figure 3–8), but if loading continues over a longer interseismic period,

sufficient strain would be accumulated to rupture in a moderate-sized earthquake like the tsunami earthquakes of 1947. While plate convergence provides a steady supply of strain, the presence of subducted seamounts and frequent slow slip appears to release most strain on the interface. This corroborates previous geodetic results from *Wallace and Beavan* [2010] that suggest shallow SSEs along the northern Hikurangi release nearly all of the accumulated strain over time. If most of the strain accumulated from plate convergence is accommodated by slow slip, it is unlikely that great earthquakes ($M_w > 8$) can nucleate in the Gisborne patch. Events 10a-14a produce a total CFS increase of 125 kPa in the shallowest part of the plate interface adjacent to seamount S1 where the March 1947 tsunami earthquake originated. Although long-term shallow strain accumulation cannot be resolved from this study, future investigations into the shallowest part of the plate interface, including planned drilling expeditions that will install borehole observatories to monitor physical, hydrologic, and chemical processes throughout the Gisborne SSE cycle, will better constrain any long-term strain accumulation that could rupture in future 1947-style earthquakes.

3.3.2 Effects of SSEs on the shallow subduction interface

An important outstanding question is how SSEs impact the stress field on the plate interface over time. To address this, we sum the changes in Coulomb failure stress over the seven modeled SSEs (Figure 3–9). Each frame incorporates the next modeled SSE showing changes in the distribution of regions of stress increase and decrease for each event with respect to tremor and earthquakes. In the northern

Tolaga Bay patch, SSEs appear to accommodate strain between the coastline and the downdip edge of seamount S2 where the May 1947 tsunami earthquake originated (Figure 3–10). While it is difficult to make strict interpretations based on the delineation of the slow slip, SSEs in this patch appear to load the shallow plate interface with ~100 kPa for the 2010 and 2011 Tolaga bay SSE cycles around the seamount and decrease stress ~150-175 kPa over the cycles between 6-15 km depth (Figure 3–9). To put these CFS changes in broader context with respect to plate convergence, the impact of these SSEs on the slip deficit must be addressed.

Figure 3–9. Cumulative CFS changes from seven SSEs between 2010 and 2014. Dark red regions represent maximum CFS increases and dark blue regions represent maximum CFS decreases. Stress decrease along the margin appears to be nearly continuous, supporting previous conclusions that SSEs in the northern Hikurangi accommodate the majority of the long-term averaged interplate coupling.

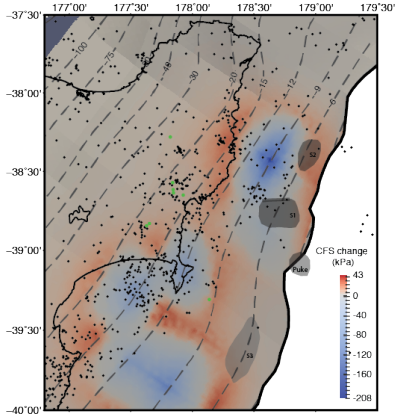

Frame 1: 10a

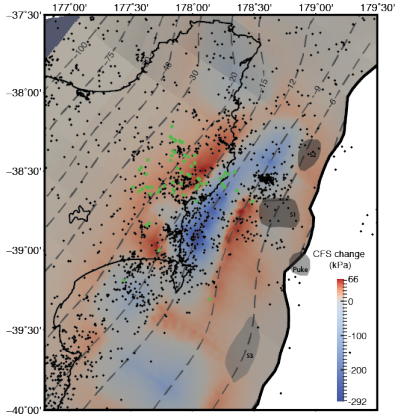

Frame 2: 10a + 10b

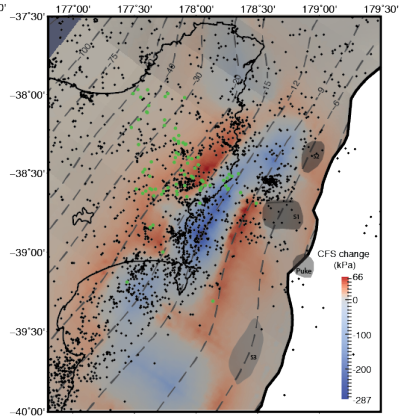

Frame 3: 10a + 10b + 11a

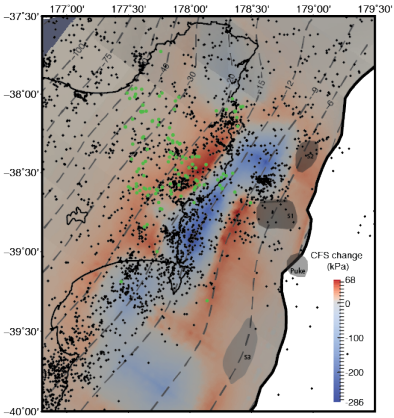

Frame 4: 10a + 10b + 11a + 11b

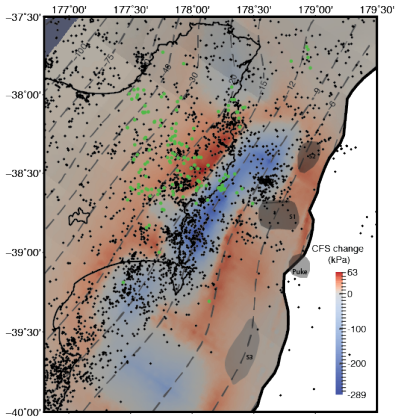

Frame 5: 10a + 10b + 11a + 11b + 11c

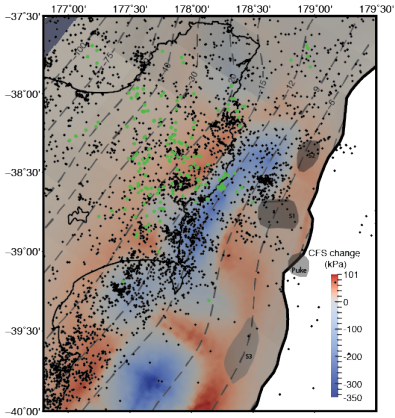

Frame 6: 10a + 10b + 11a + 11b + 11c + 13a

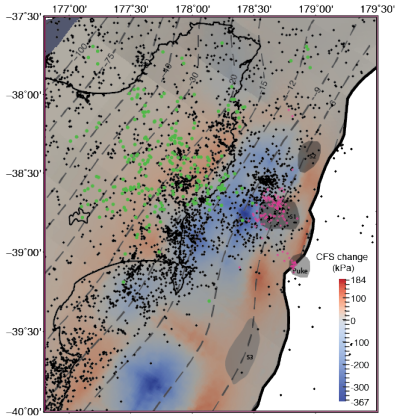

Frame 7: 10a + 10b + 11a + 11b + 11c + 13a + 14a

The central Gisborne patch experiences the greatest stress decrease along the northern Hikurangi Margin. Frames 2-6 show a full cycle between the large Gisborne SSEs of 2010 and 2014 and show that the very shallow plate interface, updip and around seamount S1 where the March 1947 tsunami earthquake occurred, experiences a net stress increase. Figure 3–10 shows that while slip from events 10a-14a may completely reduce the five-year-averaged slip deficit [*Wallace et al.*, 2012b] up to 6 km depth in the Tolaga Bay and Gisborne patches, the shallowest part of the of the interface has a remaining slip deficit. However, the full extent of remaining slip deficit is unknown because the updip limit of slow slip is poorly constrained and requires off shore geodetic measurements. Offshore tectonic tremor detected with the HOBITSS experiment is located atop seamount S1. It is possible that offshore tectonic tremor exists above all subducted seamounts in the northern Hikurangi, but detection requires an offshore seismic network. Onshore tremor episodes that accompany SSEs in the Gisborne patch are primarily located downdip of the slip patch and are concentrated in regions of CFS increase. This pattern is observed collectively with onshore tremor associated from each modeled SSEs along the northern Hikurangi Margin (Frame 7; Figure 3–9). It is unclear whether or not the same pattern exists for earthquakes because most events are too small to obtain focal mechanisms and therefore determine whether or not they are located on the plate interface. However, most onshore and offshore earthquakes associated with Gisborne SSEs are not located within 5 km depth of the plate interface (Chapter 2), and are therefore less likely to be interplate earthquakes that would be directly affected by the

CFS distribution (Figure 3–9). Although most earthquakes associated with northern Hikurangi SSEs are unlikely to be located on the plate interface, the seismic record does show that the shallow plate interface has previously ruptured in moderate magnitude tsunami earthquakes. The SSE cycle in and around the Gisborne patch appears to relieve most of the accumulated slip deficit over five years, but the SSEs produce a net stress increase of 125 kPa on the shallowest portion of the plate interface where the five-year-averaged slip deficit remains (Figure 3–10) that is added to any convergence-induced stress accumulation from interplate locking. Figure 3–10 shows that slow slip may not only completely eliminate the five-year averaged slip deficit, but that on this time scale, represents an over abundance of slip on the plate interface. This may be due to the highly productive years of 2010 and 2011 where there were numerous moderate-large SSEs along the northern Hikurangi Margin. In contrast, 2012, 2013, and 2015 did not have many SSEs. Even including the potential for anomalously high rates of SSEs, the shallow region of the plate interface has a remaining slip deficit that indicates the northern Hikurangi Margin could potentially host future tsunami earthquakes.

Figure 3–10. Slip deficit and cumulative slow slip over 5 years.
(a) Northern Hikurangi slip deficit (in mm) from *Wallace et al.* [2012b] averaged over 5 years showing the largest slip deficit at the shallowest part of the plate interface extending from the Mahia Peninsula south toward Cape Kidnappers. The dashed line represents the down dip extent of positive slip deficit in the *Wallace et al.* [2012b] model. (b) Cumulative slip from events 10a-14a in mm. (c) Difference between the 5 year averaged slip deficit and cumulative slip from events 10a-14a. Orange represents remaining regions of positive slip deficit. Updip of the dashed line, blue represents regions where slow slip has completely reduced the slip deficit.

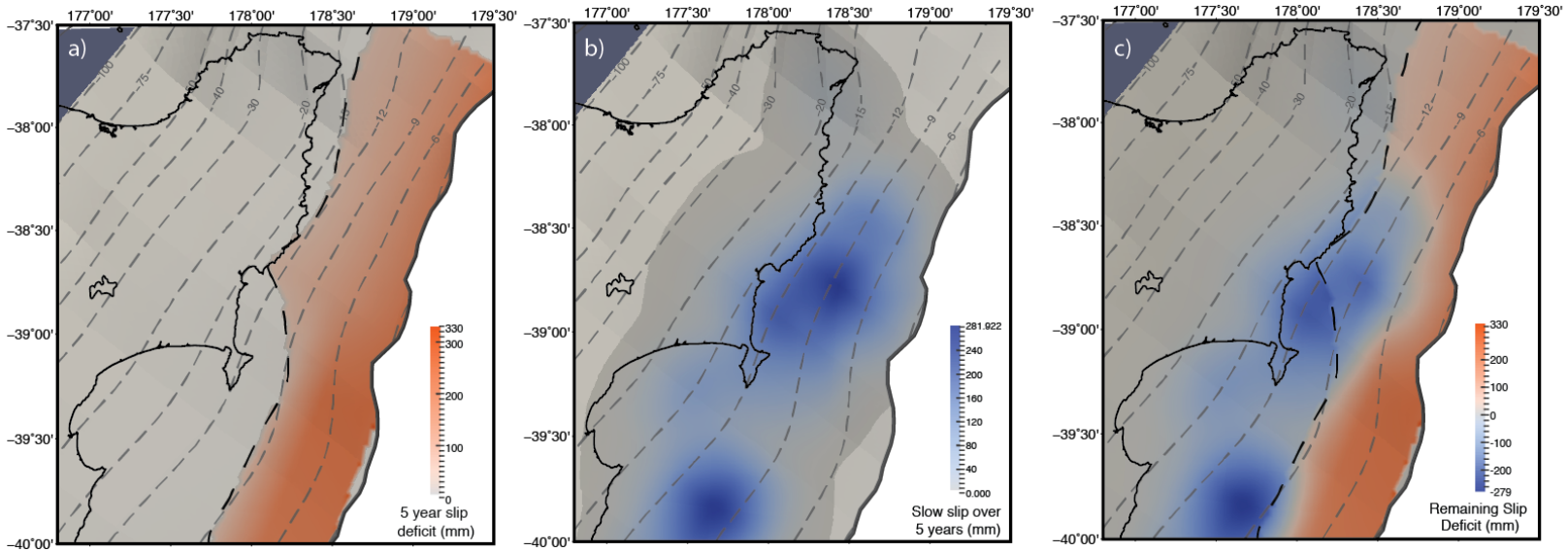
a)
b)
c)
177°00'
177°30'
178°00'
178°30'
179°00'
179°30'
-37°30'
-38°00'
-38°30'
-39°00'
-39°30'
-40°00'
100
75
60
40
30
20
15
12
9
6
330
300
200
100
0
5 year slip deficit (mm)
281.922
240
200
160
120
80
40
0.000
Slow slip over 5 years (mm)
330
200
100
0
-100
-200
-279
Remaining Slip Deficit (mm)

Southward, the Mahia and Hawke's Bay patches relieve stress in the areas near shore, but appear to load a region downdip of seamount S3. While this effect may be physically real, the apparent loading of the plate interface is uncertain due to the limited offshore resolution of the geodetically detected slip distributions. This region is far removed from the land-based cGPS network compared to the other slow slip patches and the up-dip limit of slip is not well constrained. While there is a continuous region of stress decrease between 9-15 km depth from the Tolaga Bay to the Hawke's Bay patches, the updip portion of the plate interface adjacent to seamounts S1, S2, and S3 is potentially loaded and may rupture in future tsunami earthquakes.

3.4 Conclusions

The northern Hikurangi Margin, New Zealand is in a short list of regions, including the Nicoya Peninsula, Costa Rica, the Boso Peninsula, Japan, and La Plata Island, Ecuador with rough incoming plates and shallow slow slip at depths <15 km. One of the outstanding questions about shallow slow slip is how it affects the stress state of the plate interface. Frequent slow slip events occur along the northern Hikurangi Margin with a variety of magnitudes and recurrence intervals that change along strike from small, frequent slow slip events in the north and larger, less frequent events toward the south. This along strike change in slow slip behavior mirrors the along strike change in plate coupling where the interactions between SSEs and local seismicity indicates that the entire northern Hikurangi interface is weakly coupled, close to failure, and promotes interplate slip in SSEs. By calculating the impact of

slow slip on the stress state of the megathrust for seven SSEs between 2010-2014, we find that CFS changes from one SSE influence the location of the next SSE and the along strike migration of SSE sequences. Tectonic tremor located downdip of slow slip patches and assumed to be on the plate interface, appears to be triggered by SSEs and predominately occurs in regions of CFS increase as expected. Over time through SSE cycles, the shallow-most segments of the plate interface where tsunami earthquakes have been reported in the past, experience a net increase in CFS and may be the sites of future shallow earthquakes with potentially destructive local tsunamis.

Appendices

Appendix A - Supplemental Information for Chapter 1

Table A–1. Range of parameters used in automated tremor detection and location shows the range of parameters used in the automatic tremor detection method. By varying these parameters and only using the most stable detections, this method improved the tremor detections from *Kim et al.* [2011] while decreasing the number of false detections.

Table A–1. Range of parameters used in automated tremor detection and location

Minimum number of correlating station pairs	7-10
Longitude and latitude error tolerance	0.05-0.15 degrees
Correlation coefficient	0.6-0.7
Maximum allowable correlations in earthquake frequency band	4-5
Maximum allowable correlations with reference station HIZ	2-3

Figure A–1 shows tremor episodes on 21 March 2010 comprised of a repeating LFE in part (a). This day had numerous tremor episodes associated with the March/April 2010 Gisborne SSE and part (b) shows a zoomed time window from Figure 1–4.

Figure A–2 shows all detected tremor with the slip contours for 7 slow slip events between 2010 and 2015. Slow slip is predominantly located in the shallow, offshore region of the megathrust with tremor located down dip.

Figure A–1. Repeating LFEs in tremor signal.
(a) 24 hours of 3 component seismic data from station MWZ on 21 March 2010 during the March/April 2010 Gisborne SSE with repeating LFEs plotted in red. Due to multiple local and regional earthquakes greater than M_w 2.3, the vertical scale is clipped to increase visibility. (b) LFE template found to be repeating during tremor episodes identified by automatic detection method on the vertical component. This time period is highlighted in gray in (a).

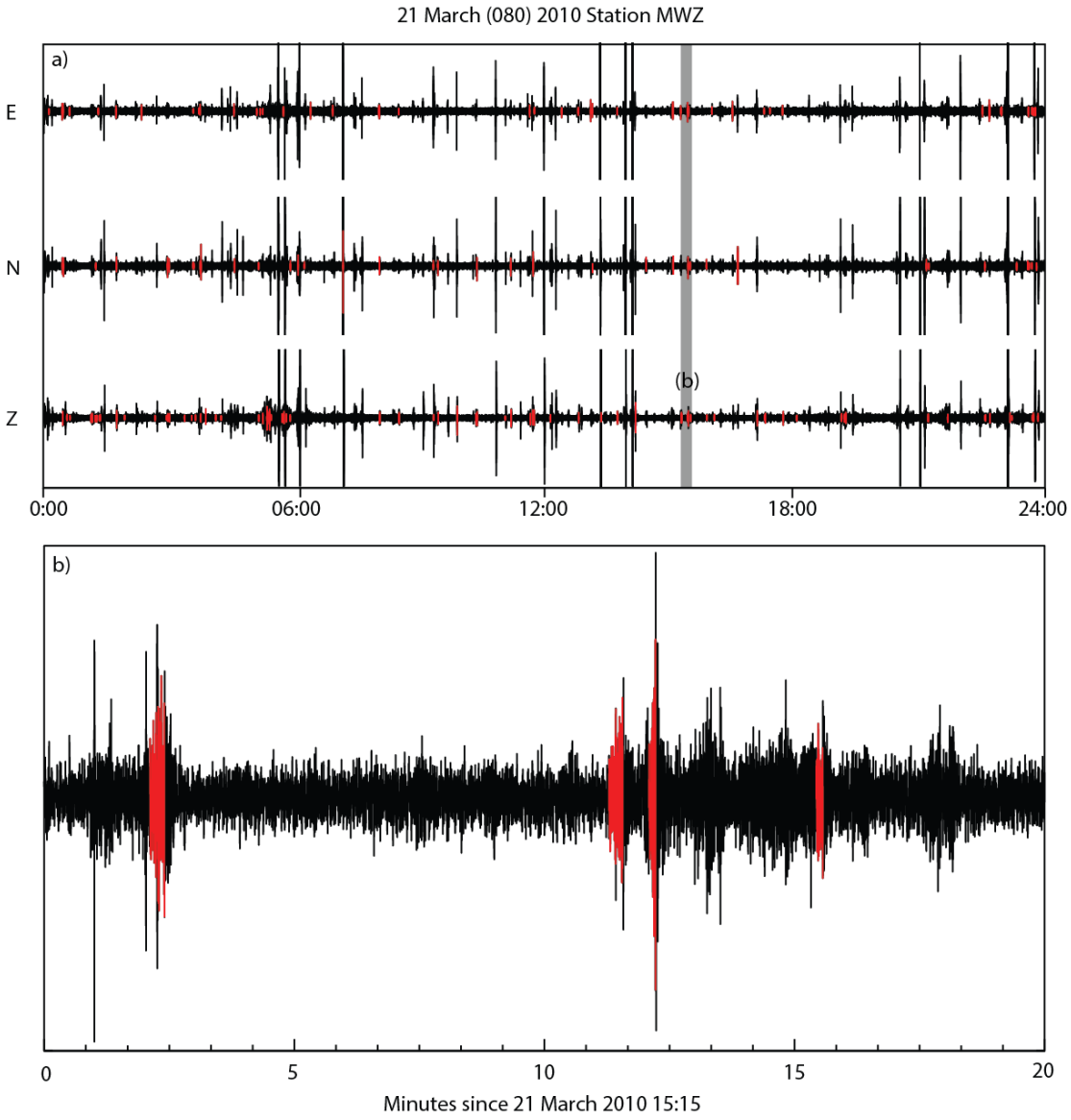
21 March (080) 2010 Station MWZ
a)
E
N
Z
(b)
0:00
06:00
12:00
18:00
24:00
b)
0
5
10
15
20
Minutes since 21 March 2010 15:15

Figure A–2. Tremor and slow slip from 7 SSEs: 2010-2015.
All detected tremor (gray circles) and slip contours (in mm) for 7 slow slip events between 2010 and 2015. Slip contours are from *Wallace and Beavan* [2010], *Wallace et al.* [2012a], and *Wallace et al.* [2016]. The plate interface depth is shown at 20 and 50 km.

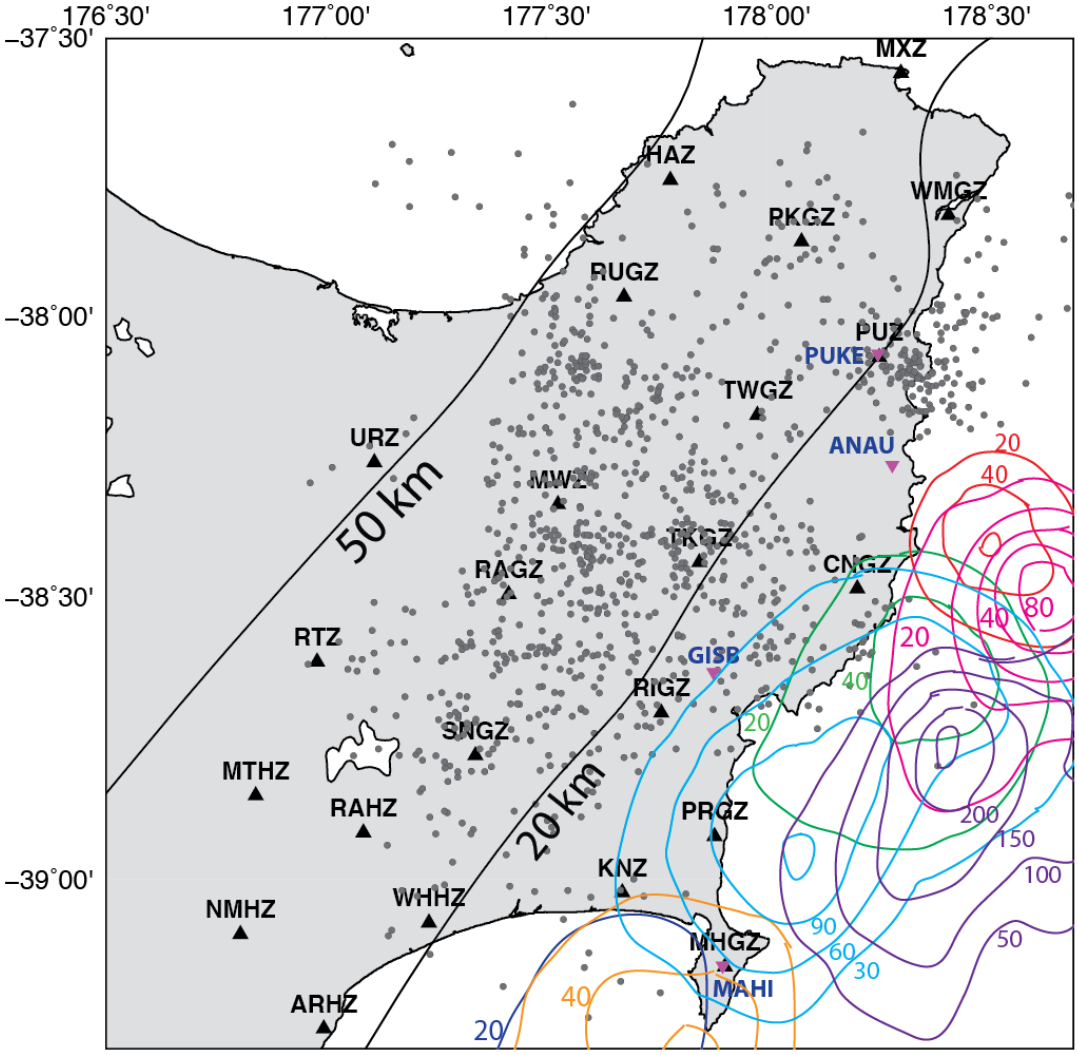
176°30'
177°00'
177°30'
178°00'
178°30'
-37°30'
-38°00'
-38°30'
-39°00'
MXZ
HAZ
WMGZ
RKGZ
RUGZ
PUZ
PUKE
TWGZ
ANAU
URZ
MWZ
TKGZ
CNGZ
RAGZ
RTZ
GISB
RIGZ
SNGZ
MTHZ
RAHZ
PRGZ
KNZ
WHHZ
NMHZ
MHGZ
MAHI
ARHZ
50 km
20 km
20
40
80
200
150
100
90
60
30
50

Appendix B - Supplemental Information from Chapter 2

Figure B–1 shows the depth of earthquakes considered to be occurring on the megathrust with respect to the plate interface. The plate interface is from the geometry used in the Coulomb failure stress calculations [*Williams et al.*, 2013]. For the purposes of this study, interplate earthquakes are defined as earthquakes limited to depths within 5 km of the plate interface. The location of subducted seamount S1 is plotted on the interface for reference. Interplate seismicity is concentrated at the downdip edge of the seamount and further downdip in the region experiencing peak displacement (> 200 mm) during the slow slip event as determined by *Wallace et al.* [2016]. Table B–1 presents the details of the original earthquake catalog from Antelope with calculated magnitudes and Table B–2 presents the NonLinLoc-relocated earthquake catalog. Magnitudes (M_L) are computed using the *mlrichter* Antelope package and the recently revised local magnitude scale from *Ristau et al.* [2016]. Note that not every earthquake in the Antelope catalog could be relocated with NonLinLoc and magnitudes could not be computed for all earthquakes.

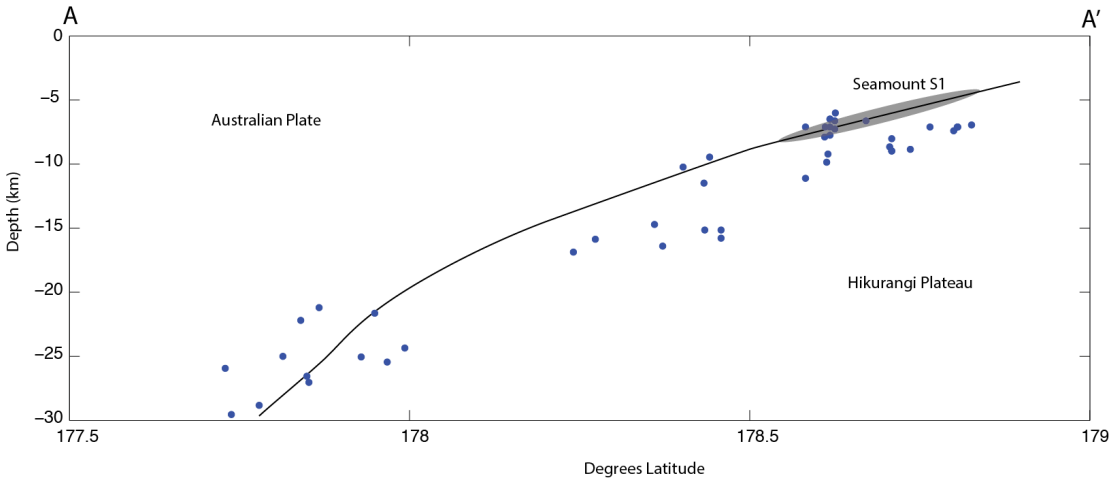

Figure B–1. Cross-sectional view of earthquakes within 5 km of the megathrust. Depths of earthquakes (circles) located within 5 km of the subducting Hikurangi Plateau interface plotted along transect A-A’ shown in Figure 2–9. Subducted seamount S1 plotted for reference. Interplate seismicity is concentrated in the peak slip patch during slow slip and near the downdip edge of seamount S1 after the end of geodetically determined slow slip.

Table B–1. September/October 2014 Antelope earthquake catalog with computed magnitudes (M_L)

Origin Time	Latitude	Longitude	Depth	M_L
2014-09-01T13:47:13	-39.0292	177.7448	13.4532	2.02
2014-09-01T14:54:06	-38.3628	178.8435	17.666	--
2014-09-01T14:58:53	-38.71	178.7448	38.1866	0.59
2014-09-01T17:27:36	-39.032	177.7594	12.7003	1.34
2014-09-01T17:32:30	-39.0129	177.7522	11.7372	1.08
2014-09-01T20:16:21	-38.8533	177.5507	14.5025	--
2014-09-01T20:31:57	-38.057	178.6027	23.0741	1.58
2014-09-01T22:45:44	-39.0223	177.7908	10.0478	--
2014-09-02T02:41:20	-39.0018	177.7191	12.9704	1.51
2014-09-02T05:59:01	-39.0123	177.7503	12.7962	--
2014-09-02T06:39:10	-37.5934	177.8072	121.3922	--
2014-09-02T10:01:20	-38.5645	178.8633	21.1907	2.15
2014-09-02T11:46:43	-37.701	178.4543	19.0733	--
2014-09-02T13:24:48	-38.0617	178.6648	19.6792	2.38
2014-09-02T14:12:05	-38.0722	178.637	9.3112	1.99
2014-09-02T16:40:59	-39.3088	177.266	23.315	--
2014-09-03T01:33:44	-38.4304	177.9658	21.6661	1.42
2014-09-03T09:16:41	-38.2619	178.8596	27.2879	1.84
2014-09-03T10:45:50	-39.0206	177.7529	13.4003	0.82
2014-09-03T13:49:13	-38.0683	178.6237	14.7114	1.25
2014-09-03T13:53:03	-39.0686	177.7802	39.041	1.4
2014-09-03T19:54:27	-38.3974	177.8789	19.7322	1.04
2014-09-03T20:40:51	-39.0825	177.5212	24.7988	0.95
2014-09-03T23:45:31	-38.7657	177.6997	16.9104	1.19
2014-09-04T03:19:39	-38.7494	177.8429	33.9668	1.43
2014-09-04T06:54:14	-38.6861	178.5467	15.7489	0.39
2014-09-04T07:40:47	-38.2065	178.0917	6.7705	1.06
2014-09-04T09:41:19	-38.8172	178.4736	37.9339	0.9
2014-09-04T09:59:29	-38.2073	178.0986	9.9838	0.96
2014-09-04T11:17:37	-39.261	177.1269	27.4645	--
2014-09-04T13:20:06	-37.8164	177.7669	40.0649	--
2014-09-04T21:11:51	-38.9183	177.193	34.9715	--
2014-09-04T23:23:53	-39.1155	177.3482	26.2267	--
2014-09-04T23:44:07	-38.4299	177.2774	35.9207	--
2014-09-05T03:53:23	-38.8614	177.9379	19.4179	1.36
2014-09-05T08:53:50	-39.1412	177.3854	25.351	--
2014-09-05T08:57:54	-38.7404	178.0283	12.6891	1.28
2014-09-05T10:12:45	-38.7741	177.995	19.6432	1.72

2014-09-05T16:48:36	-38.2465	177.3987	37.3099	--
2014-09-05T18:29:21	-38.3852	177.9795	33.4763	1.01
2014-09-05T19:20:25	-39.117	177.3497	24.8447	--
2014-09-05T23:09:43	-39.0678	177.6742	35.1057	1.65
2014-09-06T00:51:16	-38.0638	178.8959	54.971	1.66
2014-09-06T05:06:47	-39.1523	177.6859	19.8586	1.33
2014-09-06T09:55:11	-38.3893	178.5558	13.3426	2.0
2014-09-06T13:31:32	-37.9621	177.715	99.4401	--
2014-09-06T14:29:44	-39.0775	177.5175	26.7248	2.07
2014-09-06T15:54:16	-37.7458	177.3554	168.7771	--
2014-09-06T18:47:14	-38.2748	178.8892	0.0	--
2014-09-07T00:58:13	-38.7147	178.6078	39.2885	1.85
2014-09-07T01:51:42	-38.9461	178.5577	17.5217	1.42
2014-09-07T03:32:43	-38.6986	178.2313	15.312	1.49
2014-09-07T08:58:06	-38.7186	178.3069	33.887	1.33
2014-09-07T09:53:54	-38.1888	178.1292	11.3365	2.98
2014-09-07T10:27:34	-38.1337	179.414	29.8367	--
2014-09-07T10:32:35	-39.3624	177.8108	34.829	--
2014-09-07T18:58:24	-38.2128	178.0889	5.6704	2.12
2014-09-07T19:04:53	-38.2057	178.0943	5.8111	1.79
2014-09-07T23:53:02	-38.2201	178.0854	3.9501	1.85
2014-09-08T01:27:43	-38.1256	178.9502	8.5555	1.68
2014-09-08T01:34:25	-37.5286	178.2027	26.7415	--
2014-09-08T02:51:30	-38.6357	178.4261	22.3783	2.0
2014-09-08T09:16:08	-38.3397	178.6672	22.431	1.66
2014-09-08T13:54:37	-39.1001	177.2685	17.558	--
2014-09-08T14:12:05	-38.6509	178.712	12.9446	3.86
2014-09-08T16:25:00	-39.0115	177.8373	10.3283	1.51
2014-09-08T19:12:26	-37.8393	179.2832	0.0	--
2014-09-09T15:43:46	-39.2355	177.7031	32.0067	2.05
2014-09-09T16:44:34	-38.4226	178.6898	9.8782	1.46
2014-09-09T17:10:12	-38.8336	177.8935	17.9667	1.49
2014-09-09T20:59:14	-38.3281	178.592	32.014	1.65
2014-09-10T03:34:34	-39.2378	177.693	33.0424	2.0
2014-09-10T07:03:43	-37.7522	178.5152	23.0199	--
2014-09-10T12:18:39	-38.5236	178.5489	3.7144	1.12
2014-09-10T12:45:02	-38.5578	178.5547	8.0332	0.98
2014-09-10T18:41:01	-38.0909	179.0162	34.0376	2.12
2014-09-11T01:16:00	-38.8815	177.5013	0.0	0.91
2014-09-11T01:34:01	-38.1344	178.6072	21.317	--
2014-09-11T02:17:18	-38.3993	178.7593	37.5478	0.4
2014-09-11T10:20:22	-37.9303	177.8696	84.6927	--
2014-09-11T10:48:36	-38.5785	178.4789	16.7166	0.9
2014-09-11T11:55:35	-38.5669	178.4027	11.9057	1.01

2014-09-11T15:22:02	-38.4147	178.3282	14.3801	--
2014-09-11T18:52:38	-37.6888	178.6423	0.0166	--
2014-09-11T20:39:57	-38.0918	178.261	40.7996	1.76
2014-09-11T21:48:57	-37.6339	177.5771	144.8808	--
2014-09-11T22:13:45	-38.5083	178.9484	28.7685	1.47
2014-09-12T03:57:06	-39.2818	177.039	30.3476	--
2014-09-12T04:43:20	-37.7199	178.2023	35.6396	--
2014-09-12T06:46:41	-39.2917	177.029	29.9528	--
2014-09-12T07:06:33	-38.8645	177.723	15.6124	1.42
2014-09-12T07:34:20	-39.2825	177.025	30.2231	--
2014-09-12T09:59:23	-38.4687	178.0857	33.2118	1.08
2014-09-12T12:53:16	-37.6674	178.4298	22.1497	--
2014-09-12T17:01:17	-38.3784	178.6607	21.6848	2.23
2014-09-13T00:01:55	-37.7143	178.1077	64.5435	--
2014-09-13T02:48:56	-38.6692	178.6969	15.4234	0.27
2014-09-13T04:21:26	-38.9952	177.7696	52.834	2.08
2014-09-13T07:04:55	-39.0224	177.4775	21.8427	--
2014-09-13T09:44:15	-38.4723	177.5435	54.3035	2.57
2014-09-13T13:31:37	-38.497	178.6101	14.9161	1.26
2014-09-13T14:27:13	-38.3153	178.7128	36.8269	1.69
2014-09-13T16:01:31	-38.5785	177.5141	25.4053	2.21
2014-09-13T16:05:24	-38.6129	178.411	14.471	0.92
2014-09-13T22:09:56	-38.6711	177.7573	38.9874	--
2014-09-14T04:39:53	-38.0067	178.3577	18.7633	1.61
2014-09-14T06:34:46	-38.912	179.014	0.0067	2.63
2014-09-14T07:34:25	-38.639	178.6109	29.6003	1.18
2014-09-14T09:32:57	-39.3979	178.6266	36.6931	--
2014-09-14T09:57:18	-39.1486	177.7379	11.3441	1.72
2014-09-14T12:49:09	-38.2649	177.834	36.2299	1.96
2014-09-14T14:15:07	-39.4125	177.1462	27.8075	--
2014-09-14T16:44:34	-38.2151	178.6511	37.8171	--
2014-09-14T17:52:39	-38.5336	177.8486	14.352	1.5
2014-09-14T22:50:34	-38.7072	178.3767	28.6833	1.16
2014-09-15T00:31:57	-38.8184	178.5451	82.3728	--
2014-09-15T07:47:28	-37.8748	177.9628	16.3379	1.71
2014-09-15T10:24:40	-38.8878	178.6002	21.8609	0.99
2014-09-15T11:13:20	-38.6325	178.6577	12.8142	0.08
2014-09-15T11:47:00	-37.9256	177.7079	129.2701	2.15
2014-09-15T14:18:57	-38.9188	177.7813	24.66	1.08
2014-09-15T15:38:34	-37.8133	178.5686	37.7554	2.0
2014-09-15T15:41:01	-38.3222	178.0682	36.5803	1.48
2014-09-15T16:57:39	-38.8153	177.951	15.0544	1.58
2014-09-15T18:06:45	-38.8207	177.9555	16.5087	1.33
2014-09-16T05:38:46	-38.4751	178.4695	15.6271	1.33

2014-09-16T06:34:52	-39.2015	177.7602	20.0417	1.21
2014-09-16T08:05:37	-38.836	177.8437	13.619	0.52
2014-09-16T20:55:19	-38.3386	178.0917	38.0856	1.55
2014-09-17T00:13:54	-38.9926	177.9841	41.1982	1.44
2014-09-17T04:18:28	-38.8434	178.0764	50.2074	1.84
2014-09-17T04:46:48	-37.9577	178.0817	51.9249	1.98
2014-09-17T09:22:01	-38.4266	178.7006	37.1576	2.12
2014-09-17T10:13:09	-39.1188	177.4343	16.5647	2.67
2014-09-17T10:55:01	-38.8189	178.8276	13.0897	0.4
2014-09-17T11:11:17	-38.0475	178.5823	23.2707	1.39
2014-09-17T13:54:55	-39.0678	177.7892	18.2443	1.27
2014-09-17T19:47:11	-38.645	177.814	73.9772	1.27
2014-09-17T20:18:22	-38.1611	178.6775	33.3181	1.53
2014-09-18T01:55:00	-37.8621	178.6358	0.0	1.58
2014-09-18T03:47:32	-37.6041	179.0612	41.6074	2.47
2014-09-18T04:59:16	-37.5629	178.9253	17.5416	2.21
2014-09-18T05:52:12	-38.0561	178.9803	35.0555	1.87
2014-09-18T07:13:14	-37.8909	178.3624	16.9868	1.3
2014-09-18T15:15:02	-38.5485	178.8027	13.2135	1.94
2014-09-18T18:53:32	-38.4431	178.6225	18.6445	1.63
2014-09-18T19:50:31	-37.723	177.3677	63.9699	1.81
2014-09-19T05:54:09	-38.2868	178.9796	65.4552	1.06
2014-09-19T13:03:15	-38.6229	178.7806	13.4072	0.24
2014-09-19T13:22:30	-37.7525	178.2069	151.1323	2.0
2014-09-19T15:08:24	-37.9387	177.2582	136.5112	--
2014-09-19T17:40:35	-38.9497	178.5133	19.0779	1.54
2014-09-19T18:43:11	-38.5428	178.2322	22.7877	1.09
2014-09-20T02:19:14	-38.3538	178.5248	29.9675	--
2014-09-20T02:49:41	-38.4913	178.8072	44.3146	1.56
2014-09-20T09:14:35	-38.6732	178.6542	13.6338	-0.16
2014-09-20T15:10:36	-38.0291	178.7164	0.8126	1.92
2014-09-20T18:53:06	-38.8635	178.4892	38.5339	1.0
2014-09-20T19:21:37	-38.3655	177.7991	33.4034	2.0
2014-09-20T20:25:21	-38.4191	178.3416	19.9959	2.32
2014-09-21T09:31:10	-38.8898	177.9921	22.2044	1.89
2014-09-21T10:21:32	-39.1173	177.3855	18.8095	1.39
2014-09-21T10:42:26	-39.1157	177.3893	17.8631	1.6
2014-09-21T13:23:57	-39.0209	177.6802	29.4347	1.45
2014-09-21T15:14:37	-39.0314	177.7209	46.1091	2.25
2014-09-21T21:15:18	-37.6206	178.7459	0.0037	2.36
2014-09-22T07:21:24	-37.9663	177.9571	61.518	2.39
2014-09-22T08:06:04	-38.5837	178.6936	39.0305	1.89
2014-09-22T21:38:32	-38.4041	177.8559	151.1509	2.2
2014-09-23T03:39:51	-38.6203	178.4619	14.1444	--

2014-09-23T10:07:10	-39.141	177.3573	32.7593	2.15
2014-09-23T10:39:32	-38.3682	177.9268	29.1499	1.06
2014-09-23T22:43:20	-37.6438	177.0237	237.7777	2.3
2014-09-23T22:47:51	-38.6064	177.0743	84.9603	2.71
2014-09-23T23:36:05	-38.5398	178.6957	41.0663	1.97
2014-09-24T02:17:48	-38.2301	178.5249	22.7452	1.49
2014-09-24T03:49:20	-38.088	177.8439	71.8516	2.45
2014-09-24T05:14:11	-38.4077	178.2526	88.053	1.44
2014-09-24T09:30:14	-38.7733	179.2953	12.7935	1.74
2014-09-24T10:29:30	-38.4947	178.6353	14.3852	0.86
2014-09-24T15:43:58	-37.5237	177.3155	80.6771	2.32
2014-09-24T18:12:30	-38.2137	178.1859	25.5706	2.6
2014-09-24T18:17:12	-38.2163	178.1847	24.8616	1.62
2014-09-24T18:46:18	-38.702	178.806	11.0995	1.56
2014-09-24T20:29:27	-38.4621	178.637	39.7823	2.06
2014-09-24T22:07:39	-38.8201	178.7823	19.557	--
2014-09-24T23:20:40	-38.8238	178.584	15.8148	0.78
2014-09-25T01:10:41	-38.9117	177.9749	18.017	1.87
2014-09-25T02:30:33	-38.9852	177.8162	36.1988	1.78
2014-09-25T02:48:31	-38.8791	177.9803	14.9787	2.58
2014-09-25T05:38:14	-38.8873	177.0946	56.0837	2.38
2014-09-25T07:08:51	-38.5441	177.2176	77.068	2.25
2014-09-25T08:23:14	-38.7043	177.6718	19.1503	1.75
2014-09-25T14:04:31	-38.6698	178.5554	41.2215	1.52
2014-09-25T14:24:05	-38.6235	178.4444	23.0321	1.31
2014-09-25T17:59:21	-38.3219	178.0562	20.7295	1.54
2014-09-25T19:32:50	-39.1664	177.0671	25.4773	2.35
2014-09-25T19:37:28	-38.4138	177.0428	43.0097	2.29
2014-09-25T19:41:13	-38.2607	177.3428	156.1445	2.28
2014-09-25T21:58:20	-38.0416	179.0494	34.5336	3.43
2014-09-25T22:02:55	-38.9544	178.5717	14.9234	--
2014-09-26T02:36:46	-38.9448	178.7893	53.9075	1.36
2014-09-26T02:59:53	-39.1548	177.4782	32.0539	1.97
2014-09-26T03:08:50	-39.1324	178.4631	62.1542	1.59
2014-09-26T03:35:13	-38.1809	178.2723	20.6718	1.91
2014-09-26T07:04:19	-38.2145	178.48	27.9257	3.02
2014-09-26T11:23:21	-38.5671	178.4833	15.0898	0.54
2014-09-26T16:54:18	-38.4052	178.3464	17.4282	1.78
2014-09-26T17:53:01	-37.5695	177.5022	195.7507	2.64
2014-09-26T22:57:11	-38.8532	178.4799	26.1391	0.55
2014-09-27T06:30:23	-39.2491	177.0468	19.2019	2.48
2014-09-27T06:55:09	-38.3441	178.3068	48.2995	1.32
2014-09-27T08:59:30	-37.5313	177.3893	75.1567	2.24
2014-09-27T09:09:04	-38.6493	178.6689	18.447	0.45

2014-09-27T11:23:07	-38.6136	177.2217	74.2018	2.73
2014-09-27T18:44:31	-38.4751	178.756	31.2384	1.35
2014-09-27T22:42:38	-38.3368	177.7572	54.5303	1.5
2014-09-27T22:57:10	-39.0464	177.4382	19.836	--
2014-09-28T02:41:19	-39.0752	177.243	49.085	--
2014-09-28T03:47:40	-38.3697	178.7608	20.3259	2.06
2014-09-28T04:27:35	-38.2435	177.487	0.1114	--
2014-09-28T08:52:44	-39.3654	177.5253	26.2057	--
2014-09-28T09:08:54	-37.659	178.7912	7.0641	--
2014-09-28T15:55:58	-38.5575	178.8199	15.3052	1.95
2014-09-28T16:57:52	-38.5119	177.0498	87.5864	--
2014-09-28T18:15:45	-37.6887	179.1573	37.7393	--
2014-09-28T21:03:36	-38.6186	178.4353	25.5422	2.54
2014-09-28T22:20:10	-38.3836	177.9098	41.4099	2.05
2014-09-28T22:23:13	-38.9564	177.4897	22.0722	--
2014-09-29T03:04:11	-37.7144	178.0736	13.0758	2.27
2014-09-29T04:39:01	-38.7538	177.3658	81.9021	--
2014-09-29T05:52:12	-37.6281	177.3463	2.8455	--
2014-09-29T06:19:26	-38.7832	177.5724	21.1186	1.98
2014-09-29T10:05:09	-39.0447	177.4913	20.887	--
2014-09-29T10:26:59	-38.4277	178.8039	44.0445	1.8
2014-09-29T11:08:11	-39.0314	177.4712	15.4397	--
2014-09-29T11:25:36	-39.012	177.4643	26.2337	--
2014-09-29T13:15:52	-38.3555	178.1497	13.695	2.03
2014-09-29T15:20:48	-37.5324	177.2756	221.5477	--
2014-09-30T01:34:48	-38.3792	177.8817	58.3366	1.98
2014-09-30T05:14:48	-38.9114	177.9866	18.3648	1.98
2014-09-30T16:24:10	-38.8584	177.915	23.7885	1.51
2014-09-30T18:06:35	-38.2206	178.2259	8.2455	1.74
2014-09-30T18:18:29	-37.7647	177.6868	25.818	--
2014-09-30T18:26:58	-38.6045	178.4444	14.9255	1.34
2014-09-30T20:14:29	-38.7585	177.6613	15.7551	--
2014-09-30T23:00:27	-38.7037	177.1235	0.0255	--
2014-10-01T03:15:53	-38.89	177.9395	40.0111	1.19
2014-10-01T04:27:59	-38.0262	179.1708	39.1262	2.61
2014-10-01T04:32:05	-38.4459	178.9865	32.5472	1.6
2014-10-01T04:57:41	-38.8224	178.7558	19.5065	2.82
2014-10-01T07:24:50	-38.5647	178.703	80.97	--
2014-10-01T11:12:11	-38.2436	178.2497	7.5119	2.13
2014-10-01T11:54:37	-38.9496	177.5514	15.4084	1.85
2014-10-01T14:50:44	-38.6419	177.8427	15.9936	1.72
2014-10-01T16:48:46	-38.1417	178.9235	48.0305	1.93
2014-10-01T17:09:25	-38.1484	178.1954	24.5933	1.75
2014-10-01T17:33:45	-37.8919	177.66	44.7814	--

2014-10-01T18:43:54	-38.1747	178.2008	21.313	1.67
2014-10-01T20:32:05	-38.2628	178.7896	41.6559	1.63
2014-10-02T00:38:48	-38.3402	178.5172	4.8483	1.92
2014-10-02T04:59:16	-38.0439	179.0451	26.7044	2.92
2014-10-02T06:03:40	-38.6735	178.7571	26.3083	0.74
2014-10-02T10:24:46	-37.7924	178.6664	45.0819	--
2014-10-02T11:01:24	-38.352	178.4903	14.257	1.77
2014-10-02T12:22:25	-37.9642	178.3351	10.6835	--
2014-10-02T13:33:55	-37.9239	178.3926	20.6109	--
2014-10-02T17:10:57	-38.3804	177.906	29.4632	2.17
2014-10-02T18:30:22	-38.8081	178.1866	14.0833	1.64
2014-10-02T19:03:25	-38.4276	178.5291	49.3147	1.88
2014-10-02T19:33:16	-38.7949	177.9803	40.6941	4.48
2014-10-02T21:03:01	-38.4965	178.6232	55.3908	1.33
2014-10-02T21:47:10	-38.9657	177.4604	6.0093	--
2014-10-02T21:57:41	-38.7532	178.1108	15.2949	1.89
2014-10-02T22:23:11	-38.798	177.9154	46.1712	1.91
2014-10-03T02:02:12	-37.7749	178.5013	29.7157	--
2014-10-03T05:51:45	-38.0692	178.6193	7.5866	2.37
2014-10-03T07:49:21	-38.8779	177.949	70.5059	1.72
2014-10-03T11:23:01	-39.2463	177.3452	27.5653	--
2014-10-03T21:42:45	-37.9977	178.6043	37.8445	--
2014-10-03T22:28:30	-37.7943	179.3161	1.7725	--
2014-10-03T23:05:19	-38.6151	178.7074	0.0	--
2014-10-04T06:52:49	-38.7852	178.2432	7.7021	1.75
2014-10-04T07:57:08	-38.7598	178.2475	14.0583	2.1
2014-10-04T09:38:58	-38.8189	178.3161	12.5631	1.77
2014-10-04T10:55:49	-38.5219	178.0308	39.63	1.59
2014-10-04T12:01:21	-38.9611	178.389	23.7847	0.82
2014-10-04T13:41:43	-37.5502	178.648	11.4713	--
2014-10-04T14:23:35	-37.5847	178.6382	15.0243	--
2014-10-04T20:40:23	-38.4998	178.1899	23.0446	2.38
2014-10-04T22:23:18	-39.2018	177.3298	36.7031	--
2014-10-04T23:46:37	-38.2448	178.0967	15.342	1.11
2014-10-05T01:23:02	-38.6884	177.7343	37.52	1.89
2014-10-05T03:35:05	-38.8189	177.8786	11.0038	1.45
2014-10-05T07:03:21	-38.7858	177.8859	11.0297	1.4
2014-10-05T07:29:28	-38.4587	178.7788	29.596	1.44
2014-10-05T09:52:13	-39.0122	177.6547	15.912	1.07
2014-10-05T14:26:02	-38.5066	177.5852	57.4075	2.27
2014-10-05T14:51:31	-39.0251	177.5065	70.5108	2.05
2014-10-05T14:55:25	-39.0061	177.5557	67.2679	1.96
2014-10-05T15:01:12	-38.7917	177.9232	23.0095	1.64
2014-10-05T15:14:50	-38.6676	179.4852	28.8424	--

2014-10-05T15:27:47	-39.029	178.4289	24.5771	1.36
2014-10-05T21:39:02	-38.8591	178.3448	13.4255	2.03
2014-10-05T21:47:31	-38.5519	178.0172	37.8032	1.77
2014-10-06T13:40:57	-38.7935	178.2878	10.0076	1.4
2014-10-06T13:59:55	-38.2508	178.1801	15.2131	1.83
2014-10-06T15:07:45	-37.9828	178.8756	14.0115	--
2014-10-06T16:08:20	-38.9578	177.4835	20.3556	--
2014-10-06T17:58:59	-38.9231	177.4963	20.8746	--
2014-10-06T18:11:12	-38.8257	178.2756	9.8834	2.12
2014-10-06T20:10:47	-38.5575	178.576	40.7056	1.02
2014-10-07T00:11:40	-38.5686	177.4564	107.9608	--
2014-10-07T02:11:39	-38.8058	177.9437	53.4453	1.61
2014-10-07T02:34:13	-38.9558	178.5272	22.9006	1.11
2014-10-07T02:43:25	-38.9444	177.4827	24.2944	--
2014-10-07T07:27:37	-39.31	177.5699	29.7002	--
2014-10-07T09:41:16	-38.8282	178.2856	14.7726	1.46
2014-10-07T09:54:41	-37.6965	178.8973	25.9324	--
2014-10-07T10:26:47	-38.6116	178.3106	0.1385	1.19
2014-10-07T14:44:16	-38.5903	177.1748	15.3284	--
2014-10-07T16:12:36	-38.4068	178.1861	36.6154	--
2014-10-07T21:08:01	-38.3932	178.9245	115.0378	2.4
2014-10-07T22:40:15	-38.7788	178.2073	15.0776	1.52
2014-10-08T02:19:10	-38.8302	178.3562	13.5709	1.4
2014-10-08T02:37:50	-38.7709	178.1853	14.5141	1.0
2014-10-08T02:57:36	-38.8181	178.3377	13.1009	0.93
2014-10-08T04:28:18	-38.7519	178.2253	8.0975	1.18
2014-10-08T04:44:11	-38.4152	177.495	6.1752	2.3
2014-10-08T04:56:49	-38.838	178.3101	25.554	0.94
2014-10-08T05:26:11	-38.8089	177.9018	9.2826	2.12
2014-10-08T06:45:20	-39.228	177.8006	34.539	3.07
2014-10-08T07:07:02	-38.6494	178.5531	41.4544	0.5
2014-10-08T07:32:46	-38.831	178.3447	15.0874	1.37
2014-10-08T07:35:26	-38.3061	178.5681	22.0573	1.57
2014-10-08T12:41:59	-38.3062	179.0024	36.9465	2.76
2014-10-08T15:19:46	-38.7734	178.3817	10.3879	0.93
2014-10-08T15:44:41	-38.6678	178.3794	22.2257	--
2014-10-08T17:00:48	-38.8901	178.4111	22.0528	1.69
2014-10-08T19:24:48	-38.163	177.2219	113.8717	--
2014-10-08T20:50:30	-39.0752	177.7231	15.0617	1.12
2014-10-08T20:52:38	-38.8163	178.4415	11.2197	1.11
2014-10-08T21:41:00	-38.6295	177.2878	90.7224	--
2014-10-09T00:06:00	-38.7738	178.269	15.283	1.36
2014-10-09T00:32:02	-38.797	178.3367	11.9735	--
2014-10-09T05:45:35	-38.3552	177.0449	122.5258	--

2014-10-09T09:53:05	-38.481	177.9449	29.6059	1.82
2014-10-09T09:59:53	-38.4506	177.9283	19.8483	1.89
2014-10-09T12:43:19	-38.4982	178.8095	45.5646	1.77
2014-10-09T13:31:56	-39.2395	177.448	37.0401	--
2014-10-09T13:38:26	-38.9478	177.875	9.9506	1.5
2014-10-09T14:02:29	-38.8626	178.2136	13.5561	1.73
2014-10-09T15:46:49	-38.5679	178.4391	14.3693	0.61
2014-10-09T17:37:23	-39.1558	178.3808	56.1858	1.2
2014-10-10T03:07:44	-38.8302	178.4495	14.3095	0.82
2014-10-10T05:41:05	-38.3497	178.538	37.1233	1.56
2014-10-10T06:05:32	-38.1597	178.1708	27.719	2.27
2014-10-10T06:48:43	-38.2261	177.5787	72.5648	1.15
2014-10-10T07:01:24	-38.7911	178.5879	9.6419	--
2014-10-10T07:41:02	-38.2837	178.1744	15.7126	1.38
2014-10-10T09:18:02	-37.9327	177.7144	3.3544	--
2014-10-10T09:22:15	-38.1886	178.1539	14.548	1.25
2014-10-10T09:41:54	-38.7968	178.6017	8.8094	0.16
2014-10-10T09:56:21	-37.9584	177.022	0.5336	--
2014-10-10T09:57:05	-37.9753	177.029	3.9455	--
2014-10-10T11:23:34	-37.8216	178.5484	16.8429	--
2014-10-10T12:30:44	-38.4645	178.6534	29.39	1.41
2014-10-10T13:46:35	-38.8641	177.4647	35.1938	--
2014-10-10T15:18:08	-38.7142	178.3188	11.9417	1.06
2014-10-10T16:50:40	-38.7809	178.5066	37.6343	1.84
2014-10-10T18:50:01	-38.0438	177.1725	120.6747	--
2014-10-10T19:41:04	-37.885	179.161	31.282	--
2014-10-10T20:21:43	-38.5334	177.9675	27.4603	1.98
2014-10-10T21:26:03	-38.7858	179.103	22.6805	1.28
2014-10-11T04:21:27	-38.8943	178.6079	15.038	--
2014-10-11T08:36:12	-38.4528	178.4823	9.8626	1.36
2014-10-11T09:57:41	-38.8278	177.8698	11.0695	1.45
2014-10-11T10:37:53	-38.0362	177.4896	119.0944	--
2014-10-11T11:44:27	-38.9022	177.8478	18.6178	1.52
2014-10-11T12:20:08	-37.7118	178.0782	163.023	--
2014-10-11T12:44:40	-38.3635	178.1868	13.9119	1.53
2014-10-11T14:49:31	-38.5655	177.8464	14.2328	0.93
2014-10-11T16:50:52	-38.6208	178.4355	14.2271	1.78
2014-10-11T21:19:53	-38.8756	177.816	7.218	1.65
2014-10-11T22:57:55	-38.6254	179.0062	41.4968	--
2014-10-12T01:11:52	-38.7849	178.4072	15.8405	1.79
2014-10-12T05:39:20	-38.817	178.6195	6.9974	0.21
2014-10-12T06:55:57	-38.2834	178.6054	25.9663	1.7
2014-10-12T12:29:55	-37.9013	178.389	27.543	--
2014-10-12T13:10:22	-39.1842	177.5596	30.5976	1.42

2014-10-12T13:23:05	-38.6346	177.9546	28.9775	1.33
2014-10-12T13:36:35	-38.5776	178.3868	18.1871	1.61
2014-10-12T14:16:31	-38.6695	177.3465	96.2296	--
2014-10-12T14:46:09	-39.3159	177.5921	23.1538	--
2014-10-12T17:14:41	-38.6232	178.6191	40.1574	1.2
2014-10-12T20:11:03	-38.8946	177.9699	18.8456	1.61
2014-10-12T20:32:01	-38.8687	177.9817	23.4387	1.29
2014-10-12T22:15:28	-38.4282	178.1828	25.9525	1.3
2014-10-12T22:52:13	-38.8933	178.5059	23.886	0.97
2014-10-12T23:28:17	-38.8249	178.5166	20.6616	0.96
2014-10-13T00:03:20	-38.6619	178.8108	13.6337	--
2014-10-13T01:43:17	-38.7256	177.7396	14.4859	0.93
2014-10-13T03:44:57	-38.8041	178.6068	10.8919	0.24
2014-10-13T04:13:22	-38.5665	177.892	28.1512	1.8
2014-10-13T06:23:12	-38.7975	177.9554	40.5497	0.93
2014-10-13T09:25:37	-38.5576	177.865	23.6428	1.25
2014-10-13T11:32:08	-38.413	178.1328	25.6701	1.69
2014-10-13T11:56:34	-38.4125	177.7091	48.7889	1.34
2014-10-13T13:09:31	-38.4537	178.4579	42.9121	0.88
2014-10-13T13:40:09	-38.7243	178.7402	13.5052	--
2014-10-13T13:44:45	-38.695	178.6562	12.6053	0.42
2014-10-13T14:04:19	-38.8346	177.9478	18.7542	2.57
2014-10-13T14:04:19	-38.8346	177.9478	18.7542	2.57
2014-10-13T14:04:19	-38.8346	177.9478	18.7542	2.57
2014-10-13T14:04:19	-38.8346	177.9478	18.7542	2.57
2014-10-13T14:16:56	-38.1726	178.3719	9.6386	1.57
2014-10-13T15:17:38	-38.2298	177.4892	70.0088	2.77
2014-10-13T15:27:12	-38.702	177.9842	15.6598	1.13
2014-10-13T16:06:29	-38.8803	177.9068	24.3144	1.07
2014-10-13T20:59:31	-38.6342	178.4765	19.2068	0.92
2014-10-13T21:42:39	-38.946	178.4516	20.678	0.79
2014-10-13T22:05:50	-38.8037	178.6078	8.6806	0.15
2014-10-14T00:14:32	-38.3725	178.6531	85.7588	0.94
2014-10-14T00:29:10	-38.9063	178.3539	50.1656	0.95
2014-10-14T05:07:23	-38.9267	177.0095	58.2068	--
2014-10-14T06:28:47	-37.9009	177.864	59.4405	2.09
2014-10-14T10:49:20	-38.0884	178.7927	60.0965	1.43
2014-10-14T11:23:56	-38.88	177.8251	5.6649	1.18
2014-10-14T12:27:58	-39.0622	177.7832	28.0688	1.78
2014-10-14T14:10:30	-37.6228	178.6766	135.4914	1.99
2014-10-14T14:47:18	-38.8278	178.4718	14.9739	1.19
2014-10-14T20:36:56	-38.2545	177.9693	37.0675	1.59
2014-10-14T23:07:45	-38.6333	178.2028	20.8121	0.99
2014-10-15T12:09:59	-38.5508	177.2829	77.6042	--

2014-10-15T12:44:18	-37.5714	177.2765	163.905	--
2014-10-15T15:50:18	-38.2562	177.3731	102.4071	--
2014-10-15T16:51:49	-38.2021	178.6624	14.6202	1.33
2014-10-15T19:06:34	-37.8451	177.9526	104.0512	--
2014-10-15T20:30:26	-38.4137	178.6334	38.1726	1.46
2014-10-15T21:20:56	-38.8024	178.6321	7.5998	0.42
2014-10-16T11:37:24	-38.5801	178.0364	35.6265	2.0
2014-10-16T13:40:33	-39.1675	177.8865	20.4989	1.52
2014-10-16T15:37:43	-38.4001	178.6641	57.1392	1.32
2014-10-16T17:59:47	-37.6384	177.1777	240.601	--
2014-10-17T04:35:07	-37.6359	177.7459	99.4663	--
2014-10-17T08:04:20	-37.6159	178.0055	69.6298	--
2014-10-17T12:47:40	-37.8668	177.0299	51.6109	--
2014-10-17T15:43:49	-38.7957	178.6298	6.9364	0.09
2014-10-17T16:21:09	-37.9229	178.5541	37.8593	2.15
2014-10-17T17:44:04	-38.3813	177.2246	62.9747	--
2014-10-17T21:13:52	-38.4127	178.718	2.7507	--
2014-10-17T21:25:34	-38.6132	178.5608	18.0757	1.25
2014-10-18T00:55:56	-38.3049	178.1026	33.4013	1.72
2014-10-18T02:09:44	-37.67	177.2998	222.3925	--
2014-10-18T03:06:27	-39.3395	178.5728	37.4285	--
2014-10-18T05:53:13	-38.7931	178.6287	11.6439	1.09
2014-10-18T12:37:02	-38.834	177.8908	22.9272	1.81
2014-10-18T13:04:30	-38.7535	178.572	9.4209	--
2014-10-18T16:43:55	-38.7913	178.6288	2.9863	--
2014-10-18T21:43:45	-38.9267	178.799	14.4514	1.59
2014-10-19T00:35:23	-37.7413	177.4059	90.9229	--
2014-10-19T03:10:46	-38.6146	178.5418	14.7025	1.28
2014-10-19T05:27:43	-38.965	178.4463	42.7279	0.85
2014-10-19T08:20:25	-38.8788	178.3586	20.8054	2.03
2014-10-19T08:46:46	-38.885	178.3542	21.3347	2.24
2014-10-19T09:00:58	-38.8083	178.63	7.3164	0.92
2014-10-19T09:31:06	-39.2	177.4087	14.8613	--
2014-10-19T09:41:23	-37.7839	179.0353	27.1095	--
2014-10-19T10:33:51	-38.5391	178.1364	116.022	1.84
2014-10-19T16:16:55	-38.6197	177.3383	104.2272	--
2014-10-19T16:42:43	-38.4078	178.3835	21.6648	1.47
2014-10-19T23:58:30	-38.8434	178.4207	13.7004	0.69
2014-10-20T08:54:16	-39.0857	178.1931	8.7648	1.78
2014-10-20T11:11:59	-38.7468	178.6859	7.8516	0.03
2014-10-20T12:15:18	-38.4752	177.1141	99.9715	--
2014-10-20T16:02:05	-39.1664	177.0717	45.5267	--
2014-10-20T20:15:41	-38.3942	178.5321	42.4852	1.56
2014-10-20T20:51:01	-38.3368	178.5023	23.1047	1.68

2014-10-20T22:48:17	-39.327	177.101	21.2901	--
2014-10-21T01:34:20	-38.426	178.4517	18.3469	1.74
2014-10-21T01:58:59	-38.9713	179.1384	49.8972	3.45
2014-10-21T02:12:35	-38.8156	178.7506	14.8365	0.91
2014-10-21T04:37:44	-38.8009	178.3306	66.1051	2.56
2014-10-21T07:44:20	-38.584	177.8666	13.3282	0.86
2014-10-21T08:28:18	-38.6683	178.595	7.7196	1.38
2014-10-21T11:46:01	-38.5746	177.8088	17.3609	1.51
2014-10-21T13:52:37	-38.967	178.9211	0.0019	2.63
2014-10-21T23:51:19	-38.763	179.1559	10.3357	2.79
2014-10-22T00:35:58	-39.2092	178.3962	32.7655	1.81
2014-10-22T01:15:48	-39.411	177.4866	46.8082	--
2014-10-22T02:34:46	-38.8247	178.717	0.7954	--
2014-10-22T02:53:22	-38.7425	178.7622	0.0093	0.06
2014-10-22T07:59:26	-38.5149	178.6108	41.9702	1.57
2014-10-22T09:33:41	-38.7598	178.606	11.7302	1.69
2014-10-22T11:18:48	-37.5437	179.3816	17.1076	--
2014-10-22T13:37:15	-38.7835	178.7594	14.2826	2.23
2014-10-22T14:50:42	-39.3002	177.5757	29.4692	--
2014-10-22T15:54:32	-38.6855	178.6235	7.7518	0.46
2014-10-22T15:59:52	-38.7954	178.6273	7.3734	0.2
2014-10-22T17:31:38	-38.8309	178.72	0.0	0.5
2014-10-22T18:55:50	-39.2312	177.0881	26.2027	--
2014-10-22T20:11:34	-38.644	178.4788	39.1004	0.68
2014-10-22T20:38:24	-38.181	178.3017	10.2977	1.45
2014-10-22T20:46:50	-38.4852	178.5946	23.8695	1.68
2014-10-22T23:52:09	-38.7863	178.6003	8.3426	0.45
2014-10-23T00:33:41	-39.0294	177.412	39.3714	--
2014-10-23T01:40:38	-38.8008	178.6441	3.621	0.44
2014-10-23T01:42:39	-38.1917	178.3927	22.9805	1.77
2014-10-23T03:08:23	-38.9286	178.4994	0.0	1.07
2014-10-23T05:22:51	-38.6194	178.2702	29.0651	1.7
2014-10-23T10:09:09	-38.9988	178.1479	0.0	2.77
2014-10-23T11:13:08	-38.8677	178.2297	28.942	1.32
2014-10-23T12:59:14	-39.2211	177.666	18.8076	1.46
2014-10-23T21:04:09	-38.2876	177.7795	32.6757	1.78
2014-10-23T21:05:06	-38.3385	177.8513	34.9144	1.85
2014-10-23T21:06:12	-38.2694	177.7468	32.4086	2.27
2014-10-23T21:09:14	-38.1605	177.688	34.9604	2.03
2014-10-23T21:31:09	-38.3125	177.8293	33.9317	1.93
2014-10-23T21:34:38	-39.252	177.1766	30.2795	--
2014-10-23T23:53:26	-38.6386	178.4239	14.0282	2.06
2014-10-24T00:33:41	-38.7604	178.6626	8.9305	--
2014-10-24T04:57:01	-38.6269	178.4359	20.7407	1.75

2014-10-24T12:20:36	-38.5998	177.1391	79.865	--
2014-10-24T18:46:52	-38.4076	177.4744	12.4583	--
2014-10-24T19:37:23	-38.9096	178.7343	2.7992	--
2014-10-25T05:35:03	-37.8578	177.2235	2.825	--
2014-10-25T06:25:14	-38.3257	177.9573	4.9413	1.79
2014-10-25T14:32:54	-38.3918	177.9053	16.6937	1.4
2014-10-25T14:46:32	-38.3908	177.8914	19.4014	1.37
2014-10-25T14:46:59	-38.3942	177.8911	19.5939	1.4
2014-10-25T18:04:29	-37.8161	178.0247	66.197	--
2014-10-25T18:33:54	-38.2401	178.1446	22.7301	1.53
2014-10-25T18:36:49	-38.2281	178.1306	28.9645	2.06
2014-10-26T02:44:10	-38.645	177.0166	83.2574	--
2014-10-26T05:30:22	-38.1102	178.4031	10.4884	2.9
2014-10-26T07:28:54	-37.9738	177.5111	33.4829	--
2014-10-26T07:48:55	-37.5562	177.9563	164.5496	--
2014-10-26T07:56:47	-38.3223	178.5575	38.2555	1.84
2014-10-26T08:34:16	-39.0179	178.3125	25.9205	2.51
2014-10-26T09:08:13	-38.8545	178.7184	0.8478	0.81
2014-10-26T09:50:52	-39.2623	178.4887	45.1586	--
2014-10-26T10:00:00	-39.0382	177.7125	16.1019	0.58
2014-10-26T10:02:12	-38.9383	178.2441	23.9691	1.51
2014-10-26T10:05:07	-38.8397	177.936	46.7913	1.49
2014-10-26T10:25:44	-38.8157	177.9669	37.9028	1.45
2014-10-26T11:04:47	-37.6855	178.3742	14.0138	--
2014-10-26T14:44:37	-39.0322	178.3286	9.9611	1.69
2014-10-26T16:22:46	-39.1849	177.4581	36.1196	--
2014-10-26T17:09:14	-38.5146	178.4949	22.2096	1.75
2014-10-26T17:48:36	-38.5081	178.4968	21.0786	2.69
2014-10-26T18:00:08	-37.7923	178.5738	17.6453	--
2014-10-26T19:06:49	-38.5103	178.4933	23.2851	2.33
2014-10-26T23:30:33	-38.1325	177.1193	117.3335	--
2014-10-26T23:36:23	-38.8618	178.7795	6.8754	0.87
2014-10-26T23:46:21	-38.6469	178.4776	24.7992	1.03
2014-10-27T01:41:30	-38.7319	178.702	10.5927	0.98
2014-10-27T01:41:30	-38.7319	178.702	10.5927	0.98
2014-10-27T02:01:01	-38.7746	178.7081	5.9325	--
2014-10-27T07:40:42	-37.9502	178.3946	50.2101	--
2014-10-27T08:43:23	-38.557	177.9597	19.7114	2.25
2014-10-27T09:20:46	-38.4846	178.5111	21.6922	1.68
2014-10-27T09:23:51	-38.4903	177.8374	40.8676	2.07
2014-10-27T11:36:48	-38.6358	178.2401	13.94	1.09
2014-10-27T11:39:58	-38.6322	178.2374	13.3798	1.4
2014-10-27T12:22:40	-38.6365	178.2478	13.2658	1.42
2014-10-27T12:59:39	-38.7327	178.7141	2.6582	0.08

2014-10-27T14:03:40	-38.7538	178.7546	0.6435	0.35
2014-10-27T15:07:38	-38.1646	178.1725	12.4989	0.63
2014-10-27T15:09:58	-38.1745	178.1744	12.2988	1.37
2014-10-27T15:40:26	-38.4264	177.2742	85.6234	--
2014-10-27T16:18:51	-38.1378	177.2502	70.268	--
2014-10-27T19:01:25	-38.4486	177.7915	112.5909	1.91
2014-10-27T19:53:18	-39.0659	178.5627	28.4828	1.62
2014-10-27T20:23:43	-38.327	178.5433	11.4264	1.64
2014-10-27T20:48:17	-38.4904	178.6717	32.8362	1.01
2014-10-27T21:01:12	-37.7126	178.053	14.8532	--
2014-10-27T21:15:44	-39.4574	177.202	27.7935	--
2014-10-27T23:34:31	-37.6842	179.1922	23.8176	--
2014-10-28T00:12:48	-38.2122	178.2157	12.4365	1.32
2014-10-28T00:20:00	-38.1506	178.1704	13.8196	0.97
2014-10-28T00:43:50	-38.9382	178.1166	57.5419	1.49
2014-10-28T02:17:58	-38.9191	177.2272	145.5256	--
2014-10-28T11:49:08	-38.5678	177.778	34.3929	1.77
2014-10-28T19:45:54	-39.2331	177.3143	170.526	--
2014-10-28T21:32:30	-38.5674	178.7055	5.438	2.35
2014-10-28T22:27:06	-38.7322	178.6826	5.0645	--
2014-10-28T23:58:52	-38.6104	178.5326	12.3938	0.44
2014-10-29T04:37:55	-38.6892	178.6614	11.6583	3.19
2014-10-29T08:58:34	-38.7959	177.6712	12.9148	1.69
2014-10-29T13:28:58	-37.6158	178.1468	5.09	--
2014-10-29T16:05:32	-38.7884	177.306	66.8278	--
2014-10-29T17:02:12	-38.7702	178.6935	9.7655	0.22
2014-10-29T17:42:10	-38.9139	177.7933	14.2961	1.86
2014-10-29T20:35:59	-38.4751	178.5387	35.656	1.17
2014-10-29T21:34:34	-38.141	178.0112	62.8365	3.01
2014-10-29T22:17:46	-38.7251	178.722	2.9536	--
2014-10-29T22:28:25	-38.7219	178.7169	2.0223	0.01
2014-10-29T22:39:04	-37.8865	177.6544	95.5529	--
2014-10-30T00:04:31	-38.6502	177.1766	73.5982	--
2014-10-30T00:43:45	-38.7374	178.718	7.9131	0.18
2014-10-30T10:16:32	-39.1932	177.4968	33.2981	--
2014-10-30T12:26:06	-39.1165	177.4547	20.9264	--
2014-10-30T15:13:26	-38.6903	177.8934	184.7287	1.82
2014-10-30T15:52:10	-39.4652	177.4832	48.1296	--
2014-10-30T17:30:11	-37.7561	179.0197	0.0	--
2014-10-30T18:50:48	-38.0282	179.0603	38.1236	2.23
2014-10-30T18:59:04	-39.1911	177.4109	31.7511	--
2014-10-30T19:34:18	-39.1097	177.2492	22.4737	--
2014-10-30T23:31:28	-37.9603	177.9073	115.975	--
2014-10-31T01:24:00	-38.8103	178.124	221.7742	1.93

2014-10-31T05:18:11	-38.7342	178.7093	3.5327	0.33
2014-10-31T05:24:09	-38.7348	178.7098	3.0737	--
2014-10-31T08:42:19	-38.5151	178.759	46.755	1.43
2014-10-31T08:51:39	-38.5756	178.4925	20.1918	0.67
2014-10-31T09:54:28	-38.5654	178.5052	15.0673	0.82
2014-10-31T10:42:47	-37.8327	177.2122	35.92	--
2014-10-31T15:29:06	-38.5988	178.4397	27.0811	1.57
2014-10-31T23:00:30	-37.5288	179.4561	256.5187	--
2014-10-31T23:49:24	-38.7866	178.8573	12.0144	1.04

Table B–2. September/October 2014 HOBITSS earthquake catalog relocated with NonLinLoc

Origin Time	Latitude	Longitude	Depth
2014-09-01T13:47:14	-39.0194	177.738	16.2344
2014-09-01T14:54:09	-38.5191	178.765	5.6875
2014-09-01T14:58:54	-38.7284	178.74	28.8125
2014-09-01T17:27:36	-39.0226	177.765	13.3438
2014-09-01T17:32:31	-39.0325	177.754	11.0781
2014-09-01T20:16:21	-38.8657	177.594	28.6562
2014-09-01T20:31:55	-38.0679	178.609	41.1562
2014-09-01T22:45:45	-39.0259	177.777	10.9219
2014-09-02T02:41:20	-39.0259	177.723	12.9531
2014-09-02T05:59:02	-39.0357	177.75	12.7188
2014-09-02T06:39:08	-37.656	177.561	48.1875
2014-09-02T10:01:23	-38.6499	178.799	11.9375
2014-09-02T11:46:43	-37.7148	178.389	20.5312
2014-09-02T13:24:47	-38.0908	178.591	35.4531
2014-09-02T14:12:05	-38.0974	178.568	33.8906
2014-09-02T16:40:58	-39.2973	177.287	31.4688
2014-09-03T01:33:43	-38.4309	177.993	27.0156
2014-09-03T09:16:40	-38.287	178.786	48.1094
2014-09-03T10:45:51	-39.0259	177.746	12.0156
2014-09-03T11:29:27	-39.2156	177.275	48.1094
2014-09-03T13:49:12	-38.0679	178.64	38.6562
2014-09-03T13:53:01	-38.9801	177.815	48.1094
2014-09-03T19:54:27	-38.3818	177.912	23.0312
2014-09-03T20:40:50	-39.0553	177.526	29.125
2014-09-03T23:45:31	-38.7545	177.693	21.3125
2014-09-04T03:19:36	-38.7022	177.816	48.1875
2014-09-04T06:54:14	-38.6761	178.523	18.8125
2014-09-04T07:40:48	-38.2085	178.104	5.45312
2014-09-04T09:41:18	-38.8069	178.464	48.1875
2014-09-04T09:59:30	-38.202	178.097	4.98438
2014-09-04T13:20:04	-37.862	177.939	48.1094
2014-09-04T21:11:52	-38.7186	177.581	48.1094
2014-09-04T23:23:50	-39.1992	177.325	45.0625
2014-09-04T23:44:05	-38.4047	177.31	48.1094
2014-09-05T03:53:23	-38.8657	177.949	20.2188
2014-09-05T08:57:54	-38.7317	178.005	27.7969
2014-09-05T10:12:44	-38.7709	177.982	34.2031
2014-09-05T16:48:35	-38.2608	177.401	48.1094

2014-09-05T18:29:20	-38.3589	178.022	40.9219
2014-09-05T19:20:24	-39.1371	177.329	37.9531
2014-09-05T23:09:40	-39.2286	177.709	44.3594
2014-09-06T00:51:16	-38.1431	178.684	48.1094
2014-09-06T05:06:46	-39.1175	177.716	31.2344
2014-09-06T09:55:10	-38.3949	178.571	38.9688
2014-09-06T13:31:41	-38.4734	178.189	48.3438
2014-09-06T14:29:41	-39.1011	177.534	48.3438
2014-09-06T15:54:34	-38.578	178.068	48.3438
2014-09-06T18:47:19	-38.4145	178.793	-1.1875
2014-09-07T00:58:13	-38.7317	178.566	34.0469
2014-09-07T01:51:42	-38.9573	178.552	26.1562
2014-09-07T03:32:42	-38.6761	178.184	35.6875
2014-09-07T08:58:04	-38.7219	178.316	46.7812
2014-09-07T09:53:54	-38.2085	178.12	19.8281
2014-09-07T10:27:40	-38.6499	179.045	43.8125
2014-09-07T10:32:35	-39.245	177.876	48.3438
2014-09-07T18:58:25	-38.2216	178.112	5.45312
2014-09-07T19:04:54	-38.1955	178.15	16.3906
2014-09-07T23:53:03	-38.2216	178.112	5.29688
2014-09-08T01:27:45	-38.1856	178.704	12.7188
2014-09-08T01:34:15	-37.4206	177.529	48.1875
2014-09-08T02:51:29	-38.6401	178.441	38.2656
2014-09-08T09:16:07	-38.3164	178.584	17.4062
2014-09-08T14:12:04	-38.5845	178.69	26.625
2014-09-08T16:25:00	-39.0063	177.862	13.7344
2014-09-08T19:12:20	-37.4729	179.406	18.1875
2014-09-09T15:43:44	-39.2417	177.725	48.1094
2014-09-09T16:44:39	-38.5976	178.706	9.4375
2014-09-09T17:10:11	-38.8167	177.89	29.3594
2014-09-09T20:59:18	-38.5976	178.675	19.4375
2014-09-10T03:34:32	-39.2548	177.71	48.1094
2014-09-10T07:03:43	-37.8129	178.505	28.1875
2014-09-10T12:18:42	-38.5715	178.582	5.6875
2014-09-10T12:45:02	-38.5453	178.551	4.4375
2014-09-10T18:41:00	-38.1203	178.87	48.3438
2014-09-11T01:16:02	-38.8984	177.525	26.625
2014-09-11T01:34:07	-38.5453	178.674	21.3125
2014-09-11T02:17:21	-38.6892	178.754	32.875
2014-09-11T10:20:29	-38.4341	178.204	48.3438
2014-09-11T10:48:35	-38.578	178.482	28.9688
2014-09-11T11:55:34	-38.493	178.335	26.3125
2014-09-11T15:22:04	-38.5191	178.458	17.5625
2014-09-11T18:52:35	-37.4206	178.467	20.6875

2014-09-11T20:39:42	-37.4206	177.741	48.1875
2014-09-11T21:49:12	-38.4341	178.204	48.3438
2014-09-11T22:13:47	-38.5845	178.874	21.625
2014-09-12T03:57:06	-39.1796	177.116	48.3438
2014-09-12T04:43:07	-37.4206	177.408	48.1875
2014-09-12T06:46:36	-39.4935	177.179	48.3438
2014-09-12T07:06:33	-38.8559	177.729	24.5156
2014-09-12T07:34:19	-39.1927	177.101	48.3438
2014-09-12T09:59:22	-38.4734	178.097	39.2812
2014-09-12T12:53:09	-37.4206	178.316	48.1875
2014-09-12T17:01:17	-38.408	178.571	32.0938
2014-09-13T00:02:02	-38.3295	178.278	48.3438
2014-09-13T02:48:56	-38.6761	178.677	19.4375
2014-09-13T07:04:54	-39.0325	177.46	39.3594
2014-09-13T09:44:15	-38.4685	177.681	48.4609
2014-09-13T13:31:30	-38.1268	178.45	7.5625
2014-09-13T14:27:17	-38.5453	178.704	19.4375
2014-09-13T16:01:20	-38.1987	177.008	20.8438
2014-09-13T16:05:21	-38.4668	178.273	14.4375
2014-09-13T22:09:50	-38.493	177.537	48.1875
2014-09-14T04:39:53	-37.9895	178.318	19.9062
2014-09-14T06:34:48	-38.6238	178.798	43.1875
2014-09-14T07:34:24	-38.6499	178.615	35.0625
2014-09-14T09:32:57	-39.245	178.512	48.3438
2014-09-14T09:57:18	-39.1665	177.72	14.9062
2014-09-14T12:49:09	-38.3884	177.873	46.9375
2014-09-14T14:15:06	-39.3627	177.256	48.3438
2014-09-14T16:44:18	-37.4206	178.285	48.1875
2014-09-14T17:52:39	-38.5093	177.84	20.7656
2014-09-14T22:50:32	-38.7088	178.393	43.0312
2014-09-15T00:32:00	-38.8592	178.558	46.3125
2014-09-15T07:47:28	-37.996	178.021	48.1875
2014-09-15T10:24:40	-38.9115	178.621	23.1875
2014-09-15T11:13:20	-38.5976	178.613	13.1875
2014-09-15T11:47:11	-38.5845	178.075	47.875
2014-09-15T14:18:57	-38.918	177.779	27.4062
2014-09-15T15:38:44	-38.493	178.672	24.4375
2014-09-15T15:40:59	-38.3328	178.076	44.6719
2014-09-15T16:57:39	-38.8167	177.952	30.6094
2014-09-15T18:06:45	-38.8101	177.967	28.1094
2014-09-16T05:38:50	-38.6499	178.615	12.5625
2014-09-16T06:34:50	-39.2581	177.768	35.8438
2014-09-16T08:05:38	-38.8297	177.867	17.7969
2014-09-16T20:55:06	-37.7606	177.623	48.1875

2014-09-17T00:13:53	-38.9115	177.941	48.1875
2014-09-17T04:18:27	-38.8167	178.09	48.1094
2014-09-17T04:46:46	-37.9895	178.09	48.3438
2014-09-17T09:22:00	-38.4832	178.615	48.1094
2014-09-17T10:13:06	-39.1502	177.422	47.1719
2014-09-17T10:54:40	-37.4206	178.527	48.1875
2014-09-17T11:11:17	-38.0679	178.396	-1.34375
2014-09-17T13:54:51	-39.1665	177.705	47.7188
2014-09-17T19:47:12	-38.614	177.841	48.1094
2014-09-17T20:18:21	-38.2837	178.606	48.1875
2014-09-18T01:55:05	-38.0483	178.601	3.8125
2014-09-18T03:47:34	-37.9241	178.682	48.3438
2014-09-18T04:59:20	-37.9241	178.606	27.7188
2014-09-18T05:52:11	-38.1333	178.718	48.3438
2014-09-18T07:13:13	-37.9208	178.382	27.7969
2014-09-18T15:15:03	-38.5715	178.736	6.3125
2014-09-18T18:53:35	-38.6499	178.645	23.1875
2014-09-18T19:50:31	-37.9437	177.563	48.1875
2014-09-19T05:54:13	-38.6761	178.861	48.1875
2014-09-19T13:03:11	-38.4145	178.916	28.1875
2014-09-19T13:22:46	-38.833	178.711	48.1875
2014-09-19T15:08:19	-37.6821	177.015	48.1875
2014-09-19T17:40:34	-38.9638	178.498	30.6875
2014-09-19T18:42:48	-37.7345	177.015	15.6875
2014-09-20T02:19:19	-38.5976	178.644	17.5625
2014-09-20T02:49:34	-38.0222	178.357	26.9375
2014-09-20T09:14:34	-38.5715	178.582	14.4375
2014-09-20T15:10:37	-37.9895	178.79	48.3438
2014-09-20T18:53:05	-38.8853	178.527	44.4375
2014-09-20T19:21:35	-38.372	177.793	48.1094
2014-09-20T20:25:20	-38.4309	178.322	35.4531
2014-09-21T00:49:47	-38.3884	178.762	-1.1875
2014-09-21T09:31:09	-38.8951	177.999	30.6094
2014-09-21T10:21:32	-39.1142	177.395	22.4062
2014-09-21T10:42:22	-39.2188	177.256	47.7188
2014-09-21T13:23:53	-38.8984	177.463	47.875
2014-09-21T15:14:37	-38.9932	177.877	48.1094
2014-09-21T21:15:22	-37.7868	178.352	24.4375
2014-09-22T07:21:29	-38.4145	178.18	48.1875
2014-09-22T08:06:04	-38.6368	178.63	35.375
2014-09-22T21:38:46	-38.9115	178.559	48.1875
2014-09-23T01:36:31	-39.2254	178.814	48.1875
2014-09-23T03:39:51	-38.5976	178.429	21.3125
2014-09-23T10:07:11	-39.0684	177.634	48.1875

2014-09-23T10:39:31	-38.3982	177.908	41.3906
2014-09-23T22:43:25	-37.5775	177.015	48.1875
2014-09-23T22:47:46	-38.1987	177.008	48.3438
2014-09-23T23:36:03	-38.5649	178.636	48.3438
2014-09-24T02:17:47	-38.2805	178.442	36.8594
2014-09-24T03:49:20	-38.2641	177.864	48.3438
2014-09-24T05:14:16	-38.6761	178.431	48.1875
2014-09-24T09:30:14	-38.7872	179.226	42.7188
2014-09-24T10:29:29	-38.4276	178.564	27.875
2014-09-24T15:44:03	-38.0908	177.675	48.1094
2014-09-24T18:12:28	-38.2085	178.165	44.2031
2014-09-24T18:17:10	-38.2151	178.143	41.3906
2014-09-24T18:46:18	-38.7219	178.778	0.21875
2014-09-24T20:29:29	-38.6434	178.622	33.3438
2014-09-24T22:07:38	-38.8592	178.866	28.8125
2014-09-24T23:20:40	-38.8265	178.58	17.0938
2014-09-25T01:10:40	-38.9017	177.976	31.7031
2014-09-25T02:30:32	-38.9442	177.826	47.0938
2014-09-25T02:48:30	-38.8559	177.975	30.4531
2014-09-25T05:38:18	-38.8134	177.64	48.3438
2014-09-25T07:08:55	-38.6303	177.715	48.3438
2014-09-25T08:23:11	-38.6172	177.622	36.1562
2014-09-25T14:04:32	-38.7545	178.555	31.9375
2014-09-25T14:24:06	-38.7022	178.462	20.0625
2014-09-25T17:59:30	-38.6761	178.554	16.3125
2014-09-25T19:32:48	-38.9834	177.193	48.3438
2014-09-25T19:37:27	-38.4309	177.257	48.1094
2014-09-25T19:41:29	-38.7022	178.246	47.5625
2014-09-25T21:58:20	-38.1268	178.786	48.1875
2014-09-25T22:02:55	-38.99	178.622	15.0625
2014-09-25T22:19:49	-38.0974	178.873	48.1094
2014-09-26T02:36:48	-38.9638	178.745	31.3125
2014-09-26T02:59:51	-39.1305	177.515	48.1094
2014-09-26T03:08:53	-38.99	178.499	34.4375
2014-09-26T03:35:13	-38.2249	178.231	22.4062
2014-09-26T07:04:17	-38.2478	178.434	47.4844
2014-09-26T11:23:21	-38.578	178.482	26.7812
2014-09-26T16:54:17	-38.3982	178.337	30.6094
2014-09-26T17:53:22	-38.5388	178.175	48.3438
2014-09-26T22:57:08	-38.6499	178.215	37.5625
2014-09-27T06:30:21	-39.2057	177.132	48.3438
2014-09-27T06:55:11	-38.7022	178.554	48.1875
2014-09-27T08:59:34	-37.875	177.894	48.1094
2014-09-27T09:09:03	-38.6499	178.645	22.5625

2014-09-27T11:23:12	-38.7284	177.785	48.1875
2014-09-27T18:44:33	-38.5126	178.665	20.2188
2014-09-27T22:42:24	-37.8391	177.137	48.1875
2014-09-28T02:41:22	-38.9834	177.734	48.3438
2014-09-28T03:47:39	-38.3884	178.762	40.6875
2014-09-28T04:27:27	-37.8652	177.015	48.1875
2014-09-28T08:52:42	-39.4019	177.521	47.4062
2014-09-28T09:09:06	-38.323	178.684	7.875
2014-09-28T15:56:00	-38.6761	178.8	14.4375
2014-09-28T16:57:58	-38.6728	177.735	48.1094
2014-09-28T18:15:54	-38.4145	178.763	48.1875
2014-09-28T21:03:34	-38.6091	178.458	44.1641
2014-09-28T22:20:08	-38.3965	177.914	48.4609
2014-09-28T22:23:11	-38.9801	177.498	44.0469
2014-09-29T03:04:25	-38.493	178.611	5.6875
2014-09-29T04:38:54	-38.3622	177.015	20.6875
2014-09-29T05:52:11	-37.5841	177.25	48.3438
2014-09-29T06:19:24	-38.7317	177.589	41.0781
2014-09-29T10:05:06	-39.0586	177.445	48.1094
2014-09-29T10:27:00	-38.5388	178.666	40.8438
2014-09-29T11:08:11	-39.0423	177.479	23.1875
2014-09-29T11:25:34	-39.0096	177.487	48.3438
2014-09-29T13:15:52	-38.372	178.153	22.6406
2014-09-29T15:21:00	-37.6233	177.963	21.7812
2014-09-30T01:34:47	-38.3949	177.958	48.3438
2014-09-30T05:14:47	-38.9344	178.007	28.2656
2014-09-30T11:36:04	-37.4206	177.197	48.1875
2014-09-30T16:24:08	-38.8003	177.871	35.8438
2014-09-30T18:06:36	-38.2478	178.22	27.1719
2014-09-30T18:18:37	-38.2249	178.062	8.03125
2014-09-30T18:26:57	-38.5976	178.429	25.6875
2014-09-30T20:14:18	-38.493	177.015	20.6875
2014-09-30T23:00:27	-38.6728	177.142	-1.42188
2014-10-01T03:15:51	-38.8951	177.945	48.1094
2014-10-01T04:28:02	-38.2249	178.796	43.9688
2014-10-01T04:32:08	-38.6238	178.86	20.0625
2014-10-01T04:57:39	-38.8003	178.764	39.9062
2014-10-01T07:24:53	-38.833	178.773	48.1875
2014-10-01T11:12:11	-38.2674	178.205	26.8594
2014-10-01T11:54:37	-39.0226	177.611	20.8438
2014-10-01T14:50:43	-38.627	177.849	30.2969
2014-10-01T16:48:45	-38.1464	178.84	48.3438
2014-10-01T17:09:25	-38.1824	178.203	29.3594
2014-10-01T17:33:46	-38.0908	177.935	48.1094

2014-10-01T18:43:53	-38.1758	178.218	32.0156
2014-10-01T20:32:07	-38.5322	178.689	42.875
2014-10-02T00:38:50	-38.3426	178.524	21.4688
2014-10-02T04:59:15	-38.0974	178.95	48.1094
2014-10-02T06:03:39	-38.6761	178.769	29.4375
2014-10-02T10:24:44	-37.875	178.677	48.1094
2014-10-02T11:01:23	-38.3459	178.504	26.2344
2014-10-02T12:22:25	-37.9993	178.375	15.9219
2014-10-02T13:33:55	-37.9797	178.375	18.8906
2014-10-02T17:10:56	-38.4112	177.9	38.8906
2014-10-02T18:30:22	-38.8461	178.203	1.625
2014-10-02T19:03:30	-38.6499	178.645	25.0625
2014-10-02T19:33:14	-38.7529	177.961	48.4609
2014-10-02T21:03:02	-38.5715	178.674	48.1875
2014-10-02T21:47:09	-39.0455	177.483	27.9531
2014-10-02T21:57:40	-38.7807	178.125	38.8125
2014-10-02T22:23:10	-38.7971	177.967	48.1094
2014-10-03T02:02:11	-37.8195	178.543	35.8438
2014-10-03T05:51:43	-38.1595	178.795	33.3438
2014-10-03T07:49:21	-38.8036	177.967	48.1094
2014-10-03T21:42:48	-38.4407	178.549	48.1875
2014-10-03T22:28:41	-38.4407	178.978	48.1875
2014-10-03T23:05:20	-38.6499	178.738	-1.1875
2014-10-04T06:52:49	-38.8134	178.241	20.5312
2014-10-04T07:57:08	-38.7317	178.235	31.3906
2014-10-04T09:38:57	-38.833	178.249	31.3125
2014-10-04T10:55:48	-38.5289	178.025	48.1094
2014-10-04T11:29:54	-38.1824	177.89	48.1094
2014-10-04T12:01:19	-39.0161	178.376	38.1875
2014-10-04T13:41:45	-37.6364	178.479	28.0312
2014-10-04T14:23:38	-37.6756	178.388	13.3438
2014-10-04T20:40:22	-38.4995	178.189	37.0938
2014-10-04T22:23:20	-39.1273	177.766	48.3438
2014-10-04T23:46:37	-38.2478	178.074	22.1719
2014-10-05T01:23:00	-38.6793	177.742	48.1094
2014-10-05T03:35:06	-38.8134	177.886	11.1562
2014-10-05T07:03:19	-38.8134	177.886	48.3438
2014-10-05T07:29:30	-38.5845	178.751	21.625
2014-10-05T08:48:03	-38.153	178.084	48.1875
2014-10-05T09:52:08	-38.9703	177.456	48.3438
2014-10-05T14:26:04	-38.6172	177.853	48.3438
2014-10-05T14:51:34	-38.8853	177.91	48.1875
2014-10-05T14:55:28	-38.8853	177.91	48.1875
2014-10-05T15:01:09	-38.7545	177.816	46.9375

2014-10-05T15:14:53	-38.7742	179.18	40.2188
2014-10-05T15:27:44	-39.1077	178.393	44.125
2014-10-05T21:47:30	-38.5518	178.037	48.3438
2014-10-06T13:40:57	-38.8461	178.326	24.125
2014-10-06T13:59:55	-38.2543	178.197	27.4844
2014-10-06T15:07:46	-38.0745	178.693	26.3125
2014-10-06T16:08:19	-38.9573	177.502	30.8438
2014-10-06T18:11:11	-38.8265	178.303	34.5938
2014-10-06T20:10:46	-38.5976	178.583	48.1875
2014-10-07T00:11:46	-38.7219	177.9	48.3438
2014-10-07T02:11:38	-38.8003	178.009	48.3438
2014-10-07T02:34:12	-38.99	178.561	28.1875
2014-10-07T02:43:24	-38.954	177.49	40.6094
2014-10-07T07:27:35	-39.294	177.601	48.1094
2014-10-07T09:41:16	-38.8428	178.291	27.7969
2014-10-07T09:54:42	-37.8979	178.682	48.3438
2014-10-07T10:26:49	-38.6238	178.337	-1.1875
2014-10-07T14:44:15	-38.3622	177.322	10.0625
2014-10-07T16:12:34	-38.408	178.172	48.3438
2014-10-07T21:08:05	-38.2837	178.392	48.1875
2014-10-07T22:40:13	-38.7807	178.155	38.8125
2014-10-08T02:19:09	-38.833	178.341	24.4375
2014-10-08T02:27:59	-37.4206	177.801	18.1875
2014-10-08T02:37:50	-38.7415	178.139	24.125
2014-10-08T02:57:36	-38.833	178.341	23.1875
2014-10-08T04:28:18	-38.7545	178.217	-1.1875
2014-10-08T04:44:14	-38.493	177.783	-0.5625
2014-10-08T04:56:48	-38.8592	178.311	38.1875
2014-10-08T05:26:12	-38.7971	177.913	12.1719
2014-10-08T06:45:18	-39.2025	177.825	48.1094
2014-10-08T07:07:01	-38.6892	178.569	47.875
2014-10-08T07:32:45	-38.833	178.341	25.6875
2014-10-08T15:19:47	-38.7807	178.402	8.8125
2014-10-08T15:44:41	-38.6499	178.369	30.6875
2014-10-08T17:00:47	-38.869	178.377	28.2656
2014-10-08T19:24:58	-38.6172	177.961	48.3438
2014-10-08T20:50:32	-38.9703	177.656	5.53125
2014-10-08T20:52:39	-38.8069	178.433	10.0625
2014-10-08T21:41:06	-38.7349	177.87	48.3438
2014-10-09T00:06:00	-38.7807	178.279	25.6875
2014-10-09T00:32:03	-38.833	178.372	18.1875
2014-10-09T05:45:51	-38.9376	178.436	48.1875
2014-10-09T09:53:04	-38.4995	177.99	41.7812
2014-10-09T09:59:51	-38.4145	177.904	48.1875

2014-10-09T12:43:16	-38.3099	178.515	43.1875
2014-10-09T13:31:56	-39.1404	177.488	48.3438
2014-10-09T13:38:27	-38.9311	177.888	9.90625
2014-10-09T14:02:34	-38.8592	177.817	1.9375
2014-10-09T15:46:20	-37.4206	177.045	11.9375
2014-10-09T17:37:22	-39.2515	178.597	48.1875
2014-10-10T03:07:43	-38.7284	178.309	4.4375
2014-10-10T05:40:48	-37.4206	178.104	48.1875
2014-10-10T06:05:31	-38.1758	178.165	39.6719
2014-10-10T06:48:43	-38.2935	177.922	48.1094
2014-10-10T07:01:25	-38.8069	178.618	5.0625
2014-10-10T07:41:01	-38.287	178.182	31.5469
2014-10-10T09:18:04	-38.0745	177.809	48.1875
2014-10-10T09:22:14	-38.1889	178.165	26.0781
2014-10-10T09:41:55	-38.7872	178.61	6.46875
2014-10-10T09:56:22	-37.9339	177.004	-1.42188
2014-10-10T09:57:04	-37.9339	177.004	-1.42188
2014-10-10T11:23:32	-37.8293	178.524	46.7031
2014-10-10T12:30:44	-38.4995	178.634	35.2188
2014-10-10T13:46:34	-38.8494	177.49	48.1094
2014-10-10T15:18:09	-38.7545	178.371	22.5625
2014-10-10T16:50:39	-38.7872	178.441	48.3438
2014-10-10T18:50:14	-38.5518	178.052	48.3438
2014-10-10T19:41:10	-38.2772	178.782	36.1562
2014-10-10T20:21:42	-38.5224	177.956	39.5156
2014-10-10T21:25:58	-38.9376	179.455	28.1875
2014-10-11T04:21:27	-38.9115	178.621	19.4375
2014-10-11T08:36:11	-38.4636	178.515	48.1094
2014-10-11T09:57:41	-38.8232	177.89	12.6406
2014-10-11T10:37:43	-37.6037	177.015	48.1875
2014-10-11T11:44:26	-38.8363	177.852	25.6094
2014-10-11T12:20:05	-37.5252	177.5	48.1875
2014-10-11T12:44:40	-38.3655	178.183	24.2031
2014-10-11T14:49:30	-38.5518	177.929	27.7188
2014-10-11T16:50:51	-38.6074	178.41	28.1094
2014-10-11T21:19:54	-38.8624	177.829	12.3281
2014-10-11T22:42:30	-37.9077	177.719	48.1094
2014-10-11T22:57:54	-38.6499	178.83	48.1875
2014-10-12T01:11:51	-38.7644	178.39	28.1094
2014-10-12T05:39:21	-38.8069	178.618	5.0625
2014-10-12T06:56:02	-38.5715	178.674	18.8125
2014-10-12T12:29:54	-37.911	178.408	38.3438
2014-10-12T13:23:03	-38.614	177.957	46.7031
2014-10-12T13:36:36	-38.6041	178.36	14.2812

2014-10-12T14:16:37	-38.7545	177.878	48.1875
2014-10-12T14:46:09	-39.2581	177.597	30.5312
2014-10-12T17:14:41	-38.6565	178.561	34.5938
2014-10-12T20:11:02	-38.8951	177.976	35.7656
2014-10-12T20:32:00	-38.8821	177.984	42.7969
2014-10-12T22:15:27	-38.4243	178.184	36.7031
2014-10-12T22:52:13	-38.9115	178.528	27.5625
2014-10-12T23:28:17	-38.833	178.526	21.9375
2014-10-13T00:03:21	-38.6761	178.8	8.1875
2014-10-13T01:43:18	-38.7219	177.762	17.0938
2014-10-13T03:44:58	-38.8069	178.618	6.3125
2014-10-13T04:13:21	-38.5665	177.9	41.8984
2014-10-13T06:23:11	-38.7578	177.966	48.1094
2014-10-13T09:25:36	-38.5486	177.856	33.7344
2014-10-13T11:32:07	-38.4243	178.131	34.8281
2014-10-13T11:56:33	-38.4162	177.764	48.4609
2014-10-13T13:09:30	-38.4668	178.426	48.1875
2014-10-13T13:40:09	-38.7284	178.74	16.3125
2014-10-13T13:44:42	-38.5976	178.829	26.9375
2014-10-13T14:04:18	-38.8494	177.944	34.8281
2014-10-13T14:05:31	-37.6723	178.703	48.1094
2014-10-13T14:16:56	-38.1889	178.341	14.3594
2014-10-13T15:17:43	-38.5518	177.898	48.3438
2014-10-13T15:27:12	-38.7186	177.989	13.4219
2014-10-13T16:06:27	-38.8134	177.84	38.9688
2014-10-13T20:59:31	-38.6434	178.484	25.8438
2014-10-13T21:42:39	-38.9638	178.436	30.0625
2014-10-13T22:05:51	-38.8069	178.618	5.6875
2014-10-14T00:14:24	-37.8129	178.11	48.1875
2014-10-14T00:29:09	-38.8919	178.35	48.3438
2014-10-14T05:07:29	-38.9834	177.796	48.3438
2014-10-14T06:28:52	-38.3818	178.157	47.0938
2014-10-14T10:49:23	-38.3949	178.555	48.3438
2014-10-14T11:23:57	-38.8657	177.841	4.90625
2014-10-14T12:27:58	-39.0259	177.738	28.1094
2014-10-14T14:10:45	-38.6041	178.652	48.3438
2014-10-14T14:47:19	-38.8134	178.441	8.03125
2014-10-14T20:36:55	-38.3034	178.033	48.3438
2014-10-14T23:07:43	-38.6041	178.145	41.1562
2014-10-15T12:09:52	-38.1726	177.008	48.3438
2014-10-15T12:44:16	-37.4206	177.257	48.1875
2014-10-15T15:50:26	-38.6041	177.93	48.3438
2014-10-15T16:51:51	-38.3622	178.547	16.9375
2014-10-15T19:06:23	-37.4206	177.469	48.1875

2014-10-15T20:30:28	-38.5715	178.582	34.4375
2014-10-15T21:20:57	-38.7872	178.625	5.21875
2014-10-16T11:37:23	-38.5813	178.049	44.6719
2014-10-16T13:40:32	-39.1502	177.871	31.7031
2014-10-16T15:37:46	-38.4734	178.588	21.4688
2014-10-16T18:00:13	-38.6238	178.122	48.1875
2014-10-17T04:34:58	-37.4206	177.408	48.1875
2014-10-17T07:16:15	-38.4145	178.64	33.1875
2014-10-17T08:04:28	-38.3818	178.203	48.3438
2014-10-17T12:47:41	-37.9666	177.263	48.1094
2014-10-17T13:50:43	-38.3622	178.516	48.1875
2014-10-17T15:43:50	-38.7938	178.633	2.875
2014-10-17T16:21:12	-38.3164	178.462	47.0938
2014-10-17T17:44:08	-38.6172	177.761	48.3438
2014-10-17T21:13:47	-38.0745	178.724	4.4375
2014-10-17T21:25:35	-38.6565	178.53	14.9062
2014-10-18T00:55:54	-38.3034	178.11	45.2188
2014-10-18T02:10:07	-38.6238	178.091	48.1875
2014-10-18T03:06:27	-39.2581	178.528	48.3438
2014-10-18T05:53:14	-38.8003	178.626	3.65625
2014-10-18T12:37:01	-38.8134	177.902	38.6562
2014-10-18T13:04:31	-38.7742	178.625	5.84375
2014-10-18T16:43:55	-38.7938	178.633	1.625
2014-10-18T18:22:58	-38.3099	178.546	7.5625
2014-10-18T21:43:45	-38.9311	178.752	-1.34375
2014-10-19T00:35:26	-38.0728	177.681	48.4609
2014-10-19T03:10:44	-38.5191	178.458	16.9375
2014-10-19T04:51:16	-39.2188	178.914	30.2188
2014-10-19T05:27:44	-38.9376	178.498	30.6875
2014-10-19T08:20:24	-38.8624	178.369	36.3906
2014-10-19T08:46:44	-38.8886	178.392	44.9844
2014-10-19T09:00:59	-38.8003	178.626	4.59375
2014-10-19T09:31:05	-39.1927	177.411	28.0312
2014-10-19T09:41:23	-37.8456	178.817	48.3438
2014-10-19T10:33:37	-37.6821	177.046	48.1875
2014-10-19T16:17:02	-38.748	177.901	48.3438
2014-10-19T16:42:48	-38.6499	178.584	16.9375
2014-10-19T20:55:25	-37.6952	178.366	17.875
2014-10-19T23:58:30	-38.8592	178.434	16.9375
2014-10-20T08:54:21	-38.8494	177.798	6.07812
2014-10-20T11:11:59	-38.7349	178.686	3.65625
2014-10-20T12:15:26	-38.6826	177.792	48.3438
2014-10-20T16:02:09	-38.9965	177.703	48.3438
2014-10-20T20:15:45	-38.6238	178.645	21.9375

2014-10-20T20:50:59	-38.3099	178.485	47.5625
2014-10-21T01:34:22	-38.5976	178.491	22.5625
2014-10-21T01:58:57	-38.9082	178.941	46.0781
2014-10-21T02:12:34	-38.8853	178.805	5.6875
2014-10-21T04:37:44	-38.7022	178.216	48.1875
2014-10-21T07:44:20	-38.5682	177.849	25.1406
2014-10-21T08:28:17	-38.6532	178.565	-1.42188
2014-10-21T11:46:01	-38.5682	177.849	29.3594
2014-10-21T13:52:40	-38.6499	178.615	35.0625
2014-10-21T23:51:21	-38.8069	179.081	15.0625
2014-10-22T00:36:01	-38.9638	178.344	22.5625
2014-10-22T01:15:49	-39.0848	177.607	48.1094
2014-10-22T02:34:46	-38.833	178.711	-1.1875
2014-10-22T02:53:22	-38.7545	178.771	-1.1875
2014-10-22T07:59:25	-38.5616	178.509	48.1094
2014-10-22T08:01:58	-38.5845	178.383	47.875
2014-10-22T09:33:41	-38.6957	178.562	15.8438
2014-10-22T11:18:48	-37.7148	179.179	48.3438
2014-10-22T13:37:14	-38.7774	178.783	28.5781
2014-10-22T14:50:40	-39.2679	177.624	48.1094
2014-10-22T15:54:33	-38.7088	178.639	3.65625
2014-10-22T15:59:52	-38.7872	178.625	4.28125
2014-10-22T17:31:41	-38.7545	178.709	7.5625
2014-10-22T20:11:33	-38.6499	178.492	48.1875
2014-10-22T20:38:24	-38.1856	178.306	27.0938
2014-10-22T20:46:48	-38.4897	178.623	48.1094
2014-10-22T23:52:09	-38.8003	178.626	3.96875
2014-10-23T00:33:42	-38.9573	177.703	48.3438
2014-10-23T01:40:39	-38.7872	178.641	1.46875
2014-10-23T01:42:24	-37.4467	178.013	48.1875
2014-10-23T03:08:23	-38.9115	178.466	-1.1875
2014-10-23T05:22:50	-38.6238	178.276	36.3125
2014-10-23T10:09:09	-38.99	177.943	48.1875
2014-10-23T11:13:07	-38.8821	178.246	37.6406
2014-10-23T12:59:12	-39.2319	177.674	40.8438
2014-10-23T18:28:50	-38.7742	178.625	2.09375
2014-10-23T21:04:09	-38.3949	177.912	48.3438
2014-10-23T21:05:05	-38.3949	177.896	48.3438
2014-10-23T21:06:12	-38.3687	177.865	48.3438
2014-10-23T21:09:15	-38.3818	177.896	48.3438
2014-10-23T21:31:08	-38.3884	177.873	46.3125
2014-10-23T21:34:37	-39.2221	177.283	48.1094
2014-10-23T23:53:25	-38.627	178.449	37.1719
2014-10-24T00:33:41	-38.7611	178.671	5.21875

2014-10-24T04:57:01	-38.627	178.41	28.2656
2014-10-24T12:20:30	-38.2249	177.008	48.3438
2014-10-24T18:46:52	-38.4211	177.514	16.7812
2014-10-24T19:37:23	-38.8919	178.72	-1.34375
2014-10-25T05:34:57	-37.6298	177.015	20.0625
2014-10-25T06:25:17	-38.493	178.12	-1.1875
2014-10-25T14:32:53	-38.3949	177.912	27.0938
2014-10-25T14:46:32	-38.3982	177.893	28.2656
2014-10-25T14:46:59	-38.3982	177.893	28.4219
2014-10-25T18:04:35	-38.3557	178.233	48.3438
2014-10-25T18:33:53	-38.2216	178.135	34.5156
2014-10-25T18:36:48	-38.2543	178.128	37.9531
2014-10-26T02:44:06	-38.2903	177.008	48.3438
2014-10-26T05:30:30	-38.9115	178.806	5.6875
2014-10-26T07:28:56	-38.2053	177.718	48.1875
2014-10-26T07:48:52	-37.4206	177.469	48.1875
2014-10-26T07:56:53	-38.6238	178.676	21.3125
2014-10-26T08:34:14	-38.9605	178.286	43.1094
2014-10-26T09:08:15	-38.8265	178.688	-1.03125
2014-10-26T09:50:53	-39.039	178.349	48.1094
2014-10-26T10:00:00	-39.0357	177.688	20.8438
2014-10-26T10:02:11	-38.9376	178.251	34.4375
2014-10-26T10:05:06	-38.8363	177.96	48.1094
2014-10-26T10:25:42	-38.8036	177.982	48.1094
2014-10-26T11:04:59	-38.3884	178.578	19.4375
2014-10-26T14:44:38	-39.0259	178.333	6.54688
2014-10-26T16:22:46	-39.1796	177.457	38.6562
2014-10-26T17:09:13	-38.5093	178.454	34.9844
2014-10-26T17:48:34	-38.5142	178.506	46.1953
2014-10-26T18:00:15	-38.2576	178.575	21.3125
2014-10-26T19:06:47	-38.5159	178.493	42.3281
2014-10-26T23:30:44	-38.6041	177.884	48.3438
2014-10-26T23:36:23	-38.8396	178.75	-1.34375
2014-10-26T23:46:22	-38.7415	178.571	27.875
2014-10-27T01:41:31	-38.7284	178.709	8.8125
2014-10-27T02:01:02	-38.748	178.717	2.71875
2014-10-27T07:40:41	-38.0532	178.336	48.4609
2014-10-27T08:43:23	-38.5567	177.958	33.7734
2014-10-27T09:20:45	-38.4963	178.523	41.7031
2014-10-27T09:23:49	-38.5142	177.873	48.4609
2014-10-27T11:36:48	-38.627	178.249	26.8594
2014-10-27T11:39:58	-38.6303	178.238	24.2812
2014-10-27T12:22:40	-38.6303	178.253	28.0312
2014-10-27T12:59:40	-38.7284	178.709	3.1875

2014-10-27T14:03:41	-38.7349	178.747	0.53125
2014-10-27T15:07:38	-38.1856	178.199	19.9062
2014-10-27T15:09:59	-38.1889	178.18	16.7031
2014-10-27T15:40:32	-38.6434	177.838	48.3438
2014-10-27T16:18:53	-38.3557	177.528	48.3438
2014-10-27T19:01:18	-38.0222	177.259	48.1875
2014-10-27T19:53:18	-38.99	178.468	33.1875
2014-10-27T20:23:46	-38.493	178.519	25.0625
2014-10-27T20:48:19	-38.6238	178.645	30.6875
2014-10-27T21:01:04	-37.4206	177.771	48.1875
2014-10-27T23:34:28	-37.7345	179.202	48.1875
2014-10-28T00:12:48	-38.2118	178.246	25.8438
2014-10-28T00:20:00	-38.1726	178.199	18.6562
2014-10-28T00:43:34	-38.3099	177.015	21.3125
2014-10-28T02:17:56	-38.2837	177.015	48.1875
2014-10-28T11:49:07	-38.5649	177.806	48.3438
2014-10-28T19:46:15	-38.7022	178.4	26.3125
2014-10-28T21:32:32	-38.6695	178.73	-0.71875
2014-10-28T22:27:06	-38.7284	178.678	3.8125
2014-10-28T23:58:49	-38.578	178.651	42.4062
2014-10-29T04:37:54	-38.6859	178.727	27.9531
2014-10-29T08:58:34	-38.7742	177.685	28.0312
2014-10-29T13:28:57	-37.6135	178.232	27.9531
2014-10-29T16:05:35	-38.7872	177.747	48.3438
2014-10-29T17:02:13	-38.7545	178.709	7.5625
2014-10-29T17:42:10	-38.8951	177.814	23.5781
2014-10-29T20:35:57	-38.4276	178.502	47.875
2014-10-29T21:34:33	-38.2903	177.987	48.3438
2014-10-29T22:17:46	-38.7219	178.732	1.15625
2014-10-29T22:28:26	-38.7284	178.709	3.8125
2014-10-29T22:39:13	-38.4603	178.143	48.3438
2014-10-30T00:04:36	-38.7349	177.762	48.3438
2014-10-30T00:43:46	-38.7349	178.732	2.71875
2014-10-30T10:16:31	-39.1371	177.592	48.1094
2014-10-30T12:26:03	-39.1796	177.457	48.3438
2014-10-30T15:13:42	-39.0161	178.592	48.1875
2014-10-30T15:52:13	-39.1665	177.86	48.3438
2014-10-30T17:30:23	-38.2837	178.79	5.0625
2014-10-30T18:50:47	-38.0778	178.941	48.1094
2014-10-30T18:59:04	-39.2188	177.411	35.5312
2014-10-30T19:34:17	-39.1305	177.228	33.7344
2014-10-30T23:31:38	-38.4864	178.25	48.3438
2014-10-31T01:24:21	-38.7807	178.648	48.1875
2014-10-31T05:18:12	-38.7284	178.709	2.5625

2014-10-31T05:24:09	-38.7284	178.709	2.5625
2014-10-31T08:42:21	-38.5257	178.65	20.5312
2014-10-31T08:51:40	-38.5453	178.52	16.3125
2014-10-31T09:54:28	-38.578	178.498	24.9062
2014-10-31T10:42:47	-37.9274	177.354	48.1094
2014-10-31T15:29:06	-38.5976	178.398	22.5625
2014-10-31T23:00:57	-38.8853	178.929	48.1875
2014-10-31T23:49:25	-38.8134	178.826	5.53125

Appendix C - The 2011 Northern Kermadec Earthquake Doublet and Subduction Zone Faulting Interactions

Abstract.

A large intraplate earthquake doublet (July 6, 2011, M_w 7.6; October 21, 2011, M_w 7.4) occurred in the Pacific plate beneath the outer trench slope of the northern Kermadec subduction zone, seaward of a seismically-coupled region of the megathrust. The first large event, a shallow (~24 km centroid depth) normal-faulting rupture, was followed by intraplate aftershocks within minutes and by aftershocks near the megathrust within hours. The second large event, a deeper (~45 km centroid depth) thrust-faulting rupture below the northern portion of the first rupture plane, was also followed by interplate and intraplate aftershocks. The last large interplate activity in northern Kermadec involved an underthrusting doublet on January 14, 1976 (M_w 7.8, 7.9). A regional GPS station indicates that the upper plate has been moving westward in northern Kermadec since at least 2009, as expected for a seismically locked plate interface that should tend to reduce trench-slope extensional stresses. Coulomb stress change calculations using a finite-fault model determined from teleseismic body wave inversions for the normal-faulting event in the 2011 doublet favor activation of megathrust faulting. Coulomb stress changes for the October compressional event appear to reduce interplate thrust activity, but only ephemerally, as that event did not reverse the westward motion of the upper plate. The net effect of the doublet is a few bar increase of interplate thrust-fault driving

stress, which may have advanced the next large megathrust event to come. Intraplate normal faulting may serve as a harbinger, not only a response, to large megathrust ruptures.

Introduction

Subduction of oceanic lithosphere involves large-scale deformation of the stiff underthrusting plate, elastic and anelastic deformation of the overriding plate, and frictional sliding on the megathrust boundary between the two plates. The complex thermal, petrological and hydrological environment, and the wide variety of time-scales of deformation in a shallow subduction zone make it challenging to disentangle the relative roles played by elastic and anelastic deformations and to quantify the stress distribution in the subduction zone. Earthquakes provide one window into these processes, as their temporal patterns, faulting mechanisms, and magnitude of strain release directly characterize rapid time scale deformations; however, post-seismic and interseismic deformation intrinsically involve longer time scale aseismic deformations that appear to involve a mix of poroelastic, anelastic, and/or viscoelastic processes. The relationship between the relatively rapid seismic cycle processes and deformations and the million-year time scale processes by which slabs bend, sink, and unbend, is very difficult to establish.

During the past 50 years there have been many demonstrations that the stress changes associated with both interplate and intraplate earthquakes exhibit spatial and temporal patterns suggestive of significant elastic interactions, which tend to be intuitively interpretable [e.g., *Isacks et al.*, 1968; *Stauder*, 1968; *Abe*, 1972; *Ruff and*

Kanamori, 1980; *Christensen and Ruff*, 1988; *Dmowska et al.*, 1988; *Lay et al.*, 1989; *Liu and McNally*, 1993; *Taylor et al.*, 1996; *Mikumo et al.*, 1999; *Ammon et al.*, 2008; *Lay et al.*, 2009]. However; it has also been shown that viscoelastic deformation likely complicates the behavior and that intuitive-based elastic interpretations can be misleading [e.g., *Mueller et al.*, 1996a, 1996b; *Lay et al.*, 2009]. Given that our observations of subduction processes span a very limited time interval, it is valuable to document and characterize earthquake and plate deformation sequences for many environments. In this study we consider a recent earthquake sequence that exhibits interactions between intraplate earthquake faulting and megathrust faulting in the northern Kermadec subduction zone.

Intraplate earthquake activity near subduction zones is generally characterized by shallow normal-faulting ruptures with depths less than 30 km into the oceanic lithosphere, with less frequent occurrence of deeper thrust faulting [e.g., *Christensen and Ruff*, 1988]. The depth variation of faulting mechanism has generally been attributed to elastic bending stresses within the stiffest part of the shallow oceanic lithosphere [e.g., *Chapple and Forsyth*, 1979]. It has also been noted that intraplate activity appears to be modulated by the interplate earthquake cycle, with large interplate thrust events commonly activating intraplate normal faulting below the outer trench slope or in the outer rise as part of their aftershock sequence (Figure C–1). It is rare for outer rise normal faulting to occur within the several decades before a large interplate thrust event, whereas some large outer rise thrust-faulting events have been observed before megathrust failures [*Christensen and Ruff*, 1988; *Lay et al.*,

1989]. This is suggestive of a build-up or depth shallowing of intraplate compressional stresses within the subducting plate during the interseismic elastic strain accumulation interval that reduces the shallow horizontal extensional bending stresses while augmenting the deeper horizontal compressional bending stresses. This has been modeled in elastic calculations as a seismic-cycle modulation of the depth of the neutral stress surface beneath the trench [e.g., *Dmowska et al.*, 1988; *Liu and McNally*, 1993; *Taylor et al.*, 1996]. While consistent with seismicity patterns in a general sense, this notion directly juxtaposes processes acting on different time scales; the decades to century time scale of the megathrust seismic cycle and the million-year time scale of plate bending. Viscoelastic calculations [*Mueller et al.*, 1996a, 1996b] have not confirmed the viability of the intraplate thrust-faulting activity or its temporal variation being a response to the elastic strain fluctuations near the megathrust.

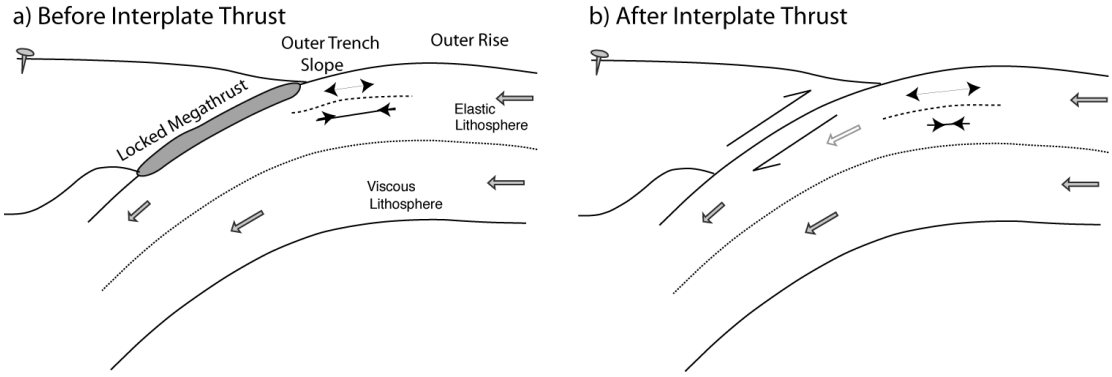

Figure C–1. Subduction zone environments before and after interplate thrust earthquakes.
Schematic subduction zone cross-sections depicting the interactions between the interplate megathrust faulting environment and the intraplate outer trench slope and outer rise environments. a) When the megathrust is locked, prior to a large underthrusting event, the intraplate environment below the trench slope may have compressional stresses superimposed on plate flexure (bending) stresses (lines with double arrow heads), reducing the in-plate extension at shallow depth and increasing the in-plate compression at greater depth within the elastic lithosphere, with a net shallowing of the neutral bending stress surface (short dotted line) within the core of the elastic lithosphere. The deeper lithosphere deforms viscously limited the depth extent of trench slope faulting, which tends to have few normal-faulting events, and some large deeper thrust-faulting events. b) After the megathrust ruptures and there is release of interplate stress, the trench slope environment may have increased shallow in-plate extension, producing large shallow normal-faulting events, with the neutral bending stress surface deepening, with reduced size and number of intraplate thrusting events. This conceptual framework is based on the ideas of *Christensen and Ruff* [1988] and *Lay et al.* [1989].

Some regions have experienced intraplate normal faulting and thrust faulting that is not clearly associated with a large interplate event, but this has been relatively rare. Outer rise faulting that is not clearly related to interplate activity occurs predominantly in subduction zones with low seismic coupling, such as the Marianas, Java and Tonga zones [*Lay and Kanamori*, 1981]. Great normal-faulting events such as the 1977 Sumba (M_w 8.3) [*Spence*, 1986; *Lynnes and Lay*, 1988] and 2009 Samoa (M_w 8.0) earthquakes [*Lay et al.*, 2010] rupture the upper oceanic lithosphere seaward

of apparently aseismic megathrusts, and likely occur as a result of strong slab pull and plate bending as the subducting plate continuously creeps into the mantle. Intraplate thrust earthquakes not related to interplate activity are much less frequent than extensional faulting, and are not as large. Most of the documented large intraplate thust faulting occurs deeper than 30 km, and typically precedes large interplate earthquakes. This pattern is consistent with the notion that without modulation by interplate seismic-cycle stresses, weakly coupled megathrust regions may have deeper elastic neutral bending stress surfaces, and hence less elastic volume for accumulating and releasing compressional stress beneath the trench. However, there are exceptions to any simple pattern as in the central Kuril Islands where a large, relatively deep intraplate thrust-faulting event in 2009 (M_w 7.4) followed the 2006 (M_w 8.3) interplate thrust event and the 2007 (M_w 8.1) trench slope normal-faulting event. It is important to recognize that we have a limited sampling of a complex process and we should avoid over-simplifying faulting interactions.

Much of the consideration about the relationship between interplate and intraplate seismicity has been dominated by compilations of observations such as *Christensen and Ruff* [1988] and *Lay et al.* [1989] which advanced the notion that the intraplate long-term (plate bending) stress regime is modulated by interplate seismic cycles. We consider a large intraplate earthquake doublet involving shallow normal faulting on July 6, 2011 (M_w 7.6) and deeper thrust faulting on October 21, 2011 (M_w 7.4) located below the northern Kermadec trench, evaluating the faulting interactions during the sequence. This 2011 Kermadec doublet, and the earlier 2009 Samoa

earthquakes near the northern end of the Tonga trench [*Beavan et al.*, 2010; *Lay et al.*, 2010] indicate that in some instances the roles may be reversed with respect to faulting interactions between the intraplate and interplate regimes.

Tectonic Framework

The Tonga-Kermadec trench extends over 2600 km from ~14.5°S, south of Samoa, to ~38°S, northeast of New Zealand (Figure C–2) with the Pacific plate underthrusting the Australian plate along the Tonga and Kermadec Islands, which are backed by the extending Lau Basin and Harve Trough, respectively [e.g., *Pelletier and Louat*, 1989; *Bevis et al.*, 1995; *Pelletier et al.*, 1998]. Near 26°S, the Louisville Ridge, a chain of seamounts on the Pacific plate, impinges obliquely on the trench, providing a major tectonic segmentation between the Tonga and Kermadec subduction zones [e.g., *Bonnardot et al.*, 2007]. The long arc complex has high levels of low and moderate magnitude shallow earthquakes, but has only a few events with M ~8 in the historic record [e.g., *McCann et al.*, 1979; *Lay et al.*, 1982; *Nishenko*, 1991], and there is large uncertainty in whether realistic potential exists for a megathrust rupture as large as M_w ~ 9.5-9.6 to occur in the region as deemed plausible by overall plate convergence characteristics [*Kagan*, 1999; *Bird and Kagan*, 2004; *McCaffrey*, 2008]. The large shallow interplate and intraplate earthquakes that have occurred in the Tonga-Kermadec region have been the subjects of several seismological studies [e.g., *Eissler and Kanamori*, 1982; *Christensen and Lay*, 1988; *Lundgren et al.*, 1989; *Houston et al.*, 1993; *Okal et al.*, 2004; *Warren et al.*, 2007;

Lay et al., 2010], and some geodetic analysis [e.g., *Beavan et al.*, 2010; *Power et al.*, 2012].

Figure C–2. Historical seismicity along the Tonga-Kermadec arc.
(Top Map) Earthquake epicenters in the Tonga-Kermadec subduction zone from the USGS National Earthquake Information Center (NEIC) catalog (1973-2012) are color coded by hypocentral depth. The epicenters of the 2011 Kermadec Doublet (yellow stars) are indicated, along with Raoul Island, approximately 175 km to the west. Velocity of the Pacific plate relative to the Australian plate for model NUVEL-1A [*DeMets et al.,* 1994] is shown by the white arrows. The dashed white box indicates the region for which large shallow events are shown in the timeline below. (Bottom Timeline) Shallow ($h < 70$ km) earthquakes with $M \geq 7.0$ from 1900 to 2012 located within the white box in the map that are listed in the PAGER-CAT Earthquake Catalog [*Allen et al.,* 2009] are shown in the timeline (the Global Centroid-Moment Tensor (GCMT) [www.globalcmt.org/CMTsearch.html] catalog is used to update the catalog from 2007 to 2012). The largest megathrust ruptures appear to be the events in 1917, 1959 and 1976, with the 1959 event locating somewhat north of the other events. The events labeled in red are intraplate events: 1955 was near the outer rise, 1986 was an intraslab rupture, and the 2011 doublet is under the trench slope. The long-term plate convergence rate varies rapidly along the Kermadec trench, decreasing southward from 90 mm/yr at 25° S to 53 mm/yr at 35° S [*Power et al.*, 2012].

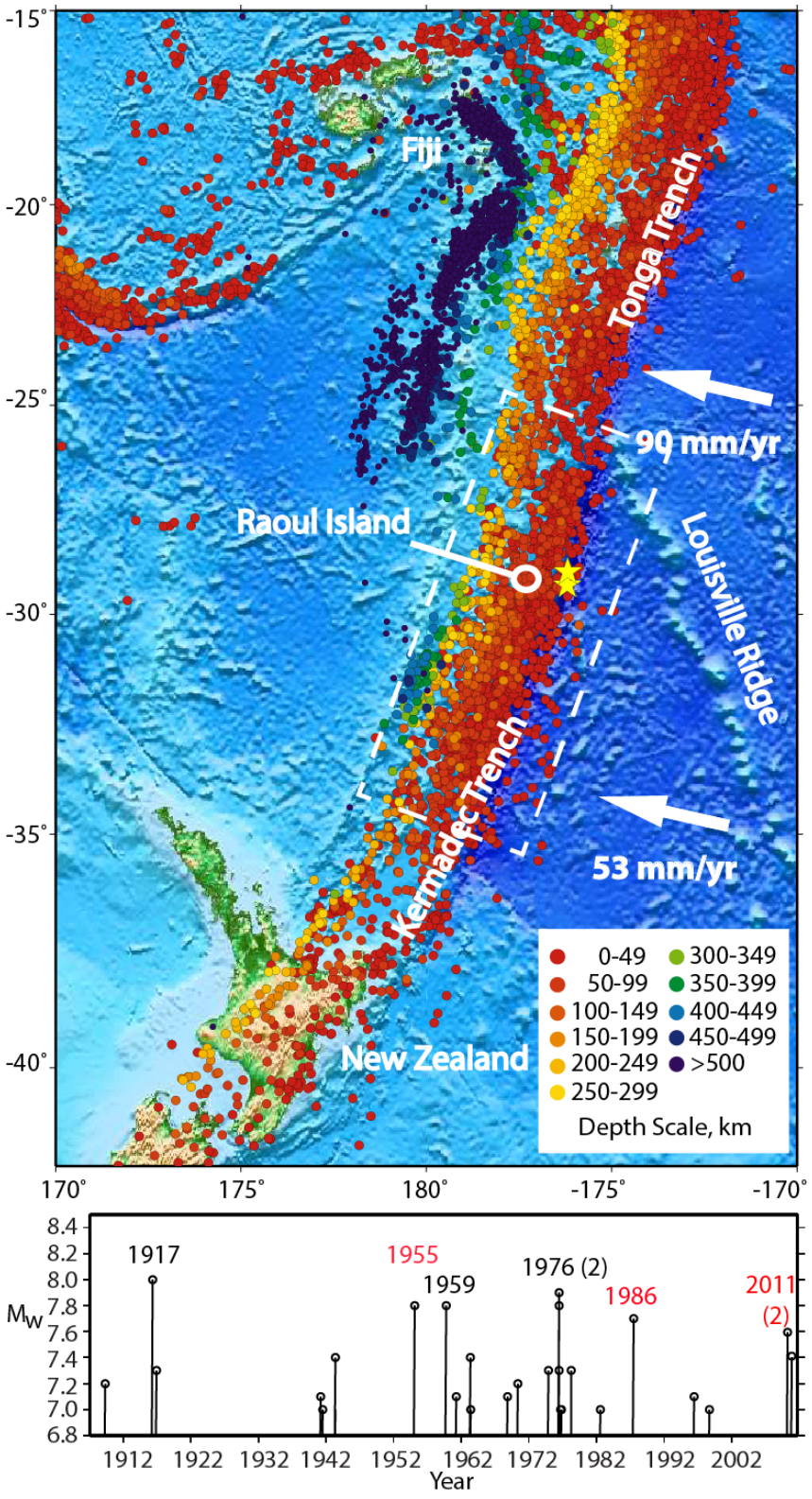
-15°
-20°
-25°
-30°
-35°
-40°
170°
175°
180°
-175°
-170°
Fiji
Tonga Trench
90 mm/yr
Raoul Island
Louisville Ridge
Kermadec Trench
53 mm/yr
New Zealand
0-49
50-99
100-149
150-199
200-249
250-299
300-349
350-399
400-449
450-499
>500
Depth Scale, km
8.4
8.2
8.0
7.8
7.6
7.4
7.2
7.0
6.8
Mw
1917
1955
1959
1976 (2)
1986
2011 (2)
1912
1922
1932
1942
1952
1962
1972
1982
1992
2002
Year

Over the last century, there have been 7 shallow (< 60 km deep) earthquakes with $M_w \geq 7.5$ along the northern Kermadec trench (Figure C–2) between 28°S and 30°S, with this being the primary concentration of large events in the subduction zone. The May 1, 1917 (M ~ 8) event and January 14, 1976 (M_w 7.8, 7.9) earthquake doublet (Figure C–3) are closely located. The 1976 events are megathrust ruptures, and the 1917 event is generally assumed to be as well [e.g., *Nishenko*, 1991], indicating a 59-year recurrence interval, compatible with a high percentage of seismic convergence. An M ~7.8 event in 1959 ruptured just to the north of those events, having been preceded in 1954 by an M 7.8 event located seaward of the trench near the outer rise. In 1986, an intraplate M_w 7.7 earthquake occurred somewhat further to the north (28.2°S) below the megathrust, apparently involving a tear in the subducting slab [*Lundgren et al.*, 1989; *Houston et al.*, 1993]. Most recently, the 2011 doublet commenced with an M_w 7.6 normal-faulting event seaward of the 1976 rupture zones, as discussed below.

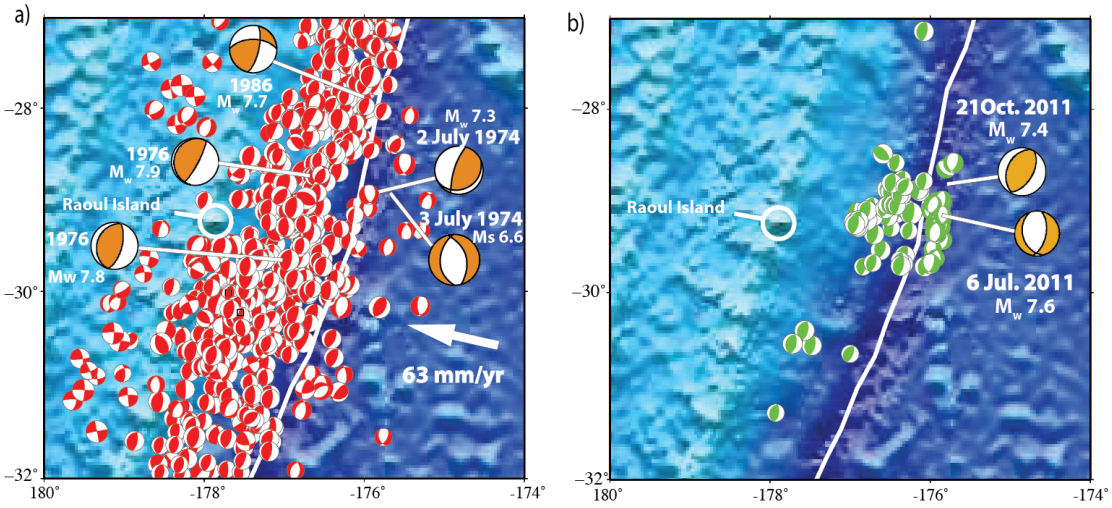

Figure C–3. Historical and current earthquake focal mechanisms.
a) Shallow earthquake focal mechanisms (GCMT lower hemisphere best double-couple solutions from January 1, 1976 to July 5, 2011, plotted at the centroid locations) in the northern Kermadec subduction zone. The large interplate events of January 14, 1976 (15:55:34.9 M_w 7.8 and 16:47:33.5 M_w 7.9), the intraslab rupture of October 20, 1986 (M_w 7.7), and the outer-trench-slope compressional and extensional doublet of July 2, 1974 (M_w 7.3) and July 3, 1974 (M_s 6.6) are shown with large brown solutions. Focal mechanisms for the 1974 doublet are from *Chapple and Forsyth* [1979]. The trench is shown by the white curve. Raoul Island is highlighted. The plate convergence arrow is from NUVEL-1A. b) The 2011 Kermadec Doublet sequence, with intraplate mainshocks of July 6, 2011 (M_w 7.6) and October 21, 2011 (M_w 7.4) (brown) and smaller interplate and intraplate event (green) GCMT solutions from July 6, 2011 to July 31, 2012 plotted at their GCMT centroid locations. The interplate aftershocks locate up-dip of the second large interplate event in 1976, in an area where there had not been much seismicity for 35 years.

Intraplate activity below the Kermadec trench preceded the 1976 megathrust doublet [*Christensen and Ruff*, 1988], with a thrust-faulting earthquake on July 2, 1974 with M_s 7.2, followed by a smaller normal-faulting earthquake on July 3, 1974 with M_s 6.6 (Figure C–3a). Just north of the subducting Louisville Ridge, an outer-trench-slope thrust earthquake in 1975 preceded a large interplate earthquake in December 19, 1982 (M_w 7.5) [*Christensen and Ruff*, 1988]. These may represent

instances of enhanced in-plate horizontal compressional stress prior to megathrust ruptures (Figure C–1a).

Power et al. [2012] infer that the northern portion of the Kermadec megathrust, in the region of the 1976 doublet, is frictionally locked at present, while the southern portion of the trench from 32°S to 38°S is not accumulating strain. If correct, this may delimit maximum size earthquakes in northern Kermadec. However, the GPS station coverage along the Kermadec trench is very sparse, with station RAUL, located on Raoul Island (part of the GeoNet network, http://www.geonet.org.nz/resources/gps/) and stations in northeastern New Zealand [e.g., *Wallace et al.*, 2004] providing the primary constraints on slip deficit. Raoul Island is the largest of the Kermadec islands and is located 175 km west of the 2011 doublet (Figure C–2, Figure C–3b). Figure C–4 shows the progressive westward movement of Raoul Island since the GPS station was installed on May 15, 2009, which indicates that the region ruptured in 1976 is currently locked. *Power et al.* [2012] infer > 80% slip deficit in the region from 28°S to 30°S based on block modeling of earthquake slip vectors and GPS velocities. The GPS data indicate that Raoul Island abruptly moved to the west in July 2011, which is assumed to be a result of the July 6, 2011 M_w 7.6 outer trench-slope normal-faulting event. Subsequently, the ground deformation has resumed its westward motion at approximately the same rate as before the earthquake and any abrupt eastward motion that may have resulted from the outer rise thrust faulting in October 2011 and interplate thrust-faulting aftershocks is not detectable above the background noise. This is a notable contrast to

the GPS observations for the September 29, 2009 Samoa normal-faulting earthquake, which showed unexpected eastward motion of the upper plate [*Beavan et al.*, 2010], later recognized to represent dynamic triggering of a large megathrust rupture [*Beavan et al.*, 2010; *Lay et al.*, 2010].

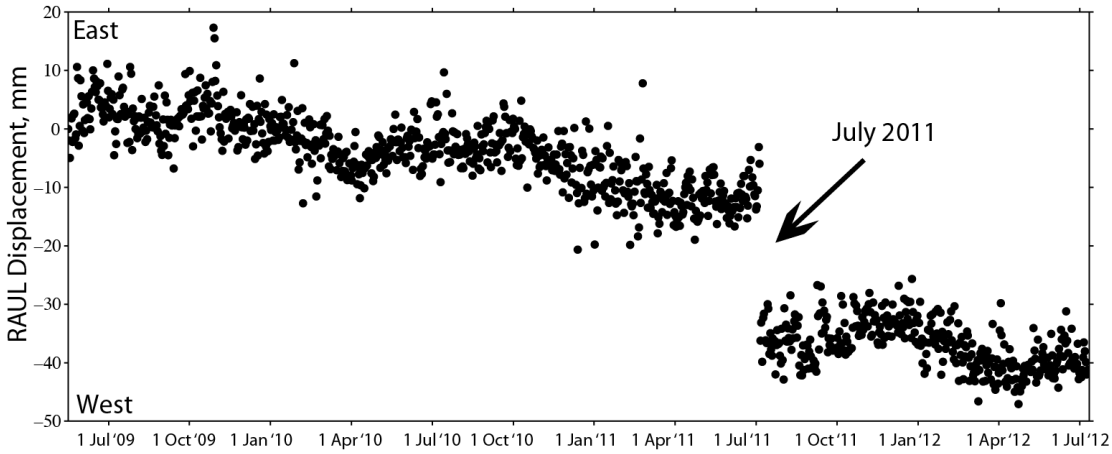

Figure C–4. cGPS record for station RAUL on Raoul Island.
GeoNet Station RAUL [www.geonet.org.nz], installed on Raoul Island on May 16, 2009, has recorded progressively westward motion, indicating a regionally-locked plate interface. Raoul Island moved ~20 mm to the west following the July 6, 2011 event, as expected for normal faulting within the subducting plate. This relatively abrupt motion is superimposed on the <10 mm/yr movement of the island preceding the July 6, 2011 earthquake. There is at most a weak signature of eastward motion for the October 21, 2011 intraplate compressional event or of the small interplate thrusting aftershocks.

2011 Kermadec doublet

On July 6, 2011 a large normal-faulting earthquake occurred below the Kermadec trench seaward of the 1976 rupture zones (Figure C–3). The US Geological Survey (USGS) source parameters (http://earthquake.usgs.gov/earthquakes/) for this earthquake are: 19:03:16.7 UTC, 29.31°S, 176.20°W, body-wave magnitude m_b = 7.0, and surface-wave magnitude M_s

= 7.4. Global Centroid Moment Tensor (www.globalcmt.org) and USGS W-phase inversions for the event yield M_w = 7.6, with centroid depth estimates of 22.7 and 15 km, respectively. Modest non-double couple components are present in both long-period solutions, with shallow plunging tension axes oriented almost perpendicular to the trench (Figure C–3b). The USGS finite-fault inversion indicates a fault plane with strike ϕ = 170°, and dip δ = 52°. A modest tsunami with peak amplitude above sea level on Raoul Island of 120 cm was reported by NOAA [http://oldwcatwc.arh.noaa.gov/about/tsunamimain.php]. This earthquake activated normal-faulting aftershocks distributed 100 km along strike of the trench, and thrust-faulting aftershocks to the west with faulting parameters consistent with plate boundary faulting [*Hayes et al*., 2012] (Figure C–3b).

The second large event of the doublet occurred on October 21, 2011, 50 km to the north of the first event, at greater depth below the outer trench-slope. The USGS source parameters are: 17:57:16.9 UTC, 29.00°S, 176.18°W, m_b = 6.9, M_s = 7.6, and M_w = 7.4. The GCMT centroid depth is 48.4 km, and the USGS W-phase centroid depth is 50 km, with minor non-double couple components and nearly horizontal compressional axes trending almost perpendicular to the trench. The USGS finite-fault inversion indicates a fault plane with ϕ = 196.1°, and δ = 48.4°. A small tsunami with peak amplitude above sea level on Raoul Island of 14 cm was reported by NOAA (http://oldwcatwc.arh.noaa.gov/about/tsunamimain.php). The doublet aftershock sequence has continued into 2012 with a mix of thrust-faulting events near the megathrust and normal-faulting events below the trench.

Doublet rupture processes

We determine finite-fault slip models for the July and October 2011 doublet events using broadband P and SH wave displacement recordings from teleseismic distances, following the methods of Kikuchi and Kanamori (http://www.eri.u-tokyo.ac.jp/ETAL/KIKUCHI/). We assume the USGS W-phase inversion fault geometry for the July earthquake with $\phi = 170°$, $\delta = 52°$, allowing variable rake. This geometry is slightly preferred relative to the orthogonal plane in the body wave inversions, and is consistent with previous findings of trenchward-dipping normal faults extending to a depth of 25-30 km along the Kermadec trench [*Warren et al.*, 2007]. For the October earthquake, it proves difficult to distinguish between the fault plane and auxiliary fault plane; and, we ultimately adopt the trenchward-dipping plane from the best double-couple of the GCMT solution with $\phi = 203°$, $\delta = 38°$, and variable rake.

Figure C–5 shows the average focal mechanism, source time function, and slip distribution for each doublet event. The July earthquake rupture is modeled as continuing for approximately 65 s, based on coherent secondary arrivals in the P waves (waveform observations and predictions are shown in Figure C–6). The subfaults were parameterized with 10 symmetric triangles with 1.5 s rise-time lagged by 1.5 s, yielding 16.5 s subfault rupture durations, and a rupture velocity of 1.5 km/s, with fault length of 150 km along strike and width of 50 km along dip. The P wave data show impulsive early ground motions and this is manifested in the spiky source time function found for the first 15 s of rupture. The inverted slip distribution has

estimated slip of up to 9 m distributed across the upper 30 km of the oceanic lithosphere (a water depth of 6 km is included in the depths in Figure C–5a) extending about 50 km along strike, with some later slip to the south about 35 s into the rupture. The large shallow slip likely generated the tsunami that was recorded regionally in the Kermadec Islands, New Zealand and Tonga (http://oldwcatwc.arh.noaa.gov/about/tsunamimain.php). The estimated seismic moment of 7.4 x 10^{20} Nm is larger than the long-period GCMT and W-phase inversions estimates of about 2.8-2.9 x 10^{20} Nm, likely due to limited resolution of the long-period component of the body wave inversion caused by use of simplified Green functions. If we consider only subfaults with at least 20% of the peak subfault moment, we obtain a moment of 6.6 x 10^{20} Nm, an average slip of 2.9 m, and static stress drop of 2.2 x 10^{16} MPa. The USGS estimates a high seismic energy release of 4.0 x 10^{16} Nm, which gives an energy magnitude M_e of 8.2. Using the USGS W-phase inversion seismic moment yields a moment-scaled energy value of 14.3 x 10^{-5}. This is a relatively high ratio even for an intraplate event [e.g., *Venkataraman and Kanamori*, 2004], comparable to the 1993 Kushiro-oki intermediate depth event, and is related to the impulsive arrivals in the ground motions.

Figure C–5. Finite-fault inversions for the July 6, 2011 and the October 21, 2011 earthquakes.
a) Source model for the July 6, 2011 normal-faulting event, including the focal mechanism strike (ϕ), dip (δ) and average rake (λ), rupture velocity (Vr), seismic moment (Mo), source time function, and model slip distribution. The P and SH waveforms used in the inversion are compared with model predictions in Figure C–6.
b) Source model for the October 21, 2011 thrust-faulting event. The P and SH waveforms used in the inversion are compared with model predictions in Figure C–7.

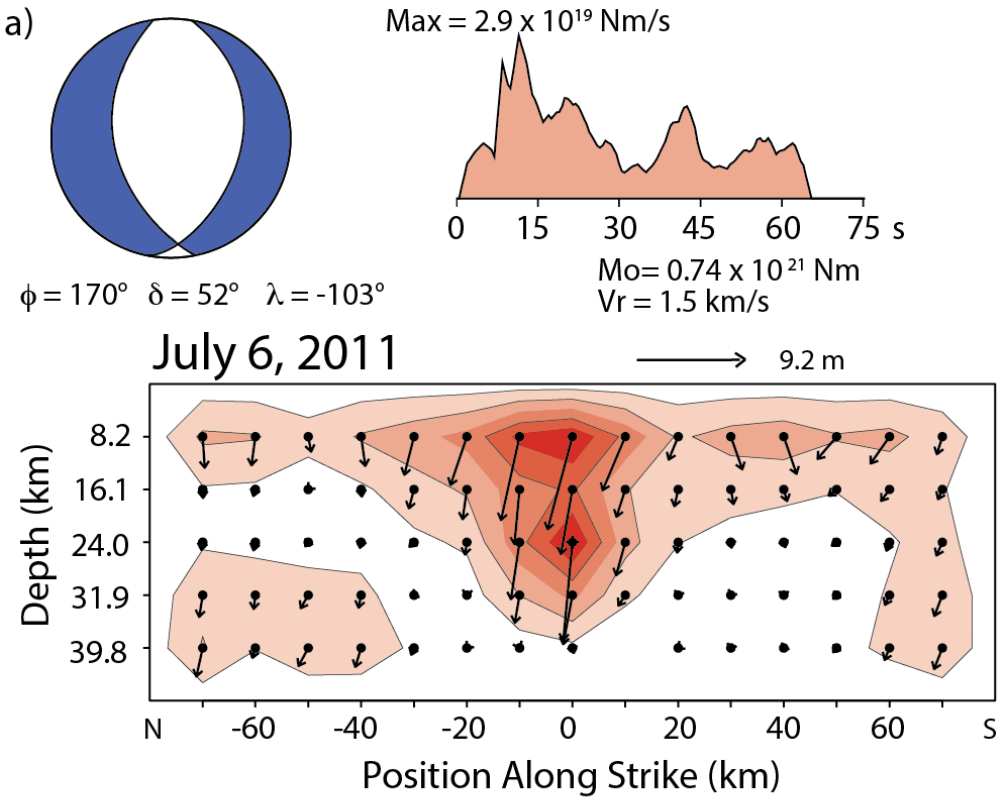
a)
Max = 2.9 x 10^19 Nm/s
0 15 30 45 60 75 s
Mo= 0.74 x 10^21 Nm
Vr = 1.5 km/s
ϕ = 170° δ = 52° λ = -103°
July 6, 2011
9.2 m
Depth (km)
8.2
16.1
24.0
31.9
39.8
N -60 -40 -20 0 20 40 60 S
Position Along Strike (km)

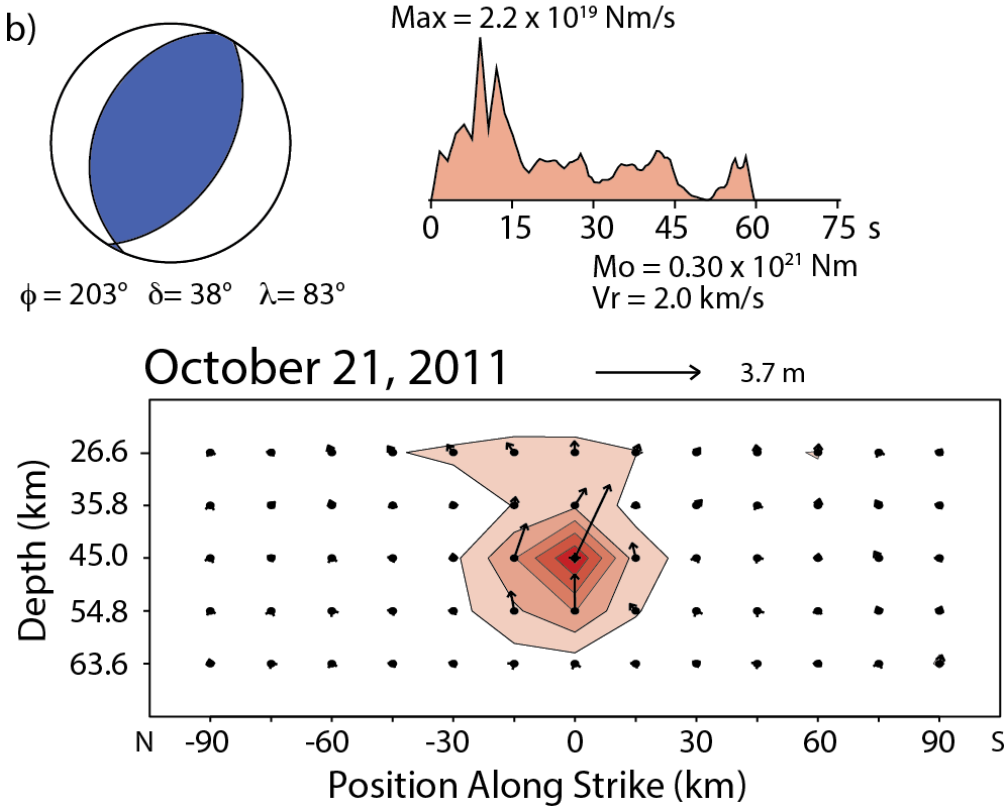
b)
Max = 2.2 x 10^19 Nm/s
0 15 30 45 60 75 s
Mo = 0.30 x 10^21 Nm
Vr = 2.0 km/s
ϕ = 203° δ= 38° λ= 83°
October 21, 2011
3.7 m
Depth (km)
26.6
35.8
45.0
54.8
63.6
N -90 -60 -30 0 30 60 90 S
Position Along Strike (km)

Located 50 km northward along trench, the October rupture lasted at least 15 s, possibly with some low amplitude seismic wave radiation as late as 60 s. We assumed Vr = 2.0 km/s and a fault extending 195 km along strike and 75 km along the 38˚ dipping plane, but the slip remained concentrated within a region extending about 45 km along strike and a centroid depth near 45 km. The subfault source time functions were parameterized with 7 symmetric triangles with 1.5 s rise-time lagged by 1.5 s, yielding 11.5 s subfault rupture durations. There are again some secondary arrivals about 30 s into the waveforms (waveform fits are shown in Figure C–7), but these may involve scattered energy not accounted for in the Green functions. The body wave inversion seismic moment of 3.0×10^{20} Nm again exceeds the long-period GCMT and W-phase inversion estimates of about 1.5×10^{20} Nm, so the peak slip estimate of 3.7 m may be overestimated by a factor of 2. If we consider only subfaults with at least 10% of the peak subfault moment, the body wave moment estimate is 2.0×10^{20} Nm, and the average slip is ~1 m with a static stress drop of 1.1×10^{16} MPa. The USGS seismic energy release estimate is 1.4×10^{15} Nm (Me 7.2) and using the W-phase inversion seismic moment gives a moment-scaled energy value of 0.9×10^{-5}. These values are over an order of magnitude lower than for the July earthquake, but the moment-scaled energy is consistent with other intraplate compressional earthquakes such as the 2009 Kuril Islands earthquake [*Lay et al.*, 2009].

Figure C–6. Observed body wave data (black) and synthetic seismograms (red) for the finite-fault inversion for the July 6, 2011 earthquake in Figure C–5a. Waveforms for P and SH (labeled) phases have true relative amplitudes except that SH signals are plotted with 0.2 times the P wave amplitudes, which is the same relative weighting as they were given in the inversion. Each station name and azimuth (ϕ) is shown.

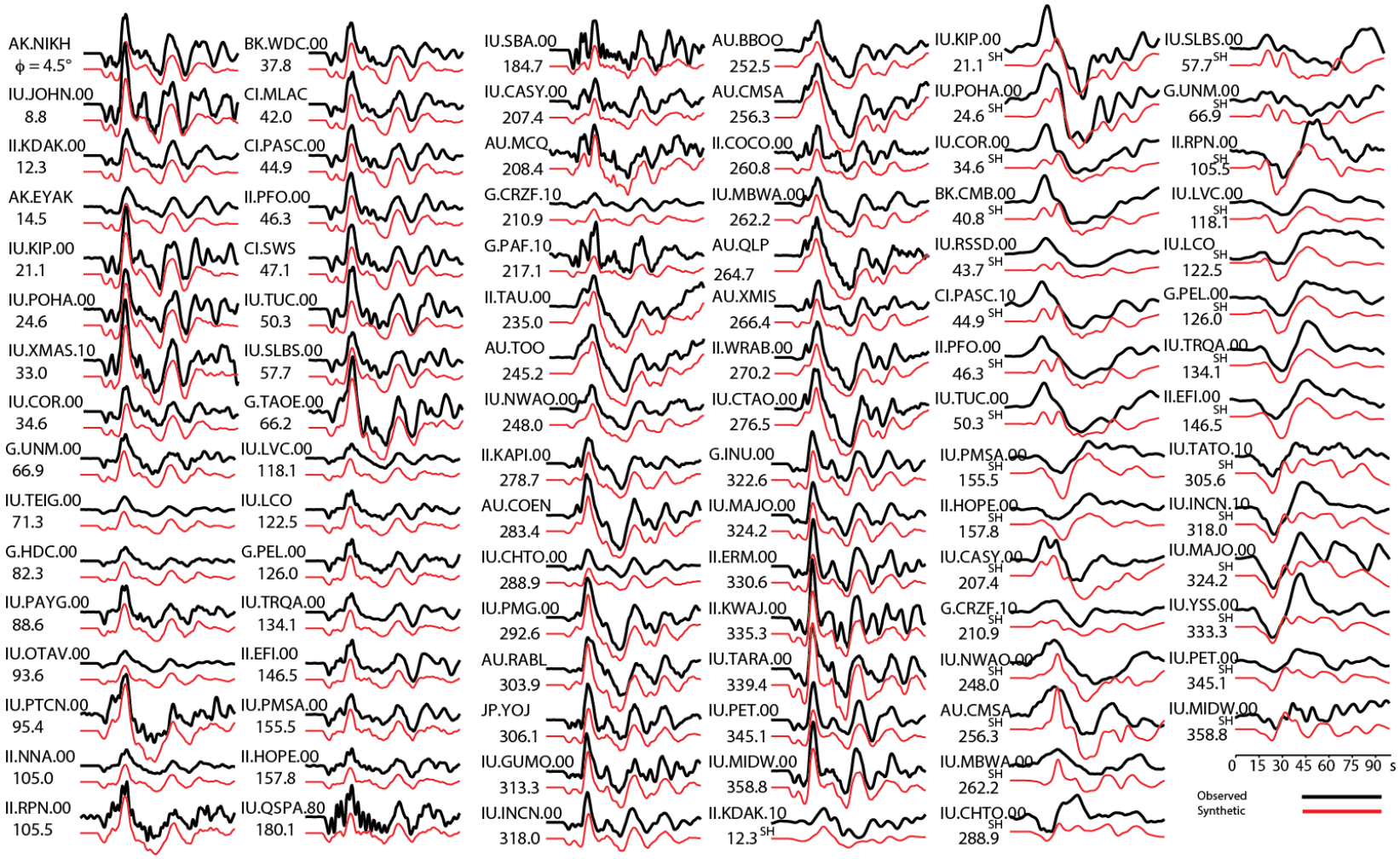
AK.NIKH
ϕ = 4.5°
IU.JOHN.00
8.8
II.KDAK.00
12.3
AK.EYAK
14.5
IU.KIP.00
21.1
IU.POHA.00
24.6
IU.XMAS.10
33.0
IU.COR.00
34.6
G.UNM.00
66.9
IU.TEIG.00
71.3
G.HDC.00
82.3
IU.PAYG.00
88.6
IU.OTAV.00
93.6
IU.PTCN.00
95.4
II.NNA.00
105.0
II.RPN.00
105.5
BK.WDC.00
37.8
CI.MLAC
42.0
CI.PASC.00
44.9
II.PFO.00
46.3
CI.SWS
47.1
IU.TUC.00
50.3
IU.SLBS.00
57.7
G.TAOE.00
66.2
IU.LVC.00
118.1
IU.LCO
122.5
G.PEL.00
126.0
IU.TRQA.00
134.1
II.EFI.00
146.5
IU.PMSA.00
155.5
II.HOPE.00
157.8
IU.QSPA.80
180.1
IU.SBA.00
184.7
IU.CASY.00
207.4
AU.MCQ
208.4
G.CRZF.10
210.9
G.PAF.10
217.1
II.TAU.00
235.0
AU.TOO
245.2
IU.NWAO.00
248.0
II.KAPI.00
278.7
AU.COEN
283.4
IU.CHTO.00
288.9
IU.PMG.00
292.6
AU.RABL
303.9
JP.YOJ
306.1
IU.GUMO.00
313.3
IU.INCN.00
318.0
AU.BBOO
252.5
AU.CMSA
256.3
II.COCO.00
260.8
IU.MBWA.00
262.2
AU.QLP
264.7
AU.XMIS
266.4
II.WRAB.00
270.2
IU.CTAO.00
276.5
G.INU.00
322.6
IU.MAJO.00
324.2
II.ERM.00
330.6
II.KWAJ.00
335.3
IU.TARA.00
339.4
IU.PET.00
345.1
IU.MIDW.00
358.8
II.KDAK.10
12.3 SH
IU.KIP.00
21.1 SH
IU.POHA.00
24.6 SH
IU.COR.00
34.6 SH
BK.CMB.00
40.8 SH
IU.RSSD.00
43.7 SH
CI.PASC.10
44.9 SH
II.PFO.00
46.3 SH
IU.TUC.00
50.3 SH
IU.PMSA.00
155.5 SH
II.HOPE.00
157.8 SH
IU.CASY.00
207.4 SH
G.CRZF.10
210.9 SH
IU.NWAO.00
248.0 SH
AU.CMSA
256.3 SH
IU.MBWA.00
262.2 SH
IU.CHTO.00
288.9 SH
IU.SLBS.00
57.7 SH
G.UNM.00
66.9 SH
II.RPN.00
105.5 SH
IU.LVC.00
118.1 SH
IU.LCO
122.5 SH
G.PEL.00
126.0 SH
IU.TRQA.00
134.1 SH
II.EFI.00
146.5 SH
IU.TATO.10
305.6 SH
IU.INCN.10
318.0 SH
IU.MAJO.00
324.2 SH
IU.YSS.00
333.3 SH
IU.PET.00
345.1 SH
IU.MIDW.00
358.8 SH
0 15 30 45 60 75 90 s
Observed
Synthetic

Figure C–7. Observed body wave data (black) and synthetic seismograms (red) for the finite-fault inversion for the October 21, 2011 earthquake in Figure C–5b. Waveforms are for both P and SH (labeled) phases and have true relative amplitudes except that SH signals are plotted with 0.2 times the P wave amplitudes, which is the same relative weighting as they were given in the inversion. Each station name and azimuth (ϕ) is shown.

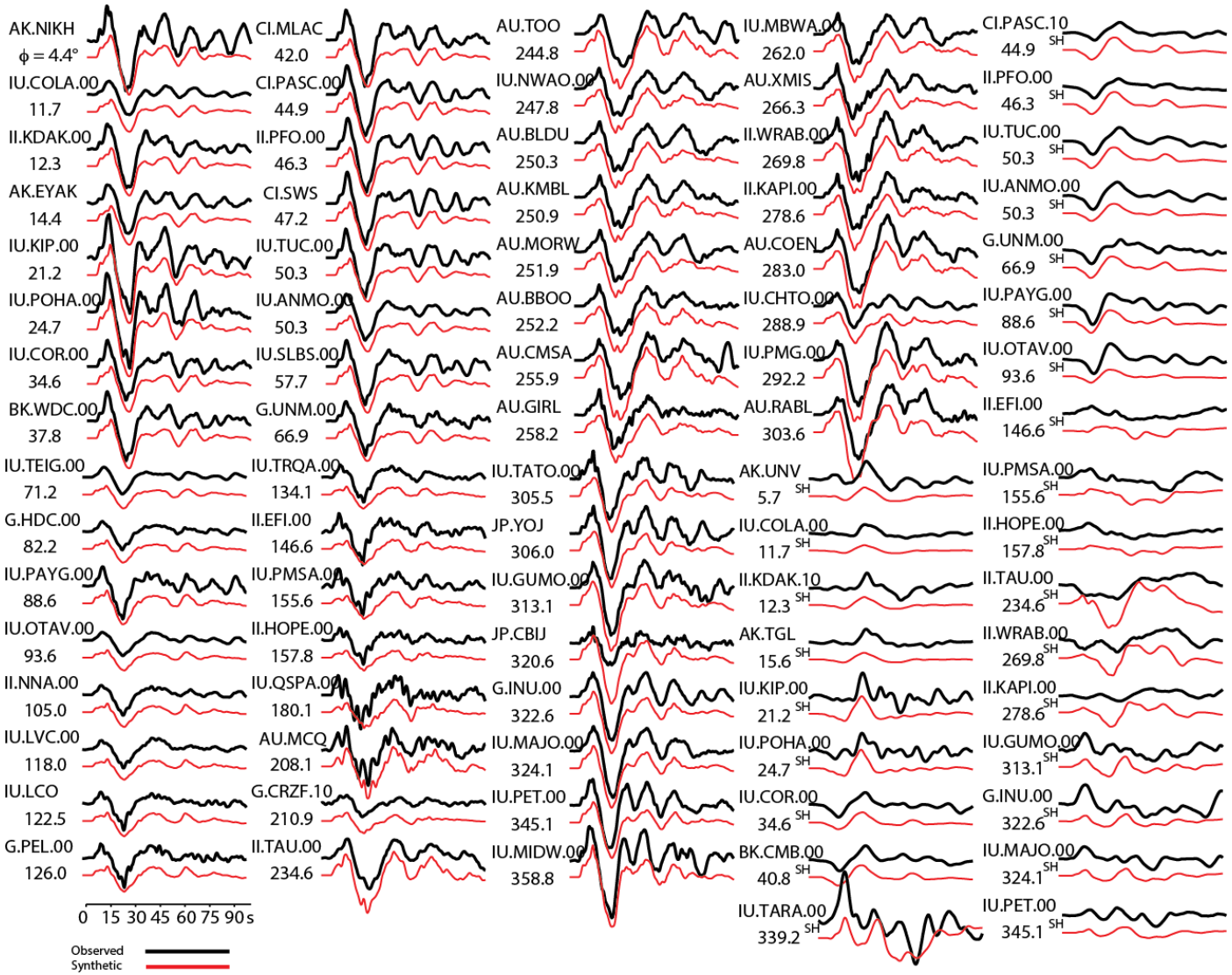
AK.NIKH
ϕ = 4.4°
IU.COLA.00
11.7
II.KDAK.00
12.3
AK.EYAK
14.4
IU.KIP.00
21.2
IU.POHA.00
24.7
IU.COR.00
34.6
BK.WDC.00
37.8
IU.TEIG.00
71.2
G.HDC.00
82.2
IU.PAYG.00
88.6
IU.OTAV.00
93.6
II.NNA.00
105.0
IU.LVC.00
118.0
IU.LCO
122.5
G.PEL.00
126.0
CI.MLAC
42.0
CI.PASC.00
44.9
II.PFO.00
46.3
CI.SWS
47.2
IU.TUC.00
50.3
IU.ANMO.00
50.3
IU.SLBS.00
57.7
G.UNM.00
66.9
IU.TRQA.00
134.1
II.EFI.00
146.6
IU.PMSA.00
155.6
II.HOPE.00
157.8
IU.QSPA.00
180.1
AU.MCQ
208.1
G.CRZF.10
210.9
II.TAU.00
234.6
AU.TOO
244.8
IU.NWAO.00
247.8
AU.BLDU
250.3
AU.KMBL
250.9
AU.MORW
251.9
AU.BBOO
252.2
AU.CMSA
255.9
AU.GIRL
258.2
IU.TATO.00
305.5
JP.YOJ
306.0
IU.GUMO.00
313.1
JP.CBIJ
320.6
G.INU.00
322.6
IU.MAJO.00
324.1
IU.PET.00
345.1
IU.MIDW.00
358.8
IU.MBWA.00
262.0
AU.XMIS
266.3
II.WRAB.00
269.8
II.KAPI.00
278.6
AU.COEN
283.0
IU.CHTO.00
288.9
IU.PMG.00
292.2
AU.RABL
303.6
AK.UNV
5.7
IU.COLA.00
11.7
II.KDAK.10
12.3
AK.TGL
15.6
IU.KIP.00
21.2
IU.POHA.00
24.7
IU.COR.00
34.6
BK.CMB.00
40.8
IU.TARA.00
339.2
CI.PASC.10
44.9
II.PFO.00
46.3
IU.TUC.00
50.3
IU.ANMO.00
50.3
G.UNM.00
66.9
IU.PAYG.00
88.6
IU.OTAV.00
93.6
II.EFI.00
146.6
IU.PMSA.00
155.6
II.HOPE.00
157.8
II.TAU.00
234.6
II.WRAB.00
269.8
II.KAPI.00
278.6
IU.GUMO.00
313.1
G.INU.00
322.6
IU.MAJO.00
324.1
IU.PET.00
345.1
SH
0 15 30 45 60 75 90 s
Observed
Synthetic

Aftershock sequence

The July 6, 2011 earthquake triggered shallow intraplate faulting within minutes reported in the USGS catalog, and activity near the megathrust updip of the 1976 rupture area within hours. For the events in the sequence large enough to obtain GCMT solutions ($M_w > 4.5$), most of the intraplate events involve normal faulting, and most of the megathrust activity is thrust faulting (Figure C–3b, Figure C–8a). The normal-faulting aftershocks may be located on the fault plane that ruptured in the mainshock or on adjacent faults of similar geometry; the source depth estimates are imprecise and no clear alignment is apparent in the cross-section in Figure C–8a. The July earthquake also triggered two deep (40-45 km) intraplate thrust-faulting aftershocks, including the October 21, 2011 earthquake. Figure C–8b shows that normal-faulting and thrust-faulting aftershocks were occurring simultaneously, indicating a stress increase on faults of similar geometry to the mainshock as well as on the megathrust interface.

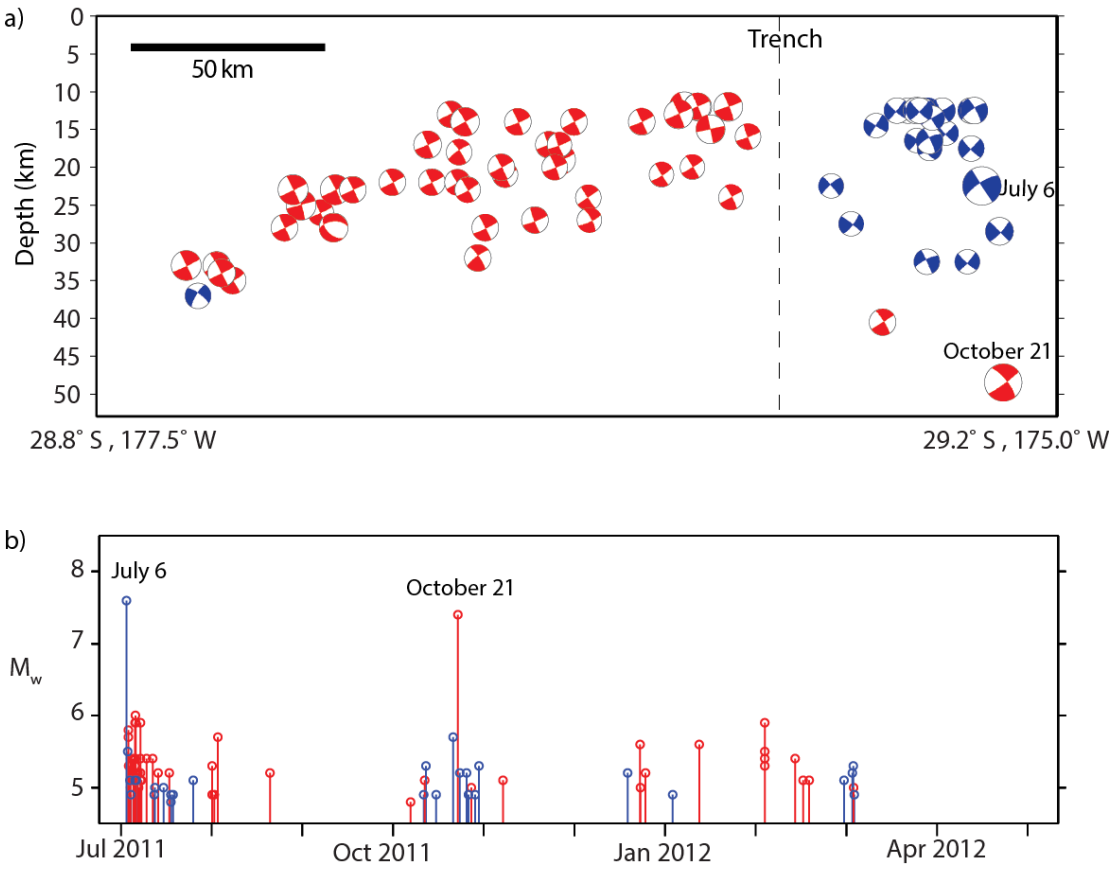

Figure C–8. Focal mechanisms and timeline of aftershock sequence.
a) Vertical cross-section perpendicular to the trench showing GCMT centroid solutions (cross-section view) plotted with depth. Thrust-faulting mechanisms are shown in red and normal-faulting mechanisms are shown in blue. The locations and depths of the thrust-faulting aftershocks arcward of the trench are largely consistent with being of the megathrust in this region. b) Timeline of the M_w values of the sequence. The July 6, 2011 and October 21, 2011 earthquakes both activate normal-faulting aftershocks in the outer trench-slope (blue) as well as thrust faulting aftershocks along the plate interface (red). After the October earthquake, the number of thrust-aftershocks triggered on the megathrust decreases for a few months but both environments continue to be active in early 2012.

The October 21, 2011 earthquake generated its own aftershock sequence of normal-faulting intraplate earthquakes and underthrusting earthquakes. As shown in Figure C–8b, the number of thrust fault aftershocks large enough for GCMT solutions

to be determined decreased for a few months after the October earthquake, possibly due to a static stress change shadow [e.g., *Toda et al.*, 2012], but picks up again in early 2012. This indicates minor influence of the intraplate thrusting on the plate interface, compatible with the lack of a significant GPS signature of the event in Figure C–4.

The GCMT depths and focal mechanisms of the thrust-faulting aftershocks west of the trench indicate that the earthquakes are likely located along the plate interface (Figure C–8a), although there is some scatter. *Hayes et al.* [2012] estimate an approximate dip of 22° for the megathrust along the Kermadec Trench and most of the thrust faulting aftershocks west of the trench have fault planes dipping between 20° and 25°. There appears to be a secondary alignment of thrust events about 10 km deeper than the primary alignment, with some of the events having slightly greater dip than the shallower events. This may indicate intraplate activity, but the events are relatively small and the depth estimates have at least 10 km uncertainty. We sought to confirm validity of the GCMT centroid depths in this region, but only a few events produced teleseismic P wave signals with high enough signal-to-noise ratios for reliable modeling. For the few events with adequate data we found good consistency between our depth estimates from P wave modeling and the GCMT depths (Appendix A), so we have no indication of a regional bias in GCMT centroid depth estimates for northern Kermadec. We focus on the likely megathrust activity, noting that there are several events near the megathrust that do clearly have mechanisms indicating

intraplate faulting (Figure C–8a), and it is possible that there are multiple activated fault structures in the region.

Stress transfer cycle

We compute stress perturbations caused by the July 6, 2011 and October 21, 2011 earthquakes for both the intraplate environment and the plate boundary. The calculations are made with Coulomb 3 software produced by S. Toda, R. Stein, J. Lin, and V. Sevilgen. A coefficient of friction of 0.4 is used in the calculations, with the basic patterns not being strongly affected by this particular choice. We use the slip distributions from our finite-fault rupture models in computing Coulomb stress changes on the primary fault geometries activated during the sequence. The July 6 normal-faulting earthquake produced Coulomb stress increases of ~1-2 bars on faults with shallow thrust fault geometries in the vicinity of the megathrust to the west (Figure C–9b). In this respect, triggering of interplate thrust aftershocks is a reasonable outcome; just as the more common reverse situation of interplate thrusting triggering outer rise normal-faulting is consistent with corresponding Coulomb stress changes. The normal-fault slip predicts larger Coulomb stress increases of ~3-5 bars on 30-50 km deep intraplate thrust-faults below the normal fault with the geometry and approximate location of the October 21 event (Figure C–9d). The October 21 faulting produced a small reduction (< 1 bar) of driving stress (a static stress change shadow) for shallow thrusting near the megathrust (Figure C–9c), consistent with the ephemeral reduction of thrusting activity, and modest increases of driving stress on

overlying normal fault geometry near the July 6 event (Figure C–9e), reconciling the occurrence of some normal-faulting aftershocks.

Figure C–9. Coulomb stress change results for July 6, 2011 and October 21, 2011 earthquakes.
a) Schematic diagram indicating the relative locations of the July 6, 2011 and October 21, 2011 earthquakes, with cross-sections perpendicular to their fault planes. b) Map view of Coulomb stress change on shallow dipping thrust faults consistent with the megathrust geometry [*Hayes et al.,* 2012] at a depth of 24 km for the finite-fault model of the July 6, 2011 event, and a vertical cross section (along AB) showing corresponding Coulomb stress changes. c) Map view of Coulomb stress change on shallow dipping thrust faults consistent with the megathrust geometry [*Hayes et al.,* 2012] at a depth of 45 km for the finite-fault model of the October 21, 2011 event, and a vertical cross section (along A'B') showing corresponding Coulomb stress changes. d) Map view of Coulomb stress change on deep trench slope compressional faults consistent with deeper compressional faulting at a depth of 45 km for the finite-fault model of the July 6, 2011 event, and a vertical cross section (along CD, which intersects the hypocenter of the October 21 event) showing corresponding Coulomb stress changes. e) Map view of Coulomb stress change on shallow trench slope extensional faults at a depth of 24 km for the finite-fault model of the October 21, 2011 event, and a vertical cross section (along C'D', which intersects the hypocenter of the July 6 event) showing corresponding Coulomb stress changes.

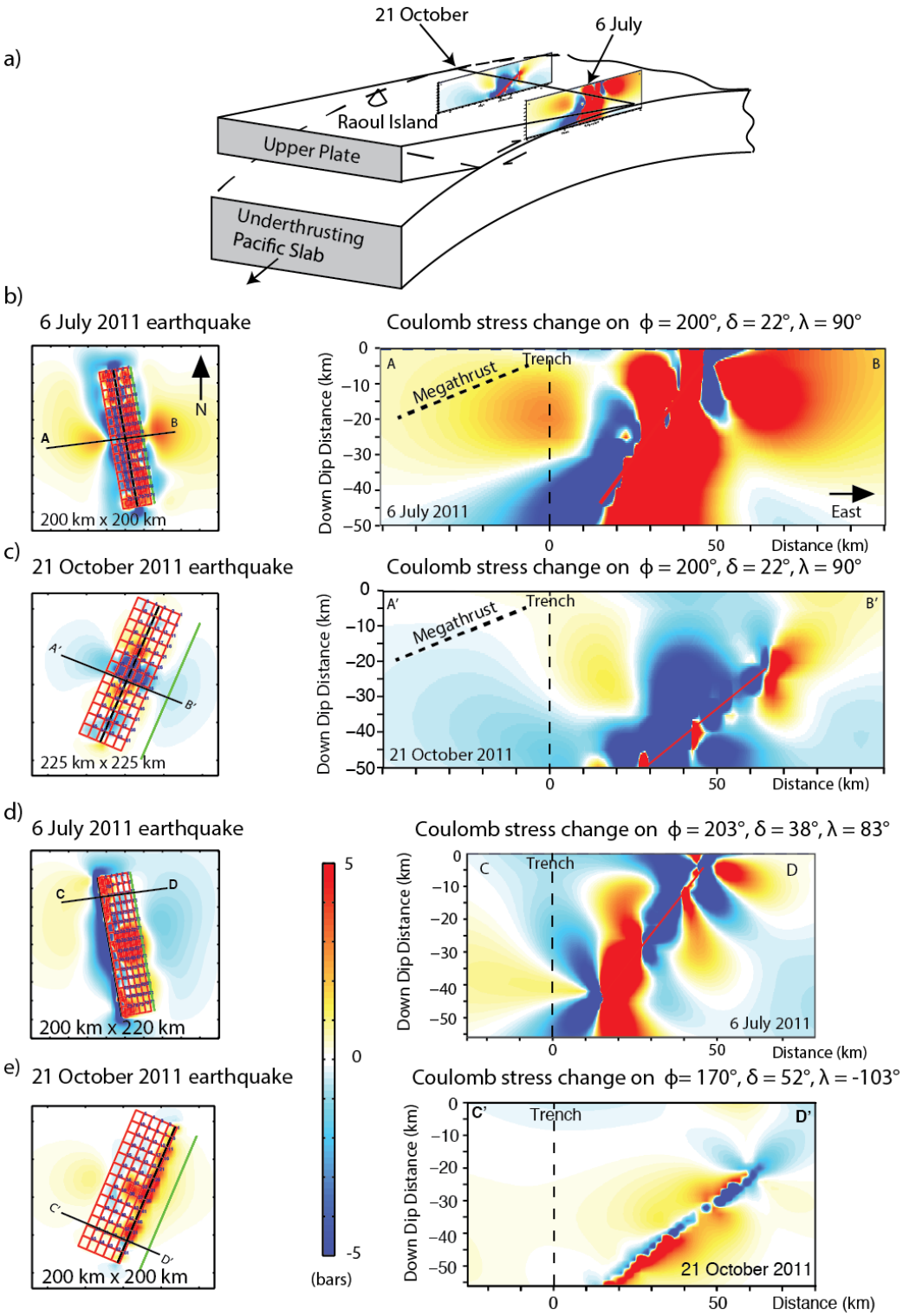
a)
21 October
6 July
Raoul Island
Upper Plate
Underthrusting Pacific Slab
b)
6 July 2011 earthquake
Coulomb stress change on ϕ = 200°, δ = 22°, λ = 90°
N
A
B
200 km x 200 km
Megathrust
Trench
6 July 2011
East
Down Dip Distance (km)
Distance (km)
c)
21 October 2011 earthquake
Coulomb stress change on ϕ = 200°, δ = 22°, λ = 90°
A′
B′
225 km x 225 km
21 October 2011
d)
6 July 2011 earthquake
Coulomb stress change on ϕ = 203°, δ = 38°, λ = 83°
C
D
200 km x 220 km
5
0
-5
(bars)
e)
21 October 2011 earthquake
Coulomb stress change on ϕ= 170°, δ = 52°, λ = -103°
C′
D′
200 km x 200 km

These calculations are made without any pre-stress in the medium, so the Coulomb stress perturbations would be superimposed on any ambient stresses from bending and flexure of the slab or interplate stress accumulation. The deeper compressional event of the Kermadec doublet is likely a consequence of combined transient stresses and longer-term bending stresses, but these calculations cannot determine the relative importance of the two. The close spatial proximity of the July normal-faulting and October thrust-faulting events, separated vertically by only ~20 km, is comparable to the separation seen between intraplate normal-faulting and thrust-faulting in other environments [e.g., *Christensen and Ruff*, 1988; *Lay et al.*, 2009]. At face value, an elastic bending interpretation would suggest that a bending stress neutral surface exists around 30-35 km deep in this region within the elastic core of the Pacific lithosphere. This implies a relatively thick elastic lithosphere of perhaps 70 km thickness, for which only the upper 2/3 or so is sufficiently brittle to experience rapid faulting. *Billen and Gurnis* [2005] analyze topography and gravity profiles parallel to the Kermadec trench and infer a dramatic decrease in plate strength due to either a decrease in flexural rigidity by 3-5 orders of magnitude or a decrease in the effective elastic thickness by more than 15 km. The latter may be consistent with a relatively shallow neutral surface in the plate, and the very occurrence of large scale faulting within the plate may provide one mechanism for weakening the subducting lithosphere. However, *Billen and Gurnis* [2005] favor such pronounced weakening of the lithosphere that it is unclear that significant elastic static stress interactions would occur between the interplate and intraplate

environment. It is possible that the interactions that are observed are influenced by dynamic stress changes that induce triggered aftershock sequences. The problem is again one of evaluating stress transfer for processes operating on vastly different time scales.

The relative roles of elastic versus anelastic processes in faulting interactions in subduction zones is not resolved, but the 2011 Kermadec doublet sequence provides additional support for importance of elastic interactions, given that the elastic Coulomb stress calculations are consistent with the observed faulting patterns and plausible long-term bending and plate interaction stresses. The Kermadec sequence is, however, distinct from typical faulting patterns that have been observed in regions with larger interplate and intraplate events, as summarized in Figure C–10. Large, shallow outer-trench-slope normal-faulting events are commonly observed following great underthrusting events in regions with strong and/or shallow seismic coupling, as in the 1896/1933 Sanriku-oki (Figure C–10a) and 2006/2007 Kuril Island (Figure C–10b) sequences. Based on these and other observations, the time delay between the great interplate rupture and the great outer-rise extensional faulting can range from minutes, as seen in the 2011 M_w 9.0 great Tohoku-oki earthquake [*Lay et al.*, 2011], to months for the 2006/2007 Kuril sequence [*Lay et al.*, 2009] to decades, as for the 1896/1933 Sanriku-oki sequence [*Kanamori*, 1971, 1972]. The varying delay time is plausibly attributable to viscoelastic and poroelastic processes, although in the Kuril sequence small intraplate activity was activated very quickly after the

thrusting [*Lay et al.*, 2009], so there is some role of dynamic triggering or elastic stress change even if the main faulting is delayed.

Figure C–10. Schematic diagrams showing examples of earthquake patterns involving large outer-trench-slope earthquakes related to megathrust earthquakes.
a) The great 1933 Sanriku-oki normal-faulting earthquake (the largest known extensional faulting earthquake) occurred 37 years after the 1896 tsunami earthquake ruptured the shallow megathrust offshore of northeastern Honshu, Japan. b) The great November 15, 2006 Kuril Islands megathrust event was followed by a great trench slope normal fault rupture 59 days later on January 13, 2007. Two years later a deeper thrust fault earthquake occurred below the trench. c) The great 2009 Samoa normal-faulting rupture beneath the outer trench slope and triggered a great megathrust rupture within one minute. d) The 2011 Kermadec Doublet sequence is distinctive in that the previous megathrust rupture was 36 years earlier in 1976 and the GPS data indicate that the megathrust is currently locked. The July 6, 2011 normal-faulting earthquake triggered aftershocks on the megathrust in addition to normal-faulting earthquakes below the trench, with a deeper, large thrust-faulting event on October 21, 2011. Stress should have increased on the 1976 rupture zone, which previously failed in 1917.

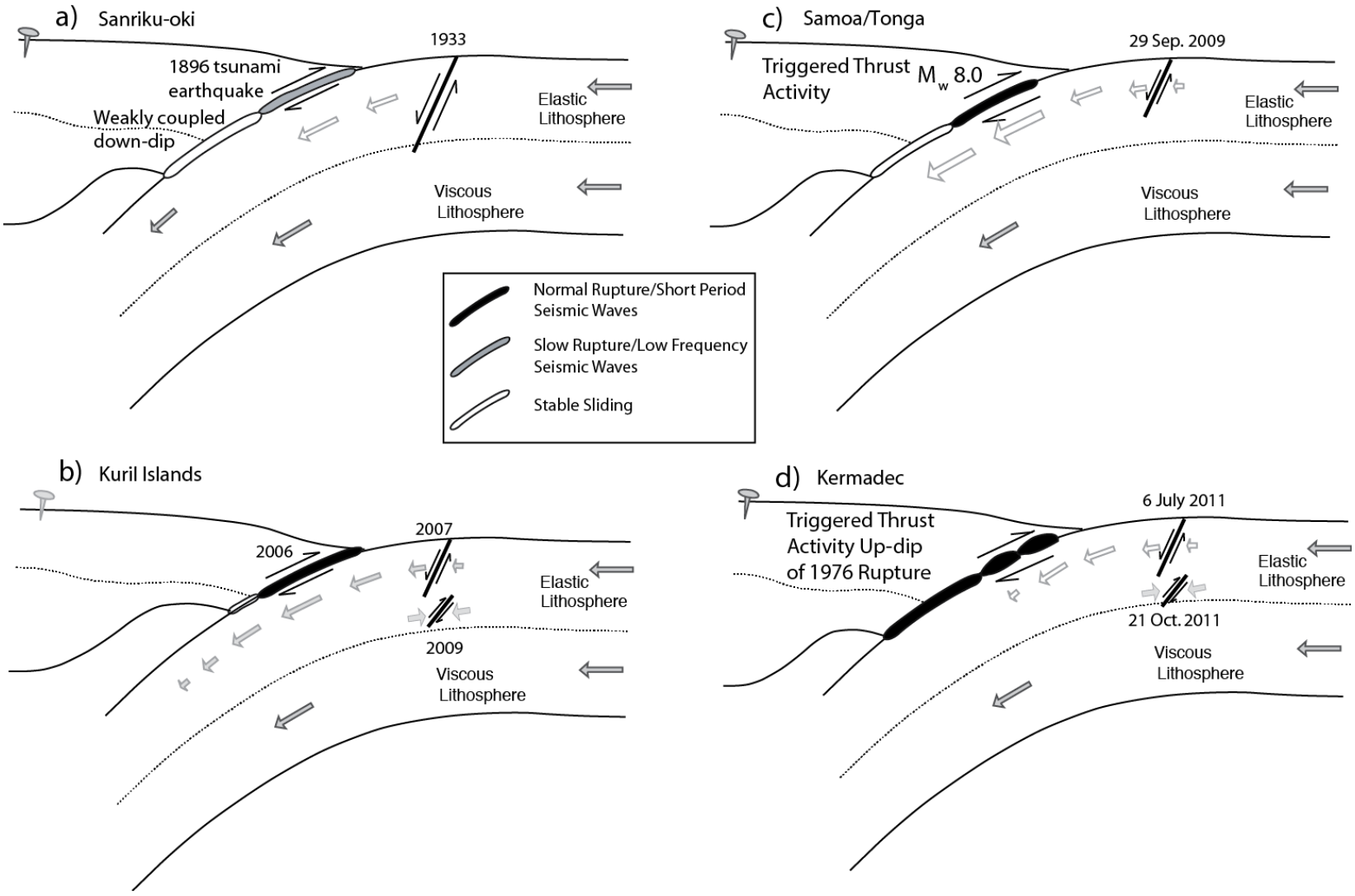
a) Sanriku-oki
1933
1896 tsunami earthquake
Weakly coupled down-dip
Elastic Lithosphere
Viscous Lithosphere
c) Samoa/Tonga
29 Sep. 2009
Triggered Thrust Activity
M_w 8.0
Elastic Lithosphere
Viscous Lithosphere
Normal Rupture/Short Period Seismic Waves
Slow Rupture/Low Frequency Seismic Waves
Stable Sliding
b) Kuril Islands
2006
2007
2009
Elastic Lithosphere
Viscous Lithosphere
d) Kermadec
6 July 2011
Triggered Thrust Activity Up-dip of 1976 Rupture
21 Oct. 2011
Elastic Lithosphere
Viscous Lithosphere

The 2009 Samoa normal-faulting event (Figure C–10c) dynamically triggered thrust-faulting on an adjacent stretch of the megathrust [*Lay et al.*, 2010], and produced far more extensive thrust-faulting aftershock activity than intraplate activity. As found here, the occurrence of megathrust faulting is a reasonable consequence of trench slope normal-faulting, although the mechanism by which large extensional stress builds up and releases if the megathrust is locked is not clear (for the Samoa event, the thrusting occurred to the south of where the normal fault ruptured, so there may be a creeping region immediately down-dip of the normal-fault that allowed slab pull stress and/or slow slip events on the megathrust to load the normal fault). The triggered thrusting may have occurred in a region of conditional stability, which was undergoing stable sliding that accelerated into earthquake faulting when the stresses abruptly increased. Much of the triggered megathrust activity in the Kermadec sequence is located in a region where few GCMT solutions were previously found (Figure C–3). The July 6, 2011 Kermadec normal-fault earthquake (Figure C–10d) is either an example of very delayed response to the 1976 interplate events similar to the Sanriku events or an example of extensional stress accumulation and release up-dip of a coupled megathrust region. Like the Samoa sequence (Figure C–10c), the trench slope faulting activated thrusting on the megthrust, but in this case, it also activated deeper intraplate compressional activity.

These diverse sequences indicate a suite of possible faulting interactions with the intraplate environment responding to changes in the interplate environment and vice versa. It is rare to observe a large normal-fault event seaward of a locked

megathrust region, but the 2011 Kermadec doublet demonstrates that this can occur and appears to load the megathrust driving stresses, likely advancing the clock for the next large megathrust failure to come. The activation of shallow megathrust faulting by the normal fault will contribute further to stress concentration on the deeper, locked megathrust. For the northern Kermadec region we have very limited knowledge of the stress state, so it is unclear what the timing or total size of the next large underthrusting event will be.

Conclusion

The July 6, 2011 (M_w 7.6) and October 21, 2011 (M_w 7.4) intraplate earthquake doublet and the accompanying aftershock sequence along the Kermadec trench allow exploration of intraplate and interplate faulting interactions and stress changes in this region. The sequence began with large shallow normal faulting on July 6, 2011 that increased driving stress on both the megathrust environment and intraplate environment, resulting in thrust-faulting and normal-faulting activity in both regions, including the October 21, 2011 thrust-faulting event ~20 km below the northern portion of the earlier normal fault rupture. Coulomb stress change calculations are consistent with the observed faulting patterns in a general sense, although the precise contribution of background plate bending and plate coupling stresses is not known quantitatively. The apparent elastic neutral stress surface depth of about 30-35 km favors a relatively thick elastic lithosphere in the region. The 2011 Kermadec doublet presents an example of intraplate faulting influencing interplate faulting, complementary to the more typical reversed situation, and the triggering of

interplate aftershocks in a region that appears to be largely seismically locked indicates that the intraplate faulting has probably advanced the timing of forthcoming interplate rupture.

C.1 Supplemental Information

We determined finite-source rupture models using P and SH waves recorded at teleseismic distances to constrain the depths of two moderate, M_w 5.9 and 6.0, underthrusting aftershocks that occurred 6 hours apart on July 9, 2011. The inversion indicates consistent centroid depths with the GCMT estimates, suggesting that there is no regional bias in GCMT depth estimates. Selected waveform fits and residual error versus assumed hypocentral depth curves are shown in Figure C–11.

Figure C–11. Selected waveforms and slip distribution for two of the largest aftershocks.
The first earthquake (a) has GCMT source parameters: -29.12, -176.77, 07/09/2011 13:54:21.5 UTC, depth=25.1 km, M_w 5.9. The second earthquake (b) occurred 6 hours later and has GCMT source parameters: -29.21, -176.80, 07/09/2011 19:35:25.4 UTC, depth= 23.1 km, M_w 5.9. Modeling results for these two events indicate that the GCMT depths are not biased in this region.

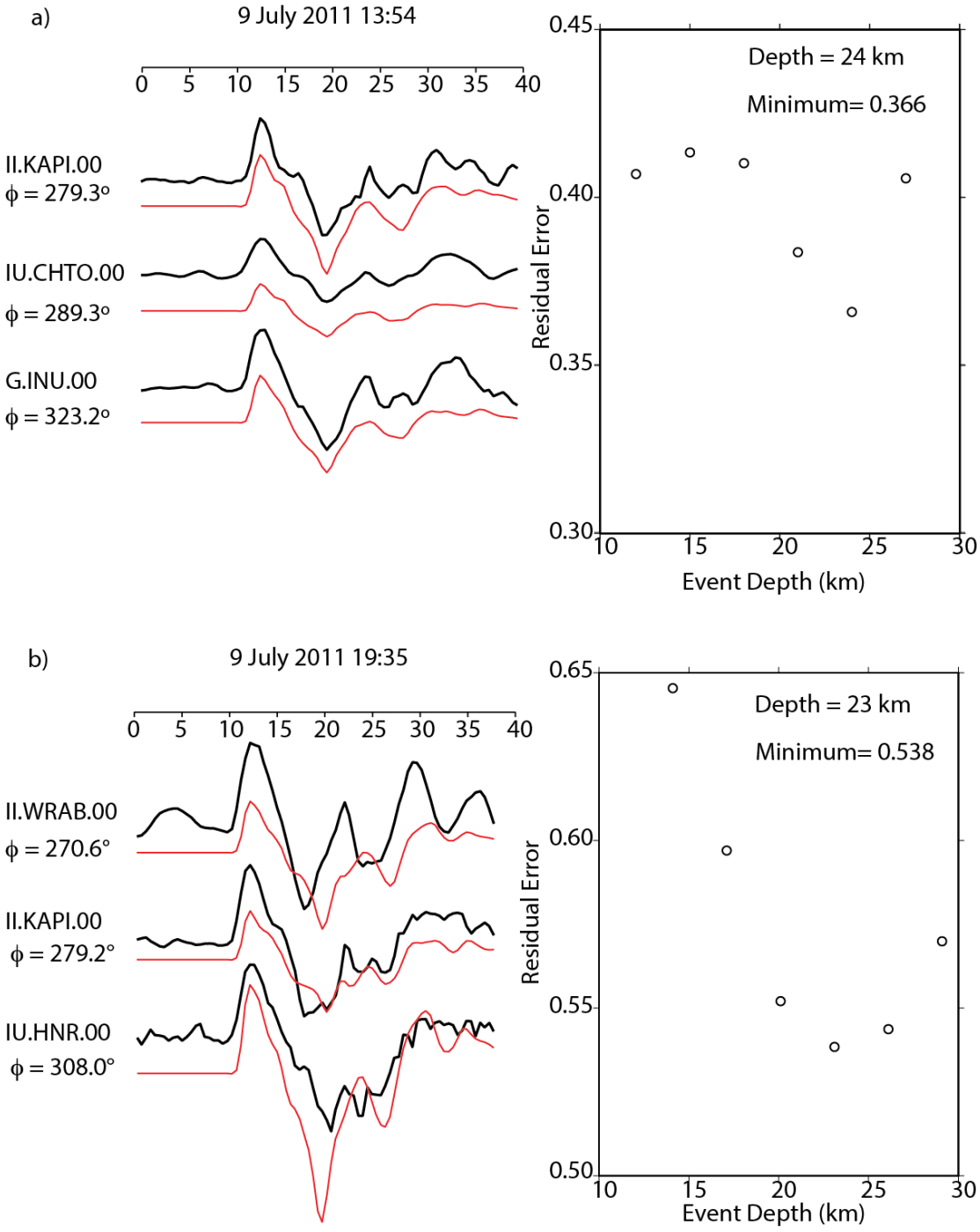
a)
9 July 2011 13:54
0 5 10 15 20 25 30 35 40
II.KAPI.00
ϕ = 279.3°
IU.CHTO.00
ϕ = 289.3°
G.INU.00
ϕ = 323.2°
Depth = 24 km
Minimum= 0.366
Residual Error
0.45
0.40
0.35
0.30
10 15 20 25 30
Event Depth (km)
b)
9 July 2011 19:35
0 5 10 15 20 25 30 35 40
II.WRAB.00
ϕ = 270.6°
II.KAPI.00
ϕ = 279.2°
IU.HNR.00
ϕ = 308.0°
Depth = 23 km
Minimum= 0.538
Residual Error
0.65
0.60
0.55
0.50
10 15 20 25 30
Event Depth (km)

References

Aagaard, B. T., M. G. Knepley, and C. A. Williams (2013), A domain decomposition approach to implementing fault slip in finite-element models of quasi-static and dynamic crustal deformation, *J. Geophys. Res. Solid Earth*, *118*(6), 3059–3079, doi:10.1002/jgrb.50217.

Aagaard, B. T., M. G. Knepley, and C. A. Williams (2016), *PyLith User Manual, Version 2.1.4*, Computational Infrastructure of Geodynamics, Davis, CA.

Abe, K. (1972), Lithospheric normal faulting beneath the Aleutian trench, *Phys. Earth Planet. Inter.*, *5*, 190–198, doi:10.1016/0031-9201(72)90091-X.

Allen, T. I., K. D. Marano, P. S. Earle, and D. J. Wald (2009), PAGER-CAT: A Composite Earthquake Catalog for Calibrating Global Fatality Models, *Seismol. Res. Lett.*, *80*(1), 57–62, doi:10.1785/gssrl.80.1.57.

Ammon, C. J., H. Kanamori, and T. Lay (2008), A great earthquake doublet and seismic stress transfer cycle in the central Kuril islands, *Nature*, *451*(7178), 561–565, doi:10.1038/nature06521.

Anderson, G., and C. Ji (2003), Static stress transfer during the 2002 Nenana Mountain-Denali Fault, Alaska, earthquake sequence, *Geophys. Res. Lett.*, *30*(6), 1310, doi:10.1029/2002GL016724.

Audet, P., and R. Bürgmann (2014), Possible control of subduction zone slow-earthquake periodicity by silica enrichment, *Nature*, *510*(7505), 389–392, doi:10.1038/nature13391.

Barker, D. H. N., R. Sutherland, S. Henrys, and S. Bannister (2009), Geometry of the Hikurangi subduction thrust and upper plate, North Island, New Zealand, *Geochem. Geophys. Geosystems*, *10*(2), Q02007, doi:10.1029/2008GC002153.

Barnes, P. M., and B. M. de Lépinay (1997), Rates and mechanics of rapid frontal accretion along the very obliquely convergent southern Hikurangi margin, New Zealand, *J. Geophys. Res. Solid Earth*, *102*(B11), 24931–24952, doi:10.1029/97JB01384.

Barnes, P. M., G. Lamarche, J. Bialas, S. Henrys, I. Pecher, G. L. Netzeband, J. Greinert, J. J. Mountjoy, K. Pedley, and G. Crutchley (2010), Tectonic and geological framework for gas hydrates and cold seeps on the Hikurangi

subduction margin, New Zealand, *Mar. Geol.*, *272*(1–4), 26–48, doi:10.1016/j.margeo.2009.03.012.

Bartlow, N. M., L. M. Wallace, R. J. Beavan, S. Bannister, and P. Segall (2014), Time-dependent modeling of slow slip events and associated seismicity and tremor at the Hikurangi subduction zone, New Zealand, *J. Geophys. Res. Solid Earth*, *119*(1), 734–753, doi:10.1002/2013JB010609.

Bassett, D., and A. B. Watts (2015), Gravity anomalies, crustal structure, and seismicity at subduction zones: 1. Seafloor roughness and subducting relief, *Geochem. Geophys. Geosystems*, *16*(5), 1508–1540, doi:10.1002/2014GC005684.

Bassett, D., R. Sutherland, S. Henrys, T. Stern, M. Scherwath, A. Benson, S. Toulmin, and M. Henderson (2010), Three-dimensional velocity structure of the northern Hikurangi margin, Raukumara, New Zealand: Implications for the growth of continental crust by subduction erosion and tectonic underplating, *Geochem. Geophys. Geosystems*, *11*(10), Q10013, doi:10.1029/2010GC003137.

Bassett, D., R. Sutherland, and S. Henrys (2014), Slow wavespeeds and fluid overpressure in a region of shallow geodetic locking and slow slip, Hikurangi subduction margin, New Zealand, *Earth Planet. Sci. Lett.*, *389*, 1–13, doi:10.1016/j.epsl.2013.12.021.

Beavan, J., L. Wallace, H. Fletcher, and A. Douglas (2007), Slow Slip Events on the Hikurangi Subduction Interface, New Zealand, in *Dynamic Planet*, edited by D. P. Tregoning and D. C. Rizos, pp. 438–444, Springer Berlin Heidelberg.

Beavan, J., X. Wang, C. Holden, K. Wilson, W. Power, G. Prasetya, M. Bevis, and R. Kautoke (2010), Near-simultaneous great earthquakes at Tongan megathrust and outer rise in September 2009, *Nature*, *466*(7309), 959–963, doi:10.1038/nature09292.

Beeler, N. M., R. W. Simpson, S. H. Hickman, and D. A. Lockner (2000), Pore fluid pressure, apparent friction, and Coulomb failure, *J. Geophys. Res. Solid Earth*, *105*(B11), 25533–25542, doi:10.1029/2000JB900119.

Bell, R., R. Sutherland, D. H. N. Barker, S. Henrys, S. Bannister, L. Wallace, and J. Beavan (2010), Seismic reflection character of the Hikurangi subduction interface, New Zealand, in the region of repeated Gisborne slow slip events, *Geophys. J. Int.*, *180*(1), 34–48, doi:10.1111/j.1365-246X.2009.04401.x.

Bell, R., C. Holden, W. Power, X. Wang, and G. Downes (2014), Hikurangi margin tsunami earthquake generated by slow seismic rupture over a subducted seamount, *Earth Planet. Sci. Lett.*, *397*, 1–9, doi:10.1016/j.epsl.2014.04.005.

Beroza, G. C., and S. Ide (2011), Slow Earthquakes and Nonvolcanic Tremor, *Annu. Rev. Earth Planet. Sci.*, *39*(1), 271–296, doi:10.1146/annurev-earth-040809-152531.

Bevis, M. et al. (1995), Geodetic observations of very rapid convergence and back-arc extension at the Tonga arc, *Nature*, *374*(6519), 249–251, doi:10.1038/374249a0.

Bilek, S. L., and T. Lay (2002), Tsunami earthquakes possibly widespread manifestations of frictional conditional stability, *Geophys. Res. Lett.*, *29*(14), 18–1, doi:10.1029/2002GL015215.

Billen, M. I., and M. Gurnis (2005), Constraints on subducting plate strength within the Kermadec trench, *J. Geophys. Res. Solid Earth*, *110*(B5), B05407, doi:10.1029/2004JB003308.

Bird, P., and Y. Y. Kagan (2004), Plate-Tectonic Analysis of Shallow Seismicity: Apparent Boundary Width, Beta, Corner Magnitude, Coupled Lithosphere Thickness, and Coupling in Seven Tectonic Settings, *Bull. Seismol. Soc. Am.*, *94*(6), 2380–2399, doi:10.1785/0120030107.

Bonnardot, M.-A., M. Régnier, E. Ruellan, C. Christova, and E. Tric (2007), Seismicity and state of stress within the overriding plate of the Tonga-Kermadec subduction zone, *Tectonics*, *26*(5), TC5017, doi:10.1029/2006TC002044.

Borghi, A., A. Aoudia, F. Javed, and R. Barzaghi (2016), Precursory slow-slip loaded the 2009 L'Aquila earthquake sequence, *Geophys. J. Int.*, *205*(2), 776–784, doi:10.1093/gji/ggw046.

Brooks, B. A., J. Foster, D. Sandwell, C. J. Wolfe, P. Okubo, M. Poland, and D. Myer (2008), Magmatically Triggered Slow Slip at Kilauea Volcano, Hawaii, *Science*, *321*(5893), 1177–1177, doi:10.1126/science.1159007.

Brown, J. R., G. C. Beroza, S. Ide, K. Ohta, D. R. Shelly, S. Y. Schwartz, W. Rabbel, M. Thorwart, and H. Kao (2009), Deep low-frequency earthquakes in tremor localize to the plate interface in multiple subduction zones, *Geophys. Res. Lett.*, *36*(19), L19306, doi:10.1029/2009GL040027.

Brown, K. M., M. D. Tryon, H. R. DeShon, L. M. Dorman, and S. Y. Schwartz (2005), Correlated transient fluid pulsing and seismic tremor in the Costa Rica subduction zone, *Earth Planet. Sci. Lett.*, *238*(1–2), 189–203, doi:10.1016/j.epsl.2005.06.055.

Brudzinski, M., E. Cabral-Cano, F. Correa-Mora, C. DeMets, and B. Márquez-Azúa (2007), Slow slip transients along the Oaxaca subduction segment from 1993 to 2007, *Geophys. J. Int.*, *171*(2), 523–538, doi:10.1111/j.1365-246X.2007.03542.x.

Brudzinski, M. R., and R. M. Allen (2007), Segmentation in episodic tremor and slip all along Cascadia, *Geology*, *35*(10), 907–910, doi:10.1130/G23740A.1.

Brudzinski, M. R., H. R. Hinojosa-Prieto, K. M. Schlanser, E. Cabral-Cano, A. Arciniega-Ceballos, O. Diaz-Molina, and C. DeMets (2010), Nonvolcanic tremor along the Oaxaca segment of the Middle America subduction zone, *J. Geophys. Res. Solid Earth*, *115*(B8), B00A23, doi:10.1029/2008JB006061.

Cervelli, P., P. Segall, K. Johnson, M. Lisowski, and A. Miklius (2002), Sudden aseismic fault slip on the south flank of Kilauea volcano, *Nature*, *415*(6875), 1014–1018, doi:10.1038/4151014a.

Chamberlain, C. J., D. R. Shelly, J. Townend, and T. A. Stern (2014), Low-frequency earthquakes reveal punctuated slow slip on the deep extent of the Alpine Fault, New Zealand, *Geochem. Geophys. Geosystems*, *15*(7), 2984–2999, doi:10.1002/2014GC005436.

Chao, K., Z. Peng, H. Gonzalez‐Huizar, C. Aiken, B. Enescu, H. Kao, A. A. Velasco, K. Obara, and T. Matsuzawa (2013), A Global Search for Triggered Tremor Following the 2011 Mw 9.0 Tohoku Earthquake, *Bull. Seismol. Soc. Am.*, *103*(2B), 1551–1571, doi:10.1785/0120120171.

Chapple, W. M., and D. W. Forsyth (1979), Earthquakes and bending of plates at trenches, *J. Geophys. Res. Solid Earth*, *84*(B12), 6729–6749, doi:10.1029/JB084iB12p06729.

Christensen, D. H., and T. Lay (1988), Large Earthquakes in the Tonga Region Associated with Subduction of the Louisville Ridge, *J. Geophys. Res. Solid Earth*, *93*(B11), 13367–13389, doi:10.1029/JB093iB11p13367.

Christensen, D. H., and L. J. Ruff (1988), Seismic coupling and outer rise earthquakes, *J. Geophys. Res. Solid Earth*, *93*(B11), 13421–13444.

Cloos, M. (1992), Thrust-type subduction-zone earthquakes and seamount asperities: A physical model for seismic rupture, *Geology*, *20*(7), 601–604, doi:10.1130/0091-7613(1992)020<0601:TTSZEA>2.3.CO;2.

Collot, J.-Y. et al. (1996), From oblique subduction to intra-continental transpression: Structures of the southern Kermadec-Hikurangi margin from multibeam bathymetry, side-scan sonar and seismic reflection, *Mar. Geophys. Res.*, *18*(2–4), 357–381, doi:10.1007/BF00286085.

Collot, J.-Y., K. Lewis, G. Lamarche, and S. Lallemand (2001), The giant Ruatoria debris avalanche on the northern Hikurangi margin, New Zealand: Result of oblique seamount subduction, *J. Geophys. Res. Solid Earth*, *106*(B9), 19271–19297, doi:10.1029/2001JB900004.

Davy, B., and J.-Y. Collot (2000), The Rapuhia Scarp (northern Hikurangi Plateau) — its nature and subduction effects on the Kermadec Trench, *Tectonophysics*, *328*(3–4), 269–295, doi:10.1016/S0040-1951(00)00211-0.

Davy, B., and R. Wood (1994), Gravity and magnetic modelling of the Hikurangi Plateau, *Mar. Geol.*, *118*(1), 139–151, doi:10.1016/0025-3227(94)90117-1.

Davy, B., K. Hoernle, and R. Werner (2008), Hikurangi Plateau: Crustal structure, rifted formation, and Gondwana subduction history, *Geochem. Geophys. Geosystems*, *9*(7), Q07004, doi:10.1029/2007GC001855.

Delahaye, E. J., J. Townend, M. E. Reyners, and G. Rogers (2009), Microseismicity but no tremor accompanying slow slip in the Hikurangi subduction zone, New Zealand, *Earth Planet. Sci. Lett.*, *277*(1–2), 21–28, doi:10.1016/j.epsl.2008.09.038.

DeMets, C., R. G. Gordon, D. F. Argus, and S. Stein (1994), Effect of recent revisions to the geomagnetic reversal time scale on estimates of current plate motions, *Geophys. Res. Lett.*, *21*(20), 2191–2194, doi:10.1029/94GL02118.

Dmowska, R., J. R. Rice, L. C. Lovison, and D. Josell (1988), Stress transfer and seismic phenomena in coupled subduction zones during the earthquake cycle, *J Geophys Res*, *93*, 7869–7884.

Dmowska, R., G. Zheng, and J. R. Rice (1996), Seismicity and deformation at convergent margins due to heterogeneous coupling, *J. Geophys. Res. Solid Earth*, *101*(B2), 3015–3029, doi:10.1029/95JB03122.

Dominguez, S., S. E. Lallemand, J. Malavieille, and R. von Huene (1998), Upper plate deformation associated with seamount subduction, *Tectonophysics*, *293*(3–4), 207–224, doi:10.1016/S0040-1951(98)00086-9.

Doser, D. I., and T. H. Webb (2003), Source parameters of large historical (1917–1961) earthquakes, North Island, New Zealand, *Geophys. J. Int.*, *152*(3), 795–832, doi:10.1046/j.1365-246X.2003.01895.x.

Douglas, A., J. Beavan, L. Wallace, and J. Townend (2005), Slow slip on the northern Hikurangi subduction interface, New Zealand, *Geophys. Res. Lett.*, *32*(16), L16305, doi:10.1029/2005GL023607.

Dragert, H., K. Wang, and T. S. James (2001), A Silent Slip Event on the Deeper Cascadia Subduction Interface, *Science*, *292*(5521), 1525–1528, doi:10.1126/science.1060152.

Dragert, H., K. Wang, and G. Rogers (2004), Geodetic and seismic signatures of episodic tremor and slip in the northern Cascadia subduction zone, *Earth Planets Space*, *56*(12), 1143–1150, doi:10.1186/BF03353333.

Eberhart-Phillips, D., and S. Bannister (2015), 3-D imaging of the northern Hikurangi subduction zone, New Zealand: variations in subducted sediment, slab fluids and slow slip, *Geophys. J. Int.*, *201*(2), 838–855, doi:10.1093/gji/ggv057.

Eberhart-Phillips, D., and M. Chadwick (2002), Three-dimensional attenuation model of the shallow Hikurangi subduction zone in the Raukumara Peninsula, New Zealand, *J. Geophys. Res. Solid Earth*, *107*(B2), ESE 3-1, doi:10.1029/2000JB000046.

Eberhart-Phillips, D., and M. Reyners (1999), Plate interface properties in the Northeast Hikurangi Subduction Zone, New Zealand, from converted seismic waves, *Geophys. Res. Lett.*, *26*(16), 2565–2568, doi:10.1029/1999GL900567.

Eberhart-Phillips, D., M. Reyners, M. Chadwick, and J.-M. Chiu (2005), Crustal heterogeneity and subduction processes: 3-D Vp, Vp/Vs and Q in the southern North Island, New Zealand, *Geophys. J. Int.*, *162*(1), 270–288, doi:10.1111/j.1365-246X.2005.02530.x.

Eberhart-Phillips, D., M. Reyners, S. Bannister, M. Chadwick, and S. Ellis (2010), Establishing a Versatile 3-D Seismic Velocity Model for New Zealand, *Seismol. Res. Lett.*, *81*(6), 992–1000, doi:10.1785/gssrl.81.6.992.

Eberhart-Phillips, D., M. Reyners, M. Faccenda, and J. Naliboff (2013), Along-strike variation in subducting plate seismicity and mantle wedge attenuation related to fluid release beneath the North Island, New Zealand, *Phys. Earth Planet. Inter.*, *225*, 12–27, doi:10.1016/j.pepi.2013.10.002.

Eiby, G. A. (1982), Two New Zealand Tsunamis, *J. R. Soc. N. Z.*, *12*(4), 338–351, doi:10.1080/03036758.1982.10415340.

Eissler, H., and H. Kanamori (1982), A large normal-fault earthquake at the junction of the Tonga trench and the Louisville ridge, *Phys. Earth Planet. Inter.*, *29*(2), 161–172, doi:10.1016/0031-9201(82)90070-X.

Ellis, S., I. Pecher, N. Kukowski, W. Xu, S. Henrys, and J. Greinert (2010), Testing proposed mechanisms for seafloor weakening at the top of gas hydrate stability on an uplifted submarine ridge (Rock Garden), New Zealand, *Mar. Geol.*, *272*(1–4), 127–140, doi:10.1016/j.margeo.2009.10.008.

Ellis, S., Å. Fagereng, D. Barker, S. Henrys, D. Saffer, L. Wallace, C. Williams, and R. Harris (2015), Fluid budgets along the northern Hikurangi subduction margin, New Zealand: the effect of a subducting seamount on fluid pressure, *Geophys. J. Int.*, *202*(1), 277–297, doi:10.1093/gji/ggv127.

François-Holden, C. et al. (2008), The Mw 6.6 Gisborne earthquake of 2007: Preliminary records and general source characterisation, *Bull New Zeal Soc Earthq Eng*, *41*(4), 266–277.

Frank, W. B., N. M. Shapiro, V. Kostoglodov, A. L. Husker, M. Campillo, J. S. Payero, and G. A. Prieto (2013), Low-frequency earthquakes in the Mexican Sweet Spot, *Geophys. Res. Lett.*, *40*(11), 2661–2666, doi:10.1002/grl.50561.

Freed, A. M. (2005), Earthquake Triggering by Static, Dynamic, and Postseismic Stress Transfer, *Annu. Rev. Earth Planet. Sci.*, *33*(1), 335–367, doi:10.1146/annurev.earth.33.092203.122505.

Fry, B., K. Chao, S. Bannister, Z. Peng, and L. Wallace (2011), Deep tremor in New Zealand triggered by the 2010 Mw8.8 Chile earthquake, *Geophys. Res. Lett.*, *38*(15), doi:http://dx.doi.org/10.1029/2011GL048319.

Fuchs, F., M. Lupi, and S. A. Miller (2014), Remotely triggered nonvolcanic tremor in Sumbawa, Indonesia, *Geophys. Res. Lett.*, *41*(12), 4185–4193, doi:10.1002/2014GL060312.

Gallego, A., R. M. Russo, D. Comte, V. Mocanu, R. E. Murdie, and J. c. VanDecar (2013), Tidal modulation of continuous nonvolcanic seismic tremor in the Chile triple junction region, *Geochem. Geophys. Geosystems*, *14*(4), 851–863, doi:10.1002/ggge.20091.

Ghosh, A., J. E. Vidale, J. R. Sweet, K. C. Creager, and A. G. Wech (2009), Tremor patches in Cascadia revealed by seismic array analysis, *Geophys. Res. Lett.*, *36*(17), L17316, doi:10.1029/2009GL039080.

Harris, R. A. (1998), Introduction to Special Section: Stress Triggers, Stress Shadows, and Implications for Seismic Hazard, *J. Geophys. Res. Solid Earth*, *103*(B10), 24347–24358, doi:10.1029/98JB01576.

Harris, R. A., and R. W. Simpson (1992), Changes in static stress on southern California faults after the 1992 Landers earthquake, *Nature*, *360*(6401), 251–254, doi:10.1038/360251a0.

Hayes, G. P., D. J. Wald, and R. L. Johnson (2012), Slab1.0: A three-dimensional model of global subduction zone geometries, *J. Geophys. Res. Solid Earth*, *117*(B1), B01302, doi:10.1029/2011JB008524.

Heki, K., S. 'ichi Miyazaki, and H. Tsuji (1997), Silent fault slip following an interplate thrust earthquake at the Japan Trench, *Nature*, *386*(6625), 595–598, doi:10.1038/386595a0.

Hill, D. P. et al. (1993), Seismicity Remotely Triggered by the Magnitude 7.3 Landers, California, Earthquake, *Science*, *260*(5114), 1617–1623.

Hirose, H., and K. Obara (2005), Repeating short- and long-term slow slip events with deep tremor activity around the Bungo channel region, southwest Japan, *Earth Planets Space*, *57*(10), 961–972, doi:10.1186/BF03351875.

Hirose, H., K. Hirahara, F. Kimata, N. Fujii, and S. 'ichi Miyazaki (1999), A slow thrust slip event following the two 1996 Hyuganada Earthquakes beneath the Bungo Channel, southwest Japan, *Geophys. Res. Lett.*, *26*(21), 3237–3240, doi:10.1029/1999GL010999.

Hornbach, M. J. et al. (2015), Permeability and pressure measurements in Lesser Antilles submarine slides: Evidence for pressure-driven slow-slip failure, *J. Geophys. Res. Solid Earth*, *120*(12), 2015JB012061, doi:10.1002/2015JB012061.

Houston, H., H. Anderson, S. L. Beck, J. Zhang, and S. Schwartz (1993), The 1986 Kermadec earthquake and its relation to plate segmentation, *Pure Appl. Geophys.*, *140*(2), 331–364, doi:10.1007/BF00879411.

Huene, R. von (2008), When Seamounts Subduct, *Science*, *321*(5893), 1165–1166, doi:10.1126/science.1162868.

von Huene, R., C. R. Ranero, W. Weinrebe, and K. Hinz (2000), Quaternary convergent margin tectonics of Costa Rica, segmentation of the Cocos Plate, and Central American volcanism, *Tectonics*, *19*(2), 314–334, doi:10.1029/1999TC001143.

Ide, S. (2010), Striations, duration, migration and tidal response in deep tremor, *Nature*, *466*(7304), 356–359, doi:10.1038/nature09251.

Ide, S. (2012), Variety and spatial heterogeneity of tectonic tremor worldwide, *J. Geophys. Res. Solid Earth*, *117*(3), doi:http://dx.doi.org/10.1029/2011JB008840.

Ide, S., G. C. Beroza, D. R. Shelly, and T. Uchide (2007a), A scaling law for slow earthquakes, *Nature*, *447*(7140), 76–79, doi:10.1038/nature05780.

Ide, S., D. R. Shelly, and G. C. Beroza (2007b), Mechanism of deep low frequency earthquakes: Further evidence that deep non-volcanic tremor is generated by shear slip on the plate interface, *Geophys. Res. Lett.*, *34*(3), L03308, doi:10.1029/2006GL028890.

Iinuma, T. et al. (2009), Aseismic slow slip on an inland active fault triggered by a nearby shallow event, the 2008 Iwate-Miyagi Nairiku earthquake (Mw6.8), *Geophys. Res. Lett.*, *36*(20), L20308, doi:10.1029/2009GL040063.

Isacks, B., J. Oliver, and L. R. Sykes (1968), Seismology and the new global tectonics, *J. Geophys. Res.*, *73*(18), 5855–5899, doi:10.1029/JB073i018p05855.

Itaba, S., and R. Ando (2011), A slow slip event triggered by teleseismic surface waves, *Geophys. Res. Lett.*, *38*(21), L21306, doi:10.1029/2011GL049593.

Ito, Y., K. Obara, K. Shiomi, S. Sekine, and H. Hirose (2007), Slow Earthquakes Coincident with Episodic Tremors and Slow Slip Events, *Science*, *315*(5811), 503–506, doi:10.1126/science.1134454.

Ito, Y. et al. (2013), Episodic slow slip events in the Japan subduction zone before the 2011 Tohoku-Oki earthquake, *Tectonophysics*, *600*, 14–26, doi:10.1016/j.tecto.2012.08.022.

Jacobs, K. M., M. K. Savage, and E. C. G. Smith (2016), Quantifying seismicity associated with slow slip events in the Hikurangi margin, New Zealand, *N. Z. J. Geol. Geophys.*, *59*(1), 58–69, doi:10.1080/00288306.2015.1127827.

Jiang, Y., S. Wdowinski, T. H. Dixon, M. Hackl, M. Protti, and V. Gonzalez (2012), Slow slip events in Costa Rica detected by continuous GPS observations, 2002–2011, *Geochem. Geophys. Geosystems*, *13*(4), Q04006, doi:10.1029/2012GC004058.

Kagan, Y. Y. (1999), Universality of the Seismic Moment-frequency Relation, in *Seismicity Patterns, their Statistical Significance and Physical Meaning*, edited by M. Wyss, K. Shimazaki, and A. Ito, pp. 537–573, Birkhäuser Basel.

Kanamori, H. (1971), Seismological evidence for a lithospheric normal faulting — the Sanriku earthquake of 1933, *Phys. Earth Planet. Inter.*, *4*(4), 289–300, doi:10.1016/0031-9201(71)90013-6.

Kanamori, H. (1972), Mechanism of tsunami earthquakes, *Phys. Earth Planet. Inter.*, *6*(5), 346–359, doi:10.1016/0031-9201(72)90058-1.

Kao, H., S.-J. Shan, H. Dragert, G. Rogers, J. F. Cassidy, K. Wang, T. S. James, and K. Ramachandran (2006), Spatial-temporal patterns of seismic tremors in northern Cascadia, *J. Geophys. Res. Solid Earth*, *111*(B3), B03309, doi:10.1029/2005JB003727.

Kaproth, B. M., and C. Marone (2013), Slow Earthquakes, Preseismic Velocity Changes, and the Origin of Slow Frictional Stick-Slip, *Science*, *341*(6151), 1229–1232, doi:10.1126/science.1239577.

Kato, A., and S. Nakagawa (2014), Multiple slow-slip events during a foreshock sequence of the 2014 Iquique, Chile Mw 8.1 earthquake, *Geophys. Res. Lett.*, *41*(15), 2014GL061138, doi:10.1002/2014GL061138.

Kato, A., K. Obara, T. Igarashi, H. Tsuruoka, S. Nakagawa, and N. Hirata (2012), Propagation of Slow Slip Leading Up to the 2011 Mw 9.0 Tohoku-Oki Earthquake, *Science*, *335*(6069), 705–708, doi:10.1126/science.1215141.

Kelleher, J., and W. McCann (1976), Buoyant zones, great earthquakes, and unstable boundaries of subduction, *J. Geophys. Res.*, *81*(26), 4885–4896, doi:10.1029/JB081i026p04885.

Kim, M. J., S. Y. Schwartz, and S. Bannister (2011), Non-volcanic tremor associated with the March 2010 Gisborne slow slip event at the Hikurangi subduction margin, New Zealand, *Geophys. Res. Lett.*, *38*(14), doi:http://dx.doi.org/10.1029/2011GL048400.

Kitajima, H., and D. M. Saffer (2012), Elevated pore pressure and anomalously low stress in regions of low frequency earthquakes along the Nankai Trough subduction megathrust, *Geophys. Res. Lett.*, *39*(23), L23301, doi:10.1029/2012GL053793.

Kodaira, S., T. Iidaka, A. Kato, J.-O. Park, T. Iwasaki, and Y. Kaneda (2004), High Pore Fluid Pressure May Cause Silent Slip in the Nankai Trough, *Science*, *304*(5675), 1295–1298, doi:10.1126/science.1096535.

Kostoglodov, V., S. K. Singh, J. A. Santiago, S. I. Franco, K. M. Larson, A. R. Lowry, and R. Bilham (2003), A large silent earthquake in the Guerrero seismic gap, Mexico, *Geophys. Res. Lett.*, *30*(15), 1807, doi:10.1029/2003GL017219.

Kukowski, N., J. Greinert, and S. Henrys (2010), Morphometric and critical taper analysis of the Rock Garden region, Hikurangi Margin, New Zealand: Implications for slope stability and potential tsunami generation, *Mar. Geol.*, *272*(1–4), 141–153, doi:10.1016/j.margeo.2009.06.004.

Lay, T., and H. Kanamori (1981), The asperity model of large earthquake sequences, in *Earthquake prediction: an international review.*, edited by D. W. Simpson and P. G. Richards, pp. 579–592, American Geophysical Union, Washington, D.C.

Lay, T., H. Kanamori, and L. Ruff (1982), The Asperity Model and the Nature of Large Subduction Zone Earthquakes, *Earthq. Predict. Res.*, *1*(1), 3–71.

Lay, T., L. Astiz, H. Kanamori, and D. H. Christensen (1989), Temporal variation of large intraplate earthquakes in coupled subduction zones, *Phys. Earth Planet. Inter.*, *54*(3), 258–312, doi:10.1016/0031-9201(89)90247-1.

Lay, T., H. Kanamori, C. J. Ammon, A. R. Hutko, K. Furlong, and L. Rivera (2009), The 2006–2007 Kuril Islands great earthquake sequence, *J. Geophys. Res. Solid Earth*, *114*(B11), B11308, doi:10.1029/2008JB006280.

Lay, T., C. J. Ammon, H. Kanamori, L. Rivera, K. D. Koper, and A. R. Hutko (2010), The 2009 Samoa-Tonga great earthquake triggered doublet, *Nature*, *466*(7309), 964–968, doi:10.1038/nature09214.

Lay, T., C. J. Ammon, H. Kanamori, M. J. Kim, and L. Xue (2011), Outer trench-slope faulting and the 2011 Mw 9.0 off the Pacific coast of Tohoku Earthquake, *Earth Planets Space*, *63*(7), 37, doi:10.5047/eps.2011.05.006.

Leeman, J., M. M. Scuderi, C. Marone, and D. Saffer (2015), Stiffness evolution of granular layers and the origin of repetitive, slow, stick-slip frictional sliding, *Granul. Matter*, *17*(4), 447–457, doi:10.1007/s10035-015-0565-1.

Lewis, K. B., and J. R. Pettinga (1993), The emerging, imbricate frontal wedge of the Hikurangi margin, *Sediment. Basins World*, *2*, 225–250.

Lewis, K. B., J.-Y. Collot, and S. E. Lallem (1998), The dammed Hikurangi Trough: a channel-fed trench blocked by subducting seamounts and their wake avalanches (New Zealand–France GeodyNZ Project), *Basin Res.*, *10*(4), 441–468, doi:10.1046/j.1365-2117.1998.00080.x.

Lewis, K. B., S. E. Lallemand, and L. Carter (2004), Collapse in a Quaternary shelf basin off East Cape, New Zealand: Evidence for passage of a subducted seamount inboard of the Ruatoria giant avalanche, *N. Z. J. Geol. Geophys.*, *47*(3), 415–429, doi:10.1080/00288306.2004.9515067.

Liu, X., and K. C. McNally (1993), Quantitative estimates of interplate coupling inferred from outer rise earthquakes, *Pure Appl. Geophys.*, *140*(2), 211–255, doi:10.1007/BF00879406.

Liu, Y., and J. R. Rice (2007), Spontaneous and triggered aseismic deformation transients in a subduction fault model, *J. Geophys. Res. Solid Earth*, *112*(B9), B09404, doi:10.1029/2007JB004930.

Lomax, A. (2011), The NonLinLoc Software Guide, version 6.0,

Lomax, A., J. Virieux, P. Volant, and C. Berge-Thierry (2000), Probabilistic Earthquake Location in 3D and Layered Models, in *Advances in Seismic Event Location*, edited by C. H. Thurber and N. Rabinowitz, pp. 101–134, Springer Netherlands.

Lundgren, P. R., E. A. Okal, and D. A. Wiens (1989), Rupture characteristics of the 1982 Tonga and 1986 Kermadec earthquakes, *J. Geophys. Res. Solid Earth*, *94*(B11), 15521–15539, doi:10.1029/JB094iB11p15521.

Lynnes, C. S., and T. Lay (1988), Source Process of the Great 1977 Sumba Earthquake, *J. Geophys. Res. Solid Earth*, *93*(B11), 13407–13420, doi:10.1029/JB093iB11p13407.

Marone, C., C. Scholz, and R. Bilham (1991), On the Mechanics of Earthquake Afterslip, *J. Geophys. Res. Solid Earth Planets*, *96*(B5), 8441–8452.

Matsuzawa, T., B. Shibazaki, K. Obara, and H. Hirose (2013), Comprehensive model of short- and long-term slow slip events in the Shikoku region of Japan, incorporating a realistic plate configuration, *Geophys. Res. Lett.*, *40*(19), 5125–5130, doi:10.1002/grl.51006.

Mattia, M. et al. (2015), A comprehensive interpretative model of slow slip events on Mt. Etna's eastern flank, *Geochem. Geophys. Geosystems*, *16*(3), 635–658, doi:10.1002/2014GC005585.

McCaffrey, R. (2008), Global frequency of magnitude 9 earthquakes, *Geology*, *36*(3), 263–266, doi:10.1130/G24402A.1.

McCaffrey, R., L. M. Wallace, and J. Beavan (2008), Slow slip and frictional transition at low temperature at the Hikurangi subduction zone, *Nat. Geosci.*, *1*(5), 316–320, doi:10.1038/ngeo178.

McCann, W. R., S. P. Nishenko, L. R. Sykes, and J. Krause (1979), Seismic gaps and plate tectonics: Seismic potential for major boundaries, *Pure Appl. Geophys.*, *117*(6), 1082–1147, doi:10.1007/BF00876211.

McCausland, W. A., K. C. Creager, M. La Rocca, and S. D. Malone (2010), Short-term and long-term tremor migration patterns of the Cascadia 2004 tremor and slow slip episode using small aperture seismic arrays, *J. Geophys. Res. Solid Earth*, *115*(B8), B00A24, doi:10.1029/2008JB006063.

Mendoza, M. M., A. Ghosh, and S. S. Rai (2016), Dynamic triggering of small local earthquakes in the central Himalaya, *Geophys. Res. Lett.*, *43*(18), 2016GL069969, doi:10.1002/2016GL069969.

Mikumo, T., S. K. Singh, and M. A. Santoyo (1999), A possible stress interaction between large thrust and normal faulting earthquakes in the Mexican subduction zone, *Bull. Seismol. Soc. Am.*, *89*(6), 1418–1427.

Mochizuki, K., T. Yamada, M. Shinohara, Y. Yamanaka, and T. Kanazawa (2008), Weak Interplate Coupling by Seamounts and Repeating M ~ 7 Earthquakes, *Science*, *321*(5893), 1194–1197, doi:10.1126/science.1160250.

Mohiuddin, M. M., and Y. Ogawa (1998), Late Paleocene–middle Miocene pelagic sequences in the Boso Peninsula, Japan: New light on northwest Pacific tectonics, *Isl. Arc*, *7*(3), 301–314, doi:10.1111/j.1440-1738.1998.00191.x.

Montgomery-Brown, E. K., and E. M. Syracuse (2015), Tremor-genic slow slip regions may be deeper and warmer and may slip slower than non-tremor-genic regions, *Geochem. Geophys. Geosystems*, *16*(10), 3593–3606, doi:10.1002/2015GC005895.

Montgomery-Brown, E. K., P. Segall, and A. Miklius (2009), Kilauea slow slip events: Identification, source inversions, and relation to seismicity, *J. Geophys. Res. Solid Earth*, *114*(B6), B00A03, doi:10.1029/2008JB006074.

Mortimer, N., and D. Parkinson (1996), Hikurangi Plateau: A Cretaceous large igneous province in the southwest Pacific Ocean, *J. Geophys. Res. Solid Earth*, *101*(B1), 687–696, doi:10.1029/95JB03037.

Mueller, S., G. L. Choy, and W. Spence (1996a), Inelastic models of lithospheric stress-I. Theory and application to outer-rise plate deformation, *Geophys. J. Int.*, *125*(1), 39–53, doi:10.1111/j.1365-246X.1996.tb06533.x.

Mueller, S., W. Spence, and G. L. Choy (1996b), Inelastic models of lithospheric stress-II. Implications for outer-rise seismicity and dynamics, *Geophys. J. Int.*, *125*(1), 54–72, doi:10.1111/j.1365-246X.1996.tb06534.x.

Murakami, M., H. Suito, S. Ozawa, and M. Kaidzu (2006), Earthquake triggering by migrating slow slip initiated by M8 earthquake along Kuril Trench, Japan, *Geophys. Res. Lett.*, *33*(9), L09306, doi:10.1029/2006GL025967.

Nadeau, R. M., and D. Dolenc (2005), Nonvolcanic Tremors Deep Beneath the San Andreas Fault, *Science*, *307*(5708), 389–389, doi:10.1126/science.1107142.

Nishenko, S. P. (1991), Circum-Pacific Seismic Potential: 1989–1999, in *Aspects of Pacific Seismicity*, edited by E. A. Okal, pp. 169–259, Birkhäuser Basel.

Obara, K. (2002), Nonvolcanic Deep Tremor Associated with Subduction in Southwest Japan, *Science*, *296*(5573), 1679–1681, doi:10.1126/science.1070378.

Obara, K., and S. Sekine (2009), Characteristic activity and migration of episodic tremor and slow-slip events in central Japan, *Earth Planets Space*, *61*(7), 853–862, doi:10.1186/BF03353196.

Obara, K., H. Hirose, F. Yamamizu, and K. Kasahara (2004), Episodic slow slip events accompanied by non-volcanic tremors in southwest Japan subduction zone, *Geophys. Res. Lett.*, *31*(23), L23602, doi:10.1029/2004GL020848.

Ohta, Y., J. T. Freymueller, S. Hreinsdóttir, and H. Suito (2006), A large slow slip event and the depth of the seismogenic zone in the south central Alaska subduction zone, *Earth Planet. Sci. Lett.*, *247*(1–2), 108–116, doi:10.1016/j.epsl.2006.05.013.

Okada, Y. (1985), Surface deformation due to shear and tensile faults in a half-space, *Bull. Seismol. Soc. Am.*, *75*(4), 1135–1154.

Okada, Y. (1992), Internal deformation due to shear and tensile faults in a half-space, *Bull. Seismol. Soc. Am.*, *82*(2), 1018–1040.

Okal, E. A., J. Borrero, and C. E. Synolakis (2004), The earthquake and tsunami of 1865 November 17: evidence for far-field tsunami hazard from Tonga, *Geophys. J. Int.*, *157*(1), 164–174, doi:10.1111/j.1365-246X.2004.02177.x.

Ougier-Simonin, A., and W. Zhu (2015), Effect of pore pressure buildup on slowness of rupture propagation, *J. Geophys. Res. Solid Earth*, *120*(12), 2015JB012047, doi:10.1002/2015JB012047.

Outerbridge, K. C., T. H. Dixon, S. Y. Schwartz, J. I. Walter, M. Protti, V. Gonzalez, J. Biggs, M. Thorwart, and W. Rabbel (2010), A tremor and slip event on the Cocos-Caribbean subduction zone as measured by a global positioning system (GPS) and seismic network on the Nicoya Peninsula, Costa Rica, *J. Geophys. Res. Solid Earth*, *115*(B10), B10408, doi:10.1029/2009JB006845.

Ozawa, S., S. Miyazaki, Y. Hatanaka, T. Imakiire, M. Kaidzu, and M. Murakami (2003), Characteristic silent earthquakes in the eastern part of the Boso peninsula, Central Japan, *Geophys. Res. Lett.*, *30*(6), 1283, doi:10.1029/2002GL016665.

Payero, J. S., V. Kostoglodov, N. Shapiro, T. Mikumo, A. Iglesias, X. Pérez-Campos, and R. W. Clayton (2008), Nonvolcanic tremor observed in the Mexican subduction zone, *Geophys. Res. Lett.*, *35*(7), L07305, doi:10.1029/2007GL032877.

Pedley, K. L., P. M. Barnes, J. R. Pettinga, and K. B. Lewis (2010), Seafloor structural geomorphic evolution of the accretionary frontal wedge in response to seamount subduction, Poverty Indentation, New Zealand, *Mar. Geol.*, *270*(1–4), 119–138, doi:10.1016/j.margeo.2009.11.006.

Pelayo, A. M., and D. A. Wiens (1992), Tsunami earthquakes: Slow thrust-faulting events in the accretionary wedge, *J. Geophys. Res. Solid Earth*, *97*(B11), 15321–15337, doi:10.1029/92JB01305.

Pelletier, B., and R. Louat (1989), Seismotectonics and present-day relative plate motions in the Tonga-Lau and Kermadec-Havre region, *Tectonophysics*, *165*(1–4), 237–250, doi:10.1016/0040-1951(89)90049-8.

Pelletier, B., S. Calmant, and R. Pillet (1998), Current tectonics of the Tonga–New Hebrides region, *Earth Planet. Sci. Lett.*, *164*(1–2), 263–276, doi:10.1016/S0012-821X(98)00212-X.

Peng, Z., and K. Chao (2008), Non-volcanic tremor beneath the Central Range in Taiwan triggered by the 2001 Mw 7.8 Kunlun earthquake, *Geophys. J. Int.*, *175*(2), 825–829, doi:10.1111/j.1365-246X.2008.03886.x.

Peng, Z., and J. Gomberg (2010), An integrated perspective of the continuum between earthquakes and slow-slip phenomena, *Nat. Geosci.*, *3*(9), 599–607, doi:10.1038/ngeo940.

Peng, Z., J. E. Vidale, A. G. Wech, R. M. Nadeau, and K. C. Creager (2009), Remote triggering of tremor along the San Andreas Fault in central California, *J. Geophys. Res. Solid Earth*, *114*(B7), B00A06, doi:10.1029/2008JB006049.

Peterson, C. L., and D. H. Christensen (2009), Possible relationship between nonvolcanic tremor and the 1998–2001 slow slip event, south central Alaska, *J. Geophys. Res. Solid Earth*, *114*(B6), B06302, doi:10.1029/2008JB006096.

Power, W., L. Wallace, X. Wang, and M. Reyners (2012), Tsunami Hazard Posed to New Zealand by the Kermadec and Southern New Hebrides Subduction Margins: An Assessment Based on Plate Boundary Kinematics, Interseismic Coupling, and Historical Seismicity, *Pure Appl. Geophys.*, *169*(1–2), 1–36, doi:10.1007/s00024-011-0299-x.

Prejean, S. G., D. P. Hill, E. E. Brodsky, S. E. Hough, M. J. S. Johnston, S. D. Malone, D. H. Oppenheimer, A. M. Pitt, and K. B. Richards-Dinger (2004), Remotely Triggered Seismicity on the United States West Coast following the Mw 7.9 Denali Fault Earthquake, *Bull. Seismol. Soc. Am.*, *94*(6B), S348–S359, doi:10.1785/0120040610.

Protti, M., V. González, T. Kato, T. Iinuma, S. Miyazaki, K. Obana, Y. Kaneda, P. La Femina, T. Dixon, and S. Schwartrz (2004), A Creep Event on the Shallow

Interface of the Nicoya Peninsula, Costa Rica Seismogenic Zone, *AGU Fall Meet. Abstr.*, *41*.

Proust, J. N., C. Martillo, F. Michaud, J. Y. Collot, and O. Dauteuil (2016), Subduction of seafloor asperities revealed by a detailed stratigraphic analysis of the active margin shelf sediments of Central Ecuador, *Mar. Geol.*, *380*, 345–362, doi:10.1016/j.margeo.2016.03.014.

Radiguet, M., H. Perfettini, N. Cotte, A. Gualandi, B. Valette, V. Kostoglodov, T. Lhomme, A. Walpersdorf, E. Cabral Cano, and M. Campillo (2016), Triggering of the 2014 Mw7.3 Papanoa earthquake by a slow slip event in Guerrero, Mexico, *Nat. Geosci.*, *9*(11), 829–833, doi:10.1038/ngeo2817.

Ranero, C. R., and R. von Huene (2000), Subduction erosion along the Middle America convergent margin, *Nature*, *404*(6779), 748–752, doi:10.1038/35008046.

Reyners, M., and S. Bannister (2007), Earthquakes triggered by slow slip at the plate interface in the Hikurangi subduction zone, New Zealand, *Geophys. Res. Lett.*, *34*(14), L14305, doi:10.1029/2007GL030511.

Reyners, M., D. Eberhart-Phillips, and G. Stuart (1999), A three-dimensional image of shallow subduction: crustal structure of the Raukumara Peninsula, New Zealand, *Geophys. J. Int.*, *137*(3), 873–890, doi:10.1046/j.1365-246x.1999.00842.x.

Reyners, M., D. Eberhart-Phillips, and S. Bannister (2011), Tracking repeated subduction of the Hikurangi Plateau beneath New Zealand, *Earth Planet. Sci. Lett.*, *311*(1–2), 165–171, doi:10.1016/j.epsl.2011.09.011.

Ristau, J., D. Harte, and J. Salichon (2016), A Revised Local Magnitude (ML) Scale for New Zealand Earthquakes, *Bull. Seismol. Soc. Am.*, *106*(2), 398–407, doi:10.1785/0120150293.

Rogers, G., and H. Dragert (2003), Episodic Tremor and Slip on the Cascadia Subduction Zone: The Chatter of Silent Slip, *Science*, *300*(5627), 1942–1943, doi:10.1126/science.1084783.

Rubin, A. M. (2008), Episodic slow slip events and rate-and-state friction, *J. Geophys. Res. Solid Earth*, *113*(B11), B11414, doi:10.1029/2008JB005642.

Rubinstein, J. L., J. E. Vidale, J. Gomberg, P. Bodin, K. C. Creager, and S. D. Malone (2007), Non-volcanic tremor driven by large transient shear stresses, *Nature*, *448*(7153), 579–582, doi:10.1038/nature06017.

Ruff, L., and H. Kanamori (1980), Seismicity and the subduction process, *Phys. Earth Planet. Inter.*, *23*(3), 240–252, doi:10.1016/0031-9201(80)90117-X.

Ruiz, S., M. Metois, A. Fuenzalida, J. Ruiz, F. Leyton, R. Grandin, C. Vigny, R. Madariaga, and J. Campos (2014), Intense foreshocks and a slow slip event preceded the 2014 Iquique Mw 8.1 earthquake, *Science*, *345*(6201), 1165–1169, doi:10.1126/science.1256074.

Saffer, D. M., and L. M. Wallace (2015), The frictional, hydrologic, metamorphic and thermal habitat of shallow slow earthquakes, *Nat. Geosci.*, *8*(8), 594–600, doi:10.1038/ngeo2490.

Sage, F., J.-Y. Collot, and C. R. Ranero (2006), Interplate patchiness and subduction-erosion mechanisms: Evidence from depth-migrated seismic images at the central Ecuador convergent margin, *Geology*, *34*(12), 997–1000, doi:10.1130/G22790A.1.

Savage, J. C., and J. P. Church (1975), Evidence for afterslip on the San Fernando fault, *Bull. Seismol. Soc. Am.*, *65*(4), 829–834.

Schwartz, S. Y., and J. M. Rokosky (2007), Slow slip events and seismic tremor at circum-Pacific subduction zones, *Rev. Geophys.*, *45*(3), RG3004, doi:10.1029/2006RG000208.

Segall, P., E. K. Desmarais, D. Shelly, A. Miklius, and P. Cervelli (2006), Earthquakes triggered by silent slip events on Kīlauea volcano, Hawaii, *Nature*, *442*(7098), 71–74, doi:10.1038/nature04938.

Segall, P., A. M. Rubin, A. M. Bradley, and J. R. Rice (2010), Dilatant strengthening as a mechanism for slow slip events, *J. Geophys. Res. Solid Earth*, *115*(B12), B12305, doi:10.1029/2010JB007449.

Shelly, D. R. (2009), Possible deep fault slip preceding the 2004 Parkfield earthquake, inferred from detailed observations of tectonic tremor, *Geophys. Res. Lett.*, *36*(17), L17318, doi:10.1029/2009GL039589.

Shelly, D. R. (2010), Migrating tremors illuminate complex deformation beneath the seismogenic San Andreas fault, *Nature*, *463*(7281), 648–652, doi:10.1038/nature08755.

Shelly, D. R., G. C. Beroza, S. Ide, and S. Nakamula (2006), Low-frequency earthquakes in Shikoku, Japan, and their relationship to episodic tremor and slip, *Nature*, *442*(7099), 188–191, doi:10.1038/nature04931.

Shelly, D. R., G. C. Beroza, and S. Ide (2007), Non-volcanic tremor and low-frequency earthquake swarms, *Nature*, *446*(7133), 305–307, doi:10.1038/nature05666.

Shibazaki, B., and Y. Iio (2003), On the physical mechanism of silent slip events along the deeper part of the seismogenic zone, *Geophys. Res. Lett.*, *30*(9), 1489, doi:10.1029/2003GL017047.

Spence, W. (1986), The 1977 Sumba earthquake series: Evidence for Slab pull force acting at a subduction zone, *J. Geophys. Res. Solid Earth*, *91*(B7), 7225–7239, doi:10.1029/JB091iB07p07225.

Stauder, W. (1968), Tensional character of earthquake foci beneath the Aleutian Trench with relation to sea-floor spreading, *J. Geophys. Res.*, *73*(24), 7693–7701, doi:10.1029/JB073i024p07693.

Stein, R. S. (1999), The role of stress transfer in earthquake occurrence, *Nature*, *402*(6762), 605–609, doi:10.1038/45144.

Stein, R. S., and M. Lisowski (1983), The 1979 Homestead Valley Earthquake Sequence, California: Control of aftershocks and postseismic deformation, *J. Geophys. Res. Solid Earth*, *88*(B8), 6477–6490, doi:10.1029/JB088iB08p06477.

Stein, R. S., G. C. P. King, and J. Lin (1992), Change in Failure Stress on the Southern San Andreas Fault System Caused by the 1992 Magnitude = 7.4 Landers Earthquake, *Science*, *258*(5086), 1328–1332.

Strong, C. P. (1994), Late Cretaceous foraminifera from Hikurangi Plateau, New Zealand, *Mar. Geol.*, *119*(1–2), 1–5, doi:10.1016/0025-3227(94)90137-6.

Szeliga, W., T. I. Melbourne, M. M. Miller, and V. M. Santillan (2004), Southern Cascadia episodic slow earthquakes, *Geophys. Res. Lett.*, *31*(16), L16602, doi:10.1029/2004GL020824.

Taylor, M. A. J., G. Zheng, J. R. Rice, W. D. Stuart, and R. Dmowska (1996), Cyclic stressing and seismicity at strongly coupled subduction zones, *J. Geophys. Res. Solid Earth*, *101*(B4), 8363–8381, doi:10.1029/95JB03561.

Thomas, A. M., R. M. Nadeau, and R. Bürgmann (2009), Tremor-tide correlations and near-lithostatic pore pressure on the deep San Andreas fault, *Nature*, *462*(7276), 1048–1051, doi:10.1038/nature08654.

Thomas, A. M., G. C. Beroza, and D. R. Shelly (2016), Constraints on the source parameters of low-frequency earthquakes on the San Andreas Fault, *Geophys. Res. Lett.*, *43*(4), 2015GL067173, doi:10.1002/2015GL067173.

Toda, S., and R. Stein (2003), Toggling of seismicity by the 1997 Kagoshima earthquake couplet: A demonstration of time-dependent stress transfer, *J. Geophys. Res. Solid Earth*, *108*(B12), 2567, doi:10.1029/2003JB002527.

Toda, S., R. S. Stein, P. A. Reasenberg, J. H. Dieterich, and A. Yoshida (1998), Stress transferred by the 1995 Mw = 6.9 Kobe, Japan, shock: Effect on aftershocks and future earthquake probabilities, *J. Geophys. Res. Solid Earth*, *103*(B10), 24543–24565, doi:10.1029/98JB00765.

Toda, S., R. S. Stein, G. C. Beroza, and D. Marsan (2012), Aftershocks halted by static stress shadows, *Nat. Geosci.*, *5*(6), 410–413, doi:10.1038/ngeo1465.

Todd, E. K., and S. Y. Schwartz (2016), Tectonic tremor along the northern Hikurangi Margin, New Zealand, between 2010 and 2015, *J. Geophys. Res. Solid Earth*, 2016JB013480, doi:10.1002/2016JB013480.

Tsumura, N. et al. (2009), A bump on the upper surface of the Philippine Sea plate beneath the Boso Peninsula, Japan inferred from seismic reflection surveys: A possible asperity of the 1703 Genroku earthquake, *Tectonophysics*, *472*(1–4), 39–50, doi:10.1016/j.tecto.2008.05.009.

Vallée, M. et al. (2013), Intense interface seismicity triggered by a shallow slow slip event in the Central Ecuador subduction zone, *J. Geophys. Res. Solid Earth*, *118*(6), 2965–2981, doi:10.1002/jgrb.50216.

Venkataraman, A., and H. Kanamori (2004), Observational constraints on the fracture energy of subduction zone earthquakes, *J. Geophys. Res. Solid Earth*, *109*(B5), B05302, doi:10.1029/2003JB002549.

Wallace, L. M., and J. Beavan (2006), A large slow slip event on the central Hikurangi subduction interface beneath the Manawatu region, North Island, New Zealand, *Geophys. Res. Lett.*, *33*(11), L11301, doi:10.1029/2006GL026009.

Wallace, L. M., and J. Beavan (2010), Diverse slow slip behavior at the Hikurangi subduction margin, New Zealand, *J. Geophys. Res. Solid Earth*, *115*(12), doi:http://dx.doi.org/10.1029/2010JB007717.

Wallace, L. M., and D. Eberhart-Phillips (2013), Newly observed, deep slow slip events at the central Hikurangi margin, New Zealand: Implications for

downdip variability of slow slip and tremor, and relationship to seismic structure, *Geophys. Res. Lett.*, *40*(20), 2013GL057682, doi:10.1002/2013GL057682.

Wallace, L. M., J. Beavan, R. McCaffrey, and D. Darby (2004), Subduction zone coupling and tectonic block rotations in the North Island, New Zealand, *J. Geophys. Res. Solid Earth*, *109*(B12), B12406, doi:10.1029/2004JB003241.

Wallace, L. M. et al. (2009), Characterizing the seismogenic zone of a major plate boundary subduction thrust: Hikurangi Margin, New Zealand, *Geochem. Geophys. Geosystems*, *10*(10), Q10006, doi:10.1029/2009GC002610.

Wallace, L. M., J. Beavan, S. Bannister, and C. Williams (2012a), Simultaneous long-term and short-term slow slip events at the Hikurangi subduction margin, New Zealand: Implications for processes that control slow slip event occurrence, duration, and migration, *J. Geophys. Res. Solid Earth*, *117*(B11), B11402, doi:10.1029/2012JB009489.

Wallace, L. M., P. Barnes, J. Beavan, R. Van Dissen, N. Litchfield, J. Mountjoy, R. Langridge, G. Lamarche, and N. Pondard (2012b), The kinematics of a transition from subduction to strike-slip: An example from the central New Zealand plate boundary, *J. Geophys. Res. Solid Earth*, *117*(B2), B02405, doi:10.1029/2011JB008640.

Wallace, L. M., N. Bartlow, I. Hamling, and B. Fry (2014), Quake clamps down on slow slip, *Geophys. Res. Lett.*, *41*(24), 2014GL062367, doi:10.1002/2014GL062367.

Wallace, L. M., S. C. Webb, Y. Ito, K. Mochizuki, R. Hino, S. Henrys, S. Y. Schwartz, and A. F. Sheehan (2016), Slow slip near the trench at the Hikurangi subduction zone, New Zealand, *Science*, *352*(6286), 701–704, doi:10.1126/science.aaf2349.

Wang, K., and S. L. Bilek (2011), Do subducting seamounts generate or stop large earthquakes?, *Geology*, *39*(9), 819–822, doi:10.1130/G31856.1.

Wang, K., and S. L. Bilek (2014), Invited review paper: Fault creep caused by subduction of rough seafloor relief, *Tectonophysics*, *610*, 1–24, doi:10.1016/j.tecto.2013.11.024.

Warren, L. M., A. N. Hughes, and P. G. Silver (2007), Earthquake mechanics and deformation in the Tonga-Kermadec subduction zone from fault plane orientations of intermediate- and deep-focus earthquakes, *J. Geophys. Res. Solid Earth*, *112*(B5), B05314, doi:10.1029/2006JB004677.

Wech, A. G., and K. C. Creager (2008), Automated detection and location of Cascadia tremor, *Geophys. Res. Lett.*, *35*(20), L20302, doi:10.1029/2008GL035458.

Wech, A. G., C. M. Boese, T. A. Stern, and J. Townend (2012), Tectonic tremor and deep slow slip on the Alpine Fault, *Geophys. Res. Lett.*, *39*(1), doi:http://dx.doi.org/10.1029/2012GL051751.

Wech, A. G., A. F. Sheehan, C. M. Boese, J. Townend, T. A. Stern, and J. A. Collins (2013), Tectonic tremor recorded by ocean bottom seismometers, *Seismol. Res. Lett.*, *84*(5), 752–758.

Williams, C. A., and L. M. Wallace (2015), Effects of material property variations on slip estimates for subduction interface slow-slip events, *Geophys. Res. Lett.*, *42*(4), 2014GL062505, doi:10.1002/2014GL062505.

Williams, C. A., D. Eberhart-Phillips, S. Bannister, D. H. Barker, S. Henrys, M. Reyners, and R. Sutherland (2013), Revised interface geometry for the Hikurangi subduction zone, New Zealand, *Seismol. Res. Lett.*, *84*(6), 1066–1073.

Wood, R., and B. Davy (1994), The Hikurangi Plateau, *Mar. Geol.*, *118*(1–2), 153–173, doi:10.1016/0025-3227(94)90118-X.

Yokota, Y., T. Ishikawa, S. Watanabe, T. Tashiro, and A. Asada (2016), Seafloor geodetic constraints on interplate coupling of the Nankai Trough megathrust zone, *Nature*, *534*(7607), 374–377, doi:10.1038/nature17632.

Yoshida, S., and N. Kato (2003), Episodic aseismic slip in a two-degree-of-freedom block-spring model, *Geophys. Res. Lett.*, *30*(13), 1681, doi:10.1029/2003GL017439.

Yoshioka, S., T. Mikumo, V. Kostoglodov, K. M. Larson, A. R. Lowry, and S. K. Singh (2004), Interplate coupling and a recent aseismic slow slip event in the Guerrero seismic gap of the Mexican subduction zone, as deduced from GPS data inversion using a Bayesian information criterion, *Phys. Earth Planet. Inter.*, *146*(3–4), 513–530, doi:10.1016/j.pepi.2004.05.006.

Zigone, D. et al. (2012), Triggering of tremors and slow slip event in Guerrero, Mexico, by the 2010 Mw 8.8 Maule, Chile, earthquake, *J. Geophys. Res. Solid Earth*, *117*(B9), B09304, doi:10.1029/2012JB009160.